Multi-responsive Microgels and Hydrogels

A thesis submitted to the University of Manchester for the degree of

Doctor of Philosophy

in the Faculty of Science and Engineering

Submitted 2020

Dongdong Lu

Department of Materials

School of Natural Sciences

The University of Manchester

Table of Contents

Word count:48206

List of Publications

1. Lu, D. D.; Zhu, M. N.; Wu, S. L; Lian, Q.; Wang, W. K.; Adlam, D. J.; Hoyland, J. A.; Saunders, B. R.,. Programmed Multiresponsive Hydrogel Assemblies with Light-Tunable Mechanical Properties, Actuation, and Fluorescence. Adv. Funct. Mater. 2020, 1909359. The relative discussion of this paper is chapter 6 in thesis.

2. Lu, D. D.; Zhu, M. N.; Wu, S. L.; Wang, W. K.; Lian, Q.; Saunders, B. R. *, Triply responsive coumarin-based microgels with remarkably large photo-switchable swelling. Polym. Chem. 2019, 10, 2516-2526. The relative discussion of this paper is chapter 5 in thesis.

3. Lu, D. D.; Zhu, M. N.; Wang, W. K.; Wu, S. L.; Adlam, D. J.; Hoyland, J. A.; Hofzumahaus, C.; Schneider, S.; Landfester, K.; Saunders, B. R*., Do the properties of gels constructed by interlinking triplyresponsive microgels follow from those of the building blocks? Soft Matter 2019, 15, 527-536. The relative discussion of this paper is chapter 4 in thesis.

4. Wu, S. L.; Zhu, M. N.; Lu, D.D; Milani, A. H.; Lian, Q.; Fielding, L.A; Saunders, B. R*.; Derry, M.J; Armes, S. P.; Adlam, D. J.; Hoyland, J. A. Self-curing super-stretchable polymer/microgel complex coacervate gels without covalent bond formation. Chem. Sci. 2019, 10, 8832-8839

5. Zhu, M. N.; Lu, D. D.; Wu, S. L.; Lian, Q.; Wang, W. K.; Lyon, L. A.; Wang, W.G; Bártolo.P; Saunders, B. R., Using green emitting pH-responsive nanogels to report environmental changes within hydrogels: a nanoprobe for versatile sensing. Nanoscale 2019, 2019, 11, 11484-11495

6. Shanks, H. R, Milani A. H; Lu, D.D; Saunders BR; Carney L; Adlam D.J.; Hoyland J.A.; Blount C.; Dickinson M., Core-shell-shell nanoparticles for NIR fluorescence imaging and NRET swelling reporting of injectable or implantable gels. Biomacromolecules 2019, 20, 2694-2702

7. Wu, S. L.; Zhu, M. N.; Lian, Q.; Lu, D.D; Spencer, B.; Adlam, D. J.; Hoyland, J. A.; Volk, K.; Karg, M.; Saunders, B. R*., Plasmonic and colloidal stability behaviours of Au-acrylic core–shell nanoparticles with thin pH-responsive shells. Nanoscale 2018, 10, 18565-18575.

8. Wang, W. K.; Lu, D. D.; Zhu, M. N.; Saunders, J. M.; Milani, A. H.; Armes, S. P.; Saunders, B. R*., Highly deformable hydrogels constructed by pH-triggered polyacid nanoparticle disassembly in aqueous dispersions. Soft Matter 2018, 14, 3510-3520.

9. Zhu, M. N.; Lu, D. D.; Wu, S. L.; Lian, Q.; Wang, W. K.; Milani, A. H.; Cui, Z. X.; Nguyen, N. T.; Chen, M.; Lyon, L. A.; Adlam, D. J.; Freemont, A. J.; Hoyland, J. A.; Saunders, B. R*., Responsive Nanogel Probe for Ratiometric Fluorescent Sensing of pH and Strain in Hydrogels. ACS Macro Lett. 2017, 6, 1245-1250

List of Figures

List of Tables

List of Abbreviations

APS	Ammonium persulfate
AA	Acrylic acid
An	(9-anthryl)methacrylate
AAm	Acrylamide
ATRP	Atomic transfer radical polymerisation
Anti-hh	Anti head-to-head
Anti-ht	Anti head-to- tail
BAC	*N,N′*-bis(acryloyl)cystamine
BDDA	1,4-butanediol diacrylate
BIS	*N,N′*-methylenebis(acrylamide)
$CHCl_3$	Chloroform
CH_2Cl_2	Dichloromethane
CMA	7-(2-methacryloyloxyethoxy)-4-methylcoumarin
CMC	Critical micelle concentration
COOH	Carboxylic acid group
CCD	Charge coupled device
DIVD	Degenrated intervertebral disc
DLS	Dynamic light scattering
DLVO	Derjaguin-Landau-Verwey-Overbeek
DMF	*N,N*-dimethylformamide
DVB	Divinylbenzene
DX MGs	Doubly crosslinked microgels
DOX	Doxorubicin hydrochloride
DTT	Dithiothreitol

DVS	Divinylsulfone
DMEM	Dulbecco's modified Eagle's medium
DLC	Drug loading content
DLE	Drug loading efficiency
DMAEMA	Dimethylamino ethyl methacrylate
DEAAm	*N,N'*-diethyl acrylamide
DD	Dimerization degree
EA	Ethyl acrylate
EGDMA	Ethylene glycol dimethacrylate
FRET	Fluorescence resonance energy transfer
FTIR	Fourier transform infrared
GMA	Glycidyl methacrylate
IVD	Intervertebral disc
IR	Infrared
KPS	Potassium persulfate
K_2CO_3	Potassium carbonate
MEO_2MA	2-(2-methoxyethoxy)ethyl methacrylate
MAA	Methacrylic acid
MGs	Microgels
MMA	Methyl methacrylate
MEMA	2-(N-morpholino)ethylmethacrylate
MeOH	Methanol
Me-RDB	Methacryloxyethyl thiocarbamoyl Rhodamine B
mol%	Mole percent
N_2	Nitrogen
NRET	Nonresonance energy transfer

NaCl	Sodium chloride
NaOH	Sodium hydroxide
NG	Nanogel
NGs	Nanogels
$NG_{Ph/An}$	Poly(methyl methacrylate-methacrylic acid-ethylene glycol dimethacrylate-(9-Phenanthryl) methyl methacrylate-(9-Anthryl) methacrylate) nanogel
NIPAM	*N*-isopropylacrylamide
NIPMAm	*N*-isopropylmethacrylamide
NIR	Near-infrared
NP	Nucleus pulposus
NMR	Nuclear magnetic resonance
NEMAM	*N*-ethylmethacrylamide
nPh	2,2'-(2-nitro-1,4-phenylene)bis(methylene)bis(oxy)bis(oxomethylene) bis(azane-diyl)bis(ethane-2,1-diyl) bis(2-methylacrylate)
nHAp	Nanohydroxyapatite
OEGMA	oligo(ethylene glycol)methacrylate
PBS	Phosphate-buffered solution
PCS	Photon correlation spectroscopy
PDI	Polydispersity index
Ph	(9-Phenanthryl) methyl methacrylate
PL	Photoluminescence
PNIPAM	Poly(*N*-isopropylacrylamide)
pNIPAM	Poly(*N*-isopropylacrylamide-*N,N'*-methylenebisacrylamide-(3-Aminopropyl)methacrylamide)

PEI	Polyethyleneimine
PEG	Poly(ethylene glycol)
PCL	Poly(ε-caprolactone)
PVCL	Poly(N-vinylcaprolactam)
PVAM	Poly(vinylamine)
PDEAEM	Poly(diethylaminoethyl methacrylate)
PDMAEM	Poly(2-(dimethylamino)ethyl methacrylate)
PCBMA	Poly(carboxybetaine methacrylate)
PEO-b-P(ETEGA-r-NBA)	Poly(ethylene oxyde) - block - poly(ethoxytri (ethyleneglycol) acrylate - random - o - nitrobenzylacrylate)
PEO-P(MEOMA-co-CMA)	Poly(ethylene oxide) and poly[2-(2-methoxyethoxy)ethyl methacrylate-co-4-methyl-[7-(methacryloyl)oxyethyloxy]coumarin]
P(3,4DHCA-co-4HCA)	Poly(3,4-dihydroxycinnamic acid-co-4-hydroxycinnamic acid)
PEA-MAA-BDDA	Poly(ethylacrylate-methacrylic acid-butanediol diacrylate)
PMMA-MAA-EGDMA	Poly(methyl methacrylate-methacrylic acid-ethyleneglycol dimethacrylate)
SP	Spiropyran
SDS	Sodium dodecyl sulfate
SEM	Scanning electron microscopy
-SH	Thiol
S-S	Disulfide
SX	Singly crosslinked
Syn-hh	Syn head-to-head
Syn-ht	Syn head-to-tail
TEM	Transmission electron microscopy
TEMED	*N,N,N′,N′*-tetramethylethane-1,2-diamine

TMS	Tetramethylsilane
TEA	Triethylamine
TPA	Two-photon absorption
UV	Ultraviolet
VPTT	Volume phase transition temperature
VCL	Vinyl caprolactam
V-50	Dihydrochloride
HPC	Hydroxypropyl cellulose
HOMO	Highest occupied molecular orbital
LUMO	Lowest unoccupied molecular orbital
LCST	Lower critical solution temperature

List of Symbols

a	Particle radius
A	Absorbance
A_1	Hamaker constants for colloid particle
A_2	Hamaker constants for medium
A_{eff}	Hamaker constant
D	Diffusion coefficient
d_z	Z-average particle size
$d_{(N)}$	Z-average particle size at a pH value of N
d_{coll}	Collapsed particle diameter
d_{swol}	Swollen diameter
d_{TEM}	Number-average diameters determined from TEM images
e	Charge
E	Efficiency of energy transfer
f	Number of effective chains formed per crosslinking monomer
G(τ)	Light intensity autocorrelation function
G'	Storage modulus
G''	Loss modulus
H	The distance between two particles
I	Initiator
I_{max}	Maximum PL intensity
k	Boltzmann constant
K_a	Dissociation constant
k_d	Rate coefficient for initiator decomposition
k_p	Rate coefficient for propagation

k_t	Rate coefficient of termination
M	Monomer
N	Number
N_A	Avogadro's constant
N_C	Effective number of polymer chains in the polymeric particle
V_0	Volume of the particle in the reference state (collapsed state)
V_S	Molar volume of the solvent
pKa	Negative logarithm of dissociation constant
q	Scattering vector
Q	Volume swelling ratio
Q(m)	Mass swelling ratio
R•	Free radicals from fractured initiator
R_p	Rate of polymerization
T	Temperature
T	Transmittance
v_1	Molar volume of the solvent
V_c	Collapsed network volume
V_{att}	Van der Waals attractive force
V_{rep}	Energy contributed by electrostatic repulsion and opposes aggregation
V_{str}	Steric stabilisation energy
V_t	Total energy of interaction
$g1(\tau)$	Normalised electric field correlation function
$g2(\tau)$	Normalised intensity correlation function
X	Number of crosslinks
z	Valence

ζ	Zeta potential
η	Viscosity
θ	Angle of the incident beam
κ	Inverse thickness of the diffuse layer
κ	Debye screening Parameter
$1/\kappa$	Thickness of the double layer
κ_2	Dipole orientation factor
λ	Wavelength
λ_{ex}	Excitation wavelength
λ_{max}	Wavelength of maximum intensity
μ	Electrophoretic mobility
ρ_s	Density of solvent
ρ_p	Density of polymer
τ	Delay time
Γ	characteristic decay rate
ϕ	Volume fraction of the polymeric particle in the swollen state
ϕ_0	Volume fraction of the polymeric particle in reference
χ	Flory solvent-polymer interaction parameter
ψ_d	Surface potential energy at the Stern layer
ε	Molar extinction coefficient
σ	Chemical shifts
v_s	Absorption frequencies of the sample and the reference
v_r	Absorption frequencies of the reference
ε_B	Breaking strain
γ^*	Yield strain

E	Modulus
Π_{don}	Donnan equilibrium
Π_{elas}	Elastic osmotic pressure
Π_{mix}	Solvent-polymer mixing osmotic pressure
Π_{total}	Total osmotic pressure of polymeric network

Abstract

Microgels (MGs) are swellable crosslinked polymer colloids. They can also be used as the only building block to construct nanostructured hydrogels which are denoted as doubly crosslinked microgels (DX MGs). Both MGs and DX MGs can be useful in biological application. This thesis presents a study of multi responsive MGs and DX MGs.

In the beginning, new triply responsive DX MG-*x*-nPh comprised of interlinked MG-*x*-nPh of oligo(ethylene glycol)methacrylate (OEGMA), 2-(2-methoxyethoxy)ethyl methacrylate (MEO_2MA), methacrylic acid (MAA), o-nitrobenzyl-based UV photocleavable crosslinker (nPh) and glycidyl methacrylate (GMA) are investigated. The MG-*x*-nPh particles swelled or collapsed in response to temperature and pH changes and also degraded when UV irradiated. The content of crosslinker (*x*) does not restrict the swelling of MG-*x*-nPh. The concentrated MGs can be formed into DX MG-*x*-nPh gels via free-radical polymerisation using the GMA vinyl groups. The DX MG-*x*-nPh gels are injectable and implanted and they are not cytotoxic to nucleus pulposus cells. DX MG-*x*-nPh also shows temperature and pH responsiveness additions UV-enhanced the gel modulus. The mechanical properties and swelling of the DX MG gels were strongly affected by *x*. The UV-C light stabilised gels have potential application as injectable gels and implants for soft tissue. Even though the photosensitive MG-*x*-nPh and gels is developed in this work, the applications are limited due to irreversibly of gel formation.

Next, I synthesised the reversibly photo-crosslinkable 7-(2-methacryloyloxyethoxy)-4-methylcoumarin (CMA) and copolymerised it with MEO_2MA and MAA to prepare triply responsive CMA-based MGs (denoted as MG-CMA). MG-CMA is also multi-responsive (pH, temperature and light). It was found that the photo-dimerisation degree of CMA is related to the size of as-made MGs. The photo-switching ability between a highly

crosslinked and de-crosslinked state was achieved using UV-irradiation. The crosslinker density was easily adjusted by switching the wavelength of UV light. Light and pH are shown to control the release of a drug from MG-CMA.

The method for preparing conventional DX MGs require addition of initiator, which limits spatial and temporal control and may adversely affect cells. At the end of the project I investigated a strategy to construct multi-responsive hydrogels utilising photo-triggered covalent interlinking of concentrated MG-CMA building blocks. This method provides precise spatial control and no other material is required to prepare the gels beyond the MG-CMA particles themselves. The multi-responsive hydrogels are reversibly responsive to light, pH and temperature. The moduli value and swelling ratios of gels are also photo-tuneable. This versatile gels show light-assisted healing, re-shaping, photo-patterning, fluorescent photo-imaging and can be built up to multi-responsive cytocompatible actuators, grippers and ON/OFF circuit components. This work provides a new strategy to construct versatile multi-responsive gels.

Declaration

I declare that no portion of the work referred to in the thesis has been submitted in support of an application for another degree or qualification of this or any other university or other institute of learning.

Dongdong Lu

Copyright Statement

Acknowledgements

There are many people helping me throughout my PhD study. I cannot go through and finish the PhD project without them. First of all, I would like to thank my supervisor, Prof. Brian Saunders for all of his help, encouragement, advice, support and expertise during my PhD. His high requirement and strong work pushed me to work harder and harder, and for that I am grateful.

I would also like to thank my cosupervisor Dr. Jonny Blaker, Dr. Steve Edmondson, Dr. Lee Fielding, Dr. Daman Adlam, Prof. Judith Hoyland, Prof. Andrew Lyon and Prof. Katharina Landfester. I have received a lot of academic support from those experts in various areas.

I would also like to thank the rest of the BRS group: Amir, Nam, Wayne, Ivan, Shanglin, Qing, Cui, Junfeng, Frank,Rosie, James, Shah, Wani, Jenny, Dou, Tong Wu and Melody. Thank you for all of your help, advice and support throughout my study, and I wish you always have happiness life.

I would also like to thank Jasmine Fernley, Polly Greensmith and Dr. Chloe Loveless for maintaining a good laboratory environment and generously providing technical support all the time.

Finally I would like to give an enormous thank my family, especially my parents, who sponsored me completing the PhD study at The University of Manchester.

Learning is like a boat sailing against the current, either forge ahead or be driven back. I hope I can keep learning and advancing with the time.

Chapter 1: Introduction

1.1 Motivation

Degenerated intervertebral disc (DIVD) leads to a loss of disc height and mechanical instability, resulting in chronic pain[1]. It is a major health problem for humans which causes reduced productivity and increased treatment costs[2]. Our group has been shown that doubly crosslinked microgels (DX MGs) assembled from the polyacid-based microgel particles (MGs) can be used as an injectable gel and provide therapeutic (load support), diagnostic (stress-strain data) and tissue regeneration capabilities for the DIVD as a non-invasive (injectable) therapy[3, 4]. Remotely monitoring and adjusting the local stress distributions of DX MGs in the DIVD in real-time, in situ are important during therapy. Some reports from our group show that the pH-responsive nanoprobes or core-shell-shell nanoparticles implanted into the DX MGs leads to gels which have capacity to monitor their environment such as local stress and pH values by fluorescent signals based on Förster resonance energy transfer (FRET)[5-7].

In this thesis, my work is developing injectable hydrogels whose swelling, mechanical property and stress distributions can be remotely controlled by light. In order to create these gels, photo-laible crosslinker or monomer were synthesised and copolymerised into MGs which were then used as building blocks construct to gels. These gels are pH-, thermal-, and light-responsive and also load bearing.

1.2 Survey of thesis

This thesis begins with a literature review in Chapter 2. This chapter introduces the theories, background and biology applications of MGs, responsive MGs (light, pH, and temperature) and DX MGs. The chapter 3 is focused on the characterisation instruments

used in this thesis. Research and discussion topics are provides in Chapters 4-6. Finally, the Chapter 7 presents an overall conclusion and future outlook.

In Chapter 4, *o*-nitrobenzyl-based UV photocleavable crosslinker (2,2'-(2-nitro-1,4-phenylene)bis(methylene)bis(oxy)bis(oxomethylene) bis(azane-diyl)bis(ethane-2,1-diyl) bis(2-methylacrylate), denoted as nPh) was synthesised firstly. A series of triply responsive MG-*x*-nPh (pH, temperature and light) containing 2-(2-methoxyethoxy)ethyl methacrylate (MEO_2MA), oligo(ethylene glycol) methacrylate (OEGMA), methacrylic acid (MAA) and different amounts of nPh were prepared by emulsion polymerisation. Afterwards, the MGs were functionalised with glycidyl methacrylate (GMA) to make vinyl functionalised MGs. The DX MG-*x*-nPh were formed through pH-induced swelling and free-radical coupling of the vinyl groups. The aim of this chapter was developing the new series of DX MGs gels with light triggered mechanical property change and swelling ratio change. Comparison of the multi-responsiveness of MG and DX MG was another motivation for this study. Hence, the sensitivity of MG-*x*-nPh and DX MG-*x*-nPh gels were investigated. The mechanism of the unexpected behaviours of light-induced MG-*x*-nPh degradation and mechanical property enhancement of DX MG-*x*-nPh gels were studied and discussed. Scheme 1.1 shows the main strategy and prospective studies. However, the light-cleavage of that crosslinker and light-enhancement of DX MG gels are irreversible, which limit their potential application. It is necessary to developing and studying the reversibly light-controllable MGs and hydrogels.

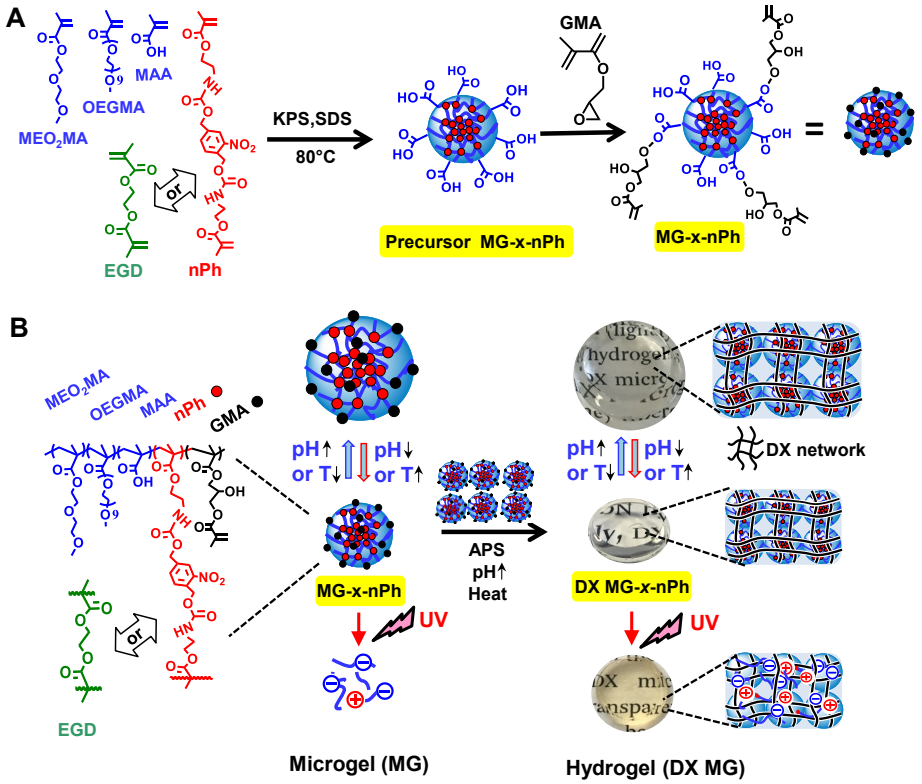

Scheme 1.1. Synthesis of triply responsive **(A)** microgels (MGs) and **(B)** DX MG gels. The structure of the control ethyleneglycol dimethacrylate (EGD) crosslinker is shown in (A). The precursor MGs were functionalised with GMA. The GMA units are crosslinked to form the DX MG gel (B).

The main idea of chapter 5 was investigating the reversibly crosslinker density and swelling changes of MGs by adjusting the wavelength of light. In this chapter, light induced-dimerisation and cleavage of a monomer (7-(2-methacryloyloxyethoxy)-4-methylcoumarin (CMA)) was investigated firstly. Four different size poly(MEO_2MA-MAA-CMA) MGs (donated as MG-CMA) were studied ranging from 25 nm to 124 nm (TEM diameters) and are photo-, pH-, temperature-responsive. They were synthesised by emulsion polymerisation of MEO_2MA, MAA and CMA (Scheme 1.2A). The light-induced changes of pH- and thermally-triggered swelling behaviours were fully studied. Light at 365 nm photo-dimerised the CMA and increased the crosslinker density while light at 254 nm photo-cleaved the dimeric CMA and decreased the crosslinker density (Scheme 1.2B). The relationship between size of as-made MGs and the light induced swelling variation was studied. The light induced volume increase upon photo-de-crosslinking was much greater than reported for other works and this was investigated.

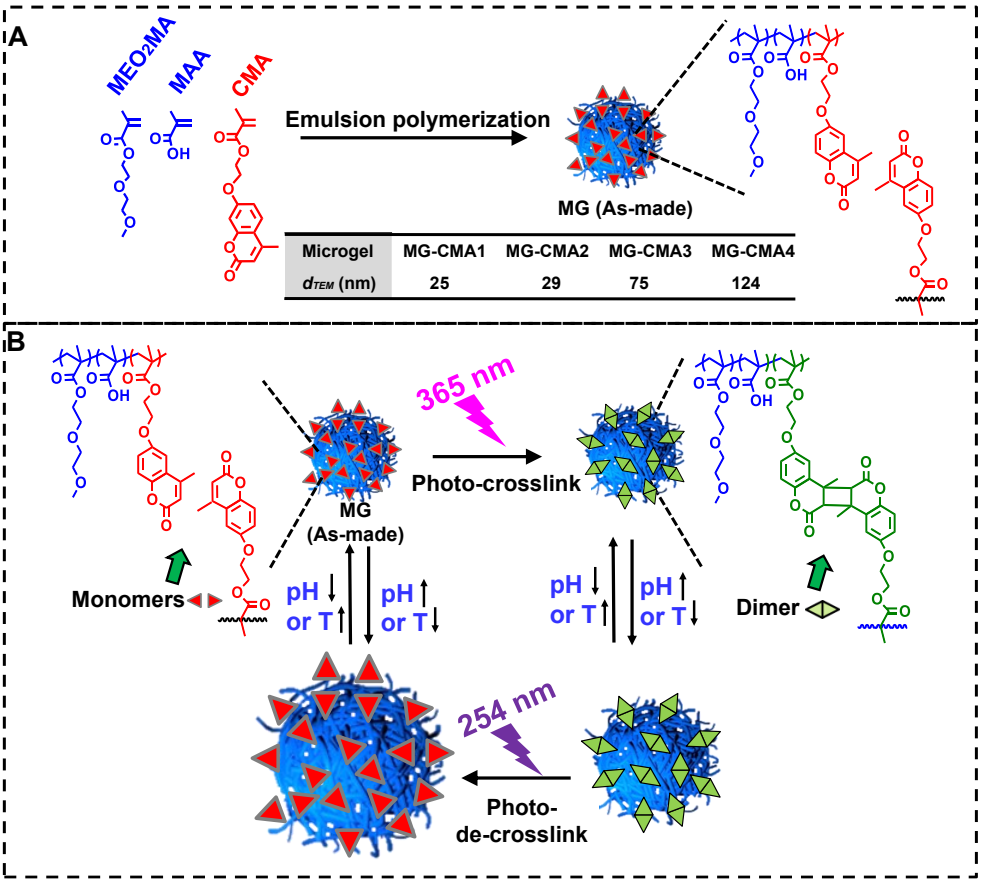

Scheme 1.2. (A) Synthesis of MG-CMA. **(B)** MGs show reversible pH-, temperature- and photo-responsive behaviours.

The light controllable mechanical property and swelling property changes was constructed successfully in chapter 4, but the method of preparing DX MG gels was free radical polymerisation, requiring the addition of initiator and accelerator which may be harmful to cell when injecting into DIVD. In Chapter 6, a multi-responsive hydrogel was constructed by light using concentrated and swollen MG-CMA as building blocks using photo-triggered dimerisation of CMA within and between MGs. This strategy is novel because it does not require adding small molecule reactants or free-radical initiator. The multi-functional nature of gel was studied including the light-triggered self-healing and re-processing to difference shapes. The photo-tuneable reversibility of the modulus value via changing wavelength of UV light was investigated. The capacity of hiding messages for anti-counterfeit applications was studied based on behaviours of light-induced fluorescent emission change. The photo-patterning to give various shapes of gels was

demostrated. The gel was also designed to construct actuators for ON/OFF circuit switching and gripping.

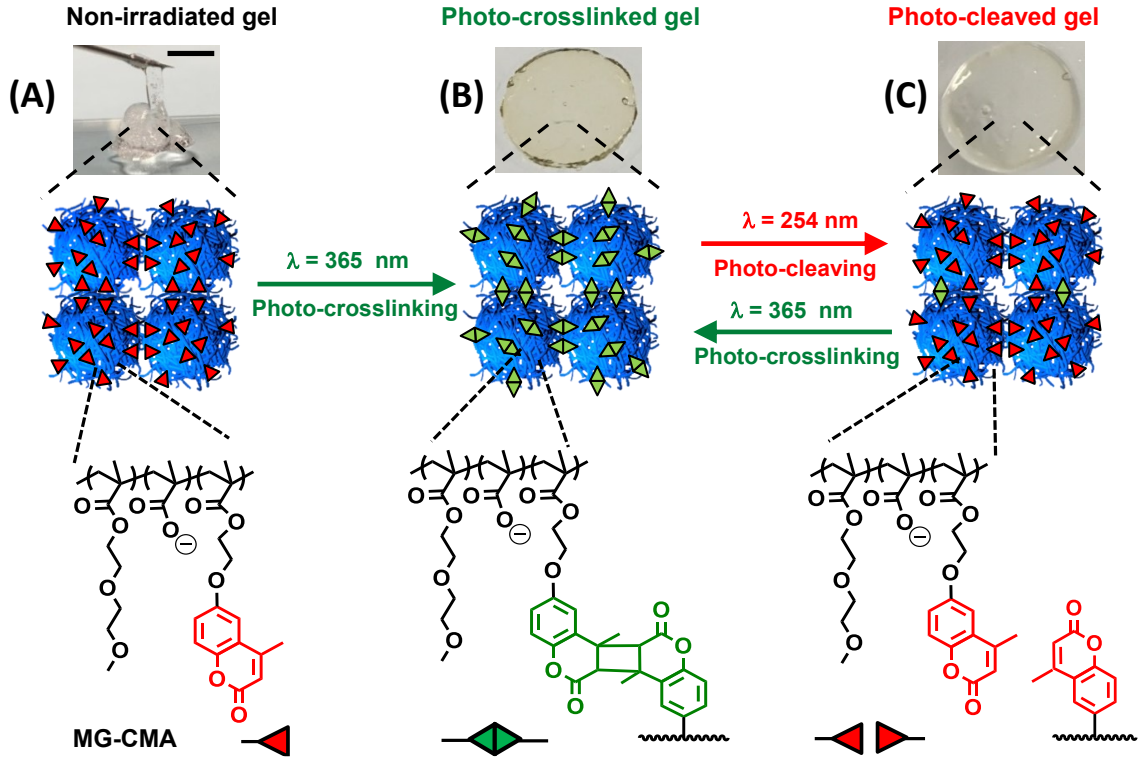

Scheme 1.3. Schematic illustration of the initial non-irradiated gel of **(A)** MG-CMA particles (no UV exposure), **(B)** photo-crosslinked gel (with 365 nm irradiation) and **(C)**photo-cleaved gel (with 254 nm irradiation), respectively. The scale bar is 5.0 mm and applies to all images.

1.3 References

1. J. Antoniou, T. Steffen, F. Nelson, N. Winterbottom, A. P. Hollander, R. A. Poole, M. Aebi and M. Alini, *J Clin Invest*, 1996, **98**, 996-1003.
2. M. Mychaskiw and J. Thomas III, *Value in Health*, 2002, **5**, 508-509.
3. A. H. Milani, A. J. Freemont, J. A. Hoyland, D. J. Adlam and B. R. Saunders, *Biomacromolecules*, 2012, **13**, 2793-2801.
4. J. M. Saunders, T. Tong, C. L. Le Maitre, T. J. Freemont and B. R. Saunders, *Soft Matter*, 2007, **3**, 486-494.
5. M. N. Zhu, D. D. Lu, S. L. Wu, Q. Lian, W. K. Wang, A. H. Milani, Z. X. Cui, N. T. Nguyen, M. Chen, L. A. Lyon, D. J. Adlam, A. J. Freemont, J. A. Hoyland and B. R. Saunders, *Acs Macro Lett*, 2017, **6**, 1245-1250.
6. M. N. Zhu, D. D. Lu, S. L. Wu, Q. Lian, W. K. Wang, L. A. Lyon, W. G. Wang, P. Bartolo and B. R. Saunders, *Nanoscale*, 2019, **11**, 11484-11495.
7. H. R. Shanks, A. H. Milani, D. D. Lu, B. R. Saunders, L. Carney, D. J. Adlam, J. A. Hoyland, C. Blount and M. Dickinson, *Biomacromolecules*, 2019, **20**, 2694-2702.

Chapter 2: Literature review

2.1 Microgels

A microgel (MG) particle is a swellable polymeric particle that contains physical or chemical crosslinking and solvent. The term "microgel" was first put forward by Baker in 1949[1]. Staudinger and Husemann first synthesised MG particles by polymerising the divinylbenzene (DVB) to obtain crosslinked polymer particles[2]. MG particles have high solvent content, high specific surface area and good colloidal stability[3]. They can swell in a good solvent[4-5] or be stimulated by physical or chemical stimulus such as temperature[6], pH[7], electricity[8], light[9] and enzyme[10]. MGs have a size between 100-1000 nm but can be larger. In collapse state (Figure 2.1A), they are hard colloid but may still contain some solvent[11]. They become soft and have a diffuse surface with dangling chains when swollen[11] (Figure 2.1B).

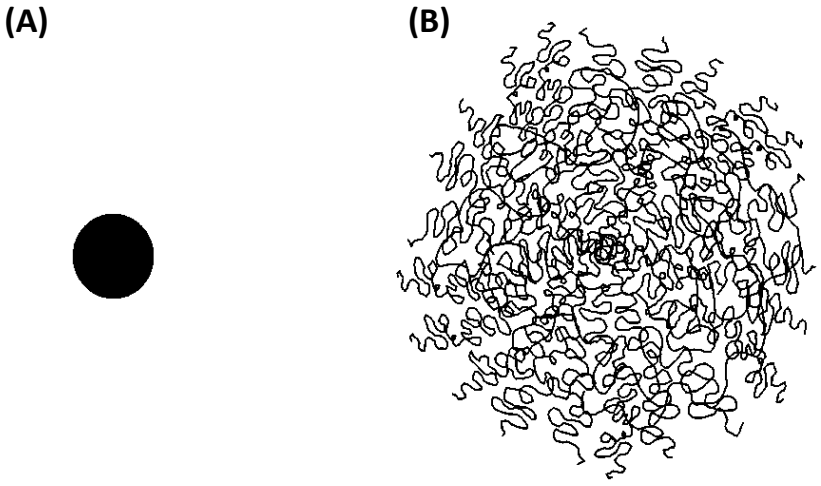

Figure 2.1. Depiction of a microgel particle at **(A)** poor and **(B)** good solvent[4].

2.1.1 Free-radical polymerisation

Free-radical polymerisation is the most used widely method to prepare of polymers from monomers with a $CH_2=CR_1R_2$ structure. There are three stages in free-radical polymerisation: initiation, propagation and termination.

2.1.1.1 Initiation

The initiation stage contains two steps. The first is creation of free-radical from an initiator and the second is formation of the active centre by free-radicals attacking the π bonds of monomers[12]. The initiator can be divided into thermal initiators, photo-initiators and redox initiators[12]. Normally, the reaction needs to be heated to above 50 °C to break the weak bond of the thermal initiator. Redox reactions are used when the temperature of free-radical polymerisation needs to be lower than 50 °C. The photochemical initiator can be decomposed using UV light irradiation which ceases as soon as the light source is removed. In this thesis, the thermal initiator was mostly used. For example, the free radical (R·) can be formed by thermolysis of persulfate in water as showed in following Figure 2.2.

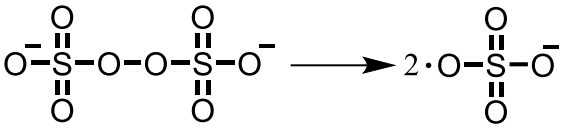

Figure 2.2. The decomposition of perselfate initiator[13].

The active centre is created when free radical (R·) attacks the π bonds of a molecule of monomers. There are two types of addition of the radical to the monomer as depicted in Figure 2.3.

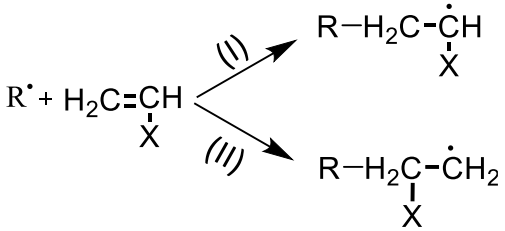

Figure 2.3. Depiction of creation of an active centre[12].

The Type (I) addition reaction is less sterically hindered for attack of the CH_2 carbon. The formed active centre in the Type (I) addition reaction is more stable due to attachment of the substituent group (X). Hence, Type (I) addition is dominated[12].

In the initiation stage, the rate of decomposition of initiator is so slow that it dominates the generation of the active centre. The latter is given by[12, 14]:

$$R_i = 2fk_d[I] \qquad (2.1)$$

where k_d is rate coefficient for initiator decomposition. f is the initiator efficiency. [I] is the concentration of initiator.

2.1.1.2 Propagation

In this stage, the polymer chain grows via sequential addition of monomer to the active centre at a rapid rate. This involves two possible types depicted below:

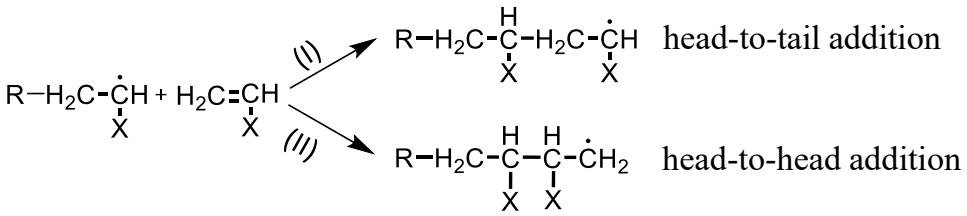

Figure 2.4. Two possible models of propagation of free-radical polymerisation[12].

Type (I) dominates for the same reasons of being less sterically hindered and formation of a more stable active centre as described above. The Type (II) pathway can be neglected except for a few monomers for which X is smal[12]. Thus, generally, the polymer chains form with head-to-tail sequences of repeat units.

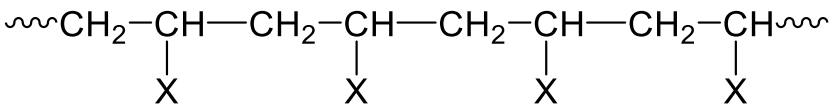

Figure 2.5. Structure of polymer chain via head-to-tail repeat units

The rate of propagation depends on the concentration of monomer ([M]), active centre ([M·]) and the rate coefficient for propagation (k_p). It is assumed that the rate of propagation is independent of the length of growing chain, which means that the k_p has a constant value. Hence, the rate of propagation can be given by[12, 14],

$R_p = k_p[M]\,[M\cdot]$ (2.2)

2.1.1.3 Termination

In this step, the active centre is consumed and propagation ceases. The two mechanisms of termination involve combination and disproportionation (see Figure 2.6). Termination by combination is the coupling together of two active centres of growing chains to form a single dead polymer molecule. For termination by disproportionation, a H atom in the penultimate C atom of one polymer chain is abstracted by another and the terminal π bond is created via joining the remaining electron in the penultimate C-H with unpaired electron on the terminal C atom. Hence, two dead polymer molecules are formed, one with an unsaturated end group and initiator fragment, and the other with a saturated end group and initiator fragment. The tendency of each termination to dominate is dependent on the monomer structure and the polymerisation conditions even though both of them take place. Generally, combination dominates termination for polymerisation of vinyl monomers (CH_2=CHX) while disproportionation dominates with α-methylvinyl monomers (CH_2=C(CH_3)X). The latter is due to the α-CH_3 group providing an additional three C-H bonds and a H atom that can be abstracted. Besides, high temperature favours the termination by disproportionation while relatively low temperature favours domination by combination[12].

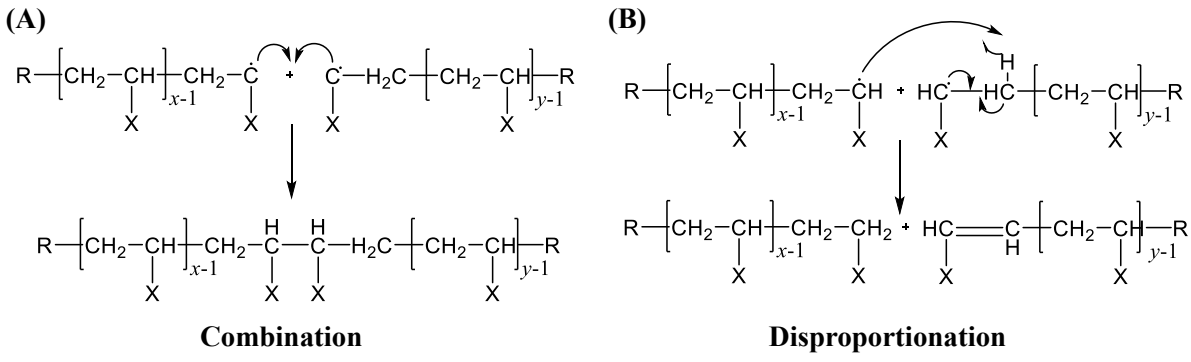

Figure 2.6. Termination by combination and disproportionation[12].

The rate of termination (R_t) is dependent on the concentration of active centres ([M·]) and the rate coefficient of termination, k_t. The latter is the combined total rate coefficient of combination and disproportionation[12, 14].

$$R_t = 2k_t[M\cdot]^2 \qquad (2.3)$$

The rate of propogation can be determined when the polymerisation is at the steady-state condition. This means that the rate of generation and consumption of [M·] are equal. Under these conditions, the rate of initiation is the same as the rate of termination[12]. This leads to:

$$R_p = k_p \left(\frac{fk_d}{k_t}\right)^{0.5}[M][I]^{0.5} \qquad (2.4)$$

2.1.2 Emulsion polymerisation

Emulsion polymerisation is a heterogeneous free-radical polymerisation. It includes the propagation reaction of free-radicals with hydrophobic monomer molecules in submicron polymer particles (0.05 - 1μm in diameter, 10^{16} - 10^{18} dm^{-3}) dispersed in a continuous aqueous phase[15]. Emulsion polymerisation was first developed by the Goodyear Tyre and Rubber Company in the 1920's[16] and is widely used for producing of plastic, paints, rubbers and coatings in industry[17]. Generally, water-soluble initiator and hydrophobic monomer are required. The monomers used for emulsion polymerisation include methacrylate ester monomer, vinyl acetate, styrene, acrylate ester monomer, and ethylene[18]. A surfactant, containing a lyophilic moiety at one end and a lyophobic head group[14], is also required to stabilise the colloidal system. Surfactant can help latex particles avoid coagulation during the early stage of polymerisation due to electrostatic repulsion between adsorbed surfactant layers[18]. Anionic surfactants (eg. sodium dodecyl sulfate (SDS), $C_{12}H_{25}OSO_3{-}Na^+$) are most common used for which the amount is 1-5%

relative to monomers[19]. The micelles contain on the order of 100 surfactants molecules and are 5-10 nm in diameter. They are formed when the surfactant concentration exceeds its critical micelle concentration (CMC) value. For example, the CMC value for the SDS is 8.3 mM in water at 25 °C[20]. The core of the micelle is hydrophobic and the hydrophilic periphery is in contact with water.

There are two main types of emulsion polymerisation mechanisms which depend on the concentration of surfactant. When the surfactant concentration is above the CMC, micellar nucleation occurs. The water-soluble radicals polymerise with the monomer dissolved in the aqueous media and form oligomeric radicals. The oligomeric radical becomes more hydrophobic with longer chain length. When the hydrophobicity reaches a certain degree, it can enter the micelles and continue to propagate. This leads to formation of the particle nuclei. When the particle nuclei size exceeds the size of the micelles, the micellar surfactant is absorbed to the surface of particle nuclei to maintain the colloidal stability of the growing particle nuclei. This stage finishes immediately when the micelles are exhausted[15].

When the surfactant concentration is below the CMC, the radicals react with the monomer in aqueous phase and create oligomeric nuclei. The surfactant molecules are absorbed to the surface of nuclei to stabilise the colloid. In this situation, a narrow particle size distribution is achieved because of the shorter particle nucleation period[15]. This step is known as interval I. In interval II, the polymerisation with the particle continues by absorption the monomers in the aqueous phase from the monomer droplets. The rate of polymerisation in this stage is constant and depends on the diffusion rate of monomer from droplets to aqueous phase. At the end of this stage, the monomer droplets are used up[19]. In interval III, the remaining monomer in particle is polymerised and the rate of

polymerisation decrease toward the end of polymerisation. Figure 2.7 shows the schematic diagram (A) and the conversion as a function of time (B) for the three intervals.

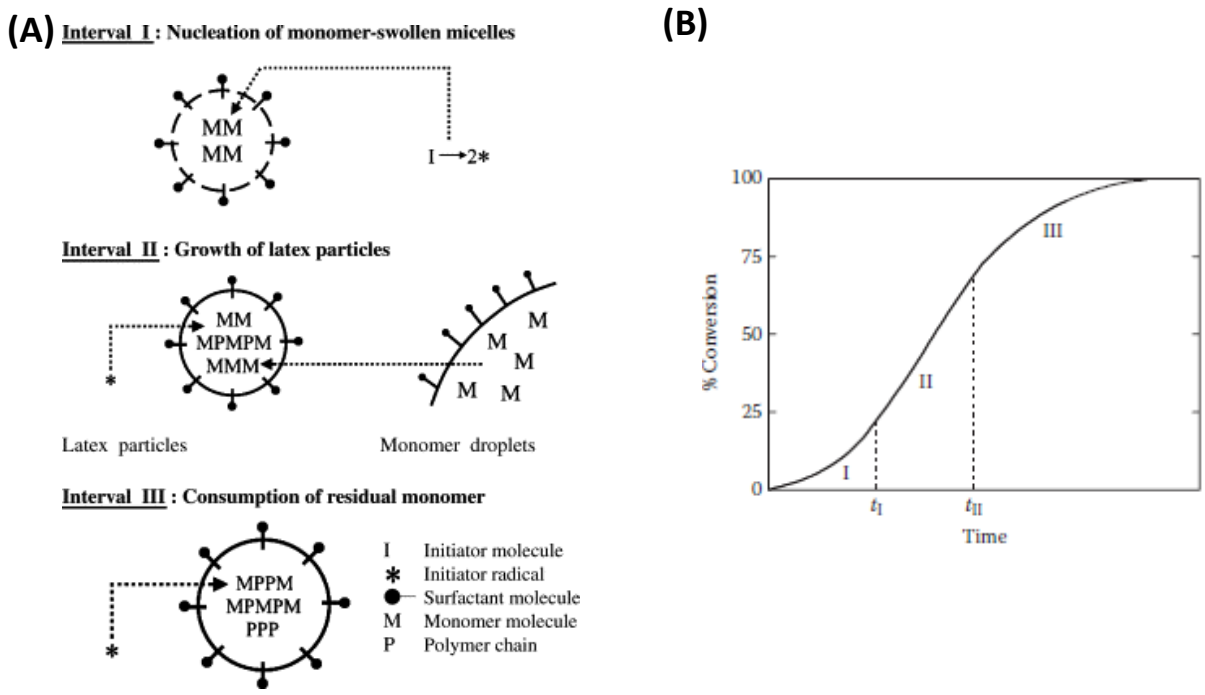

Figure 2.7. (A) The three intervals of a typical emulsion polymerisation reaction[15]. **(B)** Conversion versus reaction time for the three intervals of a classic emulsion polymerisation[19]

In this thesis, the multi-responsive MGs were synthesed by classic emulsion polymerisation process with methacrylate ester monomer 2-(2-methoxyethoxy)ethyl methacrylate (MEO_2MA)，oligo(ethylene glycol) methyl ether methacrylate (OEGMA), methacrylic acid (MAA) and a UV sensitive or normal crosslinker monomer. The anionic surfactant (SDS) and a water-soluble thermal initiator (persulfate) were used. The MGs were prepared with batch and semi-batch emulsion polymerisation. For the semi-bath emulsion polymerisation process used, the reaction ingredients (monomer, surfactant, initiator or water) are added to the reaction system throughout the reaction[15]. However, all reaction ingredients are added to system at once in the beginning of polymerisation for the batch emulsion polymerisation. The time of particle nuclei formation is longer and the particle size distribution is also broader for semi-batch emulsion polymerisation[15].

The hydrophobicity of monomers and crosslinkers in this thesis are nPh > EGD > MEO_2MA > OEGMA > MAA with the solubility for them are 0.044 mmol L^{-1}, 5.4 mmol L^{-1}, 271.0 mmol L^{-1}, 1000.0 mmol L^{-1} and 8010 mmol L^{-1} respectively[21-22]. The MEO_2MA and crosslinker (EGD and nPh) are hydrophobic, the MAA and OEGMA are more hydrophilic and they can dissolve both in comonomer and water. According to Boularas et al. study[23], when the synthesis the MG(MEO_2MA-OEGMA-MAA-EGD), fast consumption of the EGD crosslinker was consumed with a complete conversion reached in less than 15 minutes due to its higher hydrophobicity. However, complete conversion of remaining monomers converted completely in 6 hours. Hence, this multi-responsive MGs have a densely-crosslinked core and loosely-crosslinked shell microstructure with uniform distribution of monomers throughout the MGs. It is inferred that high hydrophobicity of crosslinker (EGD and nPh) has fast reaction rate and favours its partition towards the hydrophobic nuclei in the early stage of polymerization whereas less hydrophobic monomers have the almost same reaction rate.

2.2 Colloidal stability and DLVO theory

Colloidal dispersions contain two phases, one is the dispersed phase such as particles, droplets or bubbles. They have a size in the range of 1 - 1000 nm. The other phase is the continuous phase. Both of the phases can be gas, liquid or solid. Emulsions are a colloidal dispersion in which one immiscible liquid phase is dispersed in another continuous liquid phase. The colloidal particles may associate in different ways (eg. sedimentation, aggregation and coalescence). The colloid stability can be explained by DLVO theory. This was developed by Derjaguin, Landau, Verwey and Overbeek. DLVO theory involves repulsive forces induced by electric double layer and attractive forces (van der Waals forces) between colloidal species[24].

2.2.1 Electrical double layer

In a colloidal dispersion, the particles can be stabilised by the repulsive force due to the elestrostatic repulsive force that is created when particles with surface charge approach each other and their electric double layers overlap. The electric double layer is formed by a charged surface in contact with an electrolyte solution consisting of counterions and co-ions[25]. There are two layers: the inner layer and outer layer. The inner layer (Stern layer) includes absorbed counterions. The counterions are so strongly absorbed to the surface of particle that they can resist thermal motion. The outer layer (diffuse layer) formed by both co-ions and counterions around the inner layer, which is affected by thermal motion. The concentratiom of counterions decreases as the distances from the particle surface increases. Figure 2.8 depicts the electrical double layer surrounding a negatively charged particle. The Stern plane is the boundary of the Stern layer. The shear plane (or slipping plane) is a boundary to separate water that moves with shear or does not and moves with the particle surface. The electrical potential decreases from the surface through the diffusion layer as the distance from surface increases. The electrical potential at the in shear plane is called the zeta potential.

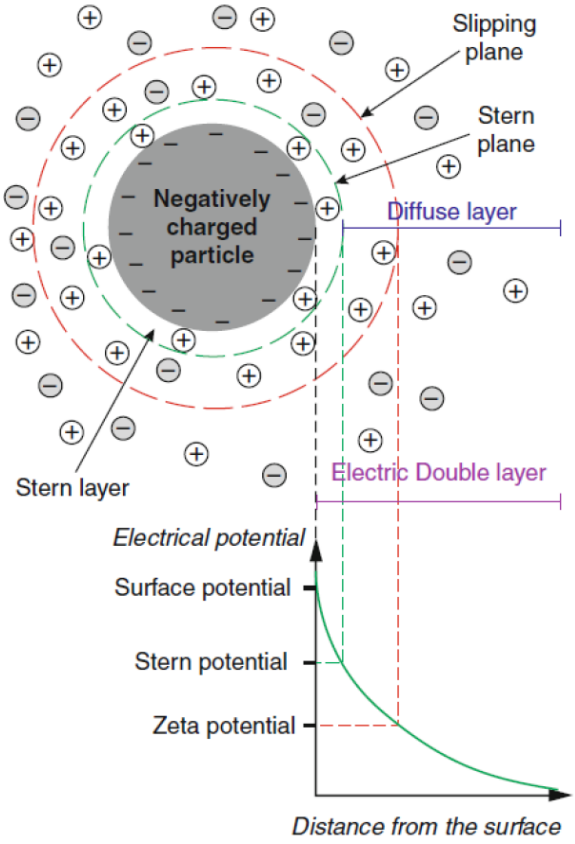

Figure 2.8. The diffuse electrical double layer of a negatively charged particle[26].

The thickness of double layer (1/κ) indicates the distance over which electrostatic interactions caused by the surface charge are significant. κ is the Debye screening parameter which is determined by the properties of medium and the electrolyte concentration. It can be calculated using the Equation (2.5) for the electrolyte at 25°C[27],

$$\kappa = 0.329 \times 10^{10} \left(\frac{cz^2}{mol\ dm^{-3}}\right)^{0.5}\ m^{-1} \qquad (2.5)$$

where *c* and *z* are the concentration and charge number of electrolyte respectively. The equation shows that 1/κ is governed by the electrolyte. The effects of the repulsion between particles can be decreased by decreasing the 1/κ. This can be achieved by increasing *c* and hence κ.

When particles approach closely to each other, their electrical double layers overlap and a repulsive force occurs. The electrostatic repulsive potential (V_R) can be calculated by Equation (2.6)[28],

$$V_R = 2\pi\varepsilon\alpha\psi_d^2 \, exp^{(-kH)} \qquad (2.6)$$

The value ε is for dielectric constant of the medium. The parameter α is the radius of the particle and ψ_d is the electrical potential at the Stern layer. H is the distance between two particles. V_R increases as ψ_d increases or H decreases.

2.2.2 Van der Waals forces

The van der Waals forces are the sum of the attractive forces when two particles are close to each other[29]. The van der Waals forces includes permanent dipole-permanent dipole, induced dipole-permanent dipole and fluctuating dipoles[30]. Instantaneous fluctuating dipoles lead to the an attractive interaction between two particles. The van der Waals force is considered for two particles with same radius (α) and separation distance (H) as shown in Figure 2.9.

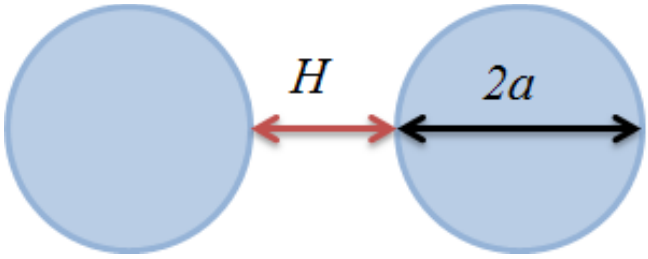

Figure 2.9. Diagram showing two particles[27].

The van der Waals forces (V_{att}) between particles can be calculated from Equation (2.7)[31] .

$$V_{att} = -\frac{A_{eff}}{12}\left[\frac{1}{x(x+2)} + \frac{1}{(x+1)^2} + 2\ln\left(\frac{x(x+2)}{(x+1)^2}\right)\right] \qquad (2.7)$$

Where A_{eff} is the effective Hamaker constant and x can be calculated as shown in the following equation.

$$x = \frac{H}{2a} \qquad (2.8)$$

The attractive force is directly related to the H and the magnitude of V_{att} greatly increases at smaller H values. If $H << a$ (i.e. $x << 1$), then the Equation 2.7 can be simplified to Equation (2.9).

$$V_{att} = -\frac{A_{eff}}{12} \cdot \frac{1}{2x} = -\frac{A_{eff} a}{12H} \qquad (2.9)$$

For a non-vacuum medium, there is an interaction between the particles and medium and this affects the A_{eff} values. The value of A_{eff} can be calculated using:

$$A_{eff} = (A_1^{0.5} - A_2^{0.5})^2 \qquad (2.10)$$

where A_1 and A_2 are the Hamaker constants for particles and the medium, respectively[32].

2.2.3 The two-particle potential energy curve

The total potential energy (V_T) can change when two particles approach each other. This can be calculated by adding the attractive force (van der waals force, V_{att}) and repulsive force (electrical double layer force, V_R) as shown in following Equation (2.11).

$$V_T = V_{att} + V_R \qquad (2.11)$$

The potential energy profile can be obtained by calculating V_T as a functional of H (see Figure 2.10). If the V_T decreases, the colloidal particles become irreversibly attracted or aggregated.

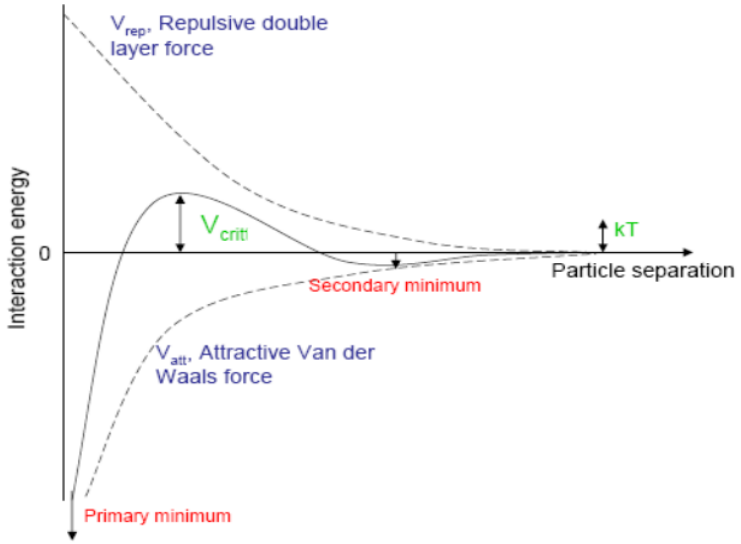

Figure 2.10. Potential energies of interaction between two colloidal particles as a function of their distance of separation[33].

2.2.4 The steric and electrostatic stabilisation of MG particles

The stabilisation of MG particles in a good solvent is more complex than the ideal particle stabilised by DLVO theory due to the polymer chain and the surface charge. When particles swell in a good solvent, the polymer chain extends outward into the solvent from the particle surface. The extended polymer chains penetrate each other as the MG particles approach and prevent MG particles flocculation or aggregation. This increases the stability of the MG dispersion. This is referred as "steric stabilisation"[34]. The MGs synthesised in this thesis contain negative charge from surfactants and neutralised acid groups and therefore electrostatic stabilisation occurs when the particle is swollen. The combination of steric and electrostatic stabilisation is called electrosteric stabilisation (Figure 2.11).

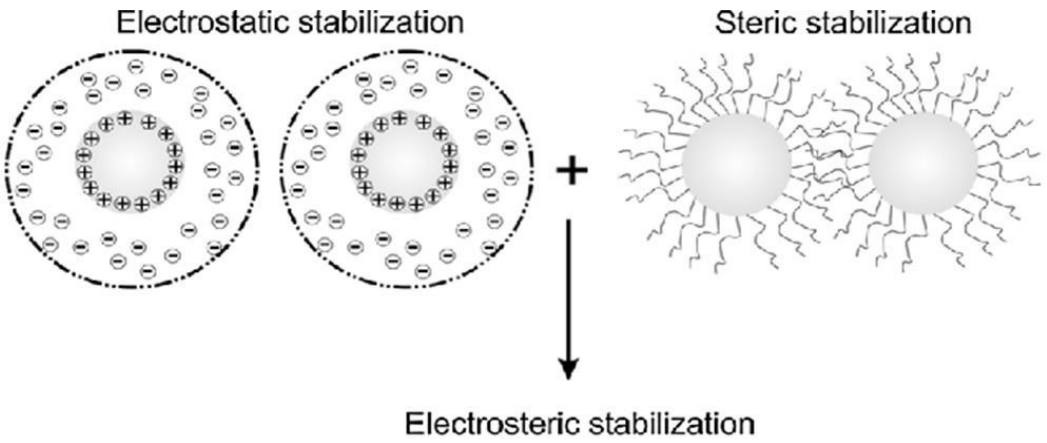

Figure 2.11. Schematic diagram of steric stabilisation and electrosteric stabilisation[35].

Those two repulsive forces should be added to the total energy of interaction between MG particles, resulting in Equation (2.12),

$$V_T = V_{att} + V_R + V_s \qquad (2.12)$$

where the V_{att} , V_R and V_s are Van der Waals interaction energy, repulsive energy due to electrical double layer and the interaction energy due to steric stabilisation, respectively[32]. The potential energy profile was shown in Figure 2.12 with considering the V_s. When the separation of particle is large (H > 100 nm), the effect of attractive force (V_{att}) and repulsive force (V_R) for the particles are negligible (region A in Figure 2.12). When the particles approach each other, both V_{att} and V_R increase. The latter increases more slowly and then V_{att} dominates. This results in a weak secondary minimum at H ~ 60 nm (region B in Figure 2.12). The aggregates in this situation are reversible and can be re-dispersed. As the particles approach more close to each other, the effect of V_R becomes stronger and reaches a point of primary maximum (H ~ 20 nm, region C in Figure 2.12). There is a large energy barrier inhibiting the close approach of the particles and thereby stabilising them against aggregation. If the kinetic energy of the particles is greater than the energy barrier, the V_{att} interaction dominates and irreversible coagulation occurs and the particles reach the primary minimum (region D in Figure 2.12).

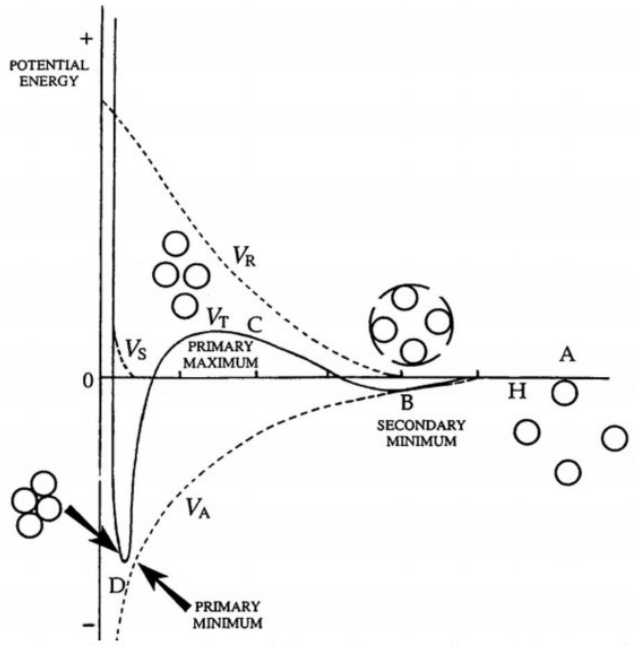

Figure 2.12. Potential energies of interaction between two colloidal particles as a function of their distance when considering the V_s [28].

When the MGs are in a good solvent, the particles are fully swollen and contain a large volume fraction of solvent. Then, $A_1 \cong A_2$ and hence $A_{eff} \cong 0$. Therefore V_{att} between the particles is small[4]. Hence, the V_T is dominated by V_R and V_s interaction and the MGs dispersion are stable. When the MGs are in a poor solvent, the particle is collapsed and V_s approaches zero[32].

2.3 Responsive MGs

Responsive MGs are the smart MGs which are capable of responding to external stimulus or internal stimulus by changing their physico-chemical properties, such as volume, water content, network permeability, charges, refractive index and hydrophilicity-hydrophobicity[3]. The external stimuli normally can be classified into light, temperature, magnetic, electricity, and ultrasound and the internal stimuli include pH, glucose, redox potential and enzymes[3, 5, 36]. Responsive MGs have attracted a lot of attention in last several decades owing to their potential for biological applications, including drug

delivery systems[37-40], bio-imaging[41], tissue regeneration[42], bone regeneration[43] and anti-bacterial[44]. For example, Zhan and coworkers synthesised a triple (pH, temperature, redox) responsive MGs by copolymerisation of *N*-isopropylacrylamide (NIPAM), acrylic acid (AA), and *N,N′*-bis(acryloyl)cystamine (BAC) as a cross-linker agent. They proved that drug release (doxorubicin) can be accelerated by elevated temperature, low pH and dithiothreitol (DTT)-induced degradation (Figure 2.12A)[45]. Zhang et. al. included graphene oxide within PNIPAM MGs and showed that the drug release could be enhanced by remote NIR light photothermal radiation treatment and then HeLa cells could be killed (Figure 2.12B)[46]. Zhu et. al. copolymerised complementary nonresonance energy transfer (NRET) dye pairs (9-phenanthryl)methyl methacrylate (Ph) and (9-anthryl)methacrylate (An) into pH responsive MGs of poly(methyl methacryate (MMA) - methacrylic acid (MAA)- ethylene glycol dimethacrylate (EGDMA)) to form MG probe for ratiometeric fluorescent sensing of pH and strain in hydrogels (Figure 2.12C)[47]. Figure 2.12D shows antibacterial MGs that were synthesised by copolymerising fluorine-containing monomer with other acrylic monomers. The durable antibacterial and bacterially antiadhesive cotton fabrics were constructed via coating the MGs into cotton fabrics[48].

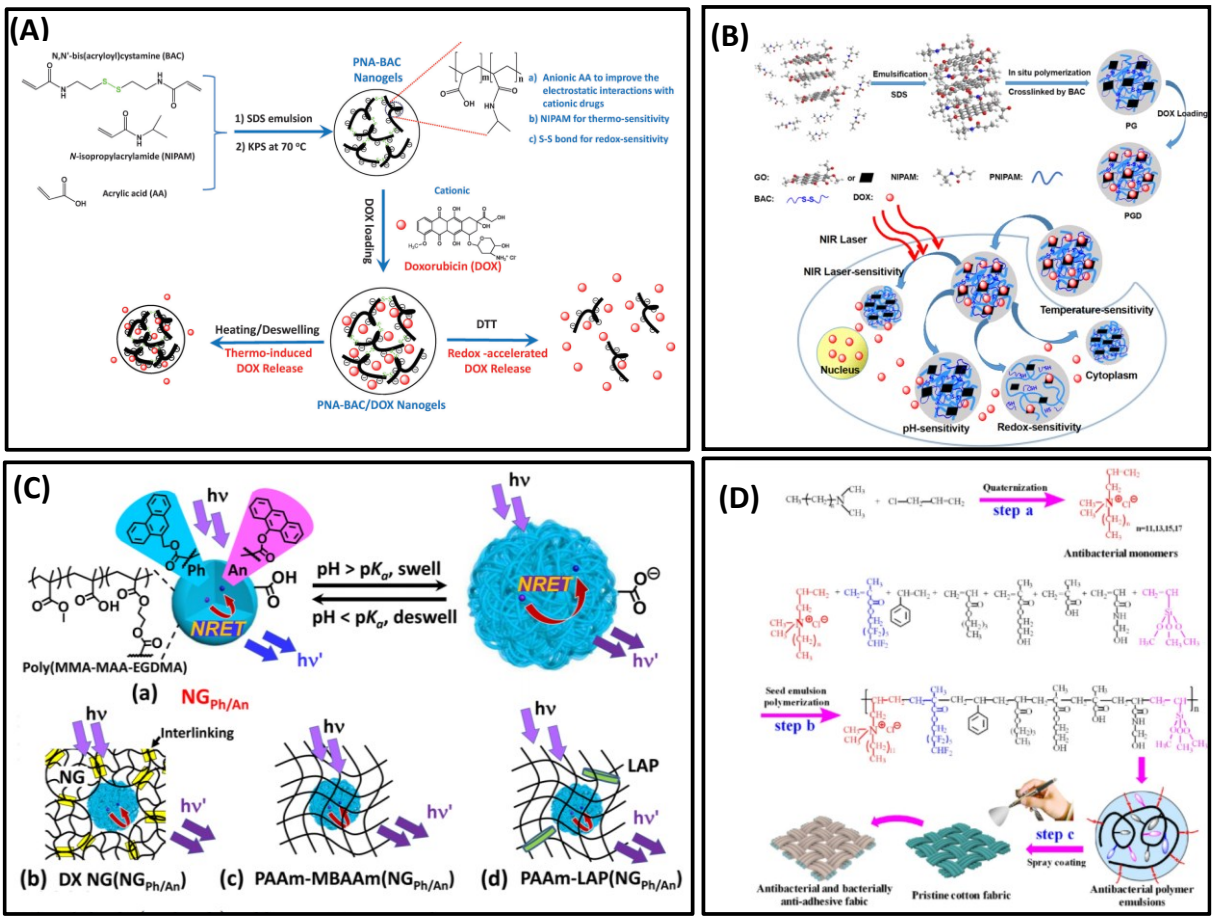

Figure 2.13. (A) Multi-responsive MG (NIPAM-AA-BAC) preparation. They act as carriers in the administration of anticancer drugs. **(B)** NIR light triggers the drug release from responsive MGs and synergistic anticancer therapy. **(C)** Dye labelling of a pH responsive MG (MMA-MAA-EGDMA) for use as a sensor. **(D)** Anti-bacterial MGs for constructing the durable antibacterial and bacterially antiadhesive cotton fabrics.

Xiong and co-workers reported a method for targeted antibiotic delivery to macrophages to treat bacterial infections via utilising MGs as the drug carrier that undergoes degradation by bacterial enzymes. The MGs contained poly(ethylene glycol) (PEG) and polyphosphoester crosslinker. The polyphosphoester crosslinker can be degraded by the active phosphatase or phospholipase produced by the bacteria to release drugs on demand (Figure 2.13A)[49]. Kumar et.al. incorporated nanohydroxyapatite (nHAp) into chitin-poly(ε-caprolactone) (PCL) based injectable composite MGs for bone defect repair. Chitin is ideal biomaterial due to its bioadhesion and biomimicking properties. PCL is widely being used for bone tissue engineering applications because the degradation

characteristics of PCL can be tuned, and its degradation products are nontoxic. HAp is the natural component of bone which can improve cell adhesion and lead to better osteointegration. These MGs show injectability, improved protein absorption, cell adhesion and cell proliferation as well as mineralisation[43](Figure 2.13B).

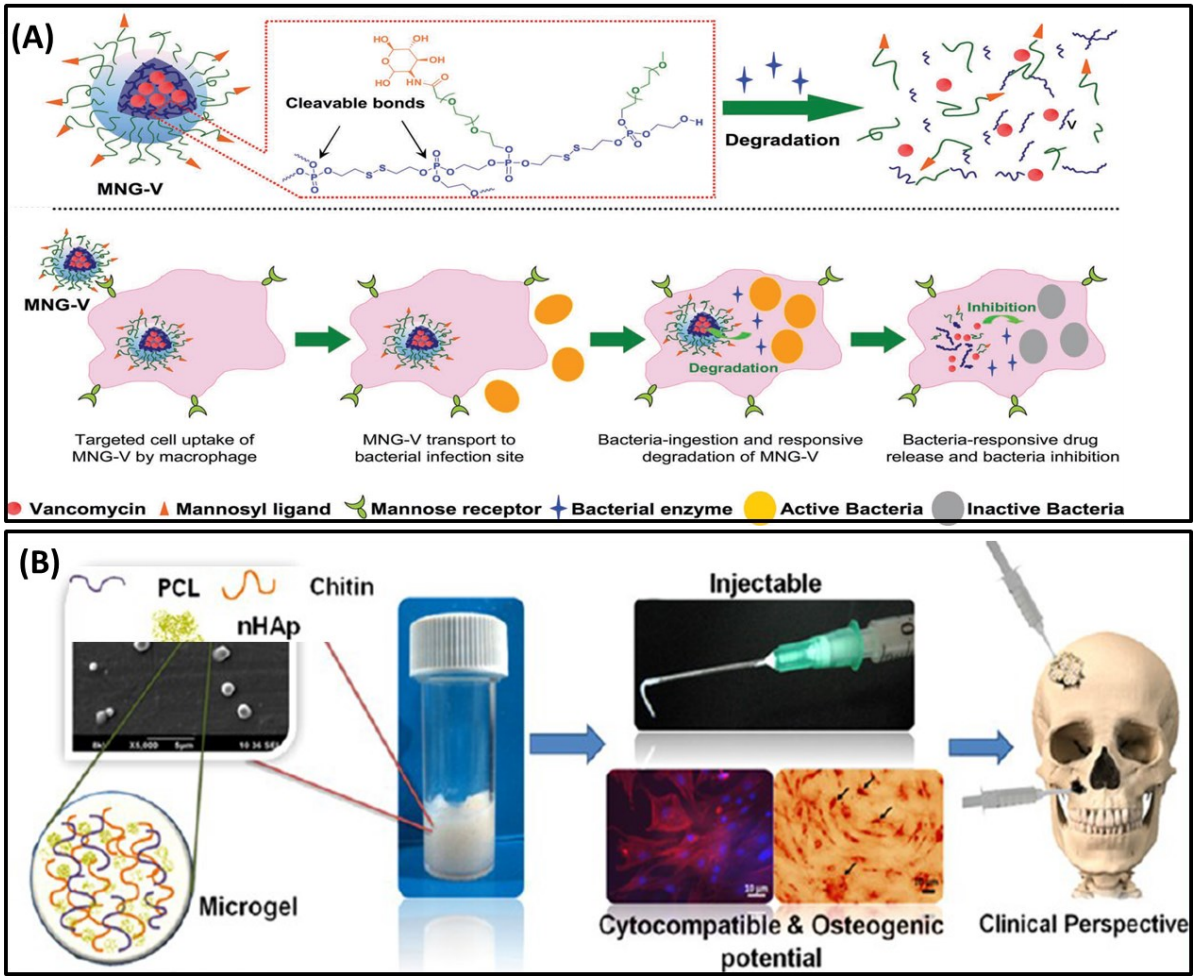

Figure 2.14. (A) Bacterial sensitive MGs for treatment of bacterial infectious disease. **(B)** Chitin-PCL-nHAp composite MGs for bone tissue engineering.

2.3.1 pH responsive MGs

pH responsive microgels are crosslinked polymer partricles whose colloid stability, size, or surface charge can be controlled by changes in pH[7]. The polyelectrolyte structures (weak acid or base) that comprise segments in the crosslinked polymer network can be ionised by protonation or deprotonation[32]. The electrostatic repulsion between polymer

segments with same charge occurs due to ionisation. As a consequence, the polymer network expands and the size of MG particle increases in responsive to pH. There has been a large amount of research reported on anionic pH-responsive MGs based on (meth)acrylic acid (MAA or AA)[50-54], which can swell with increase pH to near the pK_a. Some research of cationic pH-responsive MGs has been reported based on poly(vinylamine) (PVAM)[55], poly(diethylaminoethyl methacrylate) (PDEAEM)[56-58], poly(2-(dimethylamino)ethyl methacrylate) (PDMAEM)[59]. These types of MGs contain amine groups that can swell with decreasing pH. Polyampholyte MGs possesses both positive and negative charge and have been studied, such as poly(carboxybetaine methacrylate) (PCBMA)[59]. Polyampholyte MGs have also been studied by combining poly(methacrylic acid) and poly(diethylaminoethyl methacrylate)[60]. These MGs showed enhanced hydrophilic behaviour in aqueous medium at low and high pH but become hydrophobic and collapsed when pH is near the isoelectric point[60]. The monomer structures are shown below.

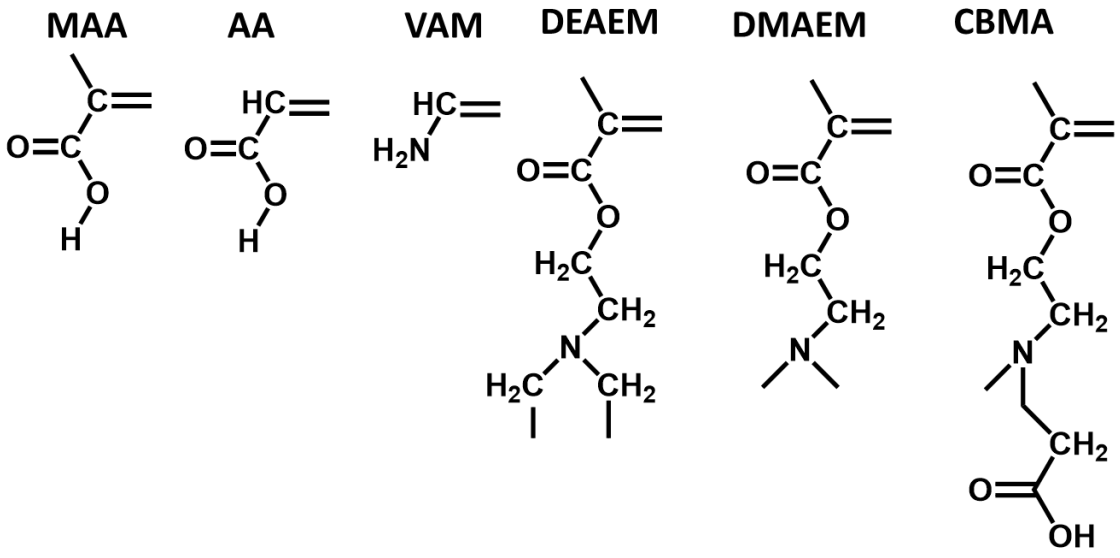

Figure 2.15. The structures of monomers used to prepared the pH responsive MGs

In my case, the MGs used in this study contain MAA and the swelling of MGs is caused by electrostatic repulsion between the neighbouring polymer chains resulting from the

deprotonation of COOH groups and formation of COO^- within the MG particle as the pH approaches the pK_a[32]. At pH values greater than the pK_a, the particles become fully swollen[61]. I selected MAA because the MGs are totally swollen and become physical gels at physiological pH (7.4) when they contain a certain amount of MAA. Such MGs are believed to be useful for biological applications such as degenerated intervertebral disc repair (DIVD)[61], drug delivery and release[62] and bio-sensors[47].

2.3.2 Thermally-responsive MGs

Thermally-responsive MGs can undergo a conformational change between hydrophilic/swollen and hydrophobic/collapsed state upon cooling or heating to below or above a certain temperature (known as the volume phase transition temperature (VPTT))[63]. This behaviour is attributed to changes of inter- and intra- molecular hydrogen bonding as well as hydrophobic interactions[64]. Some of common monomers used to prepared thermally responsive MGs are vinyl caprolactam (VCL), oligo(ethylene glycol) methacrylates (OEGMA), *N*-isopropylacrylamide (NIPAm), 2-(*N*-morpholino)ethylmethacrylate (MEMA), *N,N'*-diethyl acrylamide (DEAAm), dimethylamino ethyl methacrylate (DMAEMA) and *N*-ethylmethacrylamide (NEMAM). The structures are shown in Figure 2.15.

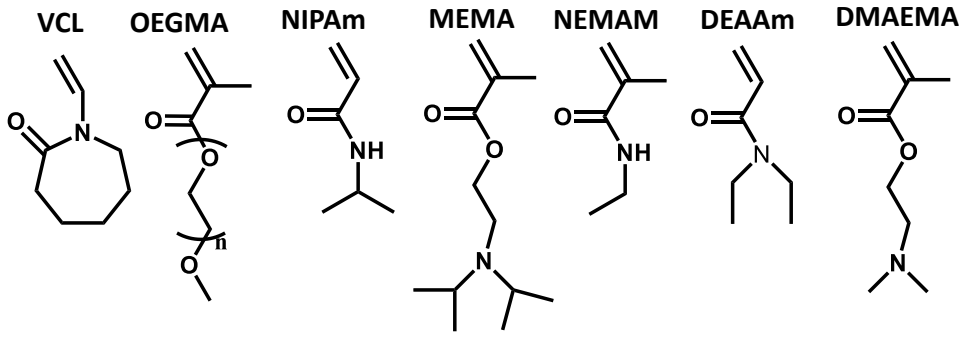

Figure 2.16. Structure of monomers used to prepared the thermally responsive MGs

PNIPAm MG exhibits a VPTT at ~32 °C and is one of the most studied thermal responsive MG due to a remarkable shrinking with increasing temperature above its

LCST[65]. The -CONH group is hydrophilic while -$CH(CH_3)_2$ is hydrophobic in the NIPAm molecule[66]. As shown in Figure 2.16A, at low temperature (< 32 °C), the C=O and N-H group form intermolecular hydrogen bonds with water, leading to expansion (swellings) of the NIPAm segments in water. While increasing the temperature above LCST disrupts such bonding and the C=O and N-H groups form intramolecular hydrogen bonds with neighbouring NIPAm segments. This leads to a dehydrated collapsed state[66] and strengthens the interactions between the hydrophobic groups (-$CH(CH_3)_2$-)[67] (Figure 2.16B).

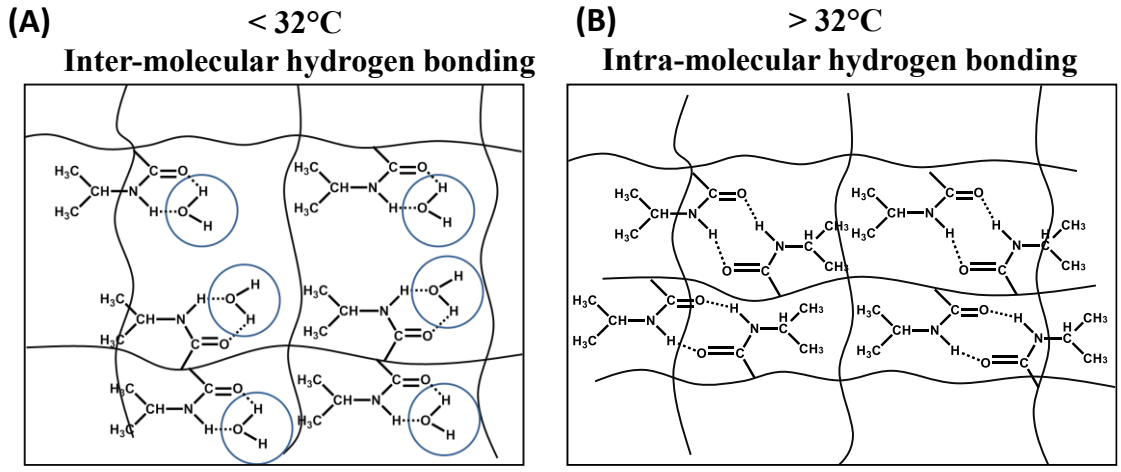

Figure 2.17. The mechanism of phase transition of PNIPAm[62].

The swelling behaviours of PNIPAm-based MG is strongly dependent on its polymer network structure (ie. comonomer structure and crosslinker concentration). A high crosslink density increases the polymer volume fraction at the swollen state and the relative swelling of MGs particles decreases[68]. MG particles with a highly crosslinked core and poorly crosslink shell have hindered the swelling of the particle core. However, the MG with a homogeneous cross-link density distribution throughout the particle can swell uniformly[69]. Some studies have also shown that the carboxylic acid group distribution with the particles (p-NIPAm (core)/p-NIPAm-AAc (shell), p-NIPAm-AAc (core)/p-NIPAm (shell) and p-NIPAm-AAc particles) affects the VPTT and thermally induced collapsed behaviours[70-71]. However, the toxicity of NIPAm and the poor

biocompatibility of PNIPAm limited the application in terms of biomaterials[72]. A broad hysteresis can be observed during the reversible phase transitions for PNIPAm polymer[73]. This may also limits its biological applications such as drug delivery. More biocompatible PVCL microgels with a VPTT of 32 - 36 °C (close to the physiological temperature), are an alternative to PNIPAm for biomedical applications[72, 74]. Unfortunately, limited amounts of carboxylic acid group can be copolymerised into PVCL-based MGs because VCL is prone to hydrolysis under acidic conditions[74]. The highly cytocompatible copolymers of OEGMA with different numbers of ethylene glycol units have arisen interest[75-77]. The VPTT of OEGMA-based MGs is directly proportional to the side chain length of oligo(ethylene glycol) units and can be tuned by different ratios of these monomers easily[78]. Studies have also shown that a high amount of carboxylic acid group (MAA) can be copolymerised with OEGMA to form the multi responsive MGs[62, 79]. Lutz and co-workers concluded that POEGMA segment-segment interactions when increasing temperature are not are due to hydrogen bonds like PNIPAM but due to weaker van der Waals interactions[80]. There are no strong hydrogen bonds donors in the molecular structure of POEGMA. Thus, the phase transitions of POEGMA polymers are reversible without hysteresis[73]. Hence, I selected OEGMA monomer to synthesis the multi-responsive and non-toxic MGs in this study.

2.3.3 Photo-responsive polymeric nanoparticles

Among the stimuli, light represents outstanding predominance for several reasons. It can be applied in a very precise manner as the light parameters (wavelength, intensity and irradiation time) are easily manipulated and are finely tuneable[81]. In addition, light can be applied with a non-physical contact from the outside the system[82-83]. This allows light to become a preferable stimuli compared to the other stimuli. Light stimulus does not require addition of a specific reagent and it can be applied to a closed reaction systems and

polymers. Furthermore, light can change polymer properties at the nano/micron-scale with millisecond temporal resolution[84]. Generally, three methods of light induced-reaction can be observed: photocleavage, photodimerisation and photoisomerisation.

The first method utilises photo-cleavable molecules such as the *o*-nitrobenzyl moiety[85], coumarin moiety[86], pyrenyl methy moiety[87] and *ρ*-methoxyphenacyl moiety[88] in polymer nanoparticles. For example, a block copolymer poly(ethylene oxyde) - block - poly(ethoxytri (ethyleneglycol) acrylate - random - o - nitrobenzylacrylate) (PEO-b-P(ETEGA-r-NBA) has been reported[89]. The LCST of this system can shift from 25 to 36 °C using UV light irradiation due to formation of the hydrophilic carboxylic acid from hydrophobic poly(*o*-nitrobenzylacrylate) in the polymer backbone (Figure 2.17A). Huang et al. synthesized two types of novel vinyl functionalised photocleavable cross-linkers based on 7-amino coumarin moieties which were used to build photoswellable and photodegradable polystyrene MGs. The variation of photodegradation and photoswelling behaviors resulted from the different cross-linking densities induced by photo-cleavage of the cross-linkers[83] (Figure 2.17B).

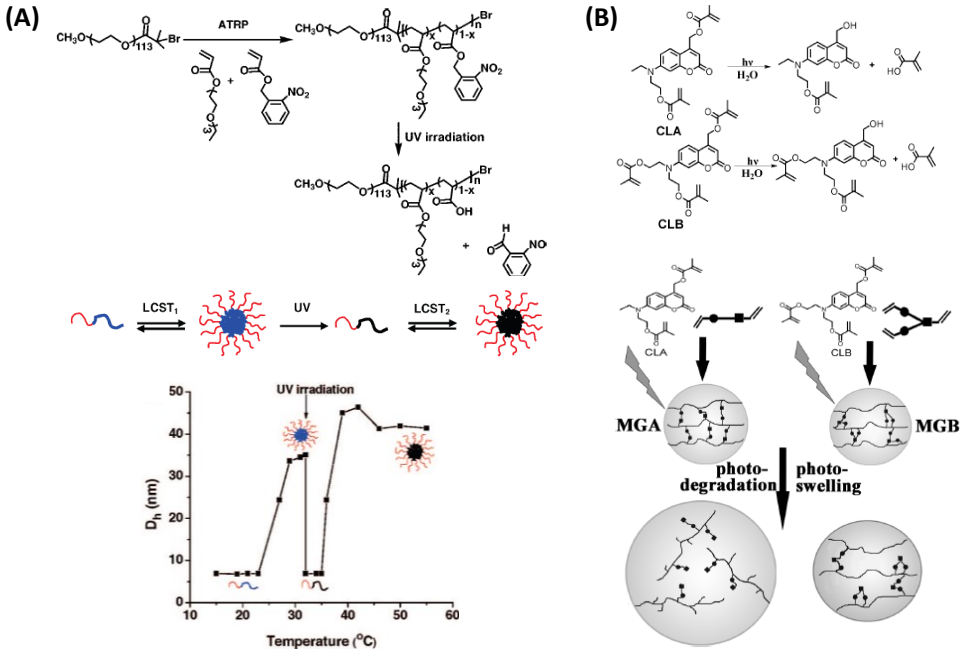

Figure 2.18. (A) Schematic representation of the (PEO-b-P(ETEGA-r-NBA)) and changes in the micellar hydrodynamic diameter with temperature and light irradiation. **(B)** Schematic representation of the photolysis of the coumarin-containing crosslinkers and photoswelling and photodegradation behavior of MGs upon irradiation.

Additionally, the reversible photo-dimerisation reactions are another strategy to confer photosensitive polymeric structures such as coumarin, anthracene and cinnamoyl derivatives[90-93]. They allow control of the crosslinking density by light-induced formation/cleavage/re-formation of crosslinking points. For example, thermo- and light-responsive nanoparticles were prepared by photo-crosslinking copolymer micelles. The diblock copolymers comprised poly(ethylene oxide) and poly[2-(2-methoxyethoxy)ethyl methacrylate-co-4-methyl-[7-(methacryloyl)oxyethyloxy]coumarin] (PEO-P(MEOMA-co-CMA)). This was photo-crosslinked to form MGs through photo-dimerisation of coumarin side groups upon absorption of $\lambda > 310$ nm light after the micelles were formed by heating a polymer solution above the LCST. The reversibility of photoinduced crosslinking density and volume change was studied by tuning the wavelength of UV light between 365 nm and 254 nm[86] (Figure 2.18A). Shi et al. synthesised bio-based cinnamate derivative copolymers particles based on poly(3,4-dihydroxycinnamic acid-

co-4-hydroxycinnamic acid) (P(3,4DHCA-co-4HCA)). They found the diameter changing due to [2 + 2] cycloaddition formation and photo-cleavage of the cinnamate groups[94] (Figure 2.18B).

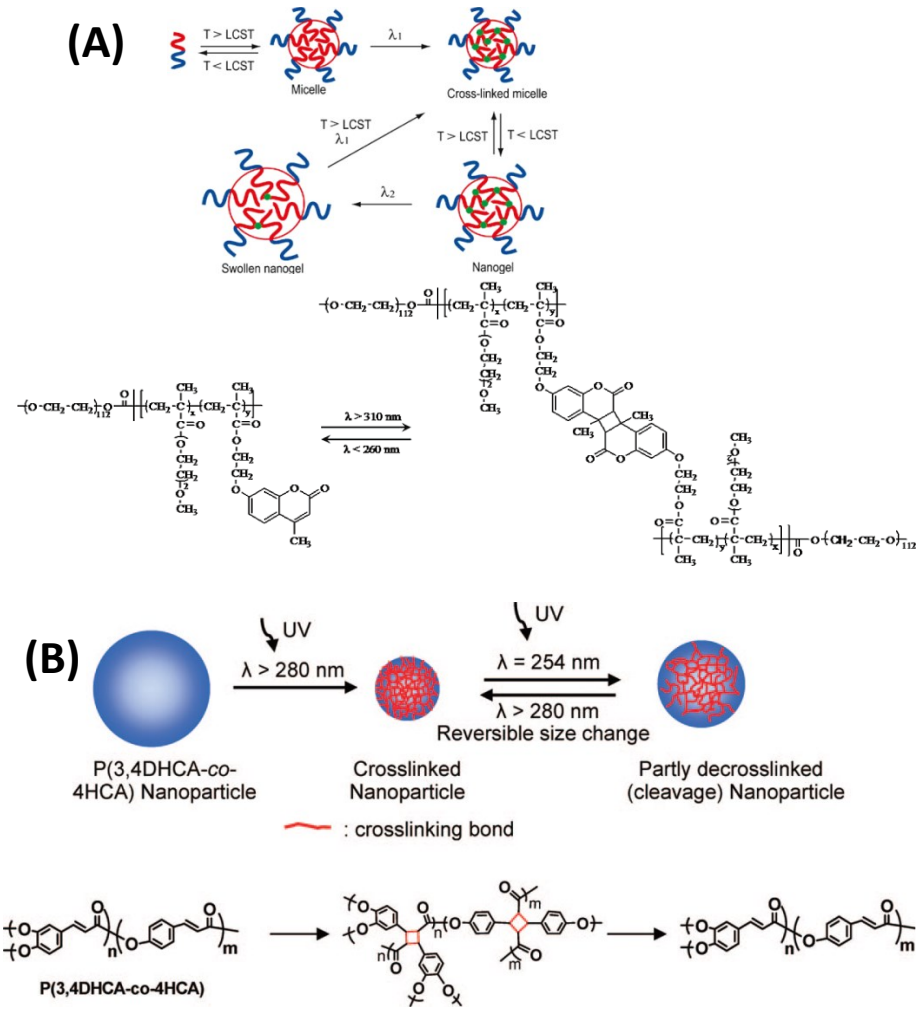

Figure 2.19. (A) Schematic representation of the PEO-P(MEOMA-co-CMA) and changes of the absorbance and diameter with irradiation. **(B)** Schematic representation of the P(3,4DHCA-co-4HCA) and changes of the absorbance and diameter with irradiation.

Another method uses the reversible photoisomerisation reaction upon irradiation by UV or visible light of photochromic molecules such as azobenzene[95-96], spiropyran[97] or dithienylethene[98] to form nanoparticle. Figure 2.19 shows several photoisomerised photochromic molecules.

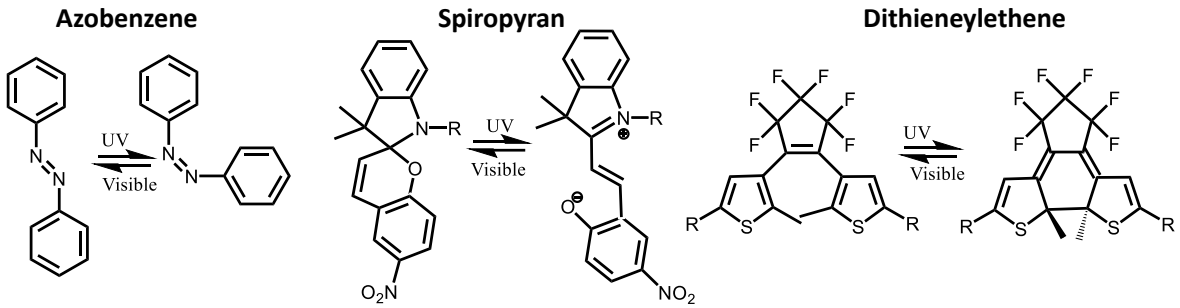

Figure 2.20. Reversible light-induced photo-isomerisable molecules.

Photoisomerisation can change the hydrophobic or hydrophilic properties of photochromic molecules. This strategy has been used to promote the formation or disruption of nanoparticles (micelles)[99-100]. Matyjaszewski and coworkers developed a poly(ethylene oxide)-blockpoly(methacrylate) with bearing spiropyran (SP) side-chains of methacrylate block (PEO-b-PMSP)[101]. The MGs disrupted and reformed upon UV (365 nm) and visible light (620 nm) irradiation. The physical crosslinks were formed due to hydrophobic- hydrophobic interaction by the aggregation of hydrophobic spiropyran groups and the MGs were intact upon visible light illumination. The spiropyran groups undergo a configuration change to a hydrophilic zwitter-ionic form, thereby disrupting the physical crosslinking points and degrading the MGs. They also demonstrated that this approach could be used for the release/encapsulation of guest molecules.

Herein, I selected the irreversible photocleavable *o*-nitrobenzyl derivatives and the reversible photo-dimerised/photocleavable coumarin as photosensitive moiety to copolymerise with temperature- and pH- responsive monomers (MEO_2MA and MAA). In this way, triple responsive MGs were synthesised. The *o*-nitrobenzyl group is one of the most useful photo-liable compounds in biology applications because of its fast photolysis kinetics[84] and biocompatibility[102]. Both the *o*-nitrobenzyl group and the residues during and after photodegradation cannot react with biomarcomolecules such as proteins, RNA or DNA[102]. The mechanism of photo-cleavage in *o*-nitrobenzyl ester has

been investigated and is depicted in Figure 2.20. The nitrobenzyl moiety (1) reacts intermolecularly from the excited state of the biradical (2) upon UV light irradiation to give hydrogen-transfer process from benzylic hydrogen atom to excited nitro group, leading to generation of nitronic acid (3)[103-104]. The nitronic acid can be converted into final products nitroso ketone (5) along with carboxylic acid (6)[84]. The intermediates (4) were identified using electrical conductivity measurement[105].

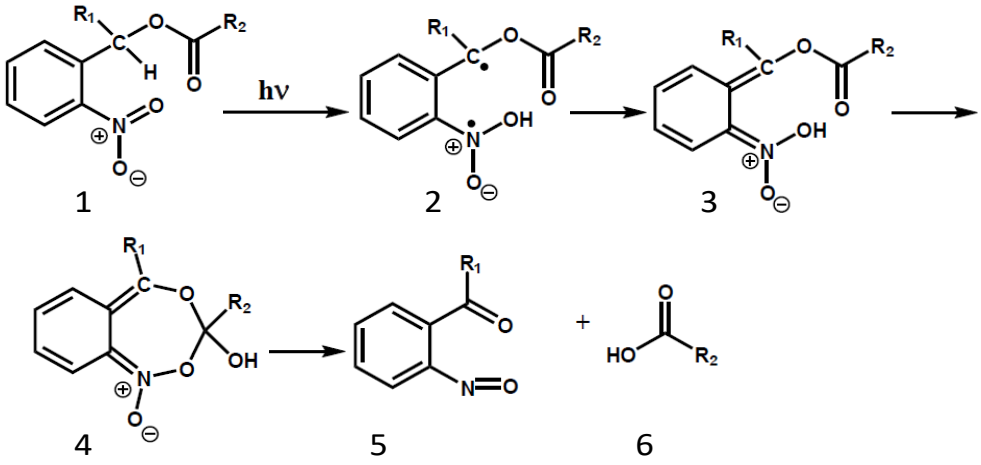

Figure 2.20. Mechanism of the photocleavage of o-nitrobenzyl ester[105].

Coumarin is a well known compound for adjusting the crosslinking degree in polymeric structure via undergoing photo-induced addition/cleavage[86, 106-107]. Under UV light of > 310 nm, two coumarin groups will dimerise via [2 + 2] photocycloaddition, forming stable covalently crosslinked bonds[108]. The crosslinked bonds will be cleaved when exposed to UV light of < 260 nm[108]. There are four photodimers: syn head-to-head (syn-hh), anti head-to-head (anti-hh), syn head-to-tail (syn-ht) and anti head-to-tail (anti-ht)[109] (Figure 2.21A). The prevalence of each species depends on the combination of UV light dose, solvent, and coumarin concentration. The anti-dimers are strongly favoured in low/non-polar solvents, but syn-dimers are formed in polar solvents and micellar solutions of cationic cetyltrimethylammonium bromide and anionic sodium dodecyl sulfate[110-111]. At high concentrations, the coumarin singlet reacts with a ground-state coumarin to form the syn-hh dimer due to face-to-face stacking of the coumarin

structure[112], while at low concentrations, inefficient intersystem crossing produces the triplet coumarin to form anti-hh dimer[113-114]. Hoffman et.al proposed that syn-dimers arise from coumarin singlet excimer state and dimerisation to syn-compounds via triplet excimers[114-115] (Figure 2. 21B).

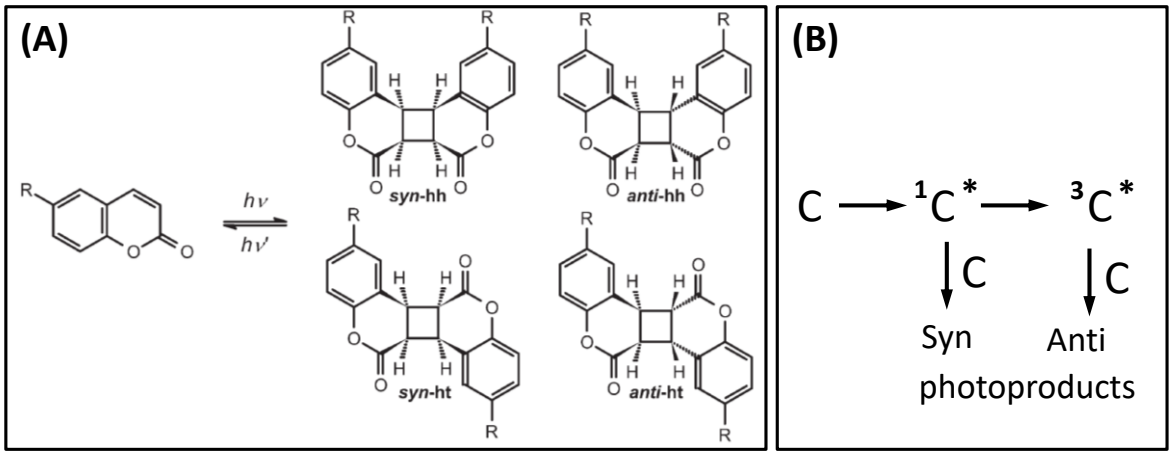

Figure 2.21. (A) Four photodimers of coumarins (R=H, alkyl)[109]. **(B)** Reaction scheme leading to the dimerisation of coumarin[114].

2.3.4 The swelling of MG particles

The volume swelling ratio (Q), indicating how much solvent can be absorbed by swelling particles, is the one of most important parameters for the stimuli responsive MGs. The Q value is determined by the crosslinker density, quality of solvent, ionisation degree and ionic strength[116]. The stimulus (e.g. pH or temperature change) causes an imbalance in osmotic pressure between the inside and outside of the particles, leading to MG swelling or de-swelling. This occurs until the same osmotic pressure is reached inside and outside the particles[117-118]. In Flory-Huggins theory, the total osmotic pressure Π_{total} is determined by three different contributions[119]. Those are the elasticity of the polymer network Π_{elas} (restricting swelling), the mixing of polymer chains with the solvent Π_m (driving swelling) and for ionic particles, a Donnan equilibrium term Π_D(driving swelling). The latter is due to the osmotic pressure from the counterions at the gel-solvent interface[120].

$$\Pi_{total} = \Pi_{elas} + \Pi_m + \Pi_D \quad (2.13)$$

When Π_{total} is zero, the osmotic pressure inside and outside particles is equal to zero. The Π_{elas}, Π_m and Π_D can be expressed as following equations[119]:

$$\Pi_{elas} = \frac{kTN_C}{V_0}[(\frac{\phi}{2\phi_0}) - (\frac{\phi}{\phi_0})^{1/3}] \quad (2.14)$$

$$\Pi_m = \frac{kTN_A}{V_S}[\phi + \ln(1-\phi) + \chi\phi^2] \quad (2.15)$$

$$\Pi_D = \frac{kTfN_C}{V_0}(\frac{\phi}{\phi_0}) \quad (2.16)$$

k is Boltzmann's constant, T is temperature, N_C is the effective number of polymer chains in the polymeric particle volume, V_0 is the volume of the particle in the reference state (collapsed state), V_S is the molar volume of the solvent (water), ϕ and ϕ_0 is the volume fraction of the polymeric particle in the swollen state and reference state (as made state) respectively, N_A is Avogadro's constant, χ is the Flory-Huggins polymer-solvent interaction parameter and means the energy change per solvent molecule when polymer-solvent contacts replaced both polymer-polymer and solvent-solvent contacts[121]. *f* is the number of counterions per chains, which describes the contribution of ionic group in MGs[119, 122].

In this thesis, the MGs swell or deswell upon the stimuli of pH, temperature and UV light. For pH stimulus, the –COOH in MGs is deprotonated to $-COO^-$ when increasing pH value of dispersion. The mechanism of swelling involves the changes of internal osmotic pressure resulting from mobile counter-ions associated with the ionised units ($-COO^-$)[116]. For the temperature stimulus, water act as good solvent and hydrogen bonding between the POEGMA segment and water maintains MGs swelling when temperature below the VPTT. The segment-solvent interactions are strong. Above the VPTT, hydrogen bonding

between the segments and water is disrupted and van der Wall interaction between segments becomes strong. The segment-segment hydrophobic interactions exceed segments-solvent interactions. In this case, the water is no longer a good solvent, resulting in particle collapse[4]. UV light can adjust the crosslinker density by photocleaving the o-nitrobenzyl moiety or photodimerising/cleaving the coumarin moiety, and then change the N_C values and Π_{elas} values.

2.4 Hydrogels

Hydrogels are cross-linked polymer networks that swell and retain a significant amount of water[123]. The crosslinking can be divided into chemical or physical nature. Chemical crosslinkers provide permanent junctions. Physical crosslinkers provide reversible junction arising from polymer chain entanglements or physical interactions such as hydrogen bond, ionic interactions or hydrophobic interaction. Responsive hydrogels that can response by shrinking or swelling with changes in external environmental conditions have attracted great attraction in recent decades due to their potential applications in biological science such as tissue regenerative engineering[124-125], drug delivery[126], cell encapsulation[127] and wound healing[128]. The external environmental conditions contain physical stimuli and chemical stimuli, where the physical stimuli including temperature, electric or magnetic field, light and pressure while the chemical stimuli including pH, solvent, ion strength[123, 129].

2.4.1 Doubly crosslinked microgels

Doubly crosslinked microgels (DX MGs) are a type of hydrogel which is prepared by crosslinking concentrated microgels. DX MGs have intra-particle crosslinking (within each MG particles) and inter-particle crosslinking (between the particles)[53]. DX MGs may be a better injectable gel compared to conventional synthetic hydrogels. This is because

conventional hydrogels are prepared using small monomer molecules and are not suitable for formation in vivo. The building blocks (MGs) for DX MGs are the physical gel with shear thinning properties before forming the covalent DX MG hydrogel.

The first DX MG hydrogel was synthesised by Hu et.al. in 2000. They first made hydroxypropyl cellulose (HPC) nanoparticles which are then mixed with divinylsulfone (DVS) to obtained a DX MG hydrogel with inter crosslinking formation by the reaction of hydroxyl group on the surface of HPC nanoparticle and the vinyl group of DVS in basic conditions (pH 12)[130]. They also prepared the dual responsive (thermal and pH) DX MG hydrogel using NIPAm-AA nanoparticle (NIPAm is *N*-isopropylacrylamide and AA is acrylic acid) as building blocks. The inter-crosslinking was formed via the reaction of carboxyl group and epichlorohydrin at 98 °C[130]. In 2006, Jia and co-worker made the biocompatible DX MG hydrogel by incubating aldehyde and hydrazide functionalised hyaluronic acid-based MG at 37 °C. They found this kind of hydrogel is good material for vocal fold regeneration because they have similar viscoelasticity as the gels[42]. Lyon et al.[131] developed a reversible sol-gel transition and thermally-and redox-sensitive DX MG hydrogel in 2012. PNIPMAm-BAC-BIS microgels was used as building block. (NIPMAm is *N*-isopropylmethacrylamide, BAC is *N,N′*-bis(acryloyl)cystamine and BIS is *N,N′*-methylenebis(acrylamide)). BIS is a non-degradable crosslinker while the disulfide group in BAC can cleave into two –SH groups in reducing conditions. The –SH group can conjugate to the disulfide group via intra- and inter- MGs in the oxidation environment and a hydrogel formed. This process was reversible and so was sol-gel polymer network formation.

A team at the University of Manchester reported pH responsive poly(ethylacrylate-methacrylic acid-butanediol diacrylate) (PEA-MAA-BDDA) and poly(methyl methacrylate-methacrylic acid-ethyleneglycol dimethacrylate) (PMMA-MAA-EGDMA)

DX MGs. The MGs were prepared by emulsion polymerisation and was then functionalised by reaction with glycidyl methacrylate (GMA) to create vinyl group at the surface of the MGs. The concentrated functionalised MGs are closely located when they are swollen in a basic environment. The inter-crosslinking can be achieved to form covalent bond between particles via free-radical reaction between vinyl group on the surface of particles at physiological conditions (37 °C and pH 7.4)[53]. This kind of injectable and biocompatible DX MG hydrogel has been shown to improve the mechanical properties of degenerated intervertebral discs (DIVD) and have potential application for restoring the mechanical properties of degenerated load-bearing soft tissue[132]. Figure 2.22 shows the method for preparing DX MG and reinforcing the degenerated soft tissue by this DX MG.

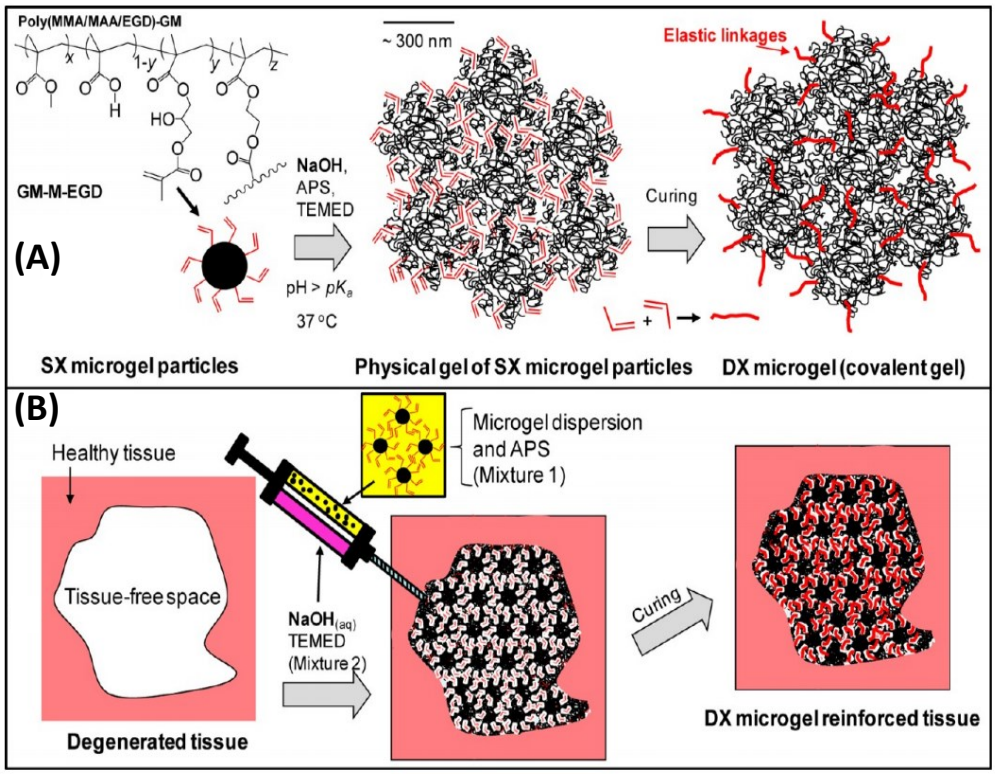

Figure 2.22. (A) Shows general method for preparing doubly crosslinked (DX) microgels using singly crosslinked (SX) GM-M-EGD microgel particles. **(B)** Shows the contents of the twin syringe used to inject the dispersion into a tissue-free space within degenerated soft tissue. APS is ammonium persulfate. TEMED is *N,N,N',N'*-tetramethylethylenediamine [132].

The aim of the present work is developing light responsive DX MG gels. This new gels can be injected into DIVD and support the degenerated load-bearing soft tissue. The mechanical property and swelling of gel located in the DIVD or tissue can be adjusted by light remotely. In Chapter 4, the preparation of the multi-responsive DX MG is based on this strategy. This uses functionalisation of GMA and formation of hydrogel via free-radical recation between vinyl groups within the MGs. In Chapter 6, GMA is replaced by reversibly photodimerised and photocleavable coumarin groups that are copolymerised within the MGs.

2.5 References

1. Baker, W. O., Microgel, a New Macromolecule - Relation to Sol and Gel as Structural Elements of Synthetic Rubber. *Ind Eng Chem* **1949,** *41* (3), 511-520.

2. Staudinger, H.; Husemann, E., Über hochpolymere Verbindungen, 116. Mitteil.: Über das begrenzt quellbare Poly-styrol. *Berichte der deutschen chemischen Gesellschaft (A and B Series)* **1935,** *68* (8), 1618-1634.

3. Zha, L. S.; Banik, B.; Alexis, F., Stimulus responsive nanogels for drug delivery. *Soft Matter* **2011,** *7* (13), 5908-5916.

4. Saunders, B. R.; Vincent, B., Microgel particles as model colloids: theory, properties and applications. *Adv Colloid Interfac* **1999,** *80* (1), 1-25.

5. Garcia, M. C.; Cuggino, J. C., Stimulus-responsive nanogels for drug delivery. *Woodh Publ Ser Biom* **2018**, 321-341.

6. Keerl, M.; Pedersen, J. S.; Richtering, W., Temperature Sensitive Copolymer Microgels with Nanophase Separated Structure. *J Am Chem Soc* **2009,** *131* (8), 3093-3097.

7. Saunders, J. M.; Tong, T.; Le Maitre, C. L.; Freemont, T. J.; Saunders, B. R., A study of pH-responsive microgel dispersions: from fluid-to-gel transitions to mechanical property restoration for load-bearing tissue. *Soft Matter* **2007,** *3* (4), 486-494.

8. Mergel, O.; Wunnemann, P.; Simon, U.; Boker, A.; Plamper, F. A., Microgel Size Modulation by Electrochemical Switching. *Chem Mater* **2015,** *27* (21), 7306-7312.

9. Zakrevskyy, Y.; Richter, M.; Zakrevska, S.; Lomadze, N.; von Klitzing, R.; Santer, S., Light-Controlled Reversible Manipulation of Microgel Particle Size Using Azobenzene-Containing Surfactant. *Adv Funct Mater* **2012,** *22* (23), 5000-5009.

10. Ogawa, K.; Wang, B.; Kokufuta, E., Enzyme-regulated microgel collapse for controlled membrane permeability. *Langmuir* **2001,** *17* (16), 4704-4707.

11. Plamper, F. A.; Richtering, W., Functional Microgels and Microgel Systems. *Accounts Chem Res* **2017,** *50* (2), 131-140.

12. Young, R. J.; Lovell, P. A., *Introduction to polymers*. 3rd ed.; CRC Press: Boca Raton, 2011; p xx, 668.

13. Needles, H. L.; Whitfield, R. E., Free-Radical Chemistry of Peptide Bonds .I. Dealkylation of Substituted Amides. *J Org Chem* **1964,** *29* (12), 3632-&.

14. Moad, G.; Solomon, D. H.; Moad, G., *The chemistry of radical polymerization*. 2nd fully rev. ed.; Elsevier: Amsterdam ; Boston, 2006; p xxvi, 639 p.

15. Chern, C. S., Emulsion polymerization mechanisms and kinetics. *Prog Polym Sci* **2006,** *31* (5), 443-486.

16. Krause, S., Polymer Chemistry: An Introduction, (Stevens, Malcolm P.). ACS Publications: 2000.

17. Klingler, J., RJ Hunter: Introduction to Modern Colloid Science, Oxford University Press, Oxford, New York, Melbourne, 1993. ISBN 0–19–855386–2, 338 Seiten, Preis: $14.95. *Berichte der Bunsengesellschaft für physikalische Chemie* **1995,** *99* (3), 591-592.

18. Chern, C.-S., *Principles and applications of emulsion polymerization*. John Wiley & Sons: 2008.

19. Young, R. J.; Lovell, P. A., *Introduction to polymers*. CRC press: 2011.

20. Miura, M.; Kodama, M., The second CMC of the aqueous solution of sodium dodecyl sulfate. I. Conductivity. *Bulletin of the Chemical Society of Japan* **1972,** *45* (2), 428-431.

21. Knapik, A.; Drelinkiewicz, A.; Szaleniec, M.; Makowski, W.; Waksmundzka-Góra, A.; Bukowska, A.; Bukowski, W.; Noworól, J. J. J. o. M. C. A. C., Hydrogenation of unsaturated carboxylic acids on functional gel-type resin supported Pd catalysts: the effect of reactant structure. **2008,** *279* (1), 47-56.

22. Hazot, P.; Delair, T.; Pichot, C.; Chapel, J.-P.; Elaissari, A. J. C. R. C., Poly (N-ethylmethacrylamide) thermally-sensitive microgel latexes: effect of the nature of the crosslinker on the polymerization kinetics and physicochemical properties. **2003,** *6* (11-12), 1417-1424.

23. Boularas, M.; Deniau-Lejeune, E.; Alard, V.; Tranchant, J.-F.; Billon, L.; Save, M. J. P. C., Dual stimuli-responsive oligo (ethylene glycol)-based microgels: insight into the role of internal structure in volume phase transitions and loading of magnetic nanoparticles to design stable thermoresponsive hybrid microgels. **2016,** *7* (2), 350-363.

24. Schramm, L. L., Emulsions, Foams, and Suspensions: Fundamentals and Applications. *Emulsions, Foams, and Suspensions: Fundamentals and Applications* **2005**, 1-448.

25. Bohinc, K.; Kralj-Iglic, V.; Iglic, A., Thickness of electrical double layer. Effect of ion size. *Electrochim Acta* **2001,** *46* (19), 3033-3040.

26. Tadros, T., *Encyclopedia of Colloid and Interface Science*. Springer: 2013.

27. Shaw,Dj - Introduction to Colloid and Surface Chemistry. *Pyrodynamic* **1967,** *5* (3), 289-&.

28. Islam, A. M.; Chowdhry, B. Z.; Snowden, M. J., Heteroaggregation in colloidal dispersions. *Adv Colloid Interfac* **1995,** *62* (2-3), 109-136.

29. Dzyaloshinskii, I. E. e.; Lifshitz, E. M.; Pitaevskii, L. P.; Priestley, M., The general theory of van der Waals forces. In *Perspectives in Theoretical Physics*, Elsevier: 1992; pp 443-492.

30. Hamaker, H. C., The London - Van Der Waals attraction between spherical particles. *Physica* **1937,** *4*, 1058-1072.

31. Hamaker, H. C., The London—van der Waals attraction between spherical particles. *physica* **1937,** *4* (10), 1058-1072.

32. Saunders, B. R.; Laajam, N.; Daly, E.; Teow, S.; Hu, X. H.; Stepto, R., Microgels: From responsive polymer colloids to biomaterials. *Adv Colloid Interfac* **2009,** *147-48*, 251-262.

33. Shaw, D. J., *Introduction to colloid and surface chemistry*. Butterworths: 1980.

34. Shaw, D. J., *Introduction to colloid and surface chemistry*. 4th ed.; Butterworth-Heinemann: Oxford ; Boston, 1992; p vi, 306 p.

35. Sehlleier, Y. H.; Abdali, A.; Schnurre, S. M.; Wiggers, H.; Schulz, C., Surface functionalization of microwave plasma-synthesized silica nanoparticles for enhancing the stability of dispersions. *J Nanopart Res* **2014,** *16* (8).

36. Cheng, R.; Meng, F. H.; Deng, C.; Klok, H. A.; Zhong, Z. Y., Dual and multi-stimuli responsive polymeric nanoparticles for programmed site-specific drug delivery. *Biomaterials* **2013,** *34* (14), 3647-3657.

37. Sivakumaran, D.; Maitland, D.; Hoare, T., Injectable Microgel-Hydrogel Composites for Prolonged Small-Molecule Drug Delivery. *Biomacromolecules* **2011,** *12* (11), 4112-4120.

38. Smeets, N. M. B.; Hoare, T., Designing responsive microgels for drug delivery applications. *J Polym Sci Pol Chem* **2013,** *51* (14), 3027-3043.

39. Vinogradov, S. V., Colloidal microgels in drug delivery applications. *Curr Pharm Design* **2006,** *12* (36), 4703-4712.

40. Qu, Y.; Chu, B. Y.; Wei, X. W.; Lei, M. Y.; Hu, D. R.; Zha, R. Y.; Zhong, L.; Wang, M. Y.; Wang, F. F.; Qian, Z. Y., Redox/pH dual-stimuli responsive camptothecin prodrug nanogels for "on-demand" drug delivery. *J Control Release* **2019,** *296*, 93-106.

41. Wolfbeis, O. S., An overview of nanoparticles commonly used in fluorescent bioimaging. *Chem Soc Rev* **2015,** *44* (14), 4743-4768.

42. Jia, X. Q.; Yeo, Y.; Clifton, R. J.; Jiao, T.; Kohane, D. S.; Kobler, J. B.; Zeitels, S. M.; Langer, R., Hyaluronic acid-based microgels and microgel networks for vocal fold regeneration. *Biomacromolecules* **2006,** *7* (12), 3336-3344.

43. Kumar, R. A.; Sivashanmugam, A.; Deepthi, S.; Iseki, S.; Chennazhi, K. P.; Nair, S. V.; Jayakumar, R., Injectable Chitin-Poly(epsilon-caprolactone)/Nanohydroxyapatite Composite Microgels Prepared by Simple Regeneration Technique for Bone Tissue Engineering. *Acs Appl Mater Inter* **2015,** *7* (18), 9399-9409.

44. Keskin, D.; Mergel, O.; van der Mei, H. C.; Busscher, H. J.; van Rijn, P., Inhibiting Bacterial Adhesion by Mechanically Modulated Microgel Coatings. *Biomacromolecules* **2019,** *20* (1), 243-253.

45. Zhan, Y.; Goncalves, M.; Yi, P. P.; Capelo, D.; Zhang, Y. H.; Rodrigues, J.; Liu, C. S.; Tomas, H.; Li, Y. L.; He, P. X., Thermo/redox/pH-triple sensitive poly(N-isopropylacrylamide-co-acrylic acid) nanogels for anticancer drug delivery. *J Mater Chem B* **2015,** *3* (20), 4221-4230.

46. Zhang, W.; Ai, S.; Ji, P.; Liu, J.; Li, Y.; Zhang, Y.; He, P., Photothermally Enhanced Chemotherapy Delivered by Graphene Oxide-Based Multiresponsive Nanogels. *ACS Applied Bio Materials* **2018,** *2* (1), 330-338.

47. Zhu, M. N.; Lu, D. D.; Wu, S. L.; Lian, Q.; Wang, W. K.; Milani, A. H.; Cui, Z. X.; Nguyen, N. T.; Chen, M.; Lyon, L. A.; Adlam, D. J.; Freemont, A. J.; Hoyland, J. A.; Saunders, B. R., Responsive Nanogel Probe for Ratiometric Fluorescent Sensing of pH and Strain in Hydrogels. *Acs Macro Lett* **2017,** *6* (11), 1245-1250.

48. Lin, J.; Chen, X. Y.; Chen, C. Y.; Hu, J. T.; Zhou, C. L.; Cai, X. F.; Wang, W.; Zheng, C.; Zhang, P. P.; Cheng, J.; Guo, Z. H.; Liu, H., Durably Antibacterial and Bacterially Antiadhesive Cotton Fabrics Coated by Cationic Fluorinated Polymers. *Acs Appl Mater Inter* **2018,** *10* (7), 6124-6136.

49. Xiong, M. H.; Li, Y. J.; Bao, Y.; Yang, X. Z.; Hu, B.; Wang, J. J. A. M., Bacteria-responsive multifunctional nanogel for targeted antibiotic delivery. **2012,** *24* (46), 6175-6180.

50. Bromberg, L.; Temchenko, M.; Alakhov, V.; Hatton, T. A., Kinetics of swelling of polyether-modified poly(acrylic acid) microgels with permanent and degradable cross-links. *Langmuir* **2005,** *21* (4), 1590-1598.

51. Bai, F.; Yang, X. L.; Li, R.; Huang, B.; Huang, W. Q., Monodisperse hydrophilic polymer microspheres having carboxylic acid groups prepared by distillation precipitation polymerization. *Polymer* **2006,** *47* (16), 5775-5784.

52. Hoare, T.; Pelton, R., Electrophoresis of functionalized microgels: morphological insights. *Polymer* **2005,** *46* (4), 1139-1150.

53. Liu, R. X.; Milani, A. H.; Freemont, T. J.; Saunders, B. R., Doubly crosslinked pH-responsive microgels prepared by particle inter-penetration: swelling and mechanical properties. *Soft Matter* **2011,** *7* (10), 4696-4704.

54. Lally, S.; Mackenzie, P.; LeMaitre, C. L.; Freemont, T. J.; Saunders, B. R., Microgel particles containing methacrylic acid: pH-triggered swelling behaviour and potential for biomaterial application. *J Colloid Interf Sci* **2007,** *316* (2), 367-375.

55. Thaiboonrod, S.; Berkland, C.; Milani, A. H.; Ulijn, R.; Saunders, B. R., Poly(vinylamine) microgels: pH-responsive particles with high primary amine contents. *Soft Matter* **2013,** *9* (15), 3920-3930.

56. Shahalom, S.; Tong, T.; Emmett, S.; Saunders, B. R., Poly(DEAEMa-co-PEGMa): A new pH-responsive comb copolymer stabilizer for emulsions and dispersions. *Langmuir* **2006,** *22* (20), 8311-8317.

57. Gao, Y.; Ahiabu, A.; Serpe, M. J., Controlled drug release from the aggregation–disaggregation behavior of pH-responsive microgels. *Acs Appl Mater Inter* **2014,** *6* (16), 13749-13756.

58. Guo, Z. R.; Chen, Q.; Gu, H. J.; He, Z. F.; Xu, W. Y.; Zhang, J. L.; Liu, Y. X.; Xiong, L. Y.; Zheng, L. Z.; Feng, Y. J., Giant Microgels with CO2-Induced On-Off, Selective, and Recyclable Adsorption for Anionic Dyes. *Acs Appl Mater Inter* **2018,** *10* (44), 38073-38083.

59. O'Bryan, C. S.; Kabb, C. P.; Sumerlin, B. S.; Angelini, T. E., Jammed Polyelectrolyte Microgels for 3D Cell Culture Applications: Rheological Behavior with Added Salts. *ACS Applied Bio Materials* **2019,** *2* (4), 1509-1517.

60. Tan, B. H.; Ravi, P.; Tam, K. C., Synthesis and characterization of novel pH-responsive polyampholyte microgels. *Macromol Rapid Comm* **2006,** *27* (7), 522-528.

61. Freemont, T. J.; Saunders, B. R., PH-responsive microgel dispersions for repairing damaged load-bearing soft tissue. *Soft Matter* **2008,** *4* (5), 919-924.

62. Zhou, T. T.; Zhao, X. B.; Liu, L.; Liu, P., Preparation of biodegradable PEGylated pH/reduction dual-stimuli responsive nanohydrogels for controlled release of an anti-cancer drug. *Nanoscale* **2015,** *7* (28), 12051-12060.

63. Dai, S.; Ravi, P.; Tam, K. C., Thermo- and photo-responsive polymeric systems. *Soft Matter* **2009,** *5* (13), 2513-2533.

64. Yildiz, I.; Yildiz, B. S., Applications of Thermoresponsive Magnetic Nanoparticles. *J Nanomater* **2015**.

65. Goodwin, J. W.; Buscall, R., *Colloidal polymer particles*. Academic Press: 1995.

66. Chen, L.; Liu, M. J.; Lin, L.; Zhang, T.; Ma, J.; Song, Y. L.; Jiang, L., Thermal-responsive hydrogel surface: tunable wettability and adhesion to oil at the water/solid interface. *Soft Matter* **2010,** *6* (12), 2708-2712.

67. Haq, M. A.; Su, Y. L.; Wang, D. J., Mechanical properties of PNIPAM based hydrogels: A review. *Mat Sci Eng C-Mater* **2017,** *70*, 842-855.

68. Varga, I.; Gilanyi, T.; Meszaros, R.; Filipcsei, G.; Zrinyi, M., Effect of cross-link density on the internal structure of Poly(N-isopropylacrylamide) microgels. *J Phys Chem B* **2001,** *105* (38), 9071-9076.

69. Acciaro, R.; Gilanyi, T.; Varga, I., Preparation of Monodisperse Poly(N-isopropylacrylamide) Microgel Particles with Homogenous Cross-Link Density Distribution. *Langmuir* **2011,** *27* (12), 7917-7925.

70. Jones, C. D.; Lyon, L. A., Synthesis and characterization of multiresponsive core-shell microgels. *Macromolecules* **2000,** *33* (22), 8301-8306.

71. Kwok, M. H.; Li, Z. F.; Ngai, T., Controlling the Synthesis and Characterization of Micrometer-Sized PNIPAM Microgels with Tailored Morphologies. *Langmuir* **2013,** *29* (30), 9581-9591.

72. Vihola, H.; Laukkanen, A.; Valtola, L.; Tenhu, H.; Hirvonen, J., Cytotoxicity of thermosensitive polymers poly(N-isopropylacrylamide), poly(N-vinylcaprolactam) and amphiphilically modified poly(N-vinylcaprolactam). *Biomaterials* **2005,** *26* (16), 3055-3064.

73. Lutz, J. F.; Akdemir, O.; Hoth, A., Point by point comparison of two thermosensitive polymers exhibiting a similar LCST: Is the age of poly(NIPAM) over? *J Am Chem Soc* **2006,** *128* (40), 13046-13047.

74. Ramos, J.; Imaz, A.; Forcada, J., Temperature-sensitive nanogels: poly(N-vinylcaprolactam) versus poly(N-isopropylacrylamide). *Polym Chem-Uk* **2012,** *3* (4), 852-856.

75. Lutz, J. F.; Stiller, S.; Hoth, A.; Kaufner, L.; Pison, U.; Cartier, R., One-pot synthesis of PEGylated ultrasmall iron-oxide nanoparticles and their in vivo evaluation as magnetic resonance imaging contrast agents. *Biomacromolecules* **2006,** *7* (11), 3132-3138.

76. Ulasan, M.; Yavuz, E.; Bagriacik, E. U.; Cengeloglu, Y.; Yavuz, M. S., Biocompatible thermoresponsive PEGMA nanoparticles crosslinked with cleavable disulfide-based crosslinker for dual drug release. *J Biomed Mater Res A* **2015,** *103* (1), 243-251.

77. Lale, S. V.; Aswathy, R. G.; Aravind, A.; Kumar, D. S.; Koul, V., AS1411 Aptamer and Folic Acid Functionalized pH-Responsive ATRP Fabricated pPEGMA-PCL-pPEGMA Polymeric Nanoparticles for Targeted Drug Delivery in Cancer Therapy. *Biomacromolecules* **2014,** *15* (5), 1737-1752.

78. Tian, Y. F.; Bian, S. S.; Yang, W. L., A redox-labile poly(oligo(ethylene glycol)methacrylate)-based nanogel with tunable thermosensitivity for drug delivery. *Polym Chem-Uk* **2016,** *7* (10), 1913-1921.

79. Boularas, M.; Deniau-Lejeune, E.; Alard, V.; Tranchant, J. F.; Billon, L.; Save, M., Dual stimuli-responsive oligo(ethylene glycol)-based microgels: insight into the role of internal structure in volume phase transitions and loading of magnetic nanoparticles to design stable thermoresponsive hybrid microgels. *Polym Chem-Uk* **2016,** *7* (2), 350-363.

80. Lutz, J. F.; Weichenhan, K.; Akdemir, O.; Hoth, A., About the phase transitions in aqueous solutions of thermoresponsive copolymers and hydrogels based on 2-(2-methoxyethoxy)ethyl methacrylate and oligo(ethylene glycol) methacrylate. *Macromolecules* **2007,** *40* (7), 2503-2508.

81. Bertrand, O.; Gohy, J. F., Photo-responsive polymers: synthesis and applications. *Polym Chem-Uk* **2017,** *8* (1), 52-73.

82. Klinger, D.; Nilles, K.; Theato, P., Synthesis of Polymeric 1-Iminopyridinium Ylides as Photoreactive Polymers. *J Polym Sci Pol Chem* **2010,** *48* (4), 832-844.

83. Huang, Q.; Bao, C. Y.; Ji, W.; Wang, Q. Y.; Zhu, L. Y., Photocleavable coumarin crosslinkers based polystyrene microgels: phototriggered swelling and release. *J Mater Chem* **2012,** *22* (35), 18275-18282.

84. Zhu, C. C.; Ninh, C.; Bettinger, C. J., Photoreconfigurable Polymers for Biomedical Applications: Chemistry and Macromolecular Engineering. *Biomacromolecules* **2014,** *15* (10), 3474-3494.

85. Jiang, J. Q.; Tong, X.; Morris, D.; Zhao, Y., Toward photocontrolled release using light-dissociable block copolymer micelles. *Macromolecules* **2006,** *39* (13), 4633-4640.

86. He, J.; Tong, X.; Zhao, Y., Photoresponsive Nanogels Based on Photocontrollable Cross-Links. *Macromolecules* **2009,** *42* (13), 4845-4852.

87. Jiang, J. Q.; Tong, X.; Zhao, Y., A new design for light-breakable polymer micelles. *J Am Chem Soc* **2005,** *127* (23), 8290-8291.

88. Bertrand, O.; Fustin, C. A.; Gohy, J. F., Multiresponsive Micellar Systems from Photocleavable Block Copolymers. *Acs Macro Lett* **2012,** *1* (8), 949-953.

89. Jiang, X.; Lavender, C. A.; Woodcock, J. W.; Zhao, B., Multiple micellization and dissociation transitions of thermo- and light-sensitive poly(ethylene oxide)-b-poly(ethoxytri(ethylene glycol) acrylate-co-o-nitrobenzyl acrylate) in water. *Macromolecules* **2008,** *41* (7), 2632-2643.

90. By Luke A. Connal, R. V., Craig J. Hawker, and Greg G. Qiao, Fabrication of Reversibly Crosslinkable, 3-Dimensionally Conformal Polymeric Microstructures. *Adv. Funct. Mater.* **2008**.

91. Marianne E. Harmon, D. K., *,†,‡ and Curtis W. Frank*,†, Photo-Cross-Linkable PNIPAAm Copolymers. 2. Effects of Constraint on Temperature and pH-Responsive Hydrogel Layers. *Macromolecules* **2003**.

92. Gui-Chao Kuang a, Y. J. a., Xin-Ru Jia a,*, Yan Li a, Er-Qiang Chen a, Zheng-Xiang Zhang a, Yen Wei b, Photoresponsive organogels: an amino acid-based dendron functionalized with p-nitrocinnamate. *Tetrahedron* **2009**.

93. Hee-Young Lee, K. K. D., † Kunshan Sun,† Tianhong Chen,‡ and Srinivasa R. Raghavan*,†, Reversible Photorheological Fluids Based on Spiropyran-Doped Reverse Micelles. *J. Am. Chem. Soc* **2011**.

94. Shi, D. J.; Matsusaki, M.; Kaneko, T.; Akashi, M., Photo-Cross-Linking and Cleavage Induced Reversible Size Change of Bio-Based Nanoparticles. *Macromolecules* **2008,** *41* (21), 8167-8172.

95. Iwaso, K.; Takashima, Y.; Harada, A., Fast response dry-type artificial molecular muscles with [c2]daisy chains. *Nat Chem* **2016,** *8* (6), 626-633.

96. Cembran, A.; Bernardi, F.; Garavelli, M.; Gagliardi, L.; Orlandi, G., On the mechanism of the cis-trans isomerization in the lowest electronic states of azobenzene: S-0, S-1, and T-1. *J Am Chem Soc* **2004,** *126* (10), 3234-3243.

97. Klajn, R., Spiropyran-based dynamic materials. *Chem Soc Rev* **2014,** *43* (1), 148-184.

98. Osuka, A.; Fujikane, D.; Shinmori, H.; Kobatake, S.; Irie, M., Synthesis and photoisomerization of dithienylethene-bridged diporphyrins. *J Org Chem* **2001,** *66* (11), 3913-3923.

99. Wang, G.; Tong, X.; Zhao, Y., Preparation of azobenzene-containing amphiphilic diblock copolymers for light-responsive micellar aggregates. *Macromolecules* **2004,** *37* (24), 8911-8917.

100. Ueki, T.; Nakamura, Y.; Lodge, T. P.; Watanabe, M., Light-Controlled Reversible Micellization of a Diblock Copolymer in an Ionic Liquid. *Macromolecules* **2012,** *45* (18), 7566-7573.

101. Lee, H. I.; Wu, W.; Oh, J. K.; Mueller, L.; Sherwood, G.; Peteanu, L.; Kowalewski, T.; Matyjaszewski, K., Light-induced reversible formation of polymeric micelles. *Angew Chem Int Edit* **2007,** *46* (14), 2453-2457.

102. Peng, K.; Kros, A., Photoresponsive hydrogels for biomedical applications. *Abstr Pap Am Chem S* **2012,** *243*.

103. Reichmanis, E.; Smith, B.; Gooden, R., O-nitrobenzyl photochemistry: Solution vs. solid-state behavior. *Journal of Polymer Science: Polymer Chemistry Edition* **1985,** *23* (1), 1-8.

104. Yip, R.; Sharma, D.; Giasson, R.; Gravel, D., Photochemistry of the o-nitrobenzyl system in solution: evidence for singlet-state intramolecular hydrogen abstraction. *The Journal of Physical Chemistry* **1985,** *89* (25), 5328-5330.

105. Wong, W.; Schupp, H.; Schnabel, W., Kinetic-mechanistic studies on the photorearrangement of o-nitrobenzyl ester groups in polymer matrices. *Macromolecules* **1989,** *22* (5), 2176-2181.

106. Jin, Q. A.; Liu, G. Y.; Li, J. A., Preparation of reversibly photo-cross-linked nanogels from pH-responsive block copolymers and use as nanoreactors for the synthesis of gold nanoparticles. *Eur Polym J* **2010,** *46* (11), 2120-2128.

107. He, J.; Tong, X.; Tremblay, L.; Zhao, Y., Corona-Cross-Linked Polymer Vesicles Displaying a Large and Reversible Temperature-Responsive Volume Transition. *Macromolecules* **2009,** *42* (19), 7267-7270.

108. He, J.; Yan, B.; Tremblay, L.; Zhao, Y., Both Core- and Shell-Cross-Linked Nanogels: Photoinduced Size Change, Intraparticle LCST, and Interparticle UCST Thermal Behaviors. *Langmuir* **2011,** *27* (1), 436-444.

109. Wolff, T.; Gorner, H., Photodimerization of coumarin revisited: Effects of solvent polarity on the triplet reactivity and product pattern. *Phys Chem Chem Phys* **2004,** *6* (2), 368-376.

110. Wolff, T.; Gorner, H., Photocleavage of dimers of coumarin and 6-alkylcoumarins. *J Photoch Photobio A* **2010,** *209* (2-3), 219-223.

111. Morrison, H.; Curtis, H.; McDowell, T., Solvent Effects on the Photodimerization of Coumarin1. *J Am Chem Soc* **1966,** *88* (23), 5415-5419.

112. Jiang, J. Q.; Shu, Q. Z.; Chen, X.; Yang, Y. Q.; Yi, C. L.; Song, X. Q.; Liu, X. Y.; Chen, M. Q., Photoinduced Morphology Switching of Polymer Nanoaggregates in Aqueous Solution. *Langmuir* **2010,** *26* (17), 14247-14254.

113. Lewis, F. D.; Barancyk, S. V., Lewis acid catalysis of photochemical reactions. 8. Photodimerization and cross-cycloaddition of coumarin. *J Am Chem Soc* **1989,** *111* (23), 8653-8661.

114. Trenor, S. R.; Shultz, A. R.; Love, B. J.; Long, T. E., Coumarins in polymers: From light harvesting to photo-cross-linkable tissue scaffolds. *Chem Rev* **2004,** *104* (6), 3059-3077.

115. Hoffman, R.; Wells, P.; Morrison, H., Organic photochemistry. XII. Further studies on the mechanism of coumarin photodimerization, observation of an unusual" heavy atom" effect. *The Journal of organic chemistry* **1971,** *36* (1), 102-108.

116. Lyon, L. A.; Serpe, M. J., *Hydrogel micro and nanoparticles*. John Wiley & Sons: 2012.

117. Fernandez-Nieves, A.; Fernandez-Barbero, A.; Vincent, B.; de las Nieves, F. J., Charge controlled swelling of microgel particles. *Macromolecules* **2000,** *33* (6), 2114-2118.

118. Lyon, L. A.; Fernandez-Nieves, A., The Polymer/Colloid Duality of Microgel Suspensions. *Annu Rev Phys Chem* **2012,** *63*, 25-43.

119. Hoare, T.; Pelton, R., Functionalized microgel swelling: Comparing theory and experiment. *J Phys Chem B* **2007,** *111* (41), 11895-11906.

120. Bamford, C. H.; Middleton, I. P., Principles of Polymer Chemistry. *Dev Hematol* **1989,** *23*, 149-193.

121. Nigro, V.; Angelini, R.; Bertoldo, M.; Ruzicka, B., Swelling of responsive-microgels: experiments versus models. *Colloids and Surfaces A: Physicochemical and Engineering Aspects* **2017,** *532*, 389-396.

122. Fernandez-Nieves, A.; Fernandez-Barbero, A.; Vincent, B.; de las Nieves, F. J., Osmotic de-swelling of ionic microgel particles. *J Chem Phys* **2003,** *119* (19), 10383-10388.

123. Ahmed, E. M., Hydrogel: Preparation, characterization, and applications: A review. *Journal of advanced research* **2015,** *6* (2), 105-121.

124. Tan, H. P.; Marra, K. G., Injectable, Biodegradable Hydrogels for Tissue Engineering Applications. *Materials* **2010,** *3* (3), 1746-1767.

125. Lin, C. C.; Anseth, K. S., PEG Hydrogels for the Controlled Release of Biomolecules in Regenerative Medicine. *Pharm Res-Dordr* **2009,** *26* (3), 631-643.

126. Li, J. Y.; Mooney, D. J., Designing hydrogels for controlled drug delivery. *Nat Rev Mater* **2016,** *1* (12).

127. Lu, S. Y.; Gao, C. M.; Xu, X. B.; Bai, X.; Duan, H. G.; Gao, N. N.; Feng, C.; Xiong, Y.; Liu, M. Z., Injectable and Self-Healing Carbohydrate-Based Hydrogel for Cell Encapsulation. *Acs Appl Mater Inter* **2015,** *7* (23), 13029-13037.

128. Qu, J.; Zhao, X.; Liang, Y. P.; Zhang, T. L.; Ma, P. X.; Guo, B. L., Antibacterial adhesive injectable hydrogels with rapid self-healing, extensibility and compressibility as wound dressing for joints skin wound healing. *Biomaterials* **2018,** *183*, 185-199.

129. Richter, A.; Paschew, G.; Klatt, S.; Lienig, J.; Arndt, K.-F.; Adler, H.-J. P., Review on hydrogel-based pH sensors and microsensors. *Sensors-Basel* **2008,** *8* (1), 561-581.

130. Hu, Z. B.; Lu, X. H.; Gao, J.; Wang, C. J., Polymer gel nanoparticle networks. *Adv Mater* **2000,** *12* (16), 1173-1176.

131. Gaulding, J. C.; Smith, M. H.; Hyatt, J. S.; Fernandez-Nieves, A.; Lyon, L. A., Reversible Inter- and Intra-Microgel Cross-Linking Using Disulfides. *Macromolecules* **2012,** *45* (1), 39-45.

132. Milani, A. H.; Freemont, A. J.; Hoyland, J. A.; Adlam, D. J.; Saunders, B. R., Injectable Doubly Cross-Linked Microgels for Improving the Mechanical Properties of Degenerated Intervertebral Discs. *Biomacromolecules* **2012,** *13* (9), 2793-2801.

Chapter 3: Characterisation methods

3.1 Dynamic light scattering

Dynamic light scattering (DLS), also called photon correlation spectroscopy (PCS), is a technique which can be used to measure the average size and size distribution of particles dispersed in a liquid. It is used to detect the size and (pH-, temperature- and light-) responses of MGs in this thesis. This technique is based on the time-dependent fluctuation and intensity of moving particles in scattered light[1]. Particles in suspension move randomly and constantly due to Brownian motion, which causes fluctuations of scattering light intensity. The velocity of moving particles is dependent on the particle size, temperature and viscosity of the medium. Smaller particles in a low viscosity of the medium move faster than larger particles in a viscous medium. The particle size can be calculated by the mean translational diffusion coefficient using the Stokes-Einstein equation. The fluctuations of scattered light are converted to mean translational diffusion coefficient[2]. A typical measurement set-up is depicted in Figure 3.1.

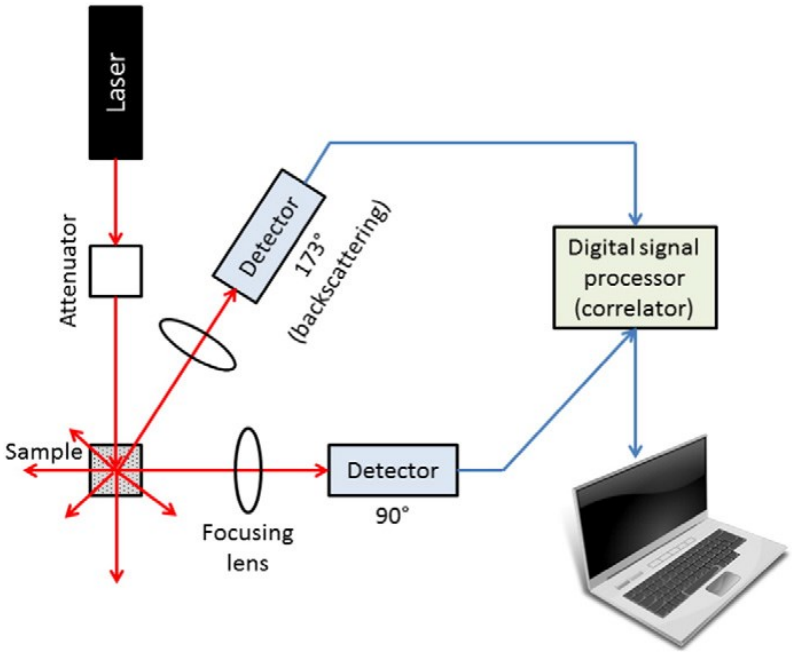

Figure 3.23. Schematic of a DLS instrument and the main components[3].

A vertically polarised laser beam passes through the sample. A detector is set up at a certain angle which is connected to a correlator. When the light passes through the particle, the irregular moving particles scatter light in all directions. The intensity of the scattered light will fluctuate over time. If small particles are measured the intensity of a scattered spot of light fluctuates quickly due to their quick motion. In contrast, the scattered intensity from large particles shows slow fluctuations because they move slowly (see Figure 3.2A and B). The fluctuating intensity at a certain angle is measured as a function of time by a detector. The intensity trace is further used to generate a correlation function (see Figure 3.2C and D). The correlation function is a measure of correlation of intensity from one moment to the next. At the beginning of the delay times, the correlation function (g_2) is linear and almost constant. Later, there is an exponential decay of the correlation function, which means that the particle is moving. Small particles move quickly so the decay of the correlation function is fast. Larger particles move more slowly and therefore the decay is delayed[4].

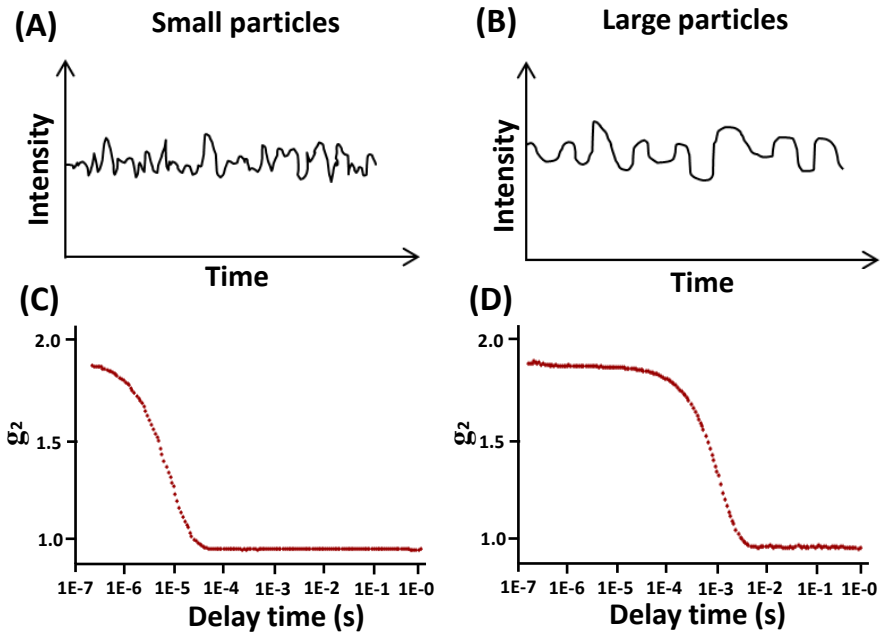

Figure 3.24 Differences in the intensity trace of small (A) and large (B) particles and correlation function of small (C) and large (D) particles. Smaller particles show faster fluctuations of the scattered light and a faster decay of the correlation function[4].

The fluctuations can be quantified by a second order correlation function given by[5],

$$g_2(t) = \frac{\langle I(t)I(t+\tau)\rangle}{\langle I(t)\rangle^2} \qquad (2.17)$$

where *I(t)* is the intensity of the scattered light at time t, and the brackets indicate averaging over all t. The correlation function depends on the delay time (τ). The latter is the amount of time that a duplicate intensity trace is shifted from the original before the averaging is performed.

For monodisperse sample, $g_2(t)$ can by analysed by the equation,

$$g_2(t) = A[1 + B\exp(-2\Gamma\tau)] \qquad (2.18)$$

where A is a constant and often called the baseline. A can be directly measured for the experiment at infinite delay. B is the spatial coherence factor, which is primarily determined by the optical properties of the system. Γ is the characteristic decay rate.

Γ can be converted to the diffusion constant *D* for the particles via relation,

$$D = \frac{\Gamma}{q^2} \qquad (2.19)$$

Here, *q* is the magnitude of the scattering vector and is given by,

$$q = \frac{4\pi n_0}{\lambda_0} \sin\frac{\theta}{2} \qquad (2.20)$$

where n_0 is the refractive index of dispersed medium, λ_0 is wavelength of light in the medium, θ is the scattering angle. The diffusion constant *D* can be used to calculated as the hydrodynamic diameter d_z of a diffusing sphere via the Stokes-Einstein equation,

$$D = \frac{\mathrm{kT}}{3\pi\eta d_z} \qquad (2.21)$$

where k is the Boltzmann constant, T is the absolute temperature and η is the viscosity of the dispersion medium.

In this study, the DLS measurements were performed using a Malvern Zetasizer NanoZS scattering apparatus at a scattering angle of 173°, fitted with a 20 mW HeNe laser. The MGs were dispersed in series of phosphate buffer at a concentration of 1.0 mg/mL. The change of hydrodynamic average size was monitored with heating from 10 to 60 °C for investigating the thermal-responsive behaviours, and was dispersed with series of phosphate buffer solution at 25 °C for investigating the pH-responsive behaviours of MGs. The samples were kept at each temperature for 300 s before testing. Each sample were run for 3 times and obtained the average values.

3.2 Ultraviolet–visible spectroscopy

Ultraviolet-visible (UV-Vis) spectra refers to the absorption spectra measured in the ultraviolet range (190 nm to 400 nm) to adjacent visible spectral regions (400 nm to 800 nm)[6]. UV-Vis spectroscopy is most commonly applied to measure solution or solid state samples. In my study, this technique is used to characterise the light induced-degradation process of photo-sensitive corsslinker (nPh) and reversible photo-dimerisation/ cleavage of photo-liable monomer (CMA) within the MGs.

When light illuminates the sample, the light with energy sufficiently are enough to excite an electron from lower energy level of the highest occupied molecular orbital (HOMO) to the higher energy level of lowest unoccupied molecular orbital (LUMO). The resulting species is called an excited state and this process refers to electronic transitions[6]. Figure 3.3 shows the electronic transitions that are involved in the UV-visible region. The energy level of each electronic state is in order: $\sigma<\pi<n<\pi^*<\sigma^*$. The usual order of energy required for electronic transitions: $n\rightarrow\pi^*$, $\pi\rightarrow\pi^*$, $n\rightarrow\sigma^*$, $\sigma\rightarrow\sigma^*$.

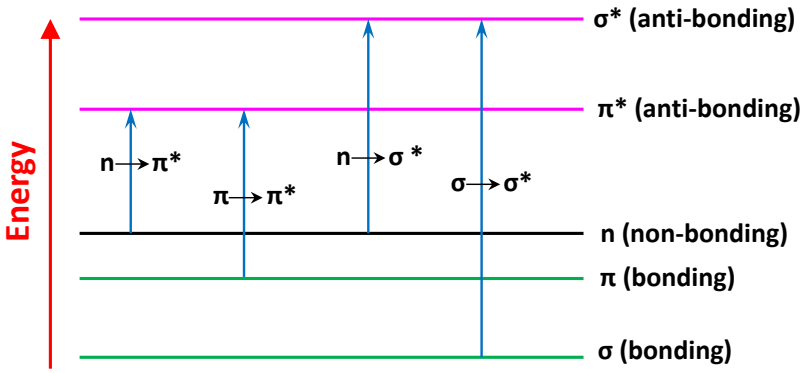

Figure 3.25. Relative energies of electronic transitions[7]

For the σ→σ* transition, an electron from a bonding σ orbital is excited to the antibonding σ orbital and the high energy is required because σ bonds are very strong. Thus, this transition does not occur in normal UV-visible regions (200-800 nm). The transition of an electron form non-bonding orbital to an antibonding σ orbital in saturated compounds containing atoms with lone pair of electron such as O,N,S is called the n→σ* transition and requires lower energy than σ→σ* transition. The π→π* transition is the promotion of an electron from a π bonding orbital to a π antibonding orbital which occurs in compounds containing one or more covalently unsaturated groups such as C=C, C=O and NO_2. This transition requires lower energy than n→σ* transition. The n→π* transition needs the lowest energy and the compounds containing double bond involving atoms (C=O, N=O) undergo such transitions. That means that the molecule containing either π bonds or atoms with non-bonding orbitals can absorb light in the region from 200 - 800 nm and can be measured using UV-Vis spectroscopy. The groups in a molecule absorbing light are known as chromophores.

Figure 3.3 shows the components of a UV-Vis spectrometer. A beam from a visible or UV light source is separated into its component wavelengths using a diffraction grating. The beam is split into two parallel equal intensity beams by a half-mirror, each of which transmits through a cuvette. One cuvette contains the sample in a transparent solvent

being studied and the other cuvette contains the solvent only as the reference. Some light will be absorbed and the remainder will be transmitted through the sample.

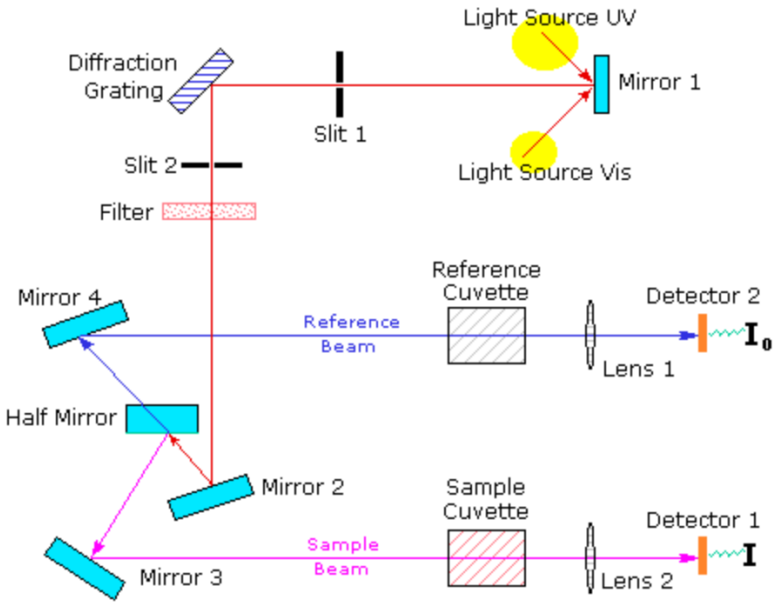

Figure 3.26. A diagram of the components of a UV-Vis spectrometer [8]

The detectors measure the intensities of light passed through reference cuvette (I_0) and sample cuvette (I). The absorbance (A) is calculated from the relationship between I_0 and I, shown in equation (2.22)[8],

$$A = log_{10}\frac{I_0}{I} \qquad (2.22)$$

The absorption can also be presented as transmittance ($T = I/I_0$)[8]. The reference beam intensity is considered as 100% Transmission (or A=0). The absorption is recorded as a function of wavelength, and the obtained absorption curve is an UV-Vis absorption spectrum.

The absorbance of a sample is proportional to its molar concentration. A corrected absorption value (the molar absorptivity (ε)) is a measure of the intensity of the absorption and used when comparing the spectra of different compounds. This can be expressed by the Beer–Lambert law[9], given as:

$$A=\varepsilon \cdot c \cdot L \qquad (2.23)$$

c is the concentration of the sample (mol L^{-1}), and L is the path length (cm), ε is called the molar extinction coefficient (L mol^{-1} cm^{-1}). The greater the probability electronic transitions of molecule, the greater the value for ε.

UV-Vis absorption of sample was measured on a PerkinElmer Lambda 25 UV/VIS spectrometer. The ε values for nPh and CMA were determined by the absorption of different concentration of nPh and CMA solution, so that the amount of CMA or nPh polymerised into MGs can be calculated based on the ε values. In order to study the photosensitivity of MG-*x*-nPh and MG-CMA via the change of absorption, the MGs solution with 0.01 wt.% was treated by UV light for pre-determined time and test its absorption.

3.3 Fourier Transform Infra-Red Spectroscopy

Fourier transform infrared (FTIR) spectroscopy is a technique used for detection of chemical bonds in a molecule by production an infrared absorption spectrum of a solid, liquid or gas. This technique usually uses the electromagnetic spectrum in the IR regions (2.5-15 μm, 4000-667 cm^{-1})[9]. When a molecule absorbs energy in IR regions, the absorbed radiation causes transitions in molecular vibrational energy levels that can change its dipole moment. This occurs when the frequency of the electromagnetic field within IR regions is equal to the vibrational frequency[10]. Planck's equation defines this frequency as $\nu = \Delta E/h$, where ΔE is the difference in energy between the upper and lower vibrational energy levels of the bond deformation and h is Planck's constant[10]. Figure 3.4 shows two types of molecular vibration: (A) stretching vibration (symmetrical stretching and asymmetrical stretching) and (B) bending vibration (scissoring, rocking, wagging and twisting)[9]. The constituent atoms responsible for dipole moments will influence the

energy requirement of vibration, allowing IR absorption peaks to be linked with chemical structure. Usually, the greater the change in dipole moment, the higher is intensity of absorption[9]. Hence, infrared spectroscopy provides information on chemical structure and bonding.

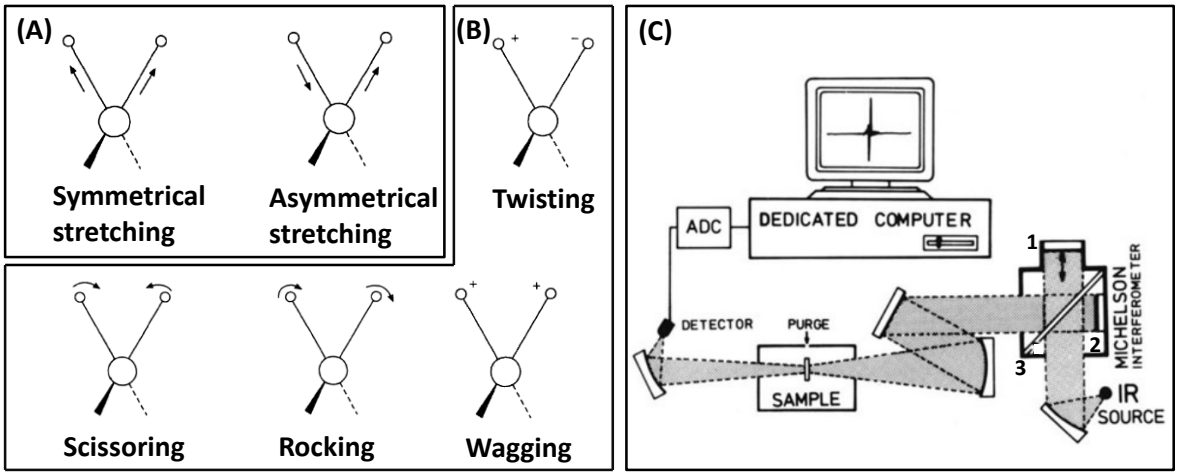

Figure 3.27. (A) Stretching vibrations and **(B)** bending vibration (+ and - means the atom moves up and down the plane respectively)[9]. **(C)** Schematic diagram of a FTIR instrument. 1 is a moving mirror; 2 is a fixed mirror; 3 is a beam splitter; ADC is an analog-digital-converter[11].

Figure 3.4C illustrates the main components of an FTIR spectrophotometer. The IR beam from an IR source is split into two equal beams by a beam splitter. One beam reflects from a fixed mirror and other beam reflects from a moving mirror which travels a short distance away from the beam splitter. The two beams recombine together after being reflected by two mirrors which creates an interference wave. When the interference light beam passed through a sample, the specific frequency of radiation is absorbed by a sample due to the excited vibration of a bond in the molecules and some radiation is transmitted. The resulting beam is recorded by a detector, digitised by analog-digital-converter and stored in a computer. The computer performs the Fourier transformation calculation and presents the data as an infrared spectrum. This plots absorbance (or transmittance) versus wavenumber. A background spectrum is recorded when analysing the result. The transmittance spectrum is obtained as following equation:

$$T\% = \frac{I_0}{I} \times 100\% \qquad (2.24)$$

where $T\%$ is the percent transmittance. I is the intensity measured from the sample and I_0 is the intensity measured from the background.

The absorbance spectrum can be calculated using the following equation (where A is the absorbance):

$$A = log_{10} \frac{1}{T} \qquad (2.24)$$

FTIR spectroscopy is applied for investigating the reversible photo-dimerisation/ cleavage of photo-labile monomer (CMA) within the MGs and hydrogels in this thesis. All samples were freeze dried to remove the solvent and obtained the dried samples before measuring. The change of absorption peak at 1620 cm^{-1} due to C=C stretching of CMA in the FTIR spectra indicates the photo-crosslinking and cleavage of MGs or hydrogels.

3.4 Proton Nuclear Magnetic Resonance Spectroscopy

Nuclear magnetic resonance (NMR) Spectroscopy is a spectroscopic method and samples absorb electromagnetic radiation in the radio-frequency region (3 MHZ to 30,000 MHZ). Nuclei of some atoms possess magnetic moments (μ) due to the spin (I) of the positive charged nuclei along the nuclear axis. The magnetic nuclei are orientated irregularly in the absence of an external magnetic field as shown in Figure 3.5A. In the presence of an external magnetic field (B_0), spinning nuclei behave like a tiny bar magnet and will orient themselves in 2I+1 way[12]. For ^1H ($I = \frac{1}{2}$), the number of orientations for their orientation is 2. One way is parallel to the applied magnetic field and other way is anti-paralled to the applied magnetic field (Figure 3.5B).

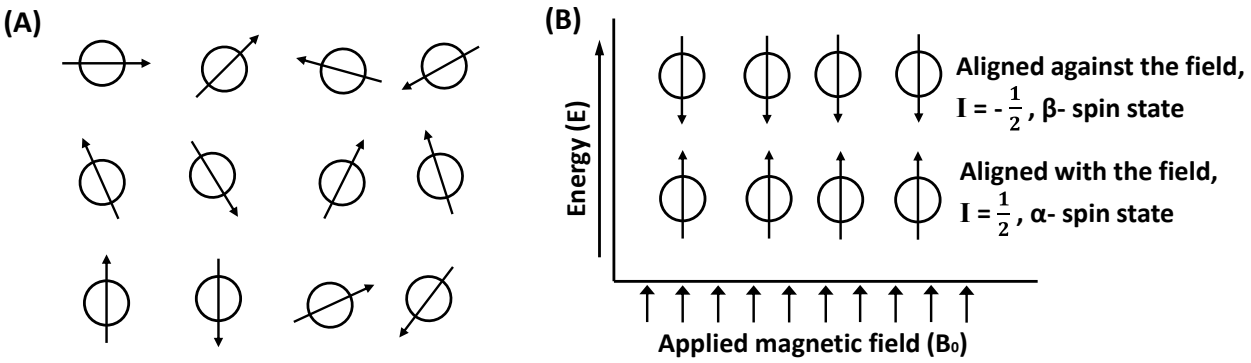

Figure 3.28. Orientation of spinning nuclei in the absence **(A)** and present **(B)** of an external magnetic field[7].

The nuclei aligned with the applied magnetic field has lower energy and refers to the α-spin state when I is $\frac{1}{2}$, while the nuclei aligned against the applied magnetic field possess higher energy. This is referred to as the β-spin state when I is $-\frac{1}{2}$. The energy difference (ΔE) between the two spin states increase with the applied magnetic field strength (Figure 3.6). The two spin states of hydrogen nuclei have the same energy when the external field is zero, but diverge as the field increases.

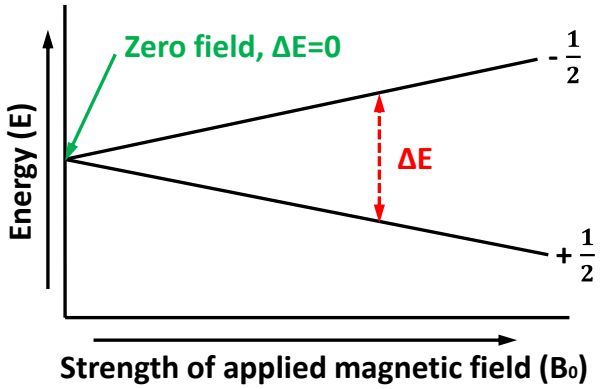

Figure 3.29. The relationship between the energy difference of two spin states and the strength of external magnetic field[12].

When the applied energy of electromagnetic radiation is equal to the ΔE, the hydrogen nuclei can transit from the more stable state to the less stable state. This indicates magnetic resonance occurs. The value of ΔE is a function of the magnetogyric ratio (γ), the strength of the external magnetic field (B_0) and Plank's constant (h).

$$\Delta E = \gamma B_0 h \qquad (2.25)$$

The electromagnetic frequency (ν) of the radiation needed to cause a transition of the hydrogen nuclei is given by equation (2.26)[13].

$$\nu = \frac{\gamma B_0}{2\pi} \qquad (2.26)$$

However, in every nucleus of molecule, a secondary magnetic field will be generated as a result of the moving of the electron surrounding the nucleus in response to an applied magnetic field (B_0). The orientation of this second field is opposite to the external field and it can shield the nucleus from the external field. Although the shielding effect is only of the order of parts per million of B_0, this can be measured using the NMR spectroscopy. A chemical group which is bonded to the hydrogen nucleus and donates electrons increases the shielding effect; whereas, if it withdraws electrons such as any group containing π bond, it can de-shield the nucleus. Hence, the hydrogen nucleus in the same molecules but in different local environment (different group) have different magnetic field (B) and absorb energy at different frequency. Hence, magnetic resonance occurs at a different frequency. The hydrogen nucleus can then be identified. The absorptions for a sample are referred to as chemical shifts compared to those of a reference standard. The tetramethylsilane (TMS), $Si(CH_3)_4$, is reference compound since its protons signal and the signal from sample cannot overlap because the silicon atom is more electropositive than carbon[7]. The chemical shifts (σ) can be calculated by the following equation:

$$\sigma \text{ (or ppm)} = \frac{v_s - v_r \text{ in } Hz}{Oscillator\ frequency \text{ in } Hz} \times 10^6 \qquad (2.27)$$

where the v_s and v_r, are the absorption frequencies of the sample and the reference in Hz, respectively[7].

Figure 3.7 shows the design for a typical NMR spectrometer. A solution of sample in a 5 mm glass tube is oriented between two strong magnets to increase the homogeneity of

magnetic field on samples. Radio frequency radiation of appropriate energy is broadcast to the sample from radio-frequency transmitter via a transmitter coil. A receiver coil surrounds the sample tube. The absorption of energy causes a tiny electric current to flow from the radio-frequency receiver via the receiver coil. The current is amplified and recorded as a signal by the recorder. A ^{1}H NMR spectrum is displayed as a plot of a series of signals (or peaks) of chemical shifts (σ). Each peak represents hydrogen protons in the same local environment and the areas under the peaks (the intensities of the peaks) are proportional to the number of hydrogen protons. ^{1}H NMR spectroscopy is used to characterise the synthesised photo-labile *o*-nitrobenzyl moiety crosslinker (nPh) and coumarin moiety monomer (CMA) in this study.

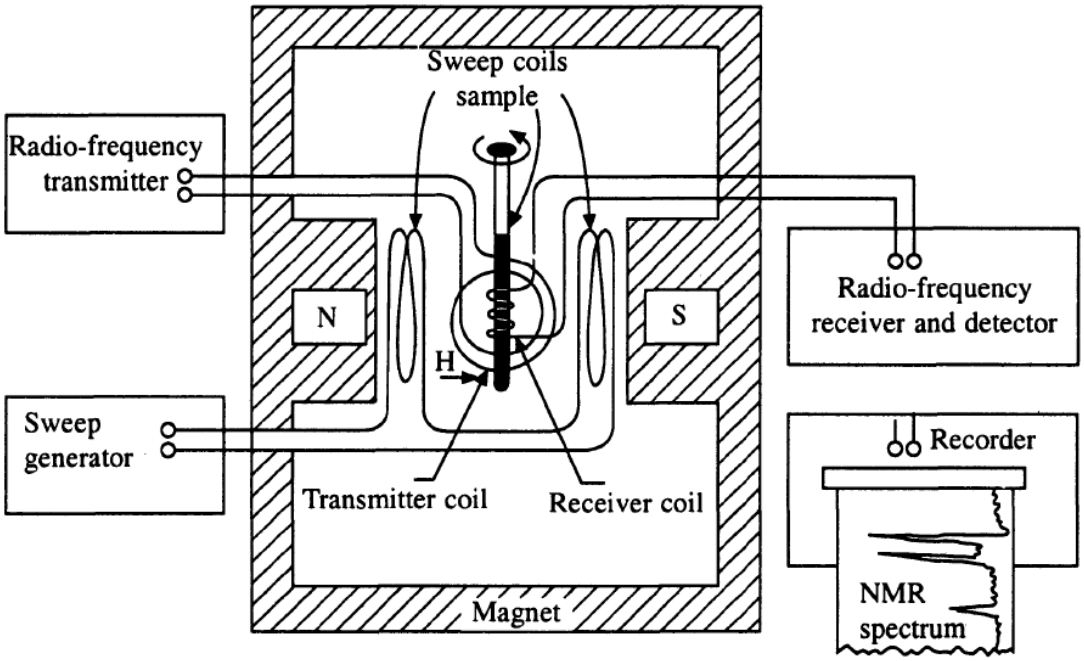

Figure 3.30. Schematic diagram of a NMR spectrometer[7].

3.5 Potentiometric titration

Potentiometric titration is a method for analysis of acidic groups and basic groups in which the change of pH is measured as a function of the added reagent volume. The change of pH is monitored using a pH electrode. Herein, it is used to measure the carboxylic acid groups (RCOOH) in MG particles and the pK_a values of MGs in this

thesis. In this way, a strong standardising base (NaOH, 0.01 M) is introduced to the mixture of MG dispersion (0.1 wt. %) and electrolyte solution (NaCl, 0.05 M), the RCOOH can be deprotonated to an anion of a conjugate base ($RCOO^-$). The electrolyte solution was used in order to keep the NaOH contacting the RCOOH fully. The deprotonation of RCOOH groups in water as shown in the following equations[14-15]:

$$RCOOH_{(aq)} + H_2O \leftrightarrow RCOO^-_{(aq)} + H_3O^+_{(aq)} \quad (2.28)$$

$$K_a = \frac{[products]}{[Reactants]} = \frac{[RCOO^-][H_3O^+]}{[RCOOH]} \quad (2.29)$$

$$pK_a = -\log_{10} K_a \quad (2.30)$$

K_a is the acid dissociation constant. *[RCOOH]* and *[$RCOO^-$]* are the molar concentrations of acid and conjugate base, respectively. The pK_a indicates the relative acidities of acids and bases. Compared with the strong acids which completely dissociate acid, the weak acids tend to dissociate partially until achieving equilibrium in an aqueous solution. Figure 3.8 shows a typical potentiometric titration plot of weak acid. It can be seen that the mixture reaches an equivalence point where the acid is neutralised.

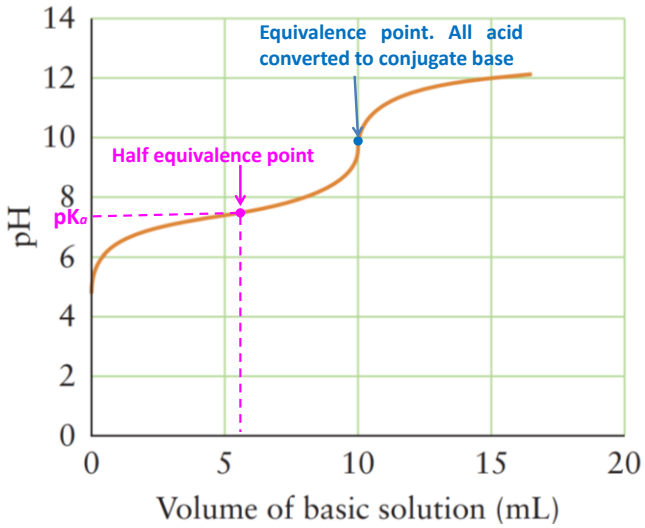

Figure 3.31. A typical plot of potential titration used to determine equivalence points and pKa values[16].

According to the Henderson-Hasselbalch, the relationship between pH and pK_a can be expressed by Equation[14] (2.31).

$$\text{pH} = pK_a + \log_{10}\frac{[RCOO^-]}{[RCOOH]} \quad (2.31)$$

The degree of neutralisation (a) can be expressed by Equation[17](2.32),

$$a = \frac{[RCOO^-]}{[RCOOH] + [RCOO^-]} \quad (2.32)$$

The Henderson-Hasselbalch equation can be further expressed as the following equation [18],

$$\text{pH} = \text{p}K_a + \log_{10}\frac{[a]}{[1-a]} \quad (2.33)$$

In the case of 50% of ionisation of the acid, a half equivalence point is attained. According to Equation 2.33, pH = pK_a can at this position. The pK_a values of MGs in this thesis were around 6.0, which means 50% of RCOOH was deprotonated to $RCOO^-$ and MGs swell due to electrostatic repulsion of negative charge. The amount of *RCOOH* can be calculated based on the consumption of NaOH when all RCOOH is converted to $RCOO^-$.

3.6 Transmission electron microscopy

Transmission electron microscopy (TEM) is a very powerful tool for visualisation of specimens in the realms of microscale to nanoscale with high-resolution. The electron microscope uses an electron beam. The resolution of microscopy depends on the wavelength of beam. Illumination with a smaller wavelength results in better resolution[19]. The electron microscope produces higher resolution images than the light microscope because the wavelength of an electron beam (~ 4×10^{-12} m with 100 keV acceleration) is much smaller than visible light (~ 500 nm). For this reason, the TEM requires a vacuum to avoid the scattering of beam from molecules present in air.

TEM has three essential systems: an electron gun, the image-producing system and the image-recording system. The electron gun is located in the top of instrument and generates the electron beam via heating the tungsten filament. The intensity and angular aperture of the beam are controlled by the condenser lens system between the gun and the specimen. Normally, two condenser lenses are employed. The first condenser lens produces a reduced image of the source, which is then imaged by the second lens onto the specimen. When the electron beam illuminates the specimen, some areas of the specimen scatter or absorb electrons and other areas transmit electrons. In the image-producing system, the scattered electrons pass through an objective lens and are focued to form the primary image. The primary image is magnified using additional lenses (Intermediate lens and Projector lens) to form a highly magnified final image. For practical reasons of image stability and brightness, the microscope is often operated to give a final magnification of 1,000-250,000× on the screen. The image-recording system consists of a charge coupled device (CCD) camera, binoculars and viewing screen. The monochromatic image is projected onto the fluorescent viewing screen to allow it visible to eye. The binoculars are used to focus the image. The image in screen is a temporary image. To collect a permanent image a CCD camera is inserted into the path of the beam and collects the image in a digital form. Figure 3.9 shows the schematic diagram of a TEM.

Herein, the size and light-induced morphology changes of MGs are characterised by TEM using a FEI Tecnai 12 BioTwin instrument at an accelerating voltage of 100 kV. The samples were stained with uranyl acetate solution and supported by 300 mesh carbon supported film on copper TEM grids. The TEM grid was plasma glow-discharged for 1 min to create a hydrophilic surface. The TEM grid was placed onto particle dispersion

droplet and then uranyl acetate solution for 1 min respectively, and then blotted with filter paper to remove excess solution. Each grid was then carefully dried at room temperature.

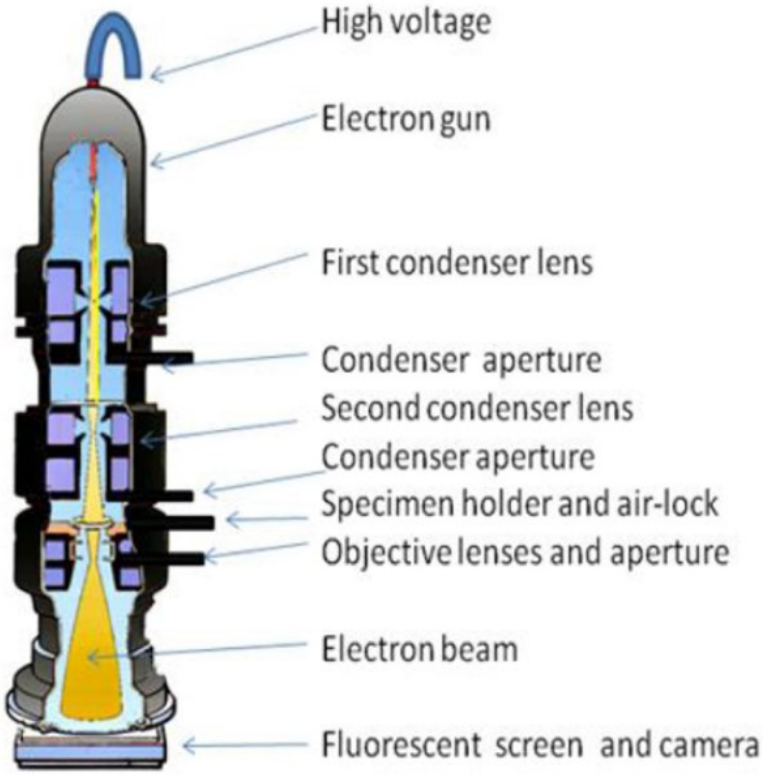

Figure 3.32. Schematic diagram of a TEM[20].

3.7 References

1. Pecora, R., *Dynamic light scattering : applications of photon correlation spectroscopy*. Plenum Press: New York, 1985; p xiv, 420 p.

2. Alexander, M.; Dalgleish, D. G., Dynamic light scattering techniques and their applications in food science. *Food Biophys* **2006,** *1* (1), 2-13.

3. Bhattacharjee, S., DLS and zeta potential - What they are and what they are not? *J Control Release* **2016,** *235*, 337-351.

4. Carvalho, P. M.; Felicio, M. R.; Santos, N. C.; Goncalves, S.; Domingues, M. M., Application of Light Scattering Techniques to Nanoparticle Characterization and Development. *Front Chem* **2018,** *6*.

5. Chu, B., *Laser light scattering: basic principles and practice*. Courier Corporation: 2007.

6. Lopez, M. D. A., Ultraviolet Spectroscopy- Visible (Uv-Vis). *Bibl Cienc* **2011,** *39*, 51-108.

7. Yadav, L. D. S., *Organic spectroscopy*. Kluwer ; Anamaya Publishers: Dordrecht Netherlands ; Boston New Delhi, 2005; p x, 324 p.

8. Perkampus, H.-H., *UV-VIS spectroscopy and its applications*. Springer-Verlag: Berlin ; New York, 1992; p ix, 244 p.

9. Anderson, R. J.; Bendell, D. J.; Groundwater, P. W.; Royal Society of Chemistry (Great Britain), *Organic spectroscopic analysis*. Royal Society of Chemistry: Cambridge, 2004; p vi, 176 p.

10. Staurt, B., Infrared spectroscopy: fundamentals and applications. *John Wiley and Sons, Ltd., West Sussex, England. DOI* **2004,** *10*, 0470011149.

11. Lin, S. Y.; Dence, C. W., *Methods in lignin chemistry*. Springer-Verlag: Berlin ; New York, 1992; p xxx, 578 p.

12. Fleming, I.; Williams, D. H., *Spectroscopic methods in organic chemistry*. McGraw-Hill New York: 1966.

13. Young, R. J., *Introduction to polymers*. Chapman and Hall: London ; New York, 1981; p viii, 331 p.

14. Po, H. N.; Senozan, N. M., The Henderson-Hasselbalch equation: Its history and limitations. *J Chem Educ* **2001,** *78* (11), 1499-1503.

15. Dell, A.; Beggs, J.; Panico, M., Principles of Biochemistry - Lehninger,A. *New Sci* **1983,** *98* (1357), 398-399.

16. Atkins, P. W.; Jones, L., *Chemical principles : the quest for insight*. W.H. Freeman: New York, 1999.

17. Meychik, N. R.; Yermakov, I. P., Ion exchange properties of plant root cell walls. *Plant Soil* **2001,** *234* (2), 181-193.

18. Fisher, S.; Kunin, R., Effect of Cross-Linking on the Properties of Carboxylic Polymers .1. Apparent Dissociation Constants of Acrylic and Methacrylic Acid Polymers. *J Phys Chem-Us* **1956,** *60* (7), 1030-1032.

19. Tanaka, N., Structure and Imaging of a Transmission Electron Microscope (TEM). *Electron Nano-Imaging: Basics of Imaging and Diffraction for Tem and Stem* **2017**, 17-28.

20. Brydson, R. M.; Hammond, C., Generic methodologies for nanotechnology: characterization. *Nanoscale Science and Technology* **2005**, 56-129.

Chapter 4: Triply-responsive hydrogels assembled from OEGMA-based microgels containing a photo-cleavable crosslinker

4.1 Abstract

In this chapter, a series of triply responsive microgels (MGs) were prepared using the co-monomers oligo(ethylene glycol) methacrylate (OEGMA), 2-(2-methoxyethoxy)ethyl methacrylate (MEO_2MA), methacrylic acid (MAA) and a synthesised o-nitrobenzyl-based UV photocleavable crosslinker (nPh) and studied fully. This MGs containing different amount of crosslinker can swell or collapse in response to pH and temperature and degradatiom when irradiated with UV light. The MGs were then functionalised with glycidyl methacrylate (GMA) to prepare GMA-functionalised MGs that were formed as doubly cross-linked microgels (DX MGs) through pH-induced swelling and free-radical coupling of the vinyl groups. The swellings and mechanical properties of OEGMA-based DX MG gels were then investigated and were pH-, temperature- and UV-light responsive. Those DX MGs were compared with the parent MGs. Unexpectedly, increasing the crosslinker content in the MGs did not restrict MG particle swelling, but the swelling ratio and mechanical properties of DX MGs were affected by crosslinker content significantly. The UV light treatment degraded the MGs but enhanced the mechanical properties of DX MGs compared with a control. This was attributed to the light-triggered polyampholyte network formation in the DX MGs. Besides, the DX MGs are injectable gels that were not cytotoxic to nucleus pulposus cells. Hence, this new family of multi-responsive DX MGs had potential application for soft tissue repair as injectable gels or as gel implants which report sterilisation.

4.2 Introduction

Multiple stimuli-responsive microgels (MGs) and hydrogels have raised considerable attention and interest in recent years for biomedical applications such as anticancer therapies[1], protein release[2, 3], drug delivery[4-6] and tissue regeneration[7-8] because of their smart properties. For smart microgels, the physico- chemical properties such as size, water content, shape, cross-linker density or hydrophilicity and hydrophobicity will change if environmental factors change. They include chemical factors (pH[9-10], ionic species[11], biological[4]) and physical factors (temperature[12], light[13], magnetic field[14]). For those stimuli, light has excellent potential. This is because light is an external stimulus that can be controlled in a very precise manner in terms of control over wavelength, intensities, and duration times and does not require physical contact[15-16].

Thermal- and pH- sensitive MGs are also well studied. Thermally responsive MGs undergo a temperature-induced swelling and deswelling transition at the volume phase transition temperature (VPTT) due to a conformational change of the polymer chains[17-18]. The introduction of functional monomer (e.g., carboxylic acids, amines) by random copolymerisation provides the pH sensitivity to the MGs. Poly(N-isopropylacrylamide) (PNIPAM) which is the most known temperature-responsive polymer[19] undergos a temperature induced phase transition with a lower critical solution temperature (LCST) at 31 °C[18]. But the toxicity of NIPAM limit may the application of this kind of microgles in biomaterial[20]. A more biocompatible alternative to PNIPAM MGs, poly(N-vinylcaprolactam) (PVCL) MGs, which exhibits an LCST of 32 - 36 °C was reported for biomedical applications[4, 20]. However, care is needed to introduce an acid-based comonomer into these MGs because VCL monomer is prone to hydrolysis under acid condition[21]. As an alternative, the POEGMA-based MGs have gained considerable interests due to its excelled biocompatibility and stability to acid conditions[22-23]. These

type of MGs can be traced to the seminal work of Lutz et al. who discovered that thermo-responsive behaviour could be obtained from copolymers of oligo(ethylene glycol) methacrylate (OEGMA) and 2-(2-methoxyethoxy)ethyl methacrylate (MEO_2MA)[24]. $PMEO_2MA$ and POEGMA have lower critical solution temperatures (LCSTs) of 29 and 90 ^oC, respectively[25]. MGs containing different ratios of these monomers have volume-phase transition temperatures (VPTTs) that can be tuned within this temperature range[26]. P(MEO_2MA-co-OEGMA-co-MAA) MGs are responsive to both pH and temperature[27-28]. For this kind of MG, MAA was distributed uniformly but the nature of hydrophobicity or hydrophilicity of crosslinker strongly affects their morphology. Boularas et al found that the ethylene glycol dimethacrylate (EGD)-crosslinked MG strongly differed from oligo(ethylene glycol) diacrylate (OEGDMA) and N,N-methylenebisacrylamide (MBA). The EGD-based MGs showed the structure of densely crosslinked core and loosely crosslinked shell, whereas the OEGDMA-based MGs showed homogeneously crosslinked distribution and MBA-crosslinked MGs showed the crosslinking enrichment in the shell with a slightly crosslinked core[29-31].

In this chapter, the photo-cleavable crosslinker, 2,2'-(2-nitro-1,4-phenylene)bis(methylene)bis(oxy)bis(oxomethylene) bis(azane-diyl)bis(ethane-2,1-diyl) bis(2-methylacrylate) (denoted as nPh), is synthesised (Shown in Scheme 4.1.) This crosslinker would degrade with irradiation by 254 nm light and form the cationic $–NH_3^+$ groups.

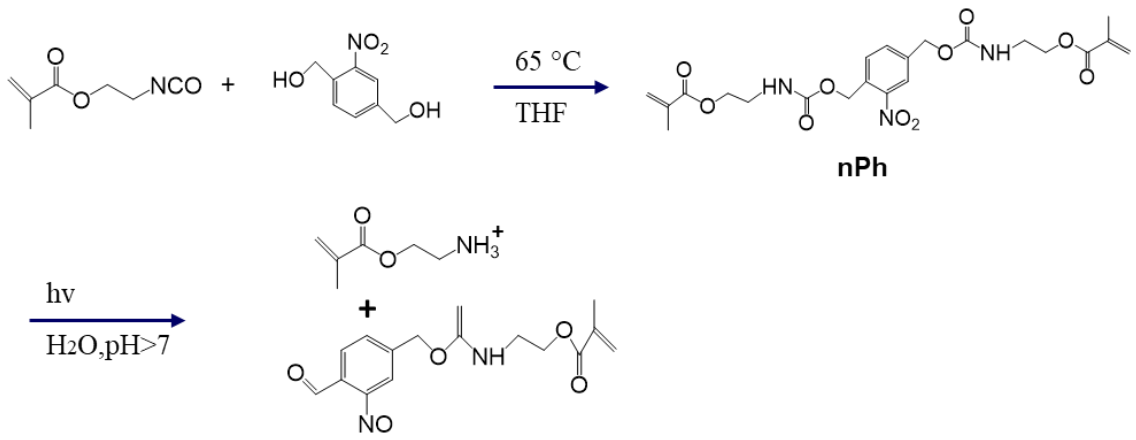

Scheme 4.1. Depiction of synthesis of nPh and photo-triggered degradation

A triple-responsive precursor MG-*x*-nPh (where *x* is the mol% of nPh used during MG synthesis) containing MEO_2MA, OEGMA, MAA and photo-cleavable crosslinker (nPh) was prepared by free-radical aqueous batch precipitation copolymerisation. Due to the hydrophobicity of nPh, I used EGD as a model crosslinker to form a control MGs (MG-*x*-EGD, where *x* is the mol% of EGD used during MG synthesis) for comparison. In contrast to an earlier MG study using nPh[32], here it has been included within a water-swellable MG for the first time. I show that OEGMA-based MGs containing nPh are pH- and thermally- responsive and UV-light degradable. The generation of cationic $–NH_3^+$ groups results from UV cleavage of nPh which leads to ionic bonding for the gels (Scheme 4.2).

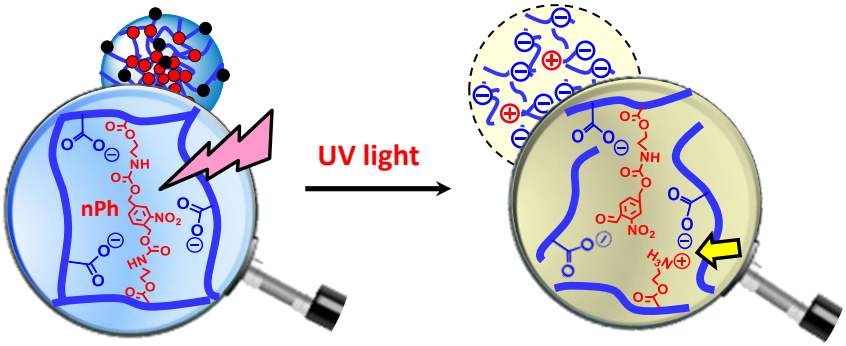

Scheme 4.2. Depiction of the UV light-triggered cleavage of nPh crosslinker resulting in ionic bond formation (yellow arrow). The ionic crosslinks are weak and the MGs disassemble in water.

Scheme 4.3A depicts the approach used to prepare the triply responsive precursor MGs. The precursor MGs were functionalised with glycidyl methacrylate (GMA) which reacted with a minor proportion of carboxylic group of MAA via an epoxide ring-opening reaction[33] to form the functionalised MGs. The concentrated MG dispersions become viscous when the pH is increased due to electrostatic repulsion of -COO^- groups. Inter-MG crosslinking was achieved via free-radical inter-MG linking in the presence of ammonium persulfate (APS) to give triply responsive DX MGs (Scheme 4.3B). The DX MG-*x*-nPh gels had two crosslink networks present; one inside the MGs that was photocleavable (via nPh) and a second from coupling between GMA.

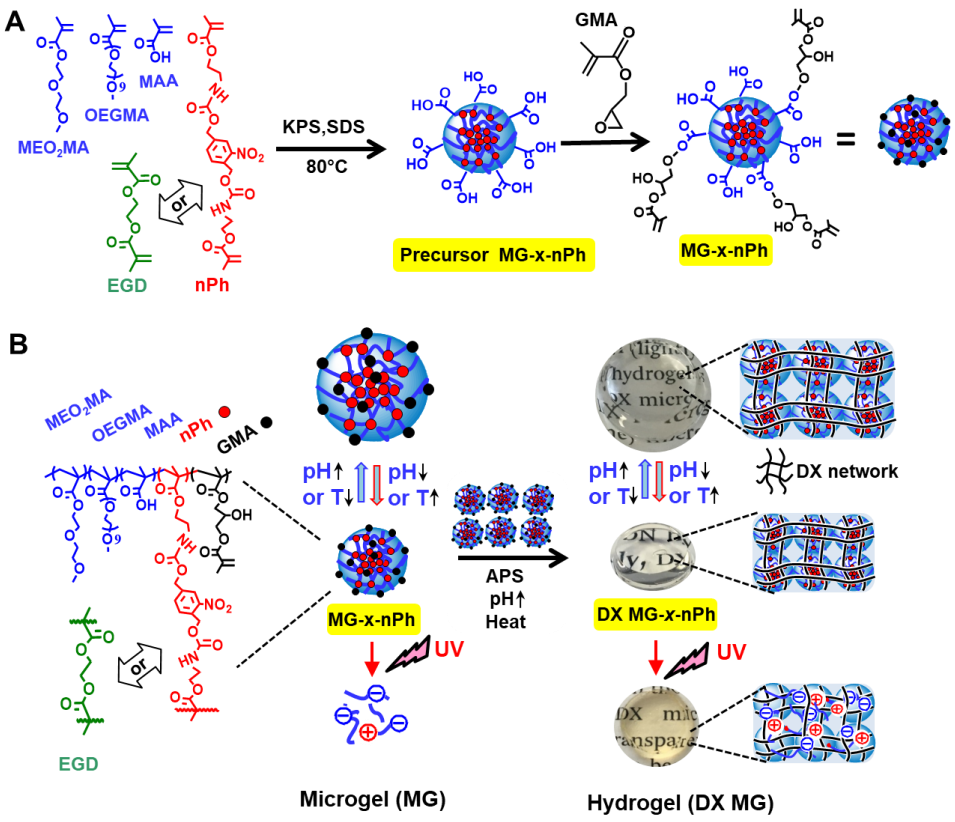

Scheme 4.3. Synthesis of triply responsive **(A)** microgels (MGs) and **(B)** DX MG gels. The pH, temperature and UV-light triggered responses are depicted. The structure of the control ethyleneglycol dimethacrylate (EGD) crosslinker is shown in (A). The precursor MGs were functionalised with GMA. The GMA units are crosslinked to form the DX MG gel (B). We propose that nPh and GMA, respectively, are relatively concentrated in each MG core and evenly distributed throughout the MGs.

This study begins with an investigation of properties of parent MG-*x*-nPh. All MGs showed significant pH- and temperature- sensitivity and light degradation behaviours. The higher concentration of nPh or EGD did not restrict the swelling behaviours of MGs due to the densely crosslinked core and loosely crosslinked shell structure. The relationship between UV light-triggered disassembly of the MG-*x*-nPh particles and nPh concentration was also investigated. I found that the lower concentration of nPh triggered faster degradation of the MGs. The DX MGs also showed the strong pH-, temperature- and UV light-dependence in swelling ratio and mechanical properties. The GMA-based crosslinking that occurs during the DX MG formation is prepared to have engaged the previously core-rich and shell-poor crosslinks. The gels are also UV light-responsive and mechanical behaviours and remarkably different to those of the parent MGs. The photo-generation of a nanostructured polyampholyte hydrogel is shown to strengthen the gel. Live/Dead assays show that the gels are not cytotoxic. These new gels have potential applications as injectable gels for soft tissue repair or as gel implants with a built-in visual display for UV-light sterilisation.

4.3 Experimental details

4.3.1 Materials

MEO_2MA (95%), OEGMA (M_n = 500 g/mol, 95%), EGD (98%), MAA (98%), GMA (97 %), sodium dodecyl sulfate (SDS, 98.5 %), *N,N,N′,N′*-tetramethylethylenediamine (TEMED, 99%), potassium persulfate (KPS, 99%), ammonium persulfate (APS, 98%,), 2-isocyanatoethyl methacrylate (98%), $CHCl_3$ (99%), methanol (99.8%), hexane (95%) and tetrahydrofuran (THF, 99%) were all purchased from Aldrich. Mono-2-(methacryloyloxy)ethyl succinate (95%) was purchased from Tokyo Chemical Industry. All chemicals were used as received. The water used was doubly filtered and deionised.

4.3.2 Synthesis of photocleavable crosslinker

The synthesis method of UV-cleavable crosslinker nPh followed that of Klinger and Landfester[32]. Briefly, mono-2-(methacryloyloxy)ethyl succinate (1.00 g, 5.5 mmol) was dissolved in anhydrous THF (10.0 mL) and added dropwise to a solution of 2-isocyanatoethyl methacrylate (1.71 g, 11.0 mmol) in anhydrous THF (15.0 mL) under nitrogen. The reaction mixture was heated to 65 °C and stirred for 24 h. After cooling to room temperature the solvent was evaporated and the residue was purified by column chromatography over silica using $CHCl_3$/MeOH (10:1) as eluent yielding 70% of nPh (1.90 g, 4.9 mmol).

4.3.3 Microgel synthesis

The MGs were prepared by aqueous precipitation copolymerisation with different comonomer compositions as shown in Table 4.1. The synthesis for MG-1.00-nPh is given as an example. Briefly, SDS (60 mg) was dissolved in water (240 mL) and the solution was purged with nitrogen gas in a three-neck reactor for 60 min. A comonomer solution

(2.765 mL) of MEO_2MA, OEGMA and MAA was prepared with a mass ratio of MEO_2MA and OEGMA of 9:1, 10.5 wt.% of MAA. This ratio was kept constant for all the MG-x-nPh systems. The nPh (84.0 mg) was added. An aqueous solution of KPS (60 mg in 12 mL water) was subsequently added after the temperature reached 70 °C. The polymerisation was continued for 6 h under a nitrogen atmosphere and cooled to room temperature. The dispersion was extensively dialysed against water for 7 days. The MG-x-EGD dispersions were prepared following the same procedure but replacing nPh with EGDMA on a mol basis (see Table 4.1).

Table 4.1 Comonomer formulations used to prepare the MGs

Microgels	MEO_2MA / wt.%	OEGMA / wt.%	MAA / wt.%	nPh / wt.%	EGD / wt.%
MG-0.15-nPh	80.2	8.9	10.5	0.4	-
MG-0.45-nPh	79.4	8.8	10.5	1.3	-
MG-0.65-nPh	79.0	8.8	10.4	1.8	-
MG-1.00-nPh	78.2	8.7	10.3	2.8	-
MG-0.15-EGD	80.3	8.9	10.6	-	0.20
MG-1.00-EGD	79.6	8.8	10.5	-	1.1

4.3.4 GMA functionalisation of the microgels

The pH of the MG dispersion (1.0 wt.%, 120 mL) was adjusted to 5.0 then GMA (0.65 mL) was added while stirring. The mole ratio of GMA to MAA used was fixed at 3.0. The dispersion was left to stir for 8 h at 40 °C. The dispersion was then washed with hexane twice and residual solvent removed by rotary evaporation.

4.3.5 DX MG preparation

DX MG gel preparations were performed at 37 or 50 °C. The gels used for cytotoxicity studies were prepared at 37 °C. All other gels were prepared at 50 °C. To prepare the DX MG at 50 °C, GMA functionalised MG (1.0 mL, 14.0 wt%) was mixed with APS (78.0

mM, 70 μL) and then NaOH (4.0 M, 30 μL) added and mixed. The mixture became viscous when the pH was adjusted to 7.4. The viscous mixture was transfered to an O-ring and sandwiched between two glass slides and then fixed using clamps and cured at 50 °C for 12 h. To prepare the DX MG at 37 °C, the NaOH solution used above was changed to alkaline TEMED solution (31 μL) which contained NaOH solution (4.0 M) and TEMED at a volume ratio of 48:2. The mixed dispersion was cured at 37 °C for 12 h. Other procedures are the same as described above.

4.3.6 Photodegradation experiments

Irradiation of MGs and DXMGs was conducted using a CL 1000 Ultraviolet Crosslinker equipped with five lamps which provided a wavelength of 254 nm and an intensity of 10 mW/cm^2 unless otherwise stated. The MG dispersions were irradiated in Quartz cuvettes. The DX MGs were sealed in a mold (inner diameter = 12.0 mm and height = 12.0 mm) with quartz slides at the ends.

4.3.7 Cytotoxicity experiments

The following experiments were conducted by Dr. Daman Adlam (School of Biological Sciences, University of Manchester). Human nucleus pulposus (NP) cells were cultured in Dulbecco's modified Eagle's medium (DMEM) supplemented with antibiotic/antimycotic (Sigma-Aldrich, UK), Glutamax and 10% fetal bovine serum (Thermo Fisher Scientific, UK). It was put in a humidified 5% CO_2 incubator at 37 °C. NP Cells were harvested by trypsinisation and seeded at a density of 5×10^4 cells per well onto 13 mm sterile glass coverslips in 24 well culture plates. In this experiment, two kinds of DX MG gel (DX MG-0.65-nPh and DX MG-1.00-EGD) were used. After overnight incubation, NP cell culture media was changed and Toroid shaped gels, sterilized in 70% ethanol for 10 mins and rehydrated with several changes of sterile phosphate buffered

saline (PBS), were introduced into the appropriate wells. Control NP cultures received an equal volume of PBS. Cells were cultured up to eight days and live/dead assays (Thermo Fisher Scientific, UK) were performed at each time-point (n=2) according to the manufacturer's instructions. Images were obtained with an Olympus BX51 fluorescence microscope and a Lietz Diavert inverted phase contrast light microscope.

4.3.8 Physical Measurements

^{1}H NMR (400 MHz) spectra of nPh were measured using a Bruker spertrometer with $CDCl_3$ as solvent. UV-Vis absorption of the nPh and microgel dispersions was measured on a PerkinElmer Lambda 25 UV/VIS spectrometer Titration measurements were used to characterize the pK_a of synthesized MG and GMA functionalised MGs in the presence of aqueous 0.05M NaCl using a Mettler Toledo Titration instrument. The titrant was aqueous NaOH solution (0.01M). Dynamic Light Scattering (DLS) measurements were performed using a Malvern Zetasizer NanoZS scattering apparatus, fitted with a 20 mW HeNe laser. Backscatter measurement were performed to characterise the size of MG and GMA functionalised MGs. TEM images were obtained using a FEI Tecnai 12 BioTwin instrument and were stained using uranyl acetate solution. The number-average diameters from TEM images were obtained using Image-J software which produces such output parameters as number of particles, maximum and minimum length, mean length and standard deviation. Uniaxial compression stress-strain data for the gels were obtained using an Instron series 5569 load frame equipped with a 10 N compression testing head. A cylindrical sample geometry with diameter of 12 mm and height of 12.5 mm was used. The volume swelling ratio values for the gels were determined by gravimetrical method. The DX MGs were placed into 0.10 M buffer solution and weighed every day for 5 days. The Q values were calculated using equation (4.1).

$$Q = \rho_p \left(\frac{Q_m}{\rho_s} + \frac{1}{\rho_p} \right) - \frac{\rho_p}{\rho_s} \qquad (4.1)$$

Where Q_m is the ratio of swollen gel mass to the dry gel mass. The parameters ρ_p and ρ_s are the density of solvent and polymer, which are taken as 1.0 and 1.2 g/mL, respectively.

4.4 Results and Discussion

4.4.1 Characterisation of nPh crosslinker

The photo-cleavable crosslinker nPh was characterised by ^{1}H NMR and UV-vis spectrum. Figure 4.1 shows the ^{1}H NMR for nPh, ^{1}H NMR ($CDCl_3$) ppm: 8.01 (s, 1H), 7.55(d, 2H), 7.50(s, 2H), 6.06(t, 2H), 5.43-5.53(s, 4H), 5.09(s, 4H), 4.18(t, 4H), 3.47(m, 4H), 1.87(s, 6H).

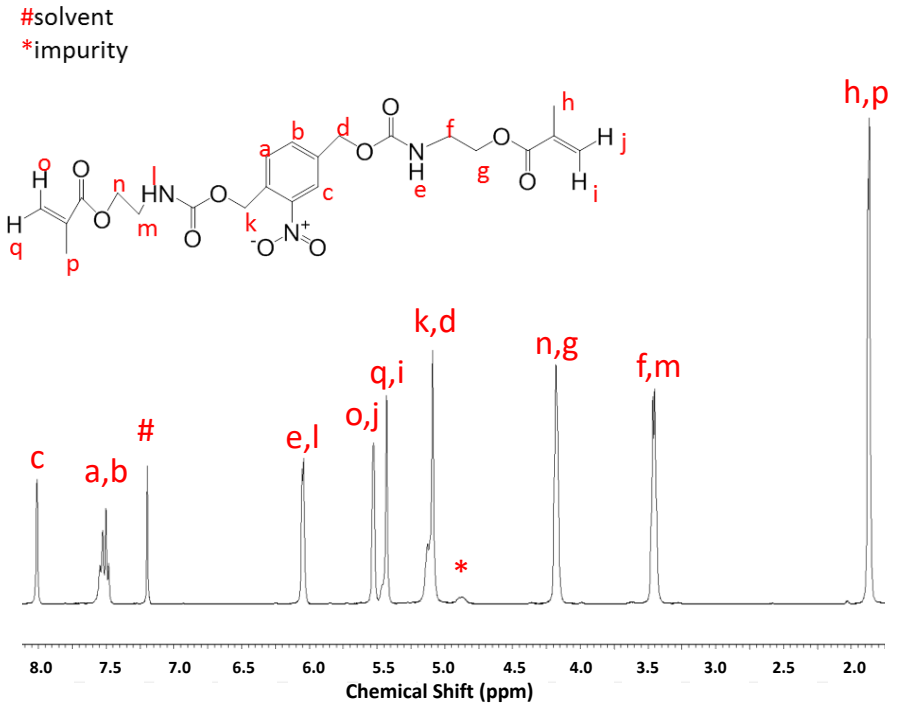

Figure 4.1.^{1}H NMR spectrum and assignments for nPh

The time-dependence UV-vis spectrum measurements for crosslinker nPh in MeOH were also measured (Figure 4.2A). Before UV treatment, nPh shows an absorption maximum at 260 nm accompanied by a tail up to 370 nm. With the UV light irradiation, the absorption peak at 260 nm decreased gradually and diminished, whereas the absorption peak at at 312 increased. This indicates the successful photoreaction which forms the nitroso-benezaldehyde photolysis product (Scheme 4.1). Although it indicates a successful photoreaction, there are no defined isosbestic points in the spectra of nP. It is impossible to find the same absorbance at all range of wavelength in inserted Figure 4.2A

during the photoreaction. This indicates the production of photoreaction side products[32]. The side products (structure was shown in Figure 4.2B), is a dimeric azobenzene compound formed by dimerisation of the primary nitroso groups at longer irradiation times[34-35] and was proved to form the new divinyl group[32]. Irradiation with light at a wavelength λ > 300 nm does not affect this new divinyl group. Light at a wavelength of 254 nm needs to be applied which is well known to cleave azobenzene groups[32]. Hence, in this study, we used the UV-C (200 - 280 nm) light to illuminate the MGs and DX MGs.

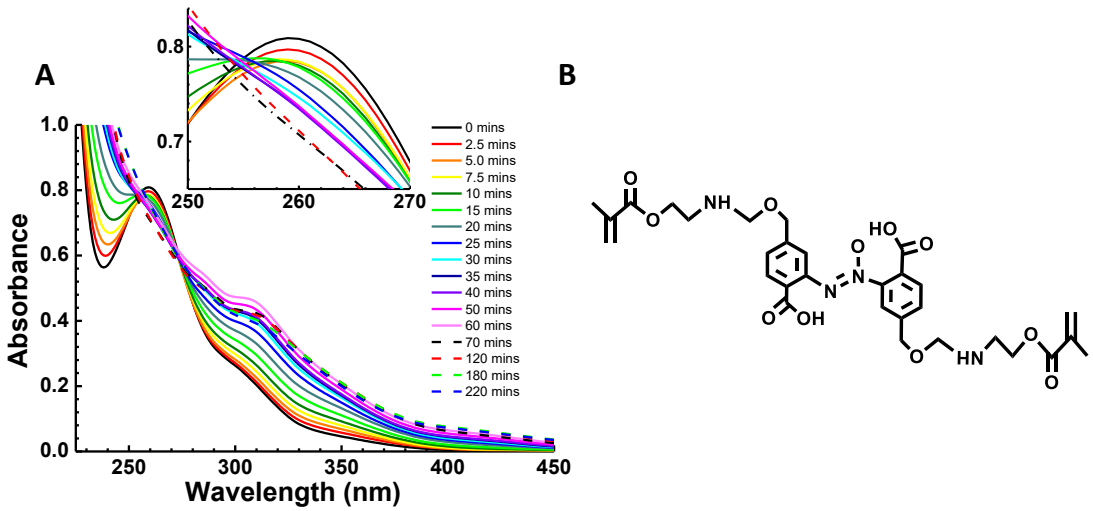

Figure 4.2. (A) Time-dependent UV-vis spectrum for the photocleavage of nPh in CH_3OH (0.15 mM) as a consequence of irradiation with UV light (365 nm). **(B)** Molecular structure of photoreaction dimeric products of nPh[32].

4.4.2 Composition and properties of the MGs

Four precursor MG-*x*-nPh were synthsised containing different amounts of crosslinker nPh (*x*) ranging from 0.15 to 1.00 mol%. Two control precursor MG-*x*-EGDs (where *x* is 0.15 and 1.00 mol%) were prepared as well. Synthesis details are given above and in Table 4.1. All precursor MGs were functionalised with GMA to form vinyl-functionalised MGs (namely, MG-0.15-nPh, MG-0.45-nPh, MG-0.65-nPh, MG-1.00-nPh, MG-0.15-EGD and MG-1.00-EGD).

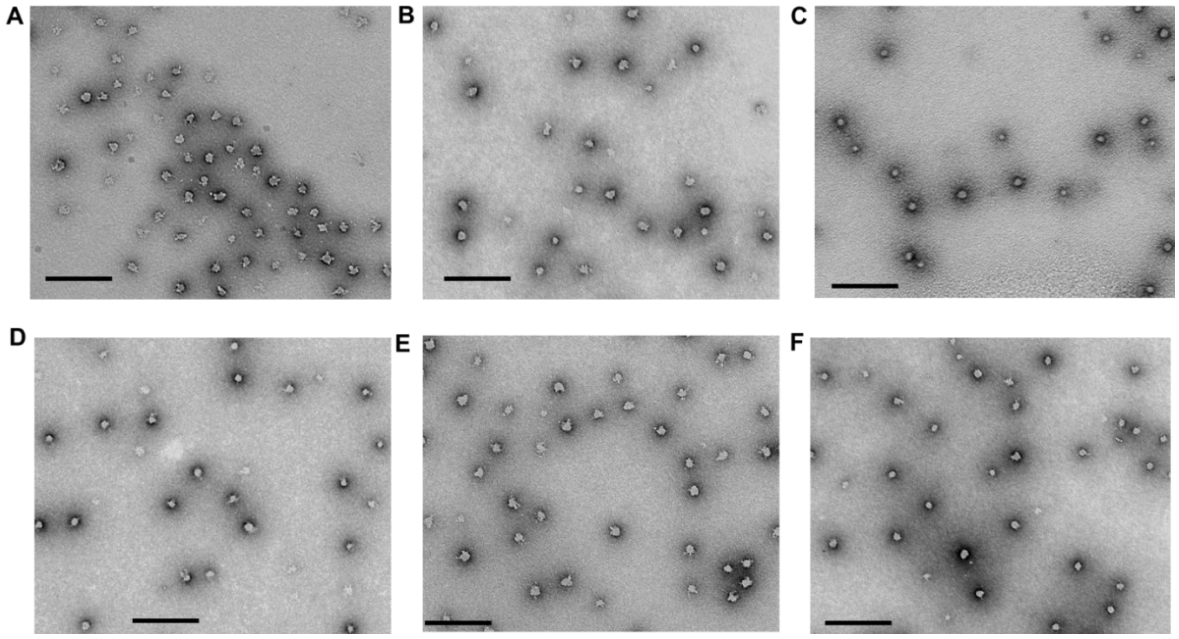

Figure 4.3. TEM images measured for **(A)** MG-0.15-nPh, **(B)** MG-0.45-nPh, **(C)** MG-0.65-nPh, **(D)** MG-1.00-nPh,**(E)** MG-0.15-EGD and **(F)** MG-1.00-EGD. The scale bars are 500 nm.

Figure 4.3 shows those six functionalized MGs are spherical particles via TEM images and have collapsed number-average diameters (d_{TEM}) in the rang 50 - 59 nm. The d_{TEM} values are smaller than the respective average diameter measured with DLS (d_z) at thre collapsed stage ie., pH 5.4 at 60 °C at 55 - 65 nm (see Table 4.2). This is because the d_z values are strongly weighted towards the largest particles and there was significant size polydispersity for each of the MGs.

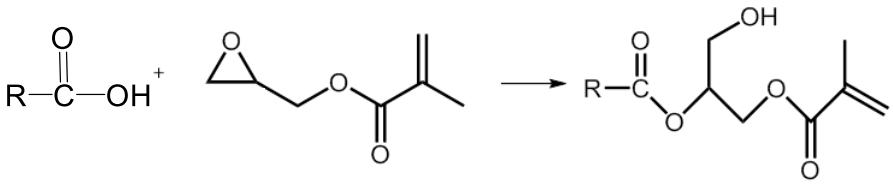

Figure 4.4. The mechanism of the GMA functionlisation reaction.

GMA reacted with the carboxylic acid group in MGs via a ring-open reaction. The mechanism is shown in Figure 4.4[36]. The carbon in epoxide ring of GMA is attacked by the R-COOH group causing a reaction. The MAA content in each MG was determined by the potentiometric titration data. The apparent pK_a is the pH value corresponding to

50 % neutralisation. The GMA content in each MG was calculated from the difference of MAA content before and after functionalisation.

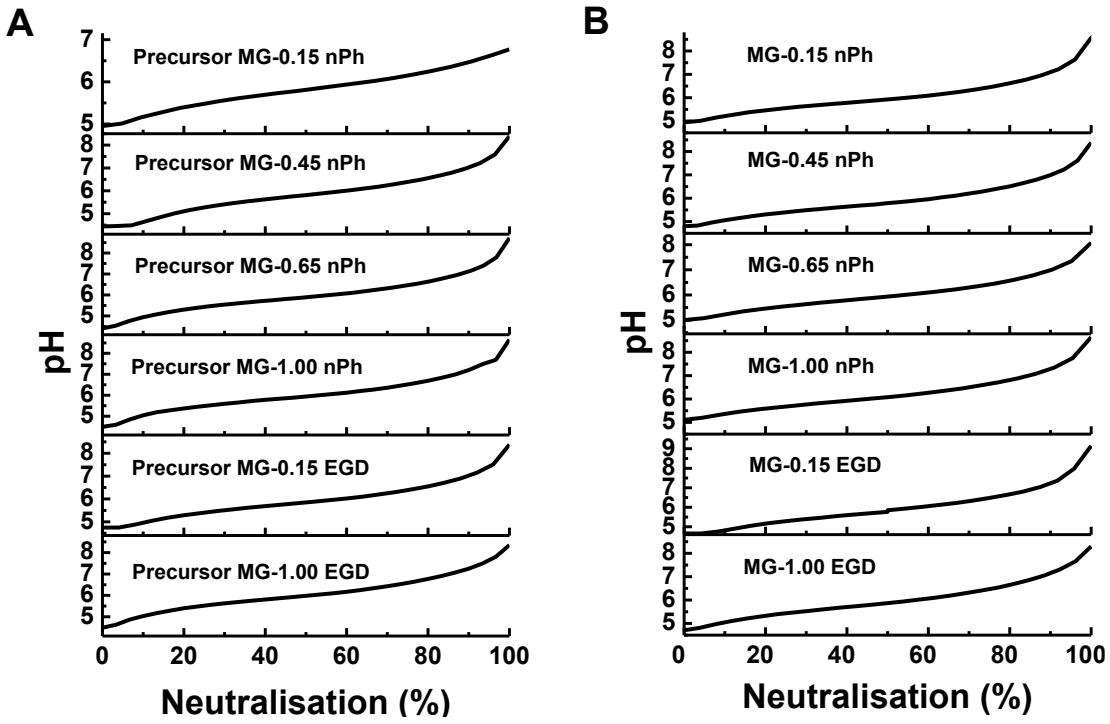

Figure 4.5. Potentiometric titration data for **(A)** precursor MG and **(B)** functionalised MG dispersions. The data were obtained at 25 °C.

The potentiometric titration data are shown in Figure 4.5A. These data showed that the precursor MG-0.15-nPh, MG-0.45-nPh, MG-0.65-nPh, MG-1.00-nPh, MG-0.15-EGD and MG-1.00-EGD contained MAA with 23.2 mol%, 24.79 mol%, 22.61 mol%, 23.32 mol%, 24.68 mol% and 23.77 mol% respectively. The functionalised MG-0.15-nPh, MG-0.45-nPh, MG-0.65-nPh, MG-1.00-nPh, MG-0.15-EGD and MG-1.00-EGD contained MAA with 18.18 mol%, 19.65 mol%, 18.53 mol%, 19.05 mol%, 20.27 mol% and 19.09 mol% as well as have GMA with 5.02 mol%, 5.17 mol%, 4.08 mol%, 4.27 mol%, 4.41 mol% and 4.68 mol%, respectively (see Figure 4.5B and Table 4.2). The mole ratio of GMA to MAA used was fixed at 3.0 during the experiment of GMA functionalisation, but only a part of GMA was functionalized with carboxylic group of MAA. It is due to hydrolysis of GMA in absence of any catalyst via the hydroxy group of water attacking

the epoxy group of GMA[37]. The pK_a for those six MGs were 5.9, 5.8, 5.9, 6.0, 5.9 and 5.9, respectively (Table 4.2). The pK_a values are much less than physiological pH (~7.4) indicating that the MG particles and DX MGs would be swollen in such an environment.

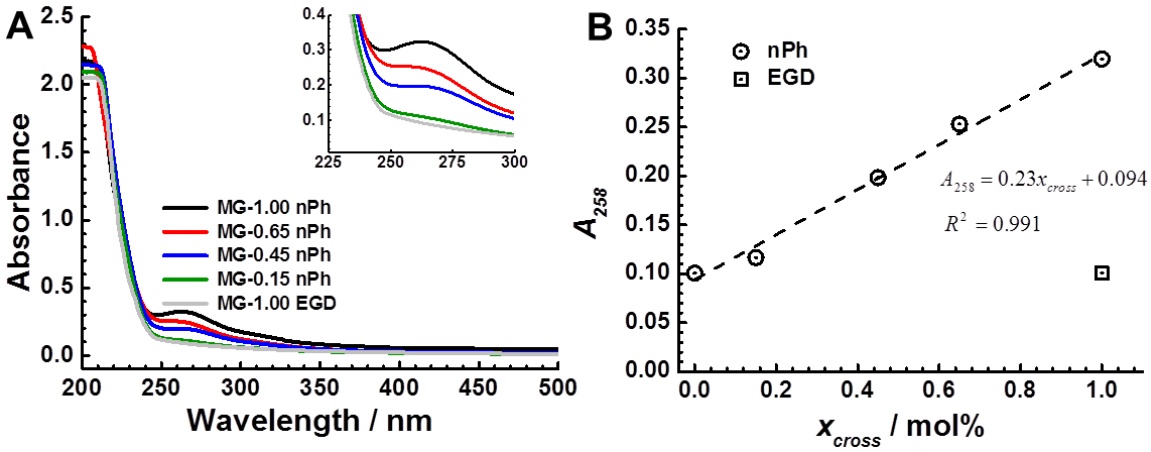

Figure 4.6. (**A**) UV-visible spectra for the MG-*x*-nPh dispersions measured at pH=7.4 and 25 °C. (**B**) Absorbance measured at 258 nm versus concentration of crosslinker used for MG. The concentration of MG dispersion is 0.01 wt.%.

The nPh content was also investigated using UV-vis spectra. In Figure 4.6A, there is a maximum absorption at 258 nm (A_{258}) for MG-*x*-nPh which is evident for nPh copolymerised in the MGs. The line of best fit between A_{258} and nominal nPh concentration for the MG-*x*-nPh dispersion data are shown (Figure 4.6B). Data measured for a MG-1.00-EGD dispersion are shown for comparison.

The composition and properties of the MGs are summerised as shown in Table 4.2. Clearly, the MAA content are still high even after functionalisation with GMA.

Table 4.2. Composition and properties of the MGs.

Microgels	MEO_2MA / mol% [a]	OEGMA / mol% [a]	MAA / mol% [b]	nPh [c] / mol%	EGD [c] / mol%	GMA / mol% [d]	pK_a [e]	VPTT (pH, 5.4)	d_{TEM} /nm [f]	d_z /nm [g] (pH 5.4, 60°C)
MG-0.15-nPh	73.68	3.10	18.18	0.15	-	5.02	5.9	25.5	51(6)	55 (0.081)
MG-0.45-nPh	71.63	3.11	19.65	0.45	-	5.17	5.8	24.4	52(9)	54 (0.089)
MG-0.65-nPh	73.65	3.16	18.53	0.65	-	4.08	5.9	24.3	50(6)	54 (0.087)
MG-1.00-nPh	72.80	3.16	19.05	1.00	-	4.27	6.0	23.4	50(7)	60 (0.058)
MG-0.15-EGD	72.44	3.09	20.27	-	0.15	4.41	5.9	23.4	59(7)	57 (0.085)
MG-1.00-EGD	70.21	3.11	19.09	-	1.00	4.68	5.9	25.0	54(7)	65 (0.074)

[a] Based on the assumption that that all OEGMA had reacted. [b] Determined from potentiometric titration data. [c] Nominal values based on formulation used. [d] Calculated using the difference of the MAA content before and after functionalisation. [e] Apparent pK_a value determined from potentiometric titration data. [f] The numbers in brackets are the standard deviation. [g] The numbers in brackets are the polydispersity index (PDI) values.

4.4.3 Study of the pH and thermal responsive of the MGs by DLS

The pH and thermal responsive behaviours of the MGs were investigated using DLS. Figure 4.7A shows the variation of d_z with different pH buffer solution for MG-1.00-nPh at 10 °C, 25 °C and 37 °C. It is clear that the diameter increases with pH increase. Also the pK_a is different for different temperatures. At 10 °C and 37 °C, respectively, the hydration between P(MEO_2MA-OEGMA) and water is maximised and minimised, respectively. This strongly influences the pH-dependence of d_z. At 37 °C and low pH, the P(MEO_2MA-OEGMA) are dehydrated and –COOH groups are deprotonated, the MGs are at the most collapsed stage. The d_z increases strongly with pH 6.0 and pK_a is 6.0. By contrast, d_z increases gradually with increasing pH without a sharp swelling transition at 10 °C. The data measured at 10 °C show a incomplete collapse at pH 4.4 which is due to hydrogen bonding of water to the P(MEO_2MA-OEGMA). Hence, at high temperature, the swelling ability of MGs was dominated by electrostatic interactions and was more affected by hydrogen bonds between the P(MEO_2MA-OEGMA) and water at low

temperature. Figure 4.7B shows the electrophoretic mobility vs pH curves for MG-1.00-nPh at 10 °C, 25 °C and 37 °C. Presumably, the negative charge near the functionalised MG surface increases in magnitude with increasing pH and reached a plateau for pH values greater than 7.4. This behaviour is due to deprotonation of the –COOH groups and confirms that an increasing concentration of -COO^- groups causes pH-triggered MG swelling. The mobility also increased with increasing temperature. This is due to local segment rearrangement with more negatively charged groups residing closer to the MG periphery.

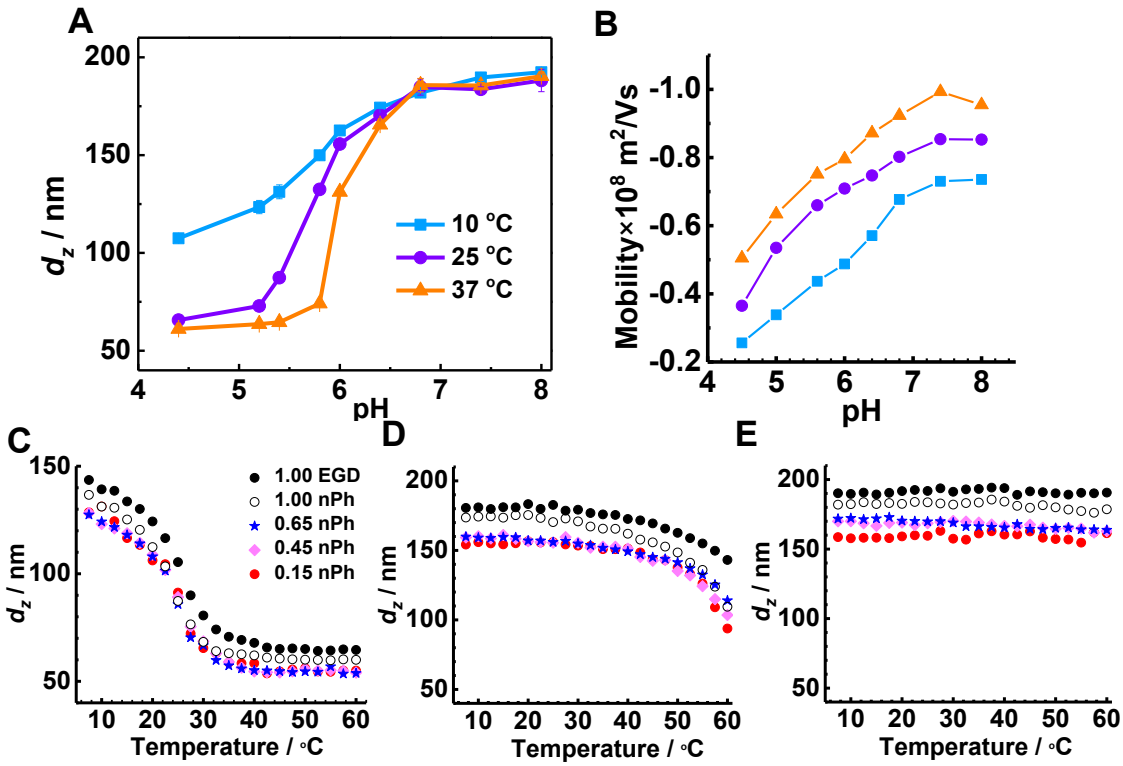

Figure 4.7. Variation of the **(A)** z-average diameter (d_z) and **(B)** electrophoretic mobility data with pH measured for MG-1.00-nPh dispersions at 10, 25 and 37 °C. The temperature-dependent d_z values measured for MG-*x*-nPh and MG-1.00-EGD dispersions at **(C)** pH 5.4, **(D)** pH 6.4 and **(E)** pH 7.4 are shown. The legend for (C) shows the mol% of nPh or EGD used and also applies to (D) and (E).

The effect of temperature was investigated. Variable temperature DLS data were measured for the MG-*x*-nPh (x = 0.15 - 1.00) and MG-1.00-EGD dispersions at pH 5.4,

6.4 and 7.4 (Figure 4.7C-E). The microgels are thermally sensitive with a decrease of d_z by increasing temperature. This is because of a decrease in solvent quality due to thermally-triggered disruption of hydrogen bonding of water to P(MEO_2MA-OEGMA). Such disruption causes attractive, hydrophobic, segment-segment interactions to dominate[25]. The VPTTs were estimated from the point of inflection of the data shown in Figure 4.6C-E. The VPTTs increased from 23.4 - 25.5 °C at pH 5.4 to ~ 60 °C at pH 6.4 (see Table 4.2). The d_z decreased around 2 times at pH 5.4 and less than 2 times at pH 6.4. This difference is due to all MGs becoming totally collapsed when T > 30 °C at pH 5.4. However, all MGs still swell at pH 6.4 even when the temperature reaches to 60 °C because electrostatic repulsion by some $–COO^-$ groups. At pH 7.4, the de-swelling behaviour was limited for all MGs and the VPTTs were much greater than 60 °C. Hence, changing the pH value of a dispersion can turn on or off the thermal responsive behaviours of these MGs.

4.4.4 The relationship between swelling behaviour and crosslinker content of the MGs

Figure 4.7C-E shows that the swelling behaviour of MGs is not restricted by crosslinker content. This trend is also shown by d_z in Figure 4.8A. The maximum d_z for all six MGs increases as the crosslinker content increases. The particle swelling ratio (Q_{MG}) was estimated using the d_z values in the fully collapsed state ($d_{z(Coll)}$) and swollen state ($d_{z(Swell)}$) via the equation $Q_{MG} = (d_{z(Swell)}/\ d_{z(Coll)})^3$. The values for $d_{z(Coll)}$ were the d_z values measured at pH 5.4 and 60 °C. The values for $d_{z(Swell)}$ were obtained at pH 7.4 and 7.5 °C from Figure 4.8A.

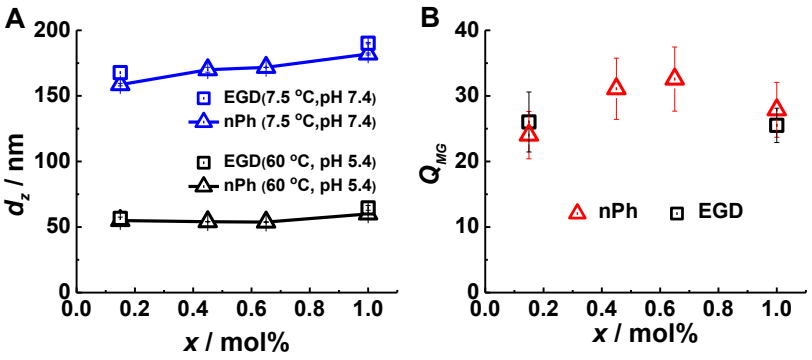

Figure 4.8. (A) Effect of crosslinker concentration (x_{cross}) and type used on the z-average diameter (d_z) measured for MG-*x*-nPh and MG-*x*-EGD dispersions. **(B)** The Q_{MG} vs. crosslinker concentration for MG-*x*-nPh and MG-*x*-EGD dispersions

Figure 4.8B shows that the Q_{MG} values do not significantly depend on *x*. This result is unexpected because increasing the concentration of crosslinker decreases particle swelling in well-studied MGs such as polystyrene and PNIPAM[38-40]. Hence, the higher crosslinker content within the MGs did not restrict the swelling behaviour of MGs. OEGMA-based MGs prepared using EGD have a core-shell structure with core-rich and shell-poor crosslinker[29-31]. Both EGD and nPh are hydrophobic and I propose that a core-shell structure was present in both MG-*x*-nPh and MG-*x*-EGD. Within the MGs, most of crosslinker (EGD or nPh) is incorporated into the core. The crosslinker in the core does not contribute shell swelling. As the separation between crosslinkers decreases the average functionality decreases[41]. Hence, closely situated crosslinkers that occupy the MG cores do not efficiently oppose particle swelling.

4.4.5 UV light-triggered degradation behaviours of the MGs

I next explored the responsive of the MG-*x*-nPh dispersion to UV-irradiation. The MG-1.00-EGD system was used to comparison. The nPh crosslinker in MGs has an absorption maximum at 258 nm that was evident in UV-visible spectra for MG-*x*-nPh dispersion (Figure 4.6).

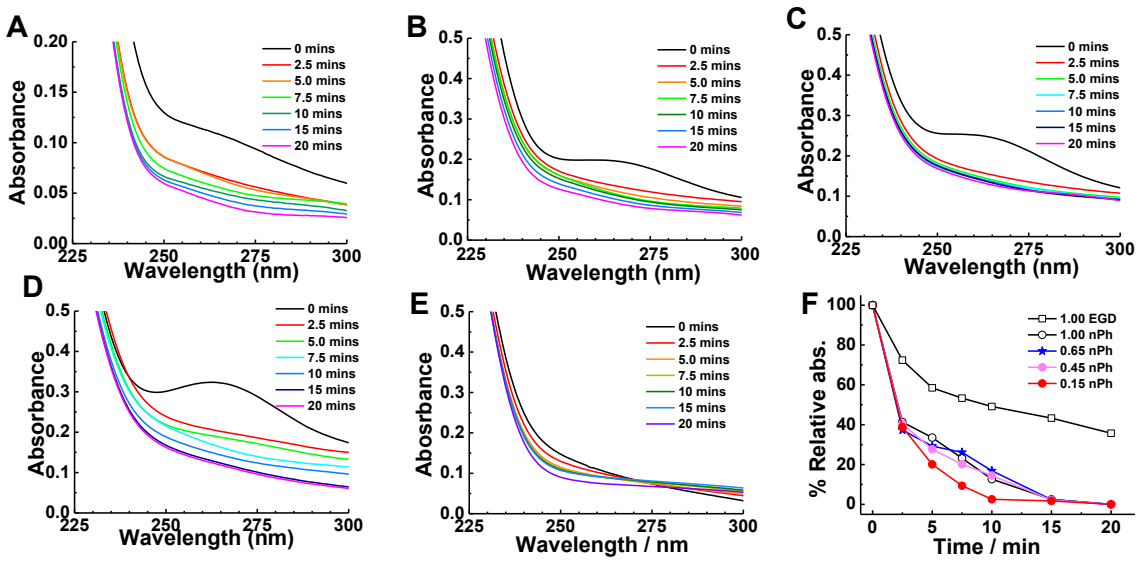

Figure 4.9. UV-visible spectra measured after different periods of UV irradiation for (**A**) MG-0.15-nPh, (**B**) MG-0.45-nPh, (**C**) MG-0.65-nPh, (**D**) MG-1.00-nPh and (**E**) MG-1.00-EGD. The pH andtemperature were 7.4 and 25 °C. **(F)** The % relative absorbance measured at 258 nm vs. UV irradiation time for MG-*x*-nPh and MG-1.00-EGD. The relative absorbance is measured relative to the baseline value.

In Figure 4.9A-D, the UV-visible spectra show that the absorption maximum at 258 nm for the MG-*x*-nPh decreased with UV light irradiation. The scattering of MG-1.00-EGD decreased with UV light irradiation (Figure 4.9E). The relative absorption at 258 nm decreased with UV light irradiation for MG-*x*-nPh as shown in Figure 4.9F. MG-0.15-nPh had the fastest decreasing relative absorption reaching 0 % in 10 min. The other nPh-based MGs needed 15 min to reach this value. The relative absorption at 258 nm for MG-1.00-EGD decreased to 40% which means limited degradation occurs. This is due to Norrish type I cleavage of ester bonds[32, 42] of EGD. Therefore, the MG-*x*-nPh with the smallest crosslinker content dissemble at the fastest rate.

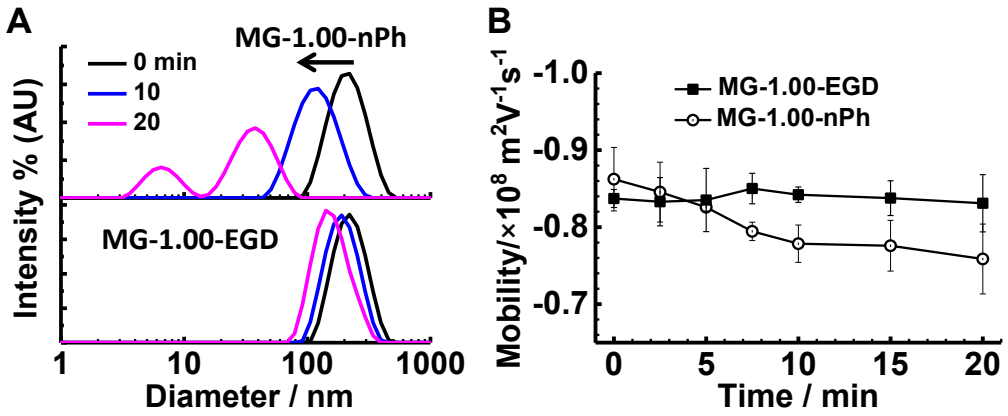

Figure 4.10. (A) DLS size distributions for MG-1.0-nPh and MG-1.0-EGD measured at 0, 10 and 20 min after UV irradiation. **(B)** Electrophoretic mobility after different irradiation times for the dispersions at pH 7.4 and 25 °C.

The change of d_z was probed by DLS for MG-1.00-nPh and MG-1.00-EGD as well after UV treatment for 0, 10 and 20 mins. Figure 4.10A shows the peak for MG-1.00-nPh moved from 200 nm to 90 nm in 10 mins and became biomodal in 20 mins. However, the peak for MG-1.00-EGD was much less affected. Moreover, in order to investigate the UV light-triggered degradation mechanism of nPh-based MGs, electrophoretic mobility data were measured for MG-1.00-nPh and MG-1.00-EGD (Figure 4.10B). The mobility becomes less negative with longer UV treatment for MG-1.00-nPh, while the mobility became stable for MG-1.00-EGD after UV treatment. This is due to an amine cationic species being photo-generated within the disassembled MG-1.00-nPh particles[32]. These cationic species are -NH_3^+ groups[32](shown in Scheme 4.2) at pH 7.4. In this case, the ionic bonds form from such groups and nearby –COO^- groups. However, ionic bonds are dynamic and not sufficiently robust to prevent MG disassembly.

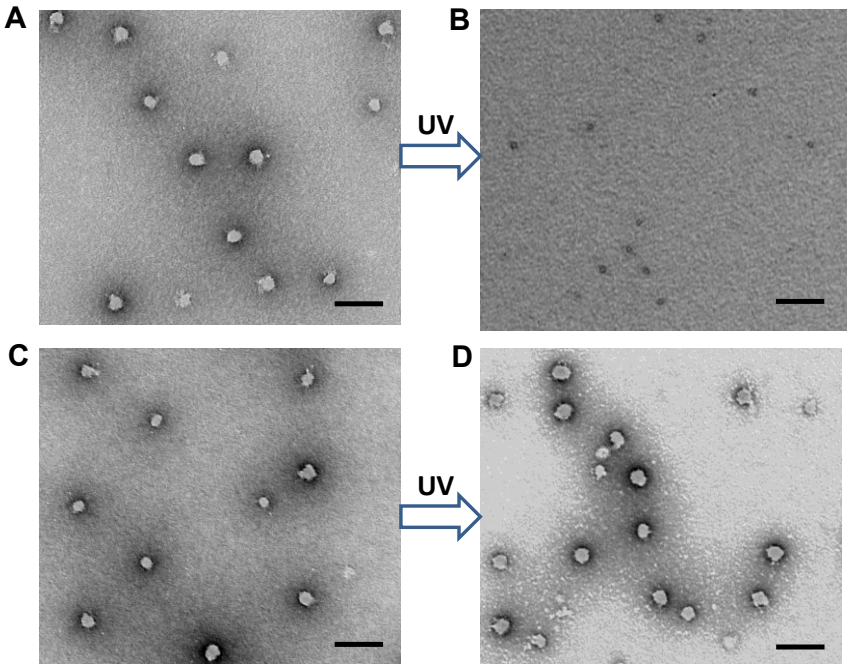

Figure 4.11. TEM images of MG-1.00-nPh deposited from solution (pH 7.4) before **(A)** and after **(B)** UV irradiation for 20 min. MG-1.00-EGD deposited from solution (pH 7.4) before **(C)** and after **(D)** UV irradiation for 20 min. The scare bars are 200 nm.

The TEM images also show that the original MG-1.00-nPh spherical particles degrade into small particle which had a diameter of about 10 nm after UV treatment for 20 min (Figure 4.11A-B). In contrast, the MG-1.00-EGD was still intact after UV treatment (Figure 4.11C-D).

4.4.6 pH and thermal responsive of the DX MGs

DX MGs were next prepared by covalently interlinking the MGs via GMA groups (Scheme 4.3B). In this study, the inter-MG crosslinker GMA were kept between 4.1 and 5.2 mol% (shown in Table 4.2). The as-made DX MGs are transparent as shown in Figure 4.12.

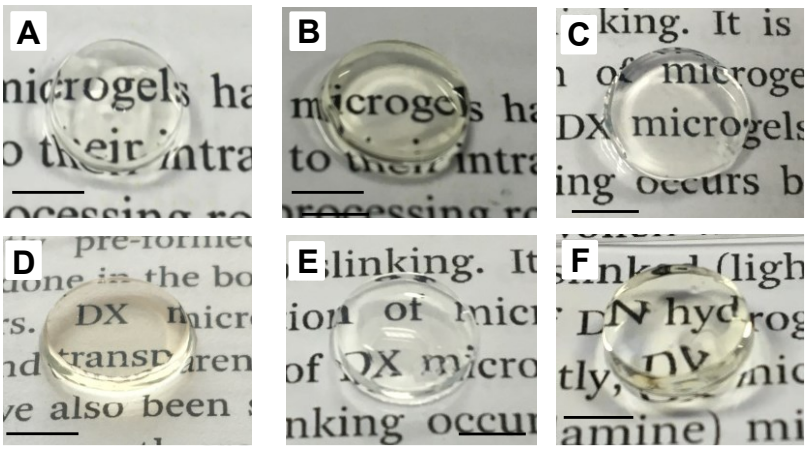

Figure 4.12. Digital photographs of **(A)** DX MG-0.15-nPh, **(B)** DX MG-0.45-nPh, **(C)** DX MG-0.65-nPh, **(D)** DX MG-1.00-nPh, **(E)** DX MG-1.00-EGD, **(F)** DX MG-0.15-EGD gels. All scale bars are 5 mm

The swelling ratio (Q_{DXMG}) of the DX MGs was investigated. They show strong pH triggered swelling at all temperatures. Taking DX MG-1.00-nPh as an example, the Q_{DXMG} increased to about 4 times from pH 5.4 to pH 7.4 at three temperatures (10 °C, 25 °C, 37 °C) (Figure 4.13A). This gel can swell most strongly when both the electrostatic repulsion is highest (pH 7.4) and hydration is strongest (10 °C). Besides, In Figure 4.13B-D, all gels have significant temperature dependent changes in Q_{DXMG} at pH 5.4, 6.4 but this is limited at pH 7.4. This matched the trend for the parent MGs (Figure 4.7C-E). The DX MG-*x*-nPh gels retains high Q_{DXMG} values at pH 7.4 and 37 °C which are potentially important as the gels should be strongly swollen at physiological conditions.

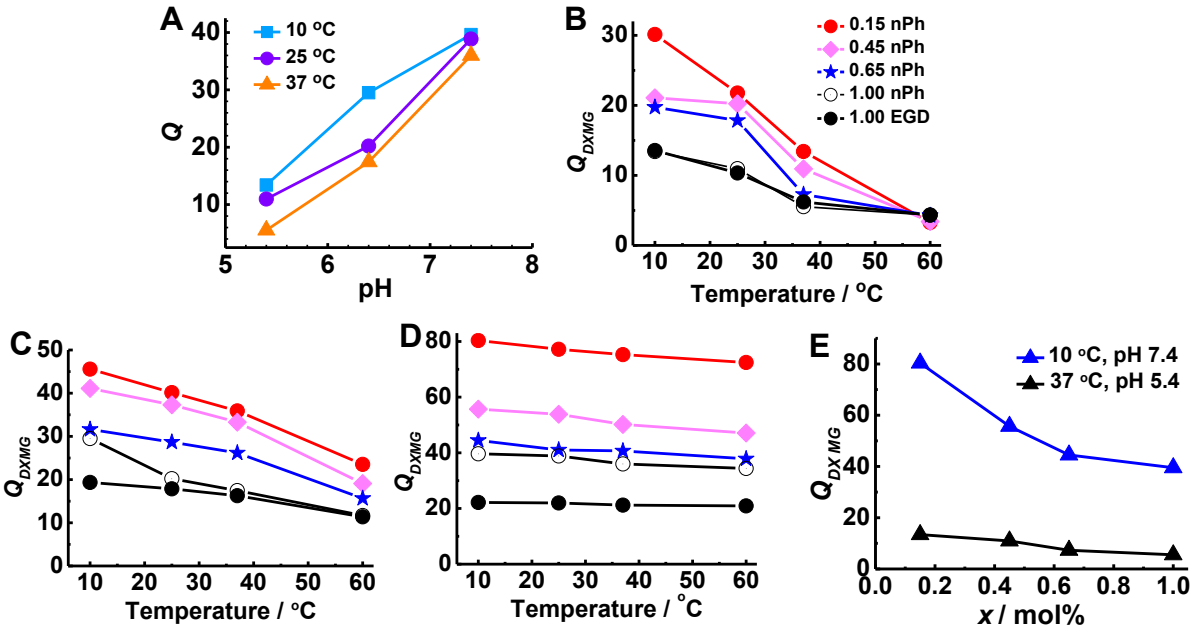

Figure 4.13. **(A)** Variation of the DX MG volume-swelling ratio (Q_{DXMG}) with pH for DX MG-1.00-nPh gels measured at 10, 25 and 37 °C. The temperature-dependence of Q_{DXMG} is shown for the gels at **(B)** pH 5.4, **(C)** pH 6.4 and **(D)** pH 7.4. The legend shown in (B) also applies to (C) and (D). (E) Dependencies of Q_{DXMG} at pH 5.4 and 7.4 on x.

Figure 4.13E shows that the Q_{DXMG} value decreases as the nPh content increases. It can be seen that at 10 °C and pH 7.4 those gels were in the fully swollen state. This agrees with the behaviour expected for conventional hydrogels[43], but it is opposite to the trend observed for the parent MGs as shown in Figure 4.8B. Hence, the Q_{DXMG} values are strongly affected by the intra-MG crosslinking.

4.4.7 The relationship between the mechanical properties and intra-MG crosslinking for the DX MGs

The compressive stress-strain properties for all gels were studied (Figure 4.14). The modulus increases (from 4.5 to 20.5 kPa) and breaking strain (ε_B) decreases (from 81.4 to 63.3 %) as crosslinker nPh increases (from 0.15 to 1.00 mol%). This trend also is shown for DX MG-x-EGD. Interestingly, the modulus for DX MG-1.00-EGD is much lower than DX MG-1.00-nPh, which means the crosslinker types affect the mechanical

properties strongly for these gels. Hence, the most deformable DX MGs are obtained with the MGs containing the lowest crosslinker contents.

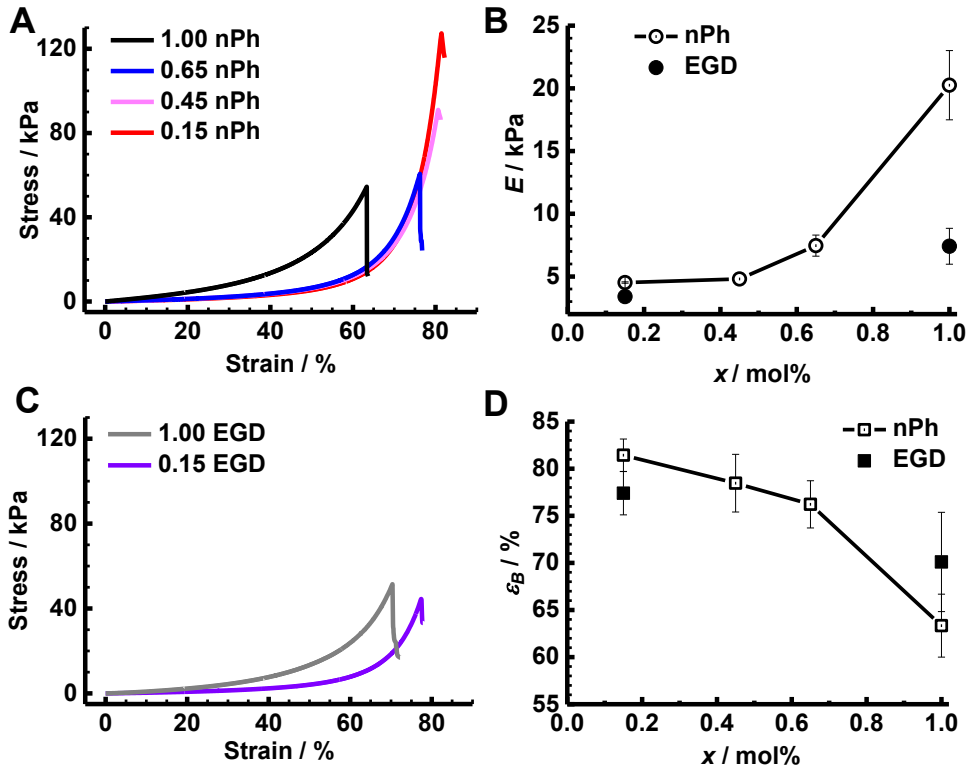

Figure 4.14. Compressive stress-strain data for **(A)** DX MG-*x*-nPh and **(C)** DX MG-*x*-EGD gels. The modulus (E) and breaking strain (ε_B) values were obtained from the data shown in (A) and (C) and are plotted as a function of the crosslinker concentration used for the MG building blocks in **(B)** and **(D)**, respectively. The data were obtained at pH 7.4 and 25 °C.

In order to prove the mechanical properties of the DX MGs can be tuned via blending. DX MG was prepared using a 50:50 blend of the MG-1.00-nPh and MG-1.00-EGD particles, which is denoted as DX MG-1.00-nPh/EGD. The modulus and breaking strain values were measured from the compressive stress-strain data and were found to be between those for the DX MG-1.00-nPh and DX MG-1.00-EGD gels (see Figure 4.15). This highlights the ability to tune the mechanical properties of these gels by using colloidal scale building blocks with different inherent stiffness.

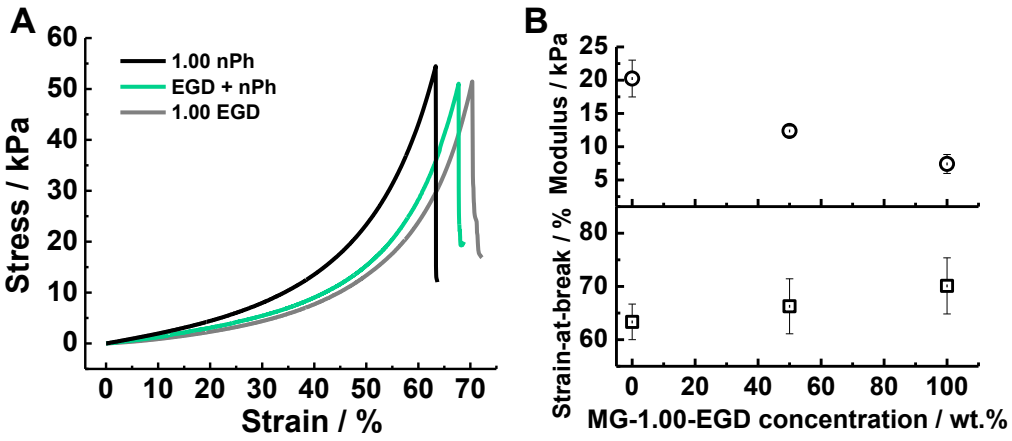

Figure 4.15. **(A)** Compression stress-strain data measured for DX MG-1.00-nPh, DX MG-1.00-EGD and DX MG-1.00-nPh/EGD. **(B)** Modulus and strain-at-break values for the gels from (A). The error bar from (B) is determined for 3 measurements for each sample.

The important question is why the intra-MG crosslinking does not contribute to the swelling behaviours for the parent MG dispersion but affects the DX MGs in swelling ratio and mechanical properties strongly? When functionalising the MGs, the temperature of dispersion is 40 °C and the pH is 5.0 which is lower than pK_a (pK_a is shown in Table 4.2). In this condition, MEO_2MA and MAA are hydrophobic. It is proposed that they both distribute uniformly within the MGs due to a similar conversion ratio of them according to Boularas et al.[44] . GMA is hydrophobic monomer with a logP of 0.34[45] and so GMA penetrates and distributes uniformly within the MGs and then reacts with –COOH via epoxide ring-opening reaction. I propose that the GMA units form a second network which provided additional linkages to the highly crosslinked cores of the MGs which enable the cores to contribute to stress distribution in the DX MG gel.

4.4.8 UV light-triggered mechanical behaviours change of the DX MGs

I next investigated UV light-triggered variation swelling ratio and mechanical properties of all DX MGs. For the colour variation of gels, the gels containing nPh became yellow after UV treatment which is due to formation of the nitroso-benezaldehyde photolysis product[32]. While for the DX MG-*x*-EGD, they remained colourless and transparent after UV treatment (Figure 4.16A).

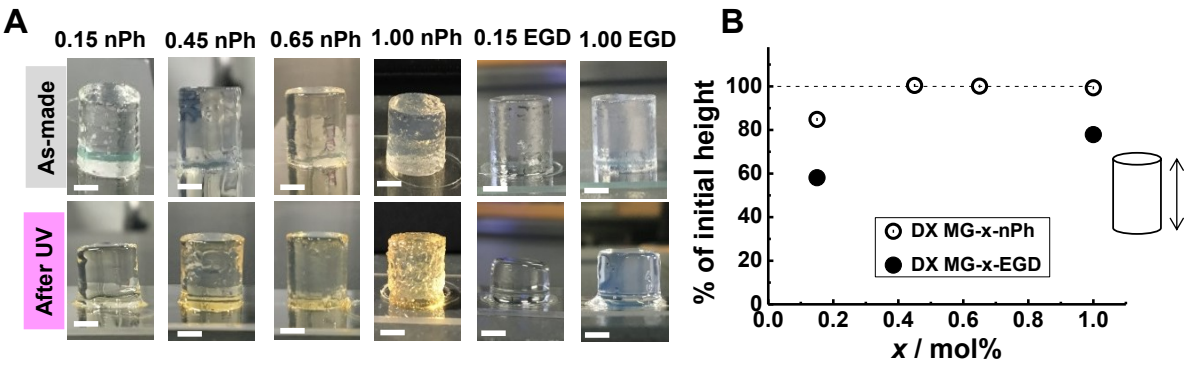

Figure 4.16 (A) Digital photographs of DX MGs before (top row) and after (bottom row) UV-irradiation. The scale bars are 5 mm. **(B)** Measured % initial gel cylinder height after UV-irradiation versus the crosslinker concentration used to prepare the parent MGs.

Figure 4.16B shows the height of DX MG-0.15-nPh and DX MG-*x*-EGD decreases noticeably as a consequence of UV irradiation. However, the heights of DX MG-0.45-nPh, DX MG-0.65-nPh and DX MG-1.00-nPh do not change. The partial dissolution of DX MG-*x*-EGD is due to Norrish type I cleavage of ester bonds[32, 42] including EGD and GMA. While for the gels containing relative high content nPh (>0.45 mol%), the photo-generated cationic species amine can associate the carboxylic acid group of MAA which avoids UV-C light weakening the gels. The UV-C light can be used to sterilise biomaterials[46]. Hence, this gel may provide a visual indication of UV-sterilsation for load-supporting soft tissue gel implants.

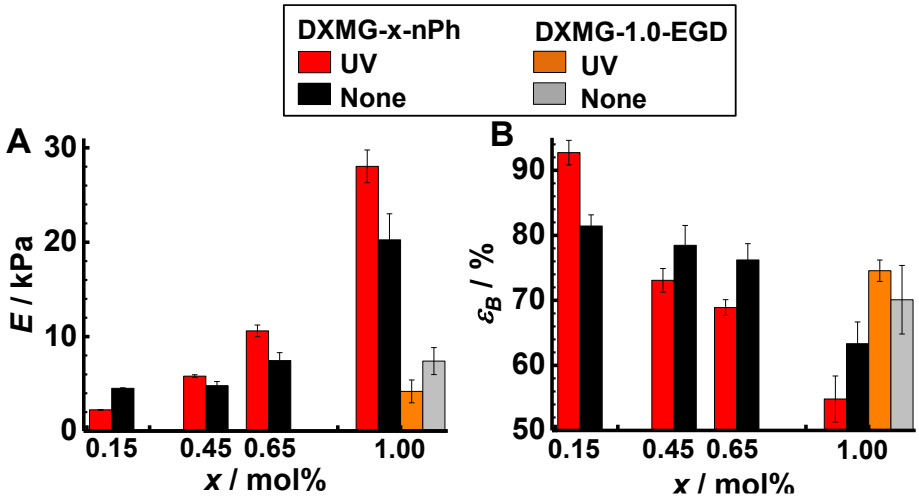

Figure 4.17. The effects of UV-irradiation on the E and ε_B values for the DX MG gels prepared using nPh and EGD are shown in **(A)** and **(B)**, respectively. The data were obtained at pH 7.4 and 25 °C.

The mechanical properties of the DX MGs change because of the UV light effect. The compressive stress-strain measurements were conducted. Figure 4.17 shows the modulus (E) and breaking strain (ε_B) values before and after UV treatment for all gels. Obviously, after UV treatment, the E values for DX MG-1.00-nPh, DX MG-0.65-nPh and DX MG-0.45-nPh increase from 20.3 to 28.0, 7.5 to 10.6 and 4.8 to 5.8 kPa, respectively. The ε_B values decrease from 63.3 to 54.8 %, 76.2 to 68.9 %, and 78.5 to 73.1 % respectively. This indicates that the UV irradiation leads to stiffening of these gels. The increase of stiffness is due to the formation of multiple ionic crosslinks between -COO^- and photogenerated –NH_3^+ groups. In contrast, the control gels (DX MG-1.00-EGD) shows the opposite trend with E value decreasing from 7.4 to 4.2 kPa and ε_B increasing from 70.1 to 74.6 %. The Norrish type I reactions of the crosslinkers contributed to these behaviours.

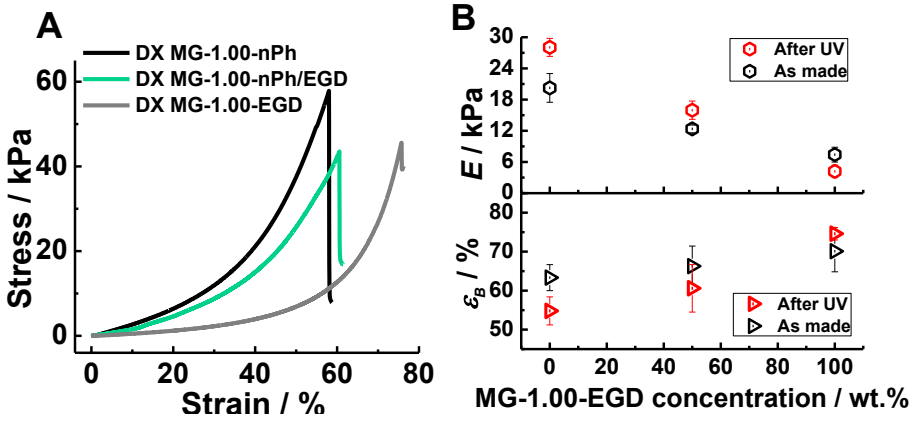

Figure 4.18. **(A)** Compression stress-strain data measured for DX MG-1.00-nPh, DX MG-1.00-EGD and DX MG-1.00-nPh/EGD after UV irradiation. **(B)** shows the effects of UV irradiation on the modulus and breaking strain values, respectively, for the gels from (A).

To address the question of whether the UV light-triggered E increase via nPh cleavage or E decrease via Norrish type I is stronger, the mechanical properties of 50:50 blend of DX MG-1.00-EGD and DX MG-1.00 nPh was measured. In Figure 4.18, the E value increases from 12.4 to 16.0 kPa and ε_B value decreases from 66.3 to 60.6 % for this gel after UV

irradiation. So the mechanical property changes caused by UV light are stronger than that caused by Norrish type I reaction.

4.4.9 Effects of UV light on swelling behaviours of the DX MGs

The effect of UV light irradiation on the Q_{DXMG} was measured as function of temperature for DX MG-1.00-nPh as shown in Figure 4.19A. The pH values of 5.4 and 7.4 were used for this study. UV irradiation caused Q_{DXMG} to decrease at pH 7.4 while it increased at pH 5.4 at the three temperatures. It is important note that Q_{DXMG} increased at two pH values for the control DX MG-1.00-EGD at 37 °C. Hence, when the pH value is higher than the pK_a of parent particle (6.0), the UV-triggered decrease Q_{DXMG} for DX MG-1.00-nPh gels is due to the association of photo-generated $-NH_3^+$ and $-COO^-$ which decreases the electrostatic repulsion within the gel. When the pH value is smaller than the pK_a, the -COOH is deprotonated and the electrostatic repulsion of $-NH_3^+$ in acid environment leads to a Q_{DXMG} increase after UV treatment. These data imply that photocleavage of the nPh crosslinker generated a polyampholyte gel.

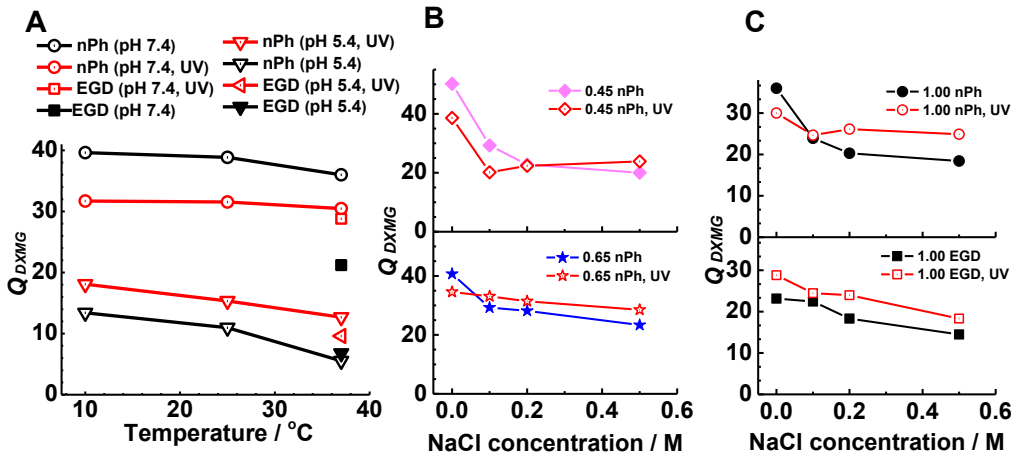

Figure 4.19. (A) Volume swelling ratios (Q_{DXMG}) for DX MG-1.00-nPh gel measured at different temperatures before and after UV irradiation. Data for control DX MG-1.00-EGD gels are also shown. The effects of NaCl concentration on the Q_{DXMG} measured for **(B)** DX MG-0.45-nPh and DX MG-0.65-nPh gel as well as **(C)** DX MG-1.00-nPh and DX MG-1.00-EGD gels before and after UV irradiation are shown. The arrows indicate cross-over points for Q_{DXMG} (see text). The data shown in (B) and (C) were measured at pH 7.4 and 37 °C.

If ionic bonds are formed as a consequence of UV irradiation, this effect can be decrease through electrostatic screening[47] when increasing the ionic strength of buffer and then increased gel swelling should be expected compared to the non-UV irradiated gel. Figure 4.19B-C shows the Q_{DXMG} in different concentration NaCl solution at pH 7.4. The Q_{DXMG} values for all non-UV light irradiated gels decrease while recover to some extent for DX MG-1.00-nPh, DX MG-0.65-nPh and DX MG-0.45-nPh when treated with UV light. This behaviour confirms that polyampholyte behaviour occurred for those gels. NaCl can disrupt the ionic bond from the photo-generated NH_3^+ and COO^- and then the swelling ratio increase. This conclusion was verified by the controlled gel DX MG-1.00-EGD. It did not show the increasing trend in Q_{DXMG} as NaCl concentration increase. The Norrish Type I cleavage of crosslinks was responsible higher Q_{DXMG} for the gel after UV irradiation compared with that without UV treatment.

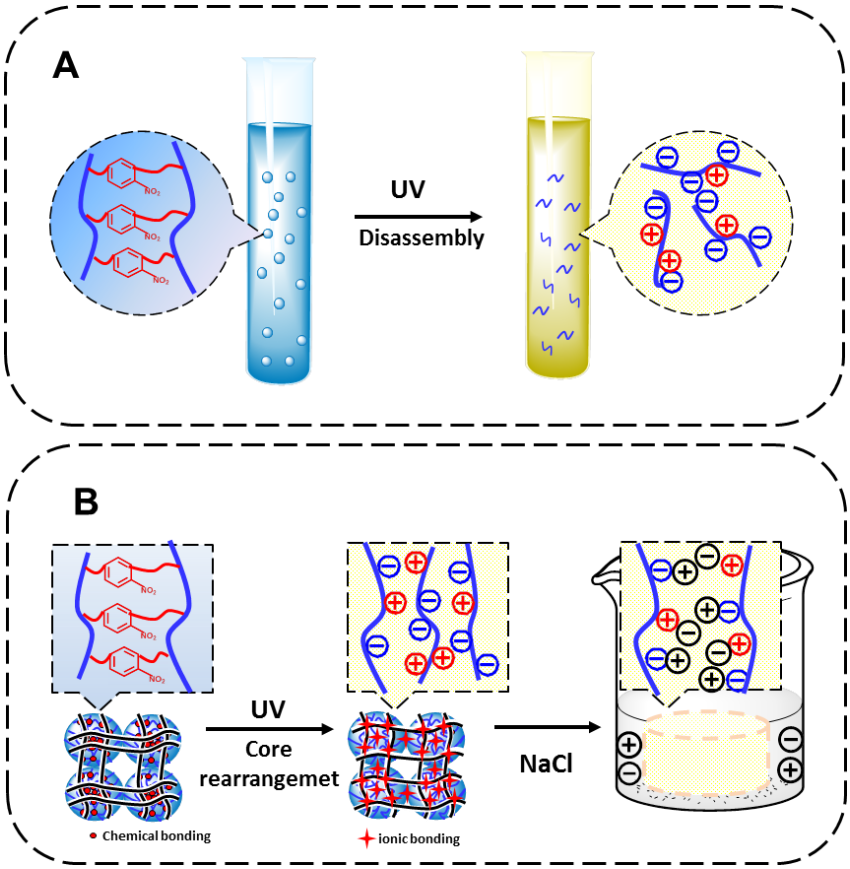

Figure 4.20. Depiction of proposed mechanisms to explain UV-light triggered MG-*x*-nPh disassembly **(A)** and DX MG-*x*-nPh de-swelling **(B)**. The UV-triggered cleavage of the nPh crosslinks groups generates positive charge which associates with nearby $–COO^-$ groups. For the MGs (A) the dynamic ionic bonds allow the MGs to disassemble. In the case of the DX MGs (B) the permanent linkages from the second DX network prevent disassembly and the segments rearrange to form multiple ionic crosslinks. The latter can be disrupted and unzipped by addition of electrolyte.

Figure 4.20 depicts the remarkably contrasting behaviours observed for the MG-*x*-nPh particles and DX MG-*x*-nPh gels as a result of UV irradiation. The MG-*x*-nPh particles degraded upon UV irradiation because the ionic crosslinks are not stabilised and are dynamic[48] (Figure 4.20A). In contrast, the DX MG-*x*-nPh gels have a second DX network formed by GMA that stabilises gel and prevents disassembly (Figure 4.20B). The photo-generated ionic bonds form and rearrange within the core of the MGs. This causes an increase in the modulus and decreased swelling. The energy of a covalent bond is 360 kJ/mol[49] (i.e., 145 kT). In contrast the ionic bonds should have an energy of ~ kT[50]. Hence,

the rearranged segments should contain multiple ionic bonds for every cleaved covalent bond and be arranged to provide cooperative bonding[50]. According to discussion above, the original nPh covalent bonds are probably closely associated within the core. This kind of nPh distribution would have decreased their average functionality[41] and decreased their efficiency in contributing elastically effective chains to a network. I propose that the inefficient stress distribution network would be replaced by a more efficient one through local rearrangement via photocleavage. The ionic bonds can be disrupted by addition of electrolyte (e.g., NaCl) due to electrostatic screening. This model implies that the UV-irradiated DX MG-*x*-nPh gels are nanostructured gels of inter-linked core-shell MGs with a polyampholyte core.

4.4.10 Cytotoxicity study of DX MGs

These gels can also be prepared at 37 °C with the aid of the accelerator TEMED. Two representative gels (DX MG-0.65-nPh and DX MG-1.00-EGD) were prepared. Since these gels have potential for injectable formulations in the context load supporting gels[51], a cell challenge test was performed. The cytotoxicity of DX MG-0.65-nPh and DX MG-1.00-EGD were studied by cultured human NP cells for 8 days and was assessed by Live/Dead assays. Live cells are distinguished by the presence of calcein (green) and dead cells are stained with ethidium homodimer-1 (red). Figure 4.21 shows the adherence and morphology of NP cells (top three rows) and live/dead assay fluorescent microscopy images of NP cells (bottom three rows). It is evident there was a very high proportion of live NP cells in contact with two gels. Hence, these gels were not cytotoxic to NP cells over a period of 8 days using Live/Dead assays.

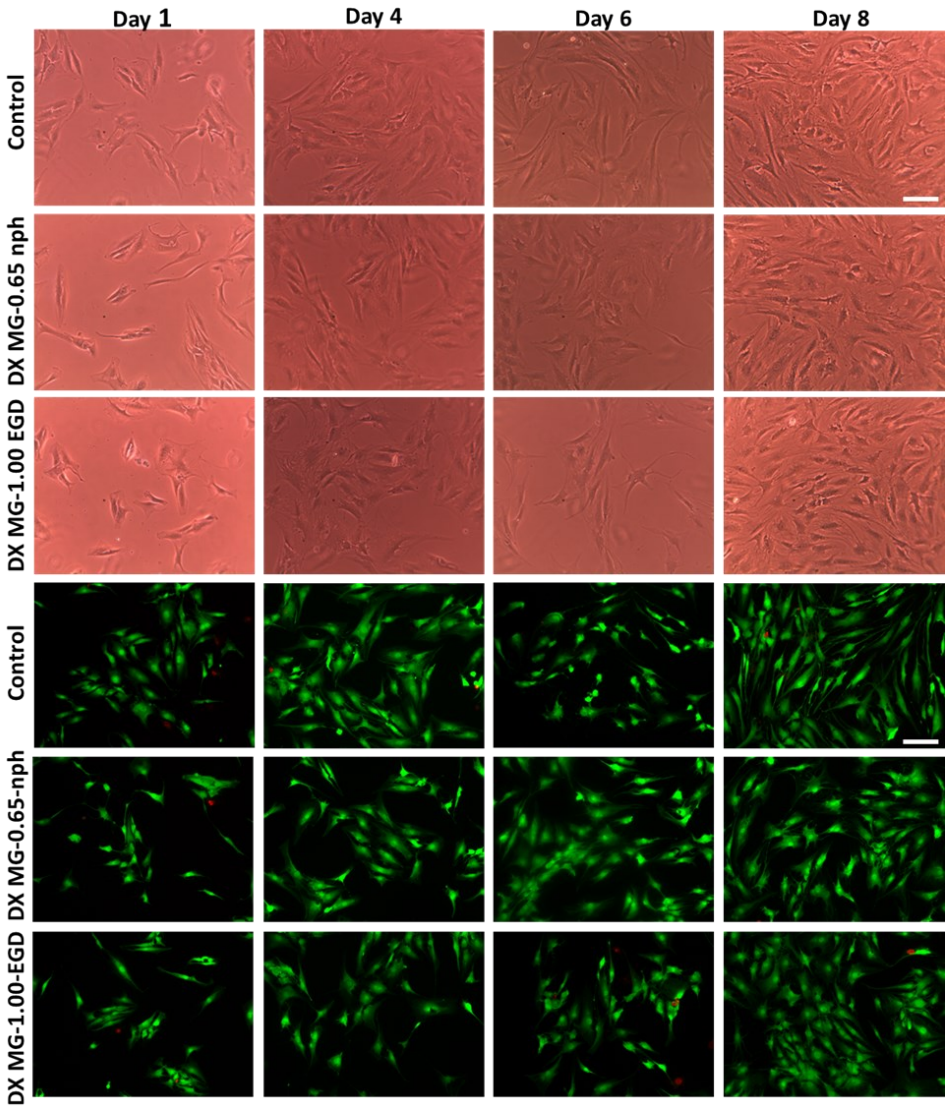

Figure 4.21. Cell challenge data for human nucleus pulposus (NP) cells in the contact of DX MG-0.65-nPh and DX MG-1.00-EGD. Cell morphology images are shown (top three rows). Live/Dead assay images (bottom three rows) were obtained using fluorescence microscope. The control group used an equal volume of PBS. The scale bar applies to all images and is 100 μm.

4.5 Conclusions

Novel OEG-based triply responsive MGs and DX MGs which are pH, temperature and UV light were prepared in this study. The effects of intra-MG-crosslinker on MGs and DX MGs are very different. Firstly, a higher content of hydrophobic crosslinker (*x*) used to prepare MGs did not affect MG swelling. This is probably due to core-rich and shell-poor crosslinker structure of the MGs. However, the modulus increases and the swelling ratio decreases as *x* increases which is opposite to the trend of parent MGs. This difference was attributed to second network from GMA which connected the previous crosslinker within MGs. Secondly, the MGs can disassemble when irradiated with UV. But the UV irradiation of the gels gave the result that the photo-cleavage of the crosslinker enhanced the strength of the gel. This result is opposite to the behaviour of the parent MGs and is attributed to stabilised ionic crosslink formation and rearrangement in the DX MG gels. The mechanical and swelling properties of the DX MG-*x*-nPh gels could be tuned via UV irradiation. This study has shown that the effect of intra-MG crosslinker and the response to UV irradiation of MG-*x*-nPh and DX MG-*x*-nPh gels can be altered by using a second network. Cytotoxicity data for an injectable version showed these gels are not cytotoxic to NP cells over a period for 8 days. This new injectable gel has potential for use in soft tissue repair. An additional potential application is in the context of visual monitoring of UV sterilsation for gel implants.

4.6 References

1. Nayak, S.; Lee, H.; Chmielewski, J.; Lyon, L. A., Folate-mediated cell targeting and cytotoxicity using thermoresponsive microgels. *J Am Chem Soc* **2004,** *126* (33), 10258-10259.

2. Murthy, N.; Thng, Y. X.; Schuck, S.; Xu, M. C.; Frechet, J. M. J., A novel strategy for encapsulation and release of proteins: Hydrogels and microgels with acid-labile acetal cross-linkers. *J Am Chem Soc* **2002,** *124* (42), 12398-12399.

3. Nochi, T.; Yuki, Y.; Takahashi, H.; Sawada, S. I.; Mejima, M.; Kohda, T.; Harada, N.; Kong, I. G.; Sato, A.; Kataoka, N.; Tokuhara, D.; Kurokawa, S.; Takahashi, Y.; Tsukada, H.; Kozaki, S.; Akiyoshi, K.; Kiyono, H., Nanogel antigenic protein-delivery system for adjuvant-free intranasal vaccines (vol 9, pg 572, 2010). *Nat Mater* **2010,** *9* (8), 685-685.

4. Wang, Y.; Nie, J. S.; Chang, B. S.; Sun, Y. F.; Yang, W. L., Poly(vinylcaprolactam)-Based Biodegradable Multiresponsive Microgels for Drug Delivery. *Biomacromolecules* **2013,** *14* (9), 3034-3046.

5. Zhou, T.; Wu, W. T.; Zhou, S. Q., Engineering oligo(ethylene glycol)-based thermosensitive microgels for drug delivery applications. *Polymer* **2010,** *51* (17), 3926-3933.

6. Kim, M. Y.; Kim, J., Chitosan Microgels Embedded with Catalase Nanozyme-Loaded Mesocellular Silica Foam for Glucose-Responsive Drug Delivery. *Acs Biomater Sci Eng* **2017,** *3* (4), 572-578.

7. Kumar, R. A.; Sivashanmugam, A.; Deepthi, S.; Iseki, S.; Chennazhi, K. P.; Nair, S. V.; Jayakumar, R., Injectable Chitin-Poly(epsilon-caprolactone)/Nanohydroxyapatite Composite Microgels Prepared by Simple Regeneration Technique for Bone Tissue Engineering. *Acs Appl Mater Inter* **2015,** *7* (18), 9399-9409.

8. Cha, C. E. Y.; Oh, J.; Kim, K.; Qiu, Y. L.; Joh, M.; Shin, S. R.; Wang, X.; Camci-Unal, G.; Wan, K. T.; Liao, R. L.; Khademhosseini, A., Microfluidics-Assisted Fabrication of Gelatin-Silica Core-Shell Microgels for Injectable Tissue Constructs. *Biomacromolecules* **2014,** *15* (1), 283-290.

9. Debord, J. D.; Lyon, L. A., Synthesis and characterization of pH-responsive copolymer microgels with tunable volume phase transition temperatures. *Langmuir* **2003,** *19* (18), 7662-7664.

10. Das, M.; Mardyani, S.; Chan, W. C. W.; Kumacheva, E., Biofunctionalized pH-responsive microgels for cancer cell targeting: Rational design. *Adv Mater* **2006,** *18* (1), 80-83.

11. Zhang, B.; Sun, B. H.; Li, X. X.; Yu, Y.; Tian, Y. Q.; Xu, X. M.; Jin, Z. Y., Synthesis of pH- and ionic strength-responsive microgels and their interactions with lysozyme. *Int J Biol Macromol* **2015,** *79*, 392-397.

12. Keerl, M.; Pedersen, J. S.; Richtering, W., Temperature Sensitive Copolymer Microgels with Nanophase Separated Structure. *J Am Chem Soc* **2009,** *131* (8), 3093-3097.

14. Klinger, D.; Landfester, K., Dual Stimuli-Responsive Poly(2-hydroxyethyl methacrylate-co-methacrylic acid) Microgels Based on Photo-Cleavable Cross-Linkers: pH-Dependent Swelling and Light-Induced Degradation. *Macromolecules* **2011,** *44* (24), 9758-9772.

14. Brugger, B.; Richtering, W., Magnetic, thermosensitive microgels as stimuli-responsive emulsifiers allowing for remote control of separability and stability of oil in water-emulsions. *Adv Mater* **2007,** *19* (19), 2973-2978.

15. Klinger, D.; Nilles, K.; Theato, P., Synthesis of Polymeric 1-Iminopyridinium Ylides as Photoreactive Polymers. *J Polym Sci Pol Chem* **2010,** *48* (4), 832-844.

16. Huang, Q.; Bao, C. Y.; Ji, W.; Wang, Q. Y.; Zhu, L. Y., Photocleavable coumarin crosslinkers based polystyrene microgels: phototriggered swelling and release. *J Mater Chem* **2012,** *22* (35), 18275-18282.

17. Sun, S. T.; Wu, P. Y., On the Thermally Reversible Dynamic Hydration Behavior of Oligo(ethylene glycol) Methacrylate-Based Polymers in Water. *Macromolecules* **2013,** *46* (1), 236-246.

18. Kubota, K.; Fujishige, S.; Ando, I., Single-Chain Transition of Poly(N-Isopropylacrylamide) in Water. *J Phys Chem-Us* **1990,** *94* (12), 5154-5158.

19. Lv, S. J.; Liu, L. Y.; Yang, W. T., Preparation of Soft Hydrogel Nanoparticles with PNIPAm Hair and Characterization of Their Temperature-Induced Aggregation. *Langmuir* **2010,** *26* (3), 2076-2082.

20. Vihola, H.; Laukkanen, A.; Valtola, L.; Tenhu, H.; Hirvonen, J., Cytotoxicity of thermosensitive polymers poly(N-isopropylacrylamide), poly(N-vinylcaprolactam) and amphiphilically modified poly(N-vinylcaprolactam). *Biomaterials* **2005,** *26* (16), 3055-3064.

21. Forcada, A. I. J., Synthesis Strategies to Incorporate Acrylic Acid intoN-Vinylcaprolactam-Based Microgels. *Polym Chem-Uk* **2011**.

22. L. Yu, Z. S., L. Gao and C. Li,, Mitigated reactive oxygen species generation leads to an improvement of cell proliferation on poly[glycidyl methacrylate-co-poly(ethylene glycol) methacrylate] functionalized polydimethylsiloxane surfaces. *J. Biomed. Mater. Res., Part A* **2015**.

23. Lutz, J. F.; Stiller, S.; Hoth, A.; Kaufner, L.; Pison, U.; Cartier, R., One-pot synthesis of PEGylated ultrasmall iron-oxide nanoparticles and their in vivo evaluation as magnetic resonance imaging contrast agents. *Biomacromolecules* **2006,** *7* (11), 3132-3138.

24. Lutz, J.-F.; Akdemir, Ö.; Hoth, A., Point by Point Comparison of Two Thermosensitive Polymers Exhibiting a Similar LCST: Is the Age of Poly(NIPAM) Over? *J. Amer. Chem. Soc.* **2006,** *128* (40), 13046-13047.

25. Lutz, J.-F., Polymerization of oligo(ethylene glycol) (meth)acrylates: Toward new generations of smart biocompatible materials. *J. Polym. Sci. A, Polym. Chem.* **2008,** *46* (11), 3459-3470.

26. Cai, T.; Marquez, M.; Hu, Z., Monodisperse Thermoresponsive Microgels of Poly(ethylene glycol) Analogue-Based Biopolymers. *Langmuir* **2007,** *23* (17), 8663-8666.

27. Mohamed Boularas, a., b Elise Deniau-Lejeune,a Valérie Alard,b; Jean-François Tranchant, b. L. B. a. a. M. S. a., Dual stimuli-responsive oligo(ethylene glycol)-based microgels: insight into the role of internal structure in volume phase transitions and loading of magnetic nanoparticles to design stable thermoresponsive hybrid microgels†. *Polym. Chem* **2016,** *7* (350–363).

28. Cazares-Cortes, E.; Espinosa, A.; Guigner, J. M.; Michel, A.; Griffete, N.; Wilhelm, C.; Menager, C., Doxorubicin Intracellular Remote Release from Biocompatible Oligo(ethylene glycol) Methyl Ether Methacrylate-Based Magnetic Nanogels Triggered by Magnetic Hyperthermia. *Acs Appl Mater Inter* **2017,** *9* (31), 25775-25788.

29. Boularas, M.; Deniau-Lejeune, E.; Alard, V.; Tranchant, J.-F.; Billon, L.; Save, M., Dual stimuli-responsive oligo(ethylene glycol)-based microgels: insight into the role of internal structure in volume phase transitions and loading of magnetic nanoparticles to design stable thermoresponsive hybrid microgels. *Polym. Chem.* **2016,** *7* (2), 350-364.

30. Gawlitza, K.; Radulescu, A.; von Klitzing, R.; Wellert, S., On the structure of biocompatible, thermoresponsive poly(ethylene glycol) microgels. *Polymer* **2014,** *55* (26), 6717-6724.

31. Wellert, S.; Radulescu, A.; Carl, A.; Klitzing, R. v.; Gawlitza, K., Evolution of Size and Structure during the Polymerization Process: A SANS Study on EG-Based Microgels. *Macromolecules* **2015,** *48* (14), 4901-4909.

32. Klinger, D.; Landfester, K., Photo-sensitive PMMA microgels: light-triggered swelling and degradation. *Soft Matter* **2011,** *7* (4), 1426-1440.

33. Reis, A. V.; Fajardo, A. R.; Schuquel, I. T. A.; Guilherme, M. R.; Vidotti, G. J.; Rubira, A. F.; Muniz, E. C., Reaction of Glycidyl Methacrylate at the Hydroxyl and Carboxylic Groups of Poly(vinyl alcohol) and Poly(acrylic acid): Is This Reaction Mechanism Still Unclear? *J. Org. Chem.* **2009,** *74* (10), 3750-3757.

34. Reichmanis, E.; Smith, B. C.; Gooden, R., Ortho-Nitrobenzyl Photochemistry - Solution Vs Solid-State Behavior. *J Polym Sci Pol Chem* **1985,** *23* (1), 1-8.

35. Ajayaghosh, A.; George, M. V.; Yamaoka, T., Photoresists Based on a Novel Photorearrangement of O-Nitrobenzylic Polymers. *J Mater Chem* **1994,** *4* (12), 1769-1773.

36. Reis, A. V.; Fajardo, A. R.; Schuquel, I. T. A.; Guilherme, M. R.; Vidotti, G. J.; Rubira, A. F.; Muniz, E. C., Reaction of Glycidyl Methacrylate at the Hydroxyl and Carboxylic Groups of Poly(vinyl alcohol) and Poly(acrylic acid): Is This Reaction Mechanism Still Unclear? *J Org Chem* **2009,** *74* (10), 3750-3757.

37. Ratcliffe, L. P.; Ryan, A. J.; Armes, S. P. J. M., From a water-immiscible monomer to block copolymer nano-objects via a one-pot RAFT aqueous dispersion polymerization formulation. **2013,** *46* (3), 769-777.

38. Saunders, B. R.; Laajam, N.; Daly, E.; Teow, S.; Hu, X.; Stepto, R., Microgels: From responsive polymer colloids to biomaterials. *Adv. Coll. Interf. Sci.* **2009,** *147-148*, 251-262.

39. Saunders, B. R.; Vincent, B., Thermal and osmotic deswelling of poly(NIPAM) microgel particles. *J. Chem. Soc., Faraday Trans.* **1996,** *92* (18), 3385-3389.

40. Bergmann, S.; Wrede, O.; Huser, T.; Hellweg, T., Super-resolution optical microscopy resolves network morphology of smart colloidal microgels. *Phys. Chem. Chem. Phys.* **2018,** *20* (7), 5074-5084.

41. Falender, J. R.; Yeh, G. S. Y.; Mark, J. E., The effect of chain length distribution on elastomeric properties. 1. Comparisons between random and highly nonrandom networks. *J. Amer. Chem. Soc.* **1979,** *101* (24), 7353-7356.

42. Conforti, P. F.; Garrison, B. J., Electronic structure calculations of radical reactions for poly(methyl methacrylate) degradation. *Chem. Phys. Lett.* **2005,** *406* (4), 294-299.

43. Flory, P. J., *Principles of polymer chemistry, Cornell University Press, NY.* **1954.**

44. Boularas, M.; Deniau-Lejeune, E.; Alard, V.; Tranchant, J. F.; Billon, L.; Save, M., Dual stimuli-responsive oligo(ethylene glycol)-based microgels: insight into the role of internal structure in volume phase transitions and loading of magnetic nanoparticles to design stable thermoresponsive hybrid microgels. *Polym Chem-Uk* **2016,** *7* (2), 350-363.

45. Clarke, D. E.; Pashuck, E. T.; Bertazzo, S.; Weaver, J. V. M.; Stevens, M. M., Self-Healing, Self-Assembled beta-Sheet Peptide Poly(gamma-glutamic acid) Hybrid Hydrogels. *J Am Chem Soc* **2017,** *139* (21), 7250-7255.

46. Claudia Fischbach, J. T., Andrea Lucke, EdithSchnell, Georg Schmeer, Torsten Blunk, Achim Göpferich, Does UV irradiation affect polymer properties relevant to tissue engineering? *Surface Science* **2001,** *491* (1), 333-345.

47. Nisato, G.; Munch, J. P.; Candau, S. J., Swelling, Structure, and Elasticity of Polyampholyte Hydrogels. *Langmuir* **1999,** *15* (12), 4236-4244.

48. Zhong, M.; Liu, Y.-T.; Xie, X.-M., Self-healable, super tough graphene oxide-poly(acrylic acid) nanocomposite hydrogels facilitated by dual cross-linking effects through dynamic ionic interactions. *J. Mater. Chem. B* **2015,** *3* (19), 4001-4008.

49. Webber, R. E.; Creton, C.; Brown, H. R.; Gong, J. P., Large Strain Hysteresis and Mullins Effect of Tough Double-Network Hydrogels. *Macromolecules* **2007,** *40* (8), 2919-2927.

50. Sun, T. L.; Kurokawa, T.; Kuroda, S.; Ihsan, A. B.; Akasaki, T.; Sato, K.; Haque, M. A.; Nakajima, T.; Gong, J. P., Physical hydrogels composed of polyampholytes demonstrate high toughness and viscoelasticity. *Nat. Mater.* **2013,** *12*, 932.

51. Milani, A. H.; Freemont, A. J.; Hoyland, J. A.; Adlam, D. J.; Saunders, B. R., Injectable Doubly Cross-Linked Microgels for Improving the Mechanical Properties of Degenerated Intervertebral Discs. *Biomacromolecules* **2012,** *13* (9), 2793-2801.

Chapter 5: Reversible light triggered swelling changes of temperature and pH-responsive OEGMA-based microgels

5.1 Abstract

In this chapter, four different size microgels (MG-CMA) ranging from 25 nm to 124 nm (TEM diameters) which are photo-, pH-, temperature- responsive are synthesised. The poly(MEO_2MA-MAA-CMA) MGs were prepared by copolymerisation of 2-(2-methoxyethoxy)ethyl methacrylate (MEO_2MA), methacrylic acid (MAA) and 7-(2-methacryloyloxyethoxy)-4-methylcoumarin (CMA) via one step precipitation polymerisation. The crosslinker density was easily controlled by alternating irradiation wavelengths of 365 nm (photo-crosslinked state) and 254 nm (photo-decrosslinked state). The pH- and temperature-triggered swelling changes for the MGs were photo-tunable. The relative volume increase upon photo-de-crosslinking is much greater than reported for other works. This is attributed to the uniform distributions of CMA and photo-induced crosslinker within the MGs. Unexpectedly, it was found that the extent of photo-induced dimerisation increased with decreasing as-made MG size. The photo-induced swelling of the MGs was used to accelerate release of the encapsulated anti-cancer drug doxorubicin (DOX) to demonstrate potential for on-demand drug release.

5.2 Introduction

Coumarin is well known molecule to prepare photoswitchable particles as reversible photo-induced formation of cyclobutane rings (dimerisation) occurs under irradiation with a wavelength (λ) > 310 nm and photocleavage of the dimers occurs under irradiation at λ < 260 nm[1, 2]. The first photocontrollable particles using coumarin were macromicelles[3]. An encapsulated solute was released via photo-de-crosslinking[3]. But the photo-tuneable change of size is negligible. He et al.[4] developed polymer micelles PEO-*b*-P(MEO_2MA-*co*-CMA) bearing coumarin methacrylate (CMA) side groups. (EO is ethylene oxide, MEO_2MA is 2-(2-methoxyethoxy)ethyl methacrylate). They found the photocleavage of coumarin could reduce the cross-linking density and lead to an increase in volume of nanoparticles by ~90%. The first pH-responsive and photo crosslink nanogel was prepared using photo-crosslinkable diblock copolymer micelles containing DMEMA and coumarin[5]. (DMEMA is 2-(diethylamino)ethyl methacrylate). Furthermore, He et al.[6] synthesised a series of nanoparticles with coumarin randomly incorporated into two polymer block P(DMA-co-CMA)-*b*-P(NIPAM-co-CMA) (DMA and NIPAM are *N,N*-dimethylacrylamide and *N*-isopropylacrylamide, respectively). They concluded the photo-controllable size change of nanoparticles was much stronger for coumarin copolymerised in both core and shell than in core or shell only. Dong et al.[7] synthesised photo-, temperature-, pH-, and ion-responsive weak polyelectrolyte spherical brushes under different modes of confinement by copolymerisation the DMEMA and CMA anchored to silica nanoparticles via surface-initiated atom transfer radical polymerisation (si-ATRP). The synthesis methods (ATRP or PAFT) for those micelle or nanoparticles involve several steps and may be difficult to scale up. In contrast, precipitation polymerisation, which is used here, provides the possibility to tune the properties of MGs conveniently and is also scalable[8].

Triply responsive MGs have been developed in recent decades for the delivery of various therapeutic agents[9-11]. Zhan et al.[12] reported biocompatible nanogels with thermos-, redox, and pH-triple sensitivity, prepared through *in situ* polymerisation of NIPAM, acrylic acid (AA) and *N*,*N*-bis(acryloyl)cystamine (BAC) as a biodegradable crosslinker. Jiang et al. [13] reported a photo-, temperature- and pH-responsive copolymer poly(DMAEMA-SP) (DMAEMA is dimethylaminoethyl methacrylate and SP is spiropyran) system which could self-assemble into nanoparticles. Hydrophobic dyes could be released upon stimulation using UV light, temperature and pH[13]. Chen et al. [14] reported a photo-, pH-, and redox-responsive MGs of poly(acrylic acid-co-spiropyran methacrylate) crosslinked by BAC. Wang et al.[15] synthesised poly(vinylcaprolactam) (PVCL)-based biodegradable MGs with BAC as cross-linker, methacrylic acid (MAA), VCL and polyethylene glycol methyl ether methacrylate (POEGMA) as comonomer. They found the VPTT shifted to higher temperature with increasing MAA content.[15] In chapter 4, I reported a triply responsive MGs copolymerised with oligo(ethylene glycol)methacrylate (OEGMA), MEO_2MA, MAA and a o-nitrobenzyl-based UV photocleavable crosslinker. The MGs showed temperature-, pH- and light- responsive behaviours. However, the photo-cleavage of that crosslinker is irreversible, which limits it potential application. This limitation is overcome in this study where we replaced that crosslinker with CMA and study reversibly photo-switchable MGs.

The previous photo-switchable particles were of a size range less than 50 nm[4, 5, 16]. Realising the potential of precipitation polymerisation (which is scalable) to provide MGs with TEM diameters in the range of 25 to 124 nm, named MG-CMA1 to MG-CMA4, respectively, were prepared based on poly(MEO_2MA-MAA-CMA). The CMA was synthesised with two steps following the reported work as shown in Scheme 5.1.

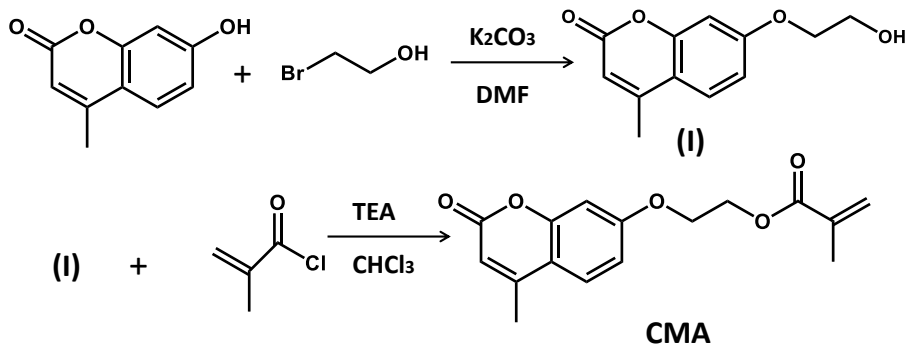

Scheme 5.1. Depiction of synthesis of CMA

The triply responsive MG-CMA copolymerizing by comonomer MEO_2MA, MAA and CMA with precipitation polymerization (Scheme 5.2A) show photo-, thermal- and pH-responsive behaviours. The pH and thermal sensitivity of the MGs can be reversibly tuned by UV light with two different wavelengths. The CMA groups present can be photo-crosslinked or de-crosslinked using 365 nm and 254 nm, respectively (Scheme 5.2B).

This study begins with the investigation of temperature- and pH-responsive behaviours properties of four MGs. The effects of photo-crosslinking and de-crosslinking on these behaviours with tuning the two wavelength of UV light (365 nm and 254 nm) are then studied as well as the reversibility of photo-switching. The crosslinked MGs could undergo reversible photocleavage leading to substantial particle volume swelling ratio increases. The photo-triggered volume ratio increases are the highest for CMA-containing responsive MGs. The release behaviour for encapsulated anti-cancer drug DOX from MG-CMA4 is investigated to demonstrate photo-triggered the potential for drug delivery. This study provides insight into the structure-property relationships for new photo-switchable MGs and also an indication that these new MGs have potential application in on-demand drug delivery.

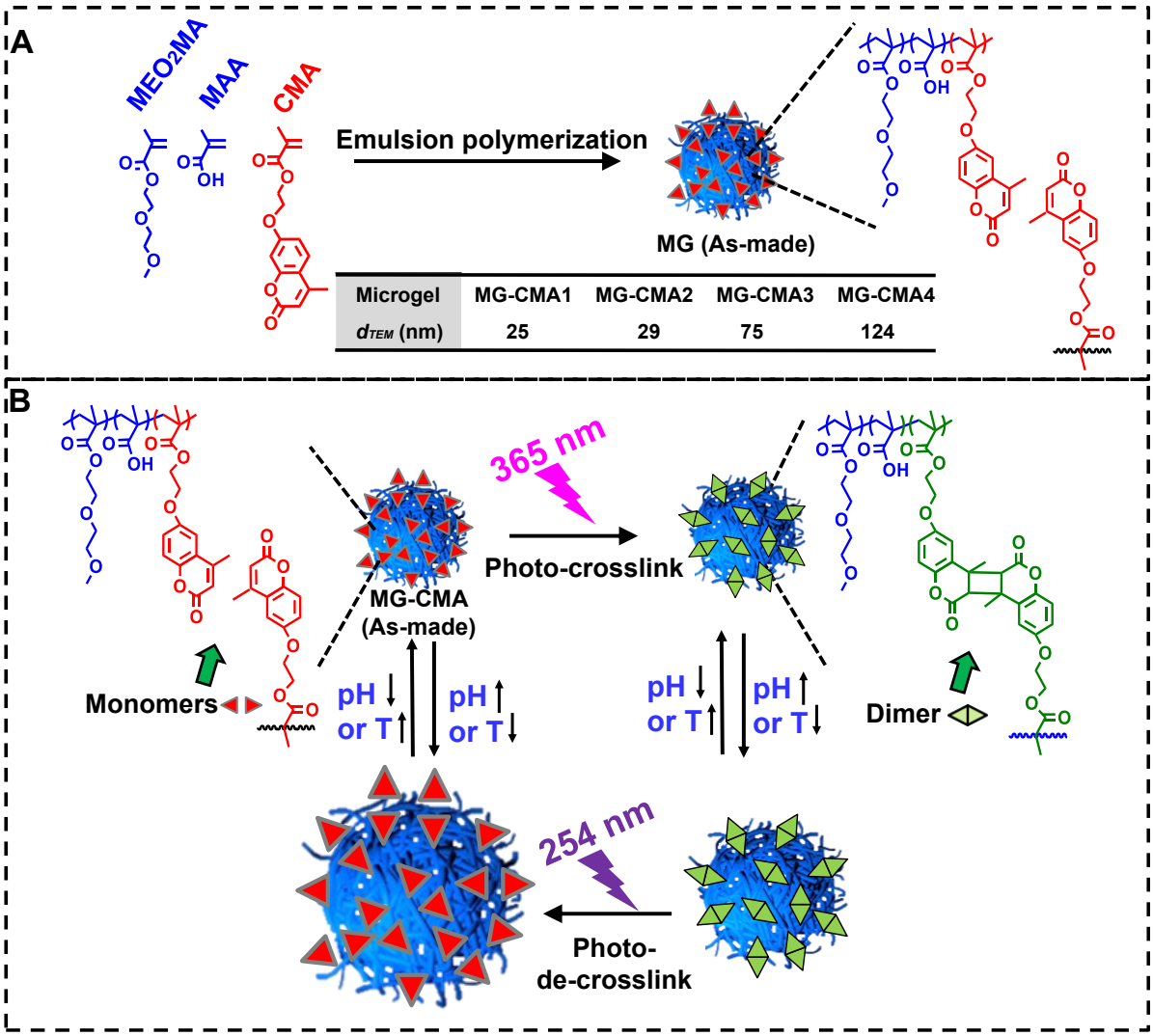

Scheme 5.2. (A) Synthesis of Poly(MEO_2MA-MAA-CMA) MGs. The table gives the as made TEM diameters of the four different MGs systems studied. (B) MGs show reversible pH-, temperature- and photo-responsive behaviours. The CMA monomers can be reversibly photo-crosslinked to give crosslinked dimers (green arrows).

5.3 Experimental detail

5.3.1 Materials

2-(2-methoxyethoxy)ethyl methacrylate (MEO_2MA, 95%), methacrylic acid (MAA, 98%), sodium dodecyl sulphate (SDS, 98.5 %), potassium persulfate (KPS, 99%), ammonium persulfate (APS, 98%,), potassium carbonate (K_2CO_3, ACS grade), chloroform ($CHCl_3$, ≥ 99.5%), chloroform-d ($CDCl_3$, 99.8 atom % D), methanol (MeOH, ≥99.9%), methacryloyl chloride (97.0%) were all purchased from Aldrich. 4-Methylumbelliferone (≥ 98%), 2-bromoethanol (95%), N,N-dimethylformamide (DMF, ACS grade), ethanol (100%), triethylamine (TEA, 99%), dichloromethane (CH_2Cl_2, ≥ 99.8%) , doxorubicin hydrochloride (DOX) were purchased from Fisher Scientific. All materials were used as received. Ultrahigh purity water was used that had been doubly filtered and deionised. The dialysis tubing (8000 MWCO) was purchased from Thermofisher Scientific.

5.3.2 Synthesis of 7-(2-methacryloyloxyethoxy)-4-methylcoumarin (CMA)

The synthesis route for CMA involved two steps[17] (Scheme 5.1). To synthesise the precursor, 7-(2-hydroxyethoxy)-4-methylcoumarin (**(I)**), 4-methylumbelliferone (4.00 g, 22.7 mmol) and K_2CO_3 (6.23 g 45.4 mmol) in anhydrous DMF (40 mL) were heated to 90 °C under a N_2 atmosphere. Then, 2-bromoethanol (2.24 mL, 34.0 mmol) was added dropwise. The reaction was refluxed for 20 h. After being cooled to room temperature the reaction mixture was poured into ice-cold water (800 mL) and then maintained at 5 °C for a further 6 h. The precipitate was collected by vacuum filtration and dried in vacuum for three days. **(I)** was obtained as a white solid (4.85 g, 97.0 % yield) which was stored in the dark until required.

To synthesise CMA, **(I)** (4.50 g, 20.4 mmol) and TEA (4.50 g, 44.2 mmol) were dissolved in $CHCl_3$ (72.0 mL). Methacryloyl chloride (4.50 g, 43.0 mmol) was added dropwise to the stirred solution at 0 °C. After being allowed to warm to room temperature the solution was stirred overnight. The solution was diluted with CH_2Cl_2, washed with brine three times and dried over $MgSO_5$. The product was concentrated using rotary evaporation. The crude product was recrystallised from ethanol to obtain CMA. The white solid (3.53 g, 60 % yield) was stored in the dark until required.

5.3.3 Synthesis of MGs

5.3.3.1 Synthesis of MG-CMA1 and MG-CMA2 using continuous precipitation copolymerisation

The first two MGs (MG-CMA1 and MG-CMA2) were synthesised via continuous precipitation copolymerisation. The total mass of comonomers used was larger for MG-CMA2 (1.80 g) compared to MG-CMA1 (1.35 g) in order to increase the final MGs size of MG-CMA2. (The comonomer mixture compositions employed are shown in Table 5.1. The synthesis for MG-CMA1 is given as an example. SDS (0.11 g) was dissolved in water (19.6 mL), and the solution purged with N_2 for 60 min to remove dissolved oxygen and heated to 80 °C. APS solution (10 mg in 0.40 g water) was added to the reaction flask. A comonomer solution containing MEO_2MA (1.13 g, 6.0 mmol), CMA (0.25 g, 0.80 mmol) and MAA (0.17 g, 2.1 mmol) was added at a uniform rate of 0.10 mL/min until the required mass had been added. The reaction was continued for 1.0 h and the nitrogen atmosphere was maintained. The reaction mixture was then cooled to room temperature and the dispersion dialysed against water for 7 days. The dispersion was washed with $CHCl_3$ three times to remove unreacted monomer and residual chloroform removed by

rotary evaporation. The pH for as made MGs was 2.8. The dispersion was protected from light using aluminium foil.

5.3.3.2 Synthesis of MG-CMA3 and MG-CMA4 using batch precipitation copolymerisation

The second two MGs systems (MG-CMA3 and MG-CMA4) were prepared by aqueous batch precipitation copolymerisation. The synthesis for MG-CMA3 is given as an example. (See Table 5.1 for composition details). Briefly, SDS (5.0 mg) was dissolved in water (20.0 mL) and the solution purged with N_2 for 60 min and heated to 70 °C. A comonomer solution containing MEO_2MA (0.17 g, 0.9 mmol), CMA (0.04 g, 0.14 mmol) and MAA (0.029 g, 0.34 mmol) was added. An aqueous KPS solution (5.0 mg in 1.0 g water) was then added quickly. The polymerisation was continued for 6 h, cooled to room temperature and the dispersion dialysed against water. The dispersion was washed with chloroform three times to remove unreacted monomer and residual chloroform removed by rotary evaporation. The pH was 3.0. The dispersion was protected from light using aluminium foil.

To probe the CMA distribution within the MG-CMA3 particles as a function of time samples were removed during particle growth to obtain the d_z value and then extensively dialysed against DMF. The content of polymerised CMA was obtained using UV-visible spectra of the dispersions, the calibration graph shown in Figure 5.2 and Beer's law.

Table 5.1 Comonomer formulations used to prepare the MGs

MGs	MEO_2MA / mol.%	MAA / mol.%	CMA / mol.%	Total mass/g[a]
MG-CMA1	66.0	24.0	10.0	1.35
MG-CMA2	66.0	24.0	10.0	1.80
MG-CMA3	65.5	24.5	10.0	0.24
MG-CMA4	60.4	23.6	16.0	0.24

[a] Total mass of monomers.

5.3.4 Photo-induced crosslinking and de-crosslinking

Irradiation of all MGs dispersion were conducted using a CL 1000 Ultraviolet Crosslinker equipped with five lamps which provided a wavelength of 365 nm and 254 nm and an intensity of 14 mW/cm^2 and 10 mW/cm^2 respectively. For obtaining UV-vis spectra and dynamic light scattering (DLS) data the MG dispersions (0.010 wt %) in quartz cuvettes were incubated at 60°C (pH 5.4) for 20 min and irradiated with UV light (365 nm) to photo-crosslink the MGs. The dispersion was then diluted in 0.10 M buffer solution of the required pH to obtain DLS data. The dispersions were irradiated with 254 nm UV light for photo-de-crosslinking in the swollen state (typically pH 7.4) and UV-vis spectra and DLS data measured. The dimerisation degree (DD) is a measure of the efficiency of photo-crosslinking and was estimated using[7]

$$DD = 100\left(1 - \frac{A_t}{A_0}\right) \qquad (5.1)$$

where A_0 and A_t are the initial absorbance and the absorbance after an irradiation time t measured using UV-vis spectroscopy.

5.3.5 Photo-induced release of DOX from MG-CMA4 particles

To load the anticancer drug DOX into photo-crosslinked MG-CMA4 particles the dispersion (0.066 wt%, 2.1 mL) was irradiated for 6 h at 365 nm. The dispersion (pH 3.8) was then mixed with aqueous DOX solution (0.50 mg/mL, 750 µL). The pH value of the mixture was adjusted to 7.4 with aqueous NaOH solution (0.50 M) to swell the particles and the dispersion stirred vigorously overnight in the dark at room temperature. The DOX-loaded crosslinked MG-CMA4 particles were then centrifuged three times to remove the free DOX. The dispersion was then diluted to 0.020 wt% with water. The final pH was 6.35.

For the determination of drug-loading content, DOX loaded MG-CMA4 particles were analysed by UV-vis spectra at 485 nm, using a calibration curve obtained with different DOX concentrations (Figure 5.16). The drug loading content (DLC) and drug loading efficiency (DLE) were calculated according to:

$$DLC = \frac{100M_o}{M_{MG}} \qquad (5.2)$$

$$DLE = \frac{100M_o}{M_{DOX(Feed)}} \qquad (5.3)$$

where M_o, M_{MG} and $M_{DOX(Feed)}$ are the original masses of DOX in the MGs, mass of the dry MGs and mass of DOX used to load the particles, respectively.

The release behaviour of the DOX-loaded MG-CMA4 was investigated at pH 6.0 and 7.4 with or without 254 nm UV light irradiation. For the release of DOX of photo-de-crosslinked MG-CMA4, the pH of the DOX-loaded particles (0.02 wt%, 0.75 mL) was adjusted to 6.0 or 7.4 with aqueous NaOH and HCl solution respectively, and then irradiated with UV light 254 nm for 2 min. For the release of DOX of photo-crosslinked MG-CMA4, the pH of the DOX-loaded particles was adjusted to 6.0 or 7.4 directly. All dispersions were then centrifuged (14,500 rpm for 60 min) and the supernatant solution (0.70 mL) analysed using UV-vis spectra at 480 nm to determine the released DOX content. The release is discussed in terms of the cumulative fractional release (M_t /M_o) of DOX from the particles where M_t is the total mass of DOX released to the supernatant at time, t.

5.3.6 Physical Measurements

^{1}H NMR spectra were measured using a B400 Bruker Avance III 400 MHz spectrometer. UV-vis spectra were measured using a PerkinElmer Lambda 25 UV/VIS spectrometer. FTIR spectra were measured using Nicolet 5700 ATR-FTIR spectrometer. Titration

measurements were conducted in the presence of aqueous NaCl (0.050 M) using a Mettler Toledo titration instrument. TEM images were obtained using a FEI Tecnai 12 BioTwin instrument and were stained using uranyl acetate solution (0.50 wt.%). Number-average diameters from TEM images were obtained using Image-J software. DLS data and electrophoretic mobility data were obtained using a Malvern Zetasizer NanoZS instrument fitted with a 20 mW HeNe laser and the angle of detection was set at 173°.

5.4 Results and Discussion

5.5.1 Characterization of the crosslinker nPh

The photo-sensitive monomer CMA was characterised by ^{1}H NMR and UV-vis spectra. Figure 5.1 shows the ^{1}H NMR spectra for the nPh. The peak positions and integrations confirmed the identify and high conversion (95%) of CMA. The calculation of the conversion is shown as below. The integrations of peak (i) and (h) are 0.96 and 3.03 respectively.

So the calculated ratio for the peak (i) and (h) is 0.317. ($^{0.96}/_{3.03}$ = 0.317)

The theoretical ratio for the peak (i) and (h) should be 0.333. ($^{1}/_{3}$ = 0.333),

Hence, the conversion can be calculated: $^{0.317}/_{0.333}$= 95.2%

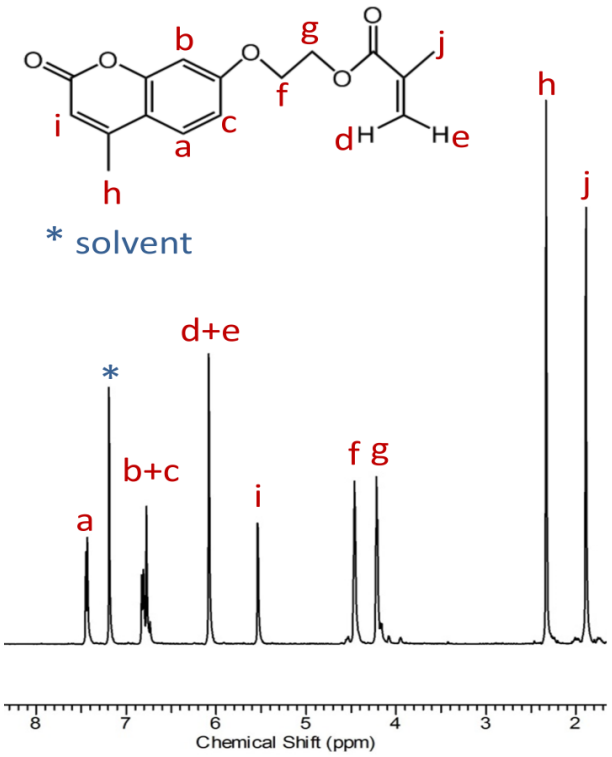

Figure 5.1.^{1}H NMR spectrum and assignments for CMA

UV-vis spectra measurements for CMA at different concentration in solvent (MeOH) were also carried out (Figure 5.2A). Figure 5.2B shows that the variation of absorbance at 320 nm is fitting well and the calculated molar extincition coefficient is 13947 mol^{-1} dm^3 cm^{-1}. The calibration graphs (Figure 5.2B) allowed the CMA contents in the MG-CMA to be determined.

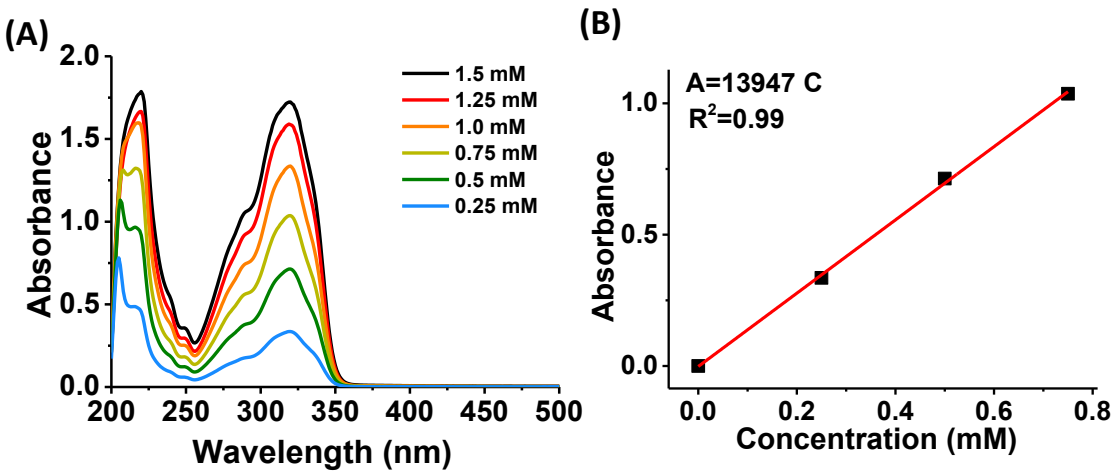

Figure 5.2. (A) UV-visible spectra for CMA at various concentrations in methanol. **(B)** Variation of absorbance at 320 nm with CMA concentration. The molar extinction coefficient was calculated from (B) as 13947 mol^{-1} dm^3 cm^{-1}.

5.5.2 Composition and properties of the MG-CMA

The synthetic methods used to prepare the four MG-CMA systems were continuous precipitation copolymerisation (for MG-CMA1 and MG-CMA2) and batch precipitation copolymerisation (for MG-CMA3 and MG-CMA4). Continuous precipitation copolymerisation uses a high surfactant concentrations together with a uniform comonomer feed rate to form sub-100 nm particles[18]. The batch precipitation copolymerisations used lower DS concentrations to grow relatively large MG-CMA3 and MG-CMA4 particles.

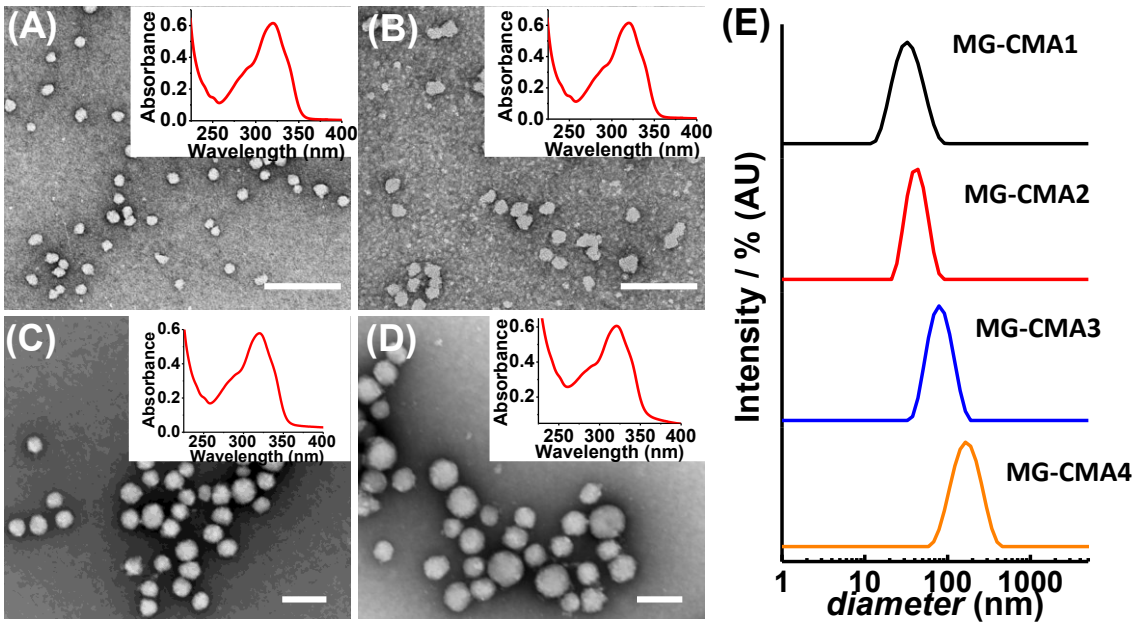

Figure 5.3. TEM images for (A) MG-CMA1, (B) MG-CMA2, (C) MG-CMA3 and (D) MG-CMA5. The scar bars are 200 nm. The inset of (D) shows the UV-Vis spectra for the MGs with a maximum due to coumarin. Similar spectra were obtained for MG-CMA1, MG-CMA2 and MG-CMA3. (E) DLS size distributions for the as made MGs measured at pH 6.0 and 65°C.

The morphology of obtained MGs is shown in Figure 5.3. TEM images measured for the MGs show that they had as-made diameters (d_{TEM}) ranging from 25 nm to 124 nm. The larger size of the d_z values compared to those measured from TEM is because the MGs contained some water at pH 6.0 and 60 ºC. DLS data obtained using the later conditions (Figure 1E) confirmed that MG-CMA1 (d_z = 28 nm) was considerably smaller than MG-CMA2 (39 nm); whereas, MG-CMA3 (77 nm) was about half the size of MG-CMA4 (150 nm). The MG-CMA1 particles were smaller than the MG-CMA2 particles because the total comonomer fed into the reactor was 25% less for the former system (Table 5.1). We discovered that the MGs size could be increased when prepared using batch precipitation polymerisation samples (MG-CMA3 and MG-CMA4) by increasing the CMA concentration used during preparation. It follows that increasing the CMA concentration decreases the colloidal stability of the initially formed pre-particles which enhances aggregation before stabilised particles grow. However, this did not translate into

significant differences in CMA contents for the purified MGs. Unreacted CMA was removed by chloroform washing.

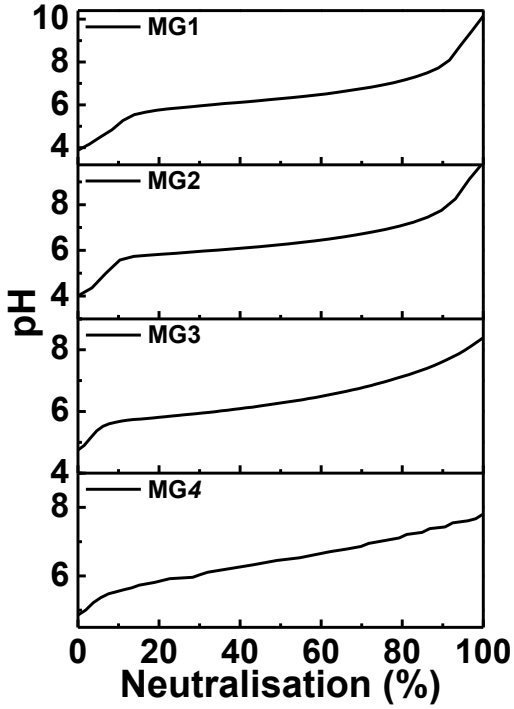

Figure 5.4. Potentiometric titration data for MG-CMA dispersions

Potentiometric titration data (Figure 5.4) were used to determine the MAA contents and these ranged from 27.9 to 30.5 mol%. The apparent pK_a values for the MGs were 5.9 to 6.2 (Table 5.2). The CMA content in the MGs was determined using UV-vis spectra and the absorption maximum at 320 nm from coumarin. The CMA content for each MG system was in the range 7.5 - 7.9 mol%. The MEO_2MA units comprised the majority of these MGs. The calculation of CMA content in MGs (take MG-CMA4 as example) is shown as below. The 320 nm absorbance of 0.0001 g/mL MG-CMA4 particle dispersion was found to be 0.605 (Figure 5.3D insert). Using the line of best fit equation given Figure 5.2B, this corresponds to CMA concentration in MG-CMA4 is:

$0.605/_{13947}$ = 4.35 $\times 10^{-5}$ mol/L= 1.27$\times 10^{-5}$ g/ mL

Therefore, 1.27$\times 10^{-5}$ g/mL $\div$0.0001 g/ mL = 12.70 wt.% = 7.5 mol%

The compositions and particle size data for the four MG-CMA are shown in Table 5.2.

Table 5.2. Composition and properties of the MGs.

MGs	MEO_2MA/ mol%	MAA / mol% [a]	CMA / mol%[b]	pK_a[c]	d_{TEM} /nm[d]	d_z /nm [e] (pH 6.0, 60°C)
MG-CMA1	64.2	27.9	7.9	6.1	25 ± 5	28 [0.060]
MG-CMA2	61.7	30.5	7.8	6.2	29 ± 5	39 [0.020]
MG-CMA3	64.1	28.1	7.8	5.9	75 ± 7	77 [0.048]
MG-CMA4	62.7	29.8	7.5	5.9	124 ± 11	150 [0.105]

[a] Determined from potentiometric titration data (Figure 5.4). [b] Calculated using the UV-vis spectra for CMA (Figure 5.2) and those for each MGs. [c] Apparent pK_a value determined from potentiometric titration data. [d] The ± values are the standard deviation. [e] z-average diameters. The numbers in brackets are the polydispersity index (PDI) values.

5.5.3 Studying the pH and thermal responsive properties of the as-made (non-irradiated) MGs by DLS

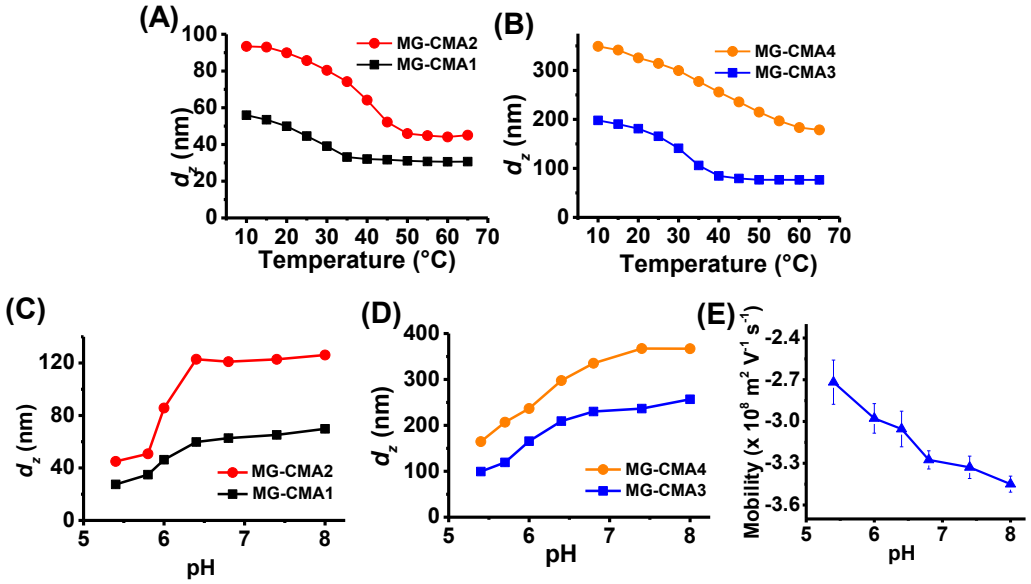

Figure 5.5. Temperature responsive properties for as-made **(A)** MG-CMA1 and MG-CMA2 and **(B)** MG-CMA3 and MG-CMA4 dispersions. The pH-responsive properties are also shown for **(C)** MG-CMA1 and MG-CMA2 and **(D)** MG-CMA3 and MG-CMA4 dispersions at 25 °C. **(E)** Variation of electrophoretic mobility with pH for as-made MG-CMA4 at 25 °C.

Variable temperature DLS data for the as-made, non-irradiated, MG dispersions at 6.0 are shown in Figure 5.5A and B. The d_z values decreased by a factor of ~ 2 when the

temperature was increased from 10 to 60 °C due to the disruption of hydrogen bond between water and P(MEO_2MA). The size distributions remained monomodal (see Figure 5.6A-D). Figures 5.5C and D show the variation of d_z with pH for all the MGs at 25 °C. The d_z values increased strongly as the pH approached the respective apparent pK_a values (of 5.9 - 6.2, Table 5.2) due to increasing electrostatic repulsion between $–COO^-$ groups. This is supported by electrophoretic mobility measurements for MG-CMA4 where the values became increasingly negative as the pH increased (Figure 5.5E).

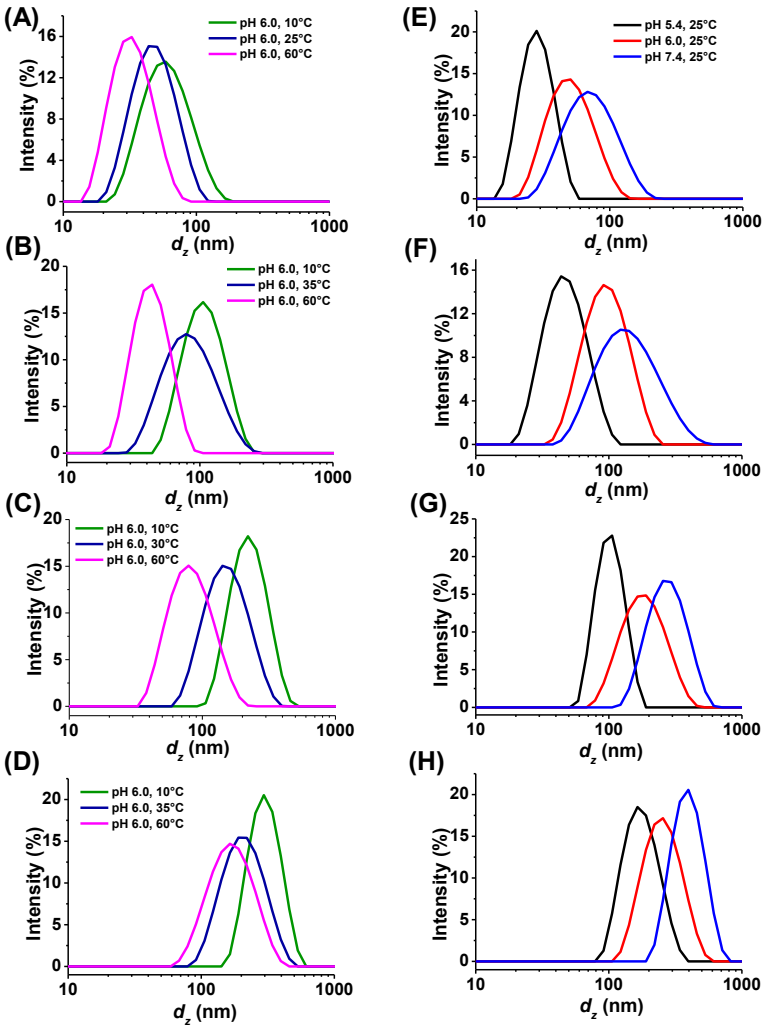

Figure 5.6. DLS size distributions for as-made (non-irradiated) MG-CMA1 **(A)**, MG-CMA2 **(B)**, MG-CMA3 **(C)** and MG-CMA4 **(D)** at different temperatures. The pH was 6.0. DLS size distributions for as-made (non-irradiated) MG-CMA1 **(E)**, MG-CMA2 **(F)**, MG-CMA3 **(G)** and MG-CMA4 **(H)** at different temperatures. The temperature was 25 °C. The scale in (E) applies to (F)-(H).

The DLS size distributions remained monomodal with no evidence of particle fragmentation as the pH increased or temperature decreased (Figure 5.6A-H). It is interesting that the microgels did not disassemble when swelling despites the fact that no crosslinking monomer was used during preparation. Self-crosslinking is not possible for methacrylate monomers cause lacking the tert-C on the main chain during synthesis[19]. The self-crosslinking is due to chain transfer reactions via the hydrogen atom on the tert-C of the polymer main chain[19]. Consequently, this result is attributed to polymer chain entanglement as well as reversible photodimerisation and cleavage through two-photon absorption of visible light of coumarins[3]. Even though we protected the MG dispersion from visible light as much as possible, some light exposure was inevitable during synthesis.

5.5.4 UV light induced MG property changes

Irradiation at 365 nm was used to form the coumarin dimer via the [2πs+ 2πs] cycloaddition formation of cyclobutane the ring (see Scheme 5.1)[1, 2]. This photoreaction added crosslinks to the MGs. The dimers also underwent photocleavage on exposure to UV light at 254 nm. This photo-crosslinking reaction is new in the context of MGs and was therefore investigated. Figure 5.7A shows the UV-vis spectra change of as-made MG-CMA4 particles upon irradiation at 365 nm. The decrease of absorption peak at 320 nm is due to photo-dimerisation of CMA and formation of crosslinks in the MG (depicted in Scheme 5.2). The time-dependent DD is shown in Figure 5.7B and reveals the DD increased relatively rapidly at first and then reached a plateau value of ~ 60% after 150 min of irradiation. It should be noted that the photo-crosslinking was performed at pH 5.4 and 60 ºC. Samples were then diluted in buffer at pH 7.4 and the DLS data measured at 25°C. These data showed that d_z decreased from 370 to 260 nm.

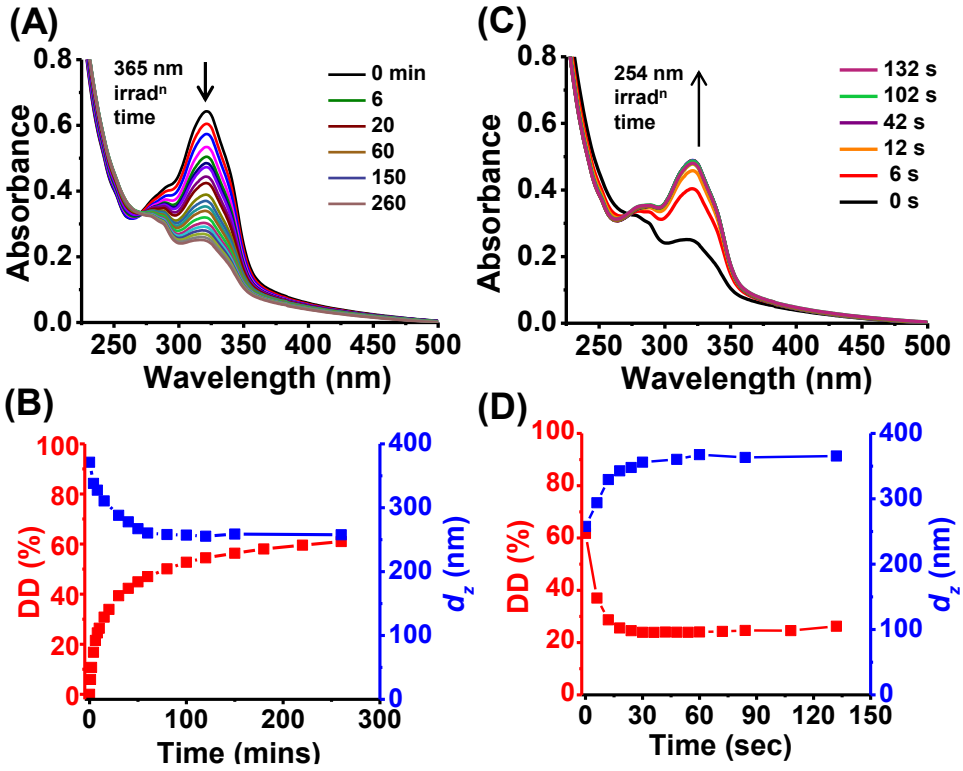

Figure 5.7. UV-vis spectra of MG-CMA4 during **(A)** photo-crosslinking at 365 nm and (**B**) variation of d_z and DD with time. (**C**) UV-vis spectra measured during photo-de-crosslinking at 254 nm and (**D**) Variation of d_z and DD with time. The pH and temperature used to obtain the d_z data were 7.4 and 25°C.

When the photo-crosslinked MG-CMA4 dispersion was subsequently irradiated at 254 nm the absorbance at 320 nm increased rapidly due to photocleavage of the dimers (see Figure 5.7C). The DD reached a minimum value of 24.9 % in only 18 sec and the d_z increased from 258 to 366 nm (see Figure 5.7D). The rate of change of DD during photo-de-crosslinking was much faster rate than photo-crosslinking. Photo-de-crosslinking was faster because the MGs were swollen (pH 7.4, 25 °C) which favoured light penetration into the particle interior. In contrast photo-crosslinking was performed using deswollen particles (pH 5.4, 60 °C). Additionally, the photocleavage activation energy is much lower than that for photo-dimerisation[20].

It can be seen from Figure 5.7D that a stable DD degree of 25 % was reached upon 254 nm irradiation. This result implies that photocleavage was incomplete. Presumably, stable

isomers of coumarin dimer components formed (e.g., anti-head-to-tail coumarin dimers) that are difficult to photocleave[21]. Additionally, upon irradiation with 254 nm light, some photo-dimerisation inevitably occurs because of the relatively high concentration of monomeric coumarin groups[22]. The diameter recovered to 366 nm even though the DD remained at 25 %. It follows that the *residual* coumarin dimers did not form elastically effective chains.

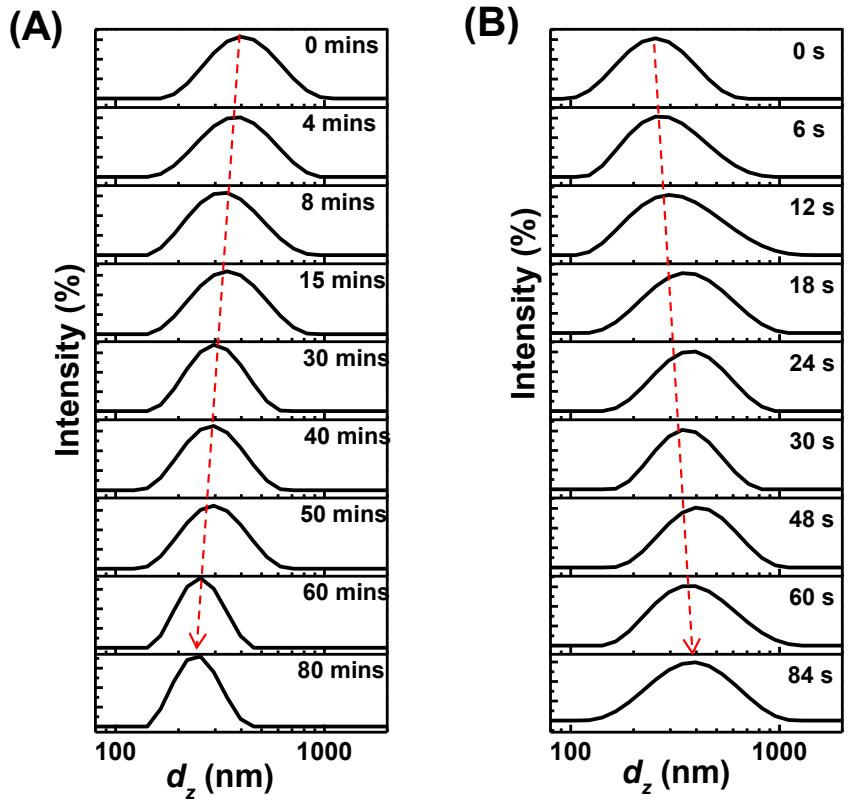

Figure 5.8. DLS size distributions measured for MG-CMA4 during (A) photo-crosslinking using 365 nm irradiation and (B) photo-de-crosslinking using 254 nm irradiation. The data were measured at pH 7.4 and 25 °C. The dotted lines highlight the changes that occurred.

The corresponding DLS distribution data (Figure 5.8) showed that the distributions remained monomodal during photo-triggered crosslinking and de-crosslinking, which shows that fragmentation of the MGs did not occur. Hence, the dz decrease and increase was due to photo-crosslinking via coumarin dimerisation.

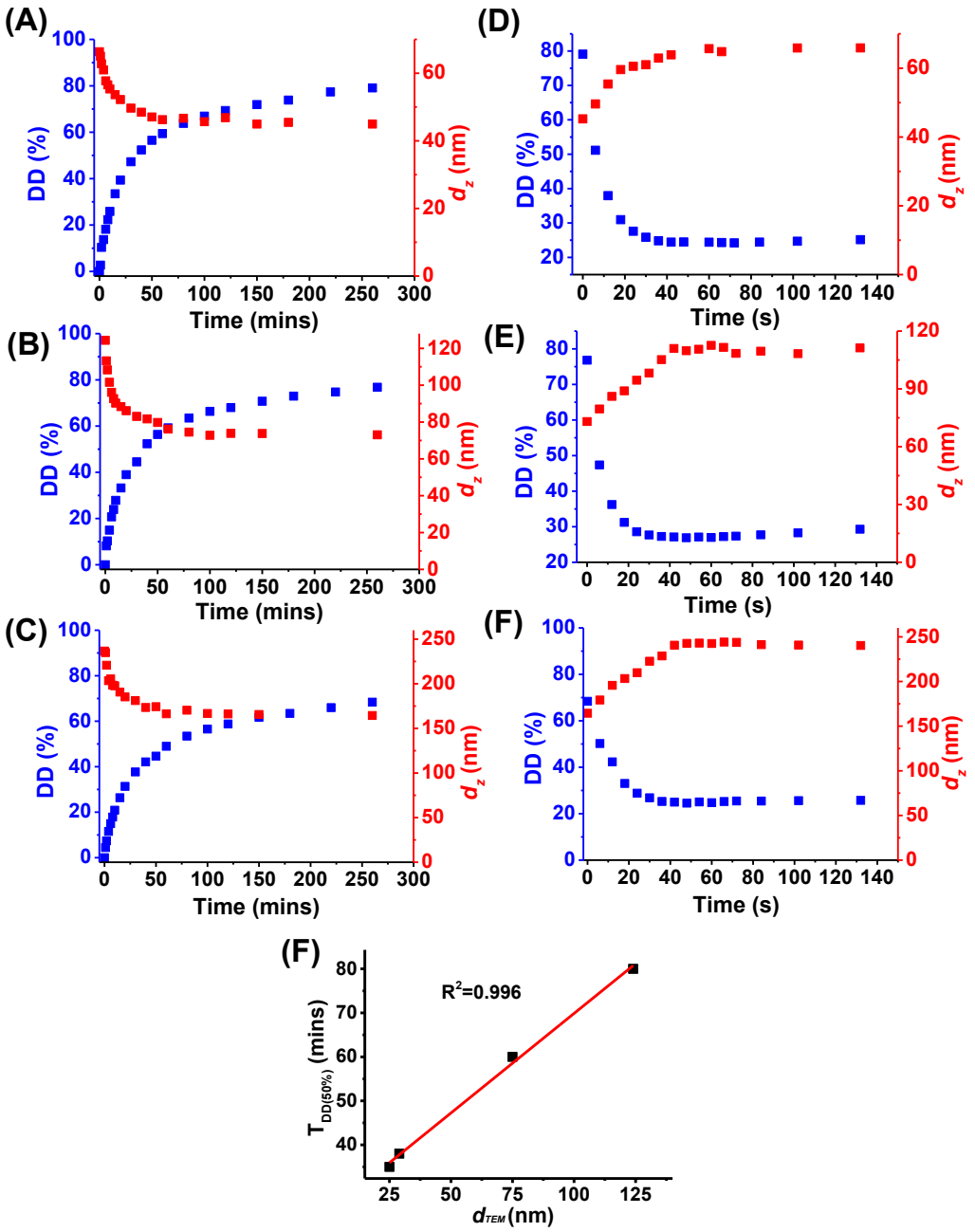

Figure 5.9. Variation of d_z and DD with time for MG-CMA1 **(A)**, MG-CMA2 **(B)**, MG-CMA3 **(C)** during UV light irradiation at 365 nm. Variation of d_z and DD with time for MG-CMA1 **(D)**, MG-CMA2 **(E)**, MG-CMA3 **(F)** during UV light irradiation at 254 nm. The pH and temperature used to obtain the d_z data were 7.4 and 25°C. **(G)** Time when DD reached to 50% vs. d_{TEM}.

The calculated DD and DLS data during irradiation (365 nm) were also measured for MG-CMA1 - MG-CMA3 (see Figure 5.9A -C). The d_z decreased from 66 nm to 45 nm, 124 nm to 73 nm and 237 nm to 165 nm for MG-CMA1, MG-CMA2 and MG-CMA3, respectively. Figure 5.9D- F shows the changes of DD and d_z during the short wavelength

of UV light (254 nm) irradiation. It can be seen that the d_z can increase back to 66 nm, 116 nm and 240 nm for MG-CMA1, MG-CMA2 and MG-CMA3, respectively. Interestingly, the time of DD reaching to 50% were 35 min, 38 min, 60 min and 80 min for MG-CMA1, MG-CMA2, MG-CMA3 and MG-CMA4, which showed a linear dependent with $d_{(TEM)}$ of as-made MGs (Figure 5.9F). This is due to the light can penetrate to the interior MGs better for the smaller size of MGs, which contributes to faster dimerization of coumairn. However, the time for DD going back to maximum is similar for all MGs causes all MGs were swollen and the cleavage process is very fast.

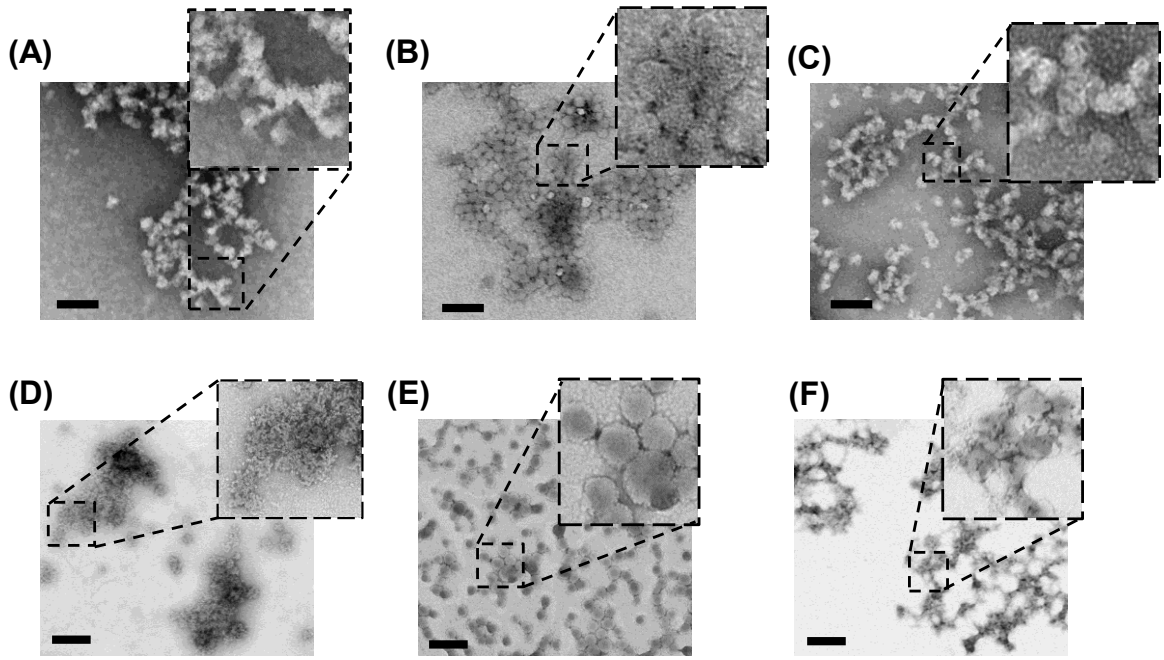

Figure 5.10. TEM images of as-made **(A)**, photo-crosslinking **(B)**, photo-de-crosslinking **(C)** MG-CMA1 and as-made **(D)**, photo-crosslinking **(E)**, photo-de-crosslinking **(F)** MG-CMA4, respectively. The pH and temperature used were 7.4 and 25°C. The scale bars for (A)-(C) are 100nm and for (D)-(E) are 400 nm, respectively.

TEM was used to study the effects of UV light on the MGs particle morphology. TEM images are shown for MG-CMA1 and MG-CMA4 (Figure 5.10). Because crosslinker monomer was not used during synthesis and inevitable dimerization at visible light, the as made MG-CMA1 and MG-CMA4 at pH 7.4 did not dissemble but tended to coalesce

(Figure 5.10A and D). However, the particles were well-defined spheres when photo-crosslinked when swollen (Figure 5.10B and E). They deformed and tended to coalesce when photo-de-crosslinked which made it difficult to clearly identify the individual particles (Figure 5.10C and F). It is well known that crosslinking opposes coalescence of MGs[23]. Our results provide indirect evidence that the extent of crosslinking was substantially changed using UV-irradiation.

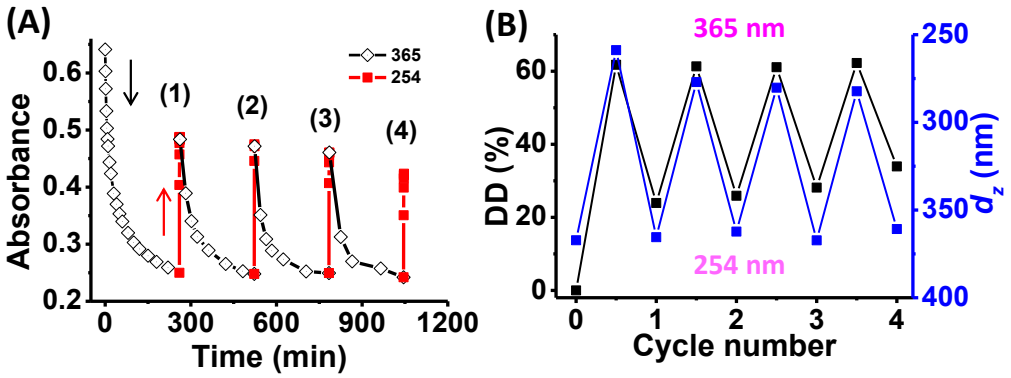

Figure 5.11. (A) Absorbance measured at 320 nm as a function of time for MG-CMA4 after four cycles of photo-crosslinking at 365 nm and photo-de-crosslinking at 254 nm. **(B)** DD and d_z values for MG-CMA4 measured during the photo-switching cycles. The d_z data were obtained at pH 7.4 and 25 °C.

Photo-switching reversibility is an important property for potential applications such as drug delivery. MG-CMA4 was subjected to four photo-crosslinking / photo-de-crosslinking cycles. The absorbance study of MG-CMA4 was shown in Figure 5.11A. Recovery to the maximum absorbance before subsequent photo-crosslinking did not occur. However, improved reversibility is evident after the first cycle. The calculated DD values as well as the d_z values are shown in Figure 5.11B. The gradual decrease in the difference between the minimum and maximum DD achieved for each cycle is due to accumulation of residual non-cleaved dimers[20] as discussed above. The reversibility for the d_z values (blue data points) was very good. Hence, it was possible to reversibly change the crosslinking for these new MGs using UV-irradiation.

5.5.5 Effects of photo-switching on MGs temperature- and pH-responsive behaviours

I next investigated the effects of photo-switching on the temperature- and pH-responsive behaviours of the MGs. Variable-temperature DLS data obtained at pH 6.0 are shown in Figure 5.12A and B. For all of the MGs systems irradiation at 254 nm (photo-de-crosslinked state) resulted in much higher swelling at 10 °C than that present for 365 nm irradiation (photo-crosslinked state) as expected. Interestingly, the VPTTs varied considerably between the photo-crosslinked and de-crosslinked states (see Figure 5.12C). (Each VPTT was determined from the point of inflection of the d_z vs. temperature data). The VPTTs for the photo-crosslinked MGs were much smaller than those for the respective photo-de-crosslinked MGs. This large VPTT difference (12 - 17 ºC) is likely because dimerised coumarin is more hydrophobic than the monomer[24]. It follows that the increased hydrophobicity of CMA dimers opposed temperature-triggered swelling. Hence, the MGs VPTT is strongly photo-switchable.

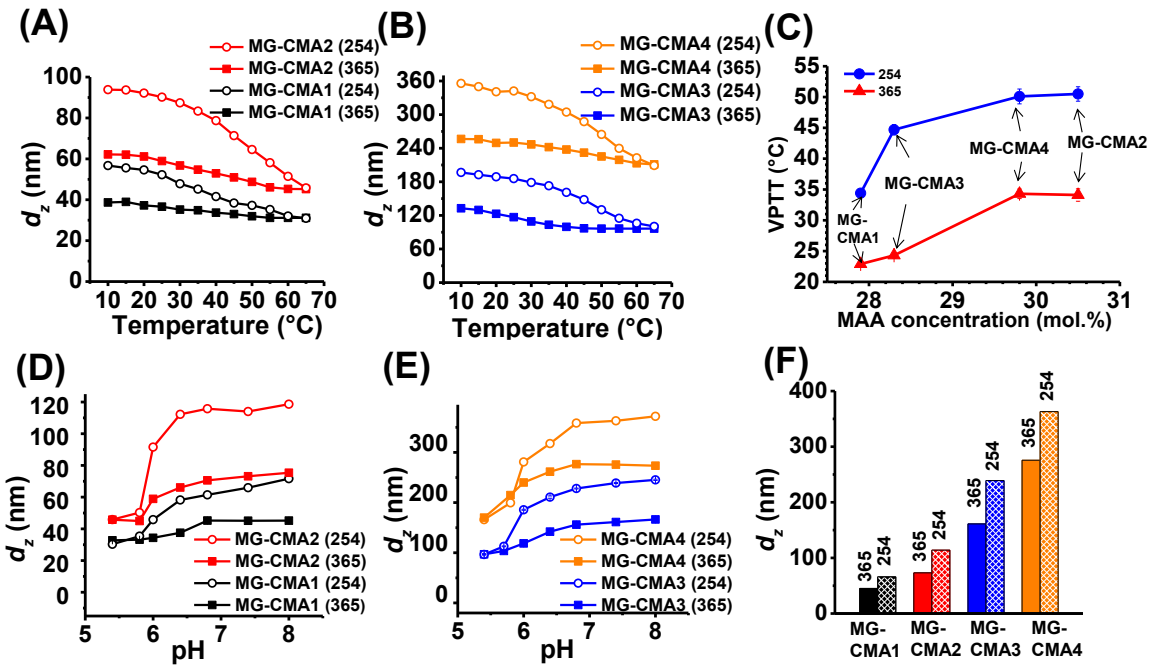

Figure 5.12. Variation of d_z with temperature at pH 6.0 for **(A)** MG-CMA1 and MG-CMA2 and **(B)** MG-CMA3 and MG-CMA4 after photo-crosslinking at 365 nm and photo-de-crosslinking at 254 nm. **(C)** Variation of the volume-phase transition temperature (VPTT) with MAA content for the microgels measured after photo-crosslinking or photo-de-crosslinking. Measured d_z values vs. pH at 25 °C for **(D)** MG-CMA1 and MG-CMA2 and **(E)** MG-CMA3 and MG-CMA4 after photo-crosslinking at 365 nm and photo-de-crosslinking at 254 nm. **(F)** Summary of d_z at pH 7.4 and 25 °C after being photo-crosslinked or photo-de-crosslinked.

Figures 5.12D and E shows the variation of d_z with pH for the MGs irradiated with 365 nm and 254 nm light at 25 °C. The d_z values for all systems increased as the pH approached the respective apparent pK_a values, as expected. Notably, the pH-induced diameter increase was less pronounced after photo-crosslinking. Figure 5.12F summarises the effect of irradiation on the d_z values in the swollen state at pH 7.5. The absolute d_z increase due to photo-de-crosslinking became more pronounced as the as-made MG size increased. The photo-switching for MG-CMA4 (the largest MG system) caused a d_z change of ~ 100 nm. This is a large photo-triggered size change compared to other CMA-containing systems[4, 5, 16].

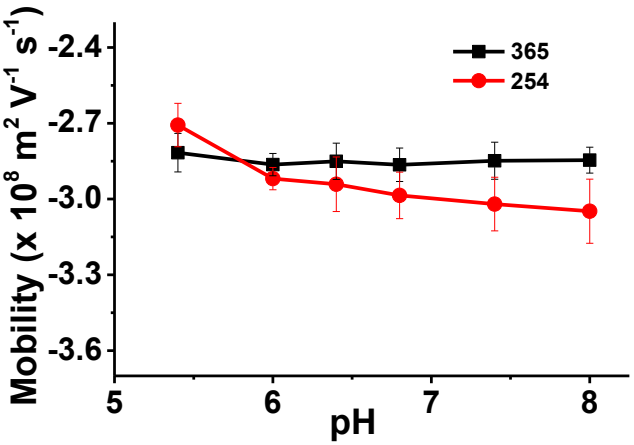

Figure 5.13. Variation of electrophoretic mobility with pH for MG-CMA4 at 25 ºC when photo-crosslinked (365 nm irradiation) or photo-decrosslinked (254 nm).

Electrophoretic mobility data for MG-CMA4 after photo-crosslinking and photo-de-crosslinking was measured to probe changes in the charge distribution at the MG periphery (see Figure 5.13). The data for the photo-crosslinked MGs were not dependent on pH which may indicate that the carboxylate groups were forced to reside inside the MGs particle periphery. In contrast, the mobilities for the photo-de-crosslinked MGs increased with increasing pH. This result implies greater conformational flexibility. The latter trend is similar to that apparent for the as-made MGs (Figure 5.5E), implying that some of the carboxylate groups in photo-de-crosslinked MG-CMA4 could reside at the periphery once again.

5.5.6 CMA distribution within the MGs and implications for photo-switching

Because of the strong photo-switching behaviour observed for the MGs in Figure 5.12, I speculated that precipitation copolymerisation resulted in a uniform distribution of CMA throughout the particles. This proposal was tested by determining the content of CMA copolymerised in the growing MG particles. These data, which were obtained using MG-CMA3, clearly show CMA was incorporated into the growing particles from the earliest time measurable (see Figure 5.14A and inset). Most of the CMA was incorporated in the

interior of the particles with less in the shell. Such an arrangement would be beneficial for "whole particle" swelling because the shell would be forced to swell in response to strong photo-triggered core swelling.

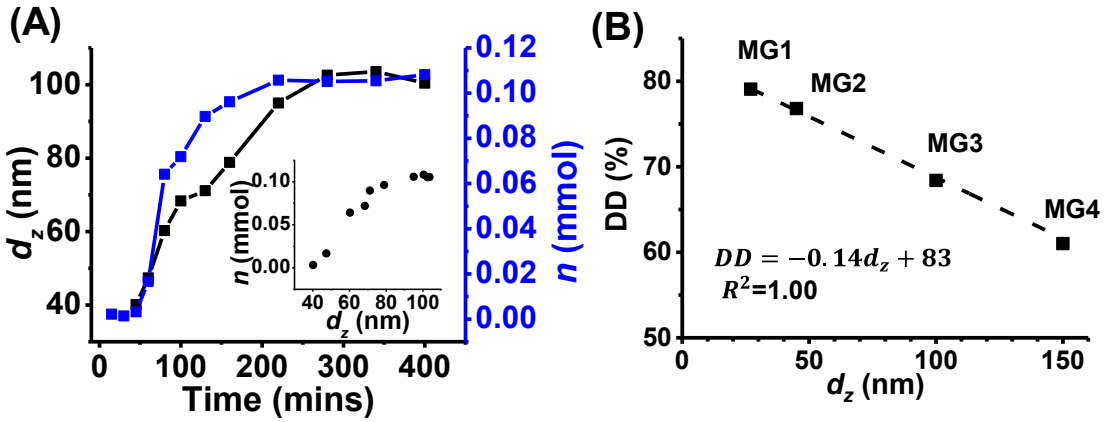

Figure 5.14. (**A**) Variation of d_z and amount (n) of CMA copolymerised within MG-CMA3 with time during synthesis. The inset shows a plot of n against d_z. The data were measured at 25 ºC and pH 5.5. (**B**) Dimerisation degree vs. d_z of the as-made deswollen particles (pH 5.4 and 60 °C).

Figure 5.14B shows the DD value (and the proportion of CMA monomers that could be photo-dimerised) increased as the size of as-made particles decreased. This is attributed to better UV light penetration of the particles due to less light scattering in the smaller MG systems. The extent of scattering is well known to decrease with decreasing colloid particle size[25].

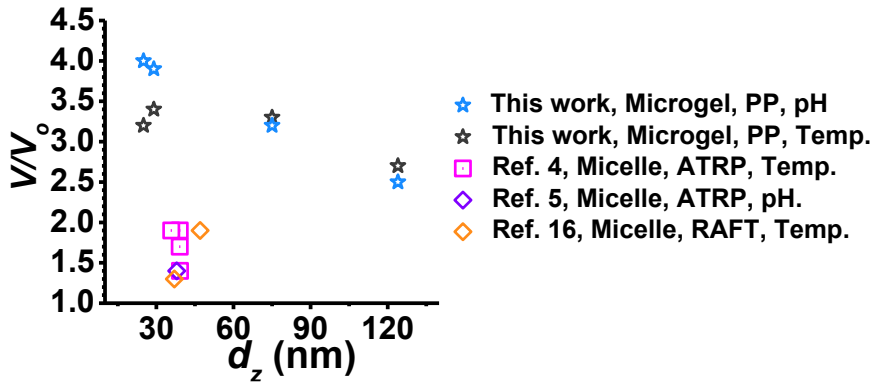

Figure 5.15. Volume ratios (*V/Vo*) for MG-CMA1 to MG-CMA4 and those from studies on related CMA-nanoparticles. The data from this study were measured using (blue stars) variable pH at 25 °C or (black stars) variable temperature at pH 6.0. PP refers to precipitation copolymerisation. The d_z values were obtained from DLS data for the de-swollen particles.

To compare the photo-switching particle size changes obtained here with other studies I use the volume ratio (V/V_o) introduced by He et al.[4]. The values for V_o and V are the average volumes determined from DLS before and after photo-de-crosslinking, respectively. A comparison of V/V_o for MG-CMA1 to MG-CMA4 with reported nanoparticles is shown in Figure 5.15. We calculated these values using particle size data reported in each study. The MGs in this work exhibit much higher V/V_o values compared to those in the related CMA-containing systems[4, 5, 16]. Those reports used methods such as RAFT or ATRP to construct copolymers and macromicelles containing CMA. In such approaches it is usually the case that CMA is added at specific locations within the copolymer. In contrast, CMA units in this work distributed more uniformly within the particle (Figure 5.14A) which contributed to the high V/V_o values. Hence, the range of diameters for the photo-switchable particles as well as their relative photo-triggered volume changes achieved here is greatly increased compared to the nanoparticles in previous studies.

5.5.7 UV-triggered release of a DOX from photo-switchable microgels

Because our MGs showed pronounced photo-switching behaviour we investigated the ability to photo-trigger release of an anticancer drug. DOX is widely used in cancer chemotherapy and was selected. DOX was encapsulated into the MG-CMA4 particles and the non-adsorbed DOX removed by centrifugation (see Experimental detail). For the determination of drug-loading content, DOX loaded MG-CMA4 particles were analysed by UV-vis spectra spectroscopy at 485 nm using a calibration curve obtained with different DOX concentrations (Figure 5.16). The drug loading content (DLC) and drug loading efficiency (DLE) were calculated to be 22.6 % and 79.1 %, respectively, using equations (5.2) and (5.3).

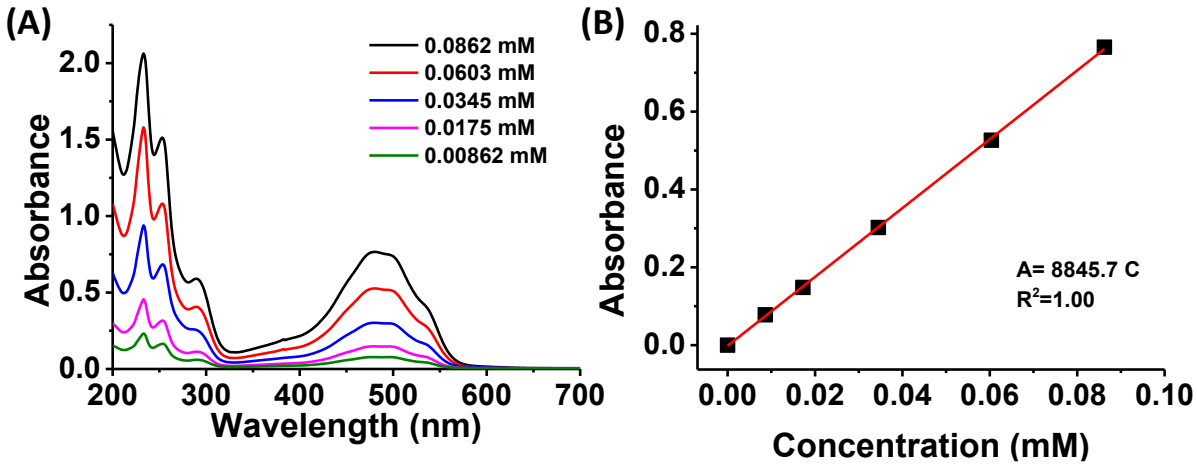

Figure 5.16. (**A**) UV-vis spectra for DOX at various concentrations. (**B**) Variation of absorbance at 480 nm with DOX concentration. The molar extinction coefficient was calculated from (B) as 8845.7 mol^{-1} dm^3 cm^{-1}.

Release experiments were performed at pH 6.0 or 7.4 and the temperature was 25 °C. These pH values were selected because they matched the pH environment in endo/lysosmal compartments (pH 5.0 - 6.0)[26, 27] and extracellular pH (of 7.4). Figure 5.17B shows the fraction of drug released (M_t/M_o) as a function of time. (M_t and M_o are the cumulative mass of DOX released at time t and the total mass of DOX initially loaded into the MG-CMA4, respectively.) The release fraction after 6 h was 0.44 and 0.12 at pH 6.0 and 7.4, respectively, for the photo-crosslinked state. At pH 6.0, there was less electrostatic attraction between positive charged ammonium ion of DOX and MGs due to increased protonation of the $RCOO^-$ groups. After photo-de-crosslinking (254 nm irradiation), DOX was released from the drug loaded MG-CMA4 much faster than that from the photo-crosslinked MG-CMA5. The cumulative release for 6 h increased to 0.75 and 0.48 at pH 6.0 and 7.4, respectively. Hence, the photo-crosslinking retarded drug release. The drug release is incomplete at pH 6.0 because ~ 50 % RCOOH was protonated to $RCOO^-$ (pK_a is 5.9 for MG-CMA4) which means the electrostatic interaction between DOX and MGs still existed. It is difficult to obtained the 100% release even at strong acid environment due to the initiator provides the negative charge in polymer network of MG.

The unreleased drug is not available for treatment, which may lead to low utilization of drug. The loaded DOX can keep stable within the MGs at this condition[28] .

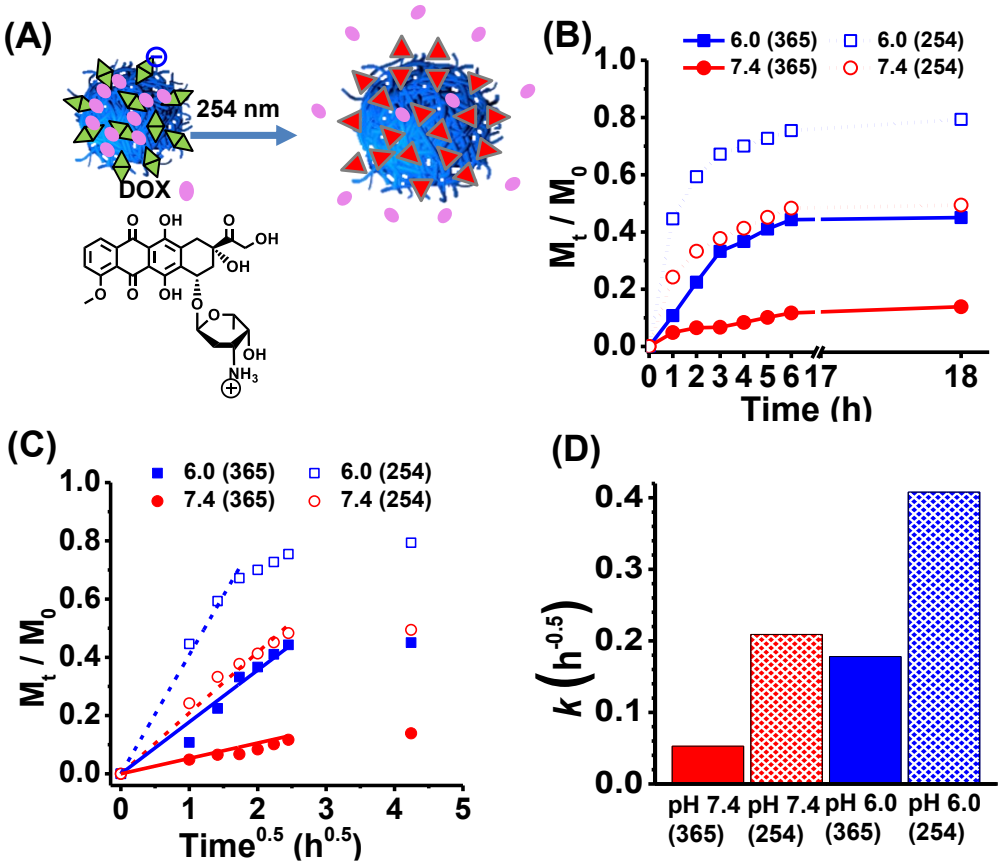

Figure 5.17. (**A**) Depiction of the proposed mechanism for photo-triggered release. (**B**) Release data for DOX from MG-CMA4 at pH 6.0 (photo-crosslinking, 365 nm), pH 6.0 (photo-de-crosslinking, 254 nm), pH 7.4 (photo-crosslinking, 365 nm) and pH 7.4 (photo-de- crosslinking, 254 nm)**.** M_t and M_0 are the cumulative mass of DOX released at time t and the mass of DOX originally loaded into MG-CMA4, respectively. The data in (**C**) are re-plotted from (B) in terms of $t^{1/2}$. (**D**) Initial rates of DOX release for the various dispersions.

Figure 5.17C shows that the fraction of DOX released exhibited a linear dependence with $t^{0.5}$. (t is releasing time). This is evidence that release was diffusion limited[29, 30]. The following equation was used to model the early-stage release data.

$$\frac{M_t}{M_0} = kt^{0.5} \qquad (5.4)$$

For the above equation k is the rate constant. This kind of time-dependent release profile has been shown to apply for conventional MGs[31]. Values for k are shown in Figure 5.17D.

The greatly increased *k* due to photo-de-crosslinking at both pH values is due to enhanced diffusion of DOX from the MG interior. Hence, DOX release was accelerated using UV light. The short wavelength UV light (254 nm used here) cannot penetrate skin effectively and might damage tissue. For potential application, two-photon absorption (TPA) using light of 532 nm should be viable[32]. The successful use of TPA has been reported for coumarin photodimer reactions[33-35]. Accordingly, the new MGs have potential application for light triggered drug release.

5.5 Conclusions

In summary, I investigated new multi-responsive photo-switchable MGs with as-made d_{TEM} values that spanned the range 25 - 124 nm. The MGs diameter could be controlled using synthesis conditions. All the MGs can be reversibly photo-cross-linked and photo-de-crosslinked using UV light of two different wavelengths. The irradiation was also shown to cause a major change of the VPTT. The results indicate that CMA is distributed reasonably uniformly within the MGs interior and this is a key reason why the photo-switching behaviours for the MGs in this work is stronger than other related systems. The photo-triggered changes in DD and d_z were found to be generally similar, but important differences were also present. The data in this work show that a significant proportion of the dimerised CMA monomer was not involved in controlling the swelling of the MG particles. An unexpected discovery of this study is that DD increased with decreasing size of as made particles. This result demonstrates the importance of MGs size to the photo-response and was proposed to be due to better UV light penetration of smaller particles. The release for encapsulated DOX showed considerable enhancement upon photo-de-crosslinking which indicates good potential for future photo-switchable MGs for on-demand drug delivery.

5.6 References

1. Wolff, T.; Gorner, H., Photodimerization of coumarin revisited: Effects of solvent polarity on the triplet reactivity and product pattern. *Phys Chem Chem Phys* **2004,** *6* (2), 368-376.

2. Mal, N. K.; Fujiwara, M.; Tanaka, Y., Photocontrolled reversible release of guest molecules from coumarin-modified mesoporous silica. *Nature* **2003,** *421* (6921), 350-353.

3. Jiang, J. Q.; Qi, B.; Lepage, M.; Zhao, Y., Polymer micelles stabilization on demand through reversible photo-cross-linking. *Macromolecules* **2007,** *40* (4), 790-792.

4. He, J.; Tong, X.; Zhao, Y., Photoresponsive Nanogels Based on Photocontrollable Cross-Links. *Macromolecules* **2009,** *42* (13), 4845-4852.

5. Qiao Jin, G. L., Jian Ji, Preparation of reversibly photo-cross-linked nanogels from pH-responsive block copolymers and use as nanoreactors for the synthesis of gold nanoparticles. *Eur. Polym. J.* **2010,** *46*, 2120–2128.

6. Jie He, B. Y., Luc Tremblay, Yue Zhao, Both Core- and Shell-Cross-Linked Nanogels: Photoinduced Size Change, Intraparticle LCST, and Interparticle UCST Thermal Behaviors. *Langmuir* **2011,** *27*, 436-445.

7. Zhixin Dong, J. M., Dapeng Wang, Muquan Yang, Xiangling Ji, Synthesis and Multi-Stimuli-Responsive Behavior of Poly(N,N-dimethylaminoethyl methacrylate) Spherical Brushes under Different Modes of Confinement in Solution. *Langmuir* **2015,** *31*, 8930−8939.

8. Pich, A. R., W, Chemical Design of Responsive Microgels. *Adv. Polym. Sci.* **2010,** *234*, 1.

9. Wang, J.; Cooper, R. C.; He, H. L.; Li, B. X.; Yang, H., Polyamidoamine Dendrimer Microgels: Hierarchical Arrangement of Dendrimers into Micrometer

Domains with Expanded Structural Features for Programmable Drug Delivery and Release. *Macromolecules* **2018,** *51* (15), 6111-6118.

10. Zhang, Q.; Colazo, J.; Berg, D.; Mugo, S. M.; Serpe, M. J., Multiresponsive Nanogels for Targeted Anticancer Drug Delivery. *Mol Pharmaceut* **2017,** *14* (8), 2624-2628.

11. Hoare, T.; Pelton, R., Impact of Microgel Morphology on Functionalized Microgel−Drug Interactions. *Langmuir* **2008,** *24* (3), 1005-1012.

12. Zhan, Y.; Goncalves, M.; Yi, P. P.; Capelo, D.; Zhang, Y. H.; Rodrigues, J.; Liu, C. S.; Tomas, H.; Li, Y. L.; He, P. X., Thermo/redox/pH-triple sensitive poly(N-isopropylacrylamide-co-acrylic acid) nanogels for anticancer drug delivery. *J Mater Chem B* **2015,** *3* (20), 4221-4230.

13. Jiang, F. J.; Chen, S.; Cao, Z. Q.; Wang, G. J., A photo, temperature, and pH responsive spiropyran-functionalized polymer: Synthesis, self-assembly and controlled release. *Polymer* **2016,** *83*, 85-91.

14. Chen, S.; Bian, Q.; Wang, P. J.; Zheng, X. W.; Lv, L.; Dang, Z. M.; Wang, G. J., Photo, pH and redox multi-responsive nanogels for drug delivery and fluorescence cell imaging. *Polym Chem-Uk* **2017,** *8* (39), 6150-6157.

15. Wang, Y.; Nie, J. S.; Chang, B. S.; Sun, Y. F.; Yang, W. L., Poly(vinylcaprolactam)-Based Biodegradable Multiresponsive Microgels for Drug Delivery. *Biomacromolecules* **2013,** *14* (9), 3034-3046.

16. He, J.; Yan, B.; Tremblay, L.; Zhao, Y., Both Core- and Shell-Cross-Linked Nanogels: Photoinduced Size Change, Intraparticle LCST, and Interparticle UCST Thermal Behaviors. *Langmuir* **2011,** *27* (1), 436-445.

17. Kabb, C. P.; O'Bryan, C. S.; Deng, C. C.; Angelini, T. E.; Sumerlin, B. S., Photoreversible Covalent Hydrogels for Soft-Matter Additive Manufacturing. *Acs Appl Mater Inter* **2018,** *10* (19), 16793-16801.

18. Nunes, J. D.; Asua, J. M., Theory-Guided Strategy for Nanolatex Synthesis. *Langmuir* **2012,** *28* (19), 7333-7342.

19. Smith, M. H.; Herman, E. S.; Lyon, L. A., Network Deconstruction Reveals Network Structure in Responsive Microgels. *J. Phys. Chem. B.* **2011,** *115* (14), 3761-3765.

20. Chen, Y.; Jean, C. S., Polyethers containing coumarin dimer components in the main chain. II. Reversible photocleavage and photopolymerization. *Journal of applied polymer science* **1997,** *64* (9), 1759-1768.

21. Chen, Y.; Geh, J.-L., Copolymers derived from 7-acryloyloxy-4-methylcoumarin and acrylates: 2. Reversible photocrosslinking and photocleavage. *Polymer* **1996,** *37* (20), 4481-4486.

22. Chen, Y.; Chen, K. H., Synthesis and reversible photocleavage of novel polyurethanes containing coumarin dimer components. *Journal of Polymer Science Part A: Polymer Chemistry* **1997,** *35* (4), 613-624.

23. Cui, Z. X.; Wang, W. K.; Obeng, M.; Chen, M.; Wu, S. L.; Kinloch, I.; Saunders, B. R., Using intra-microgel crosslinking to control the mechanical properties of doubly crosslinked microgels. *Soft Matter* **2016,** *12* (33), 6985-6995.

24. Zhao, Y.; Tremblay, L.; Zhao, Y., Phototunable LCST of Water-Soluble Polymers: Exploring a Topological Effect. *Macromolecules* **2011,** *44* (10), 4007-4011.

25. Everett, D. H., Basice principles of colloid science. *RSC Paperbacks, Cambridge* **1988**.

26. Motoi Oishi, S. S., and Yukio Nagasaki, On−Off Regulation of 19F Magnetic Resonance Signals Based on pH-Sensitive PEGylated Nanogels for Potential Tumor-Specific Smart 19F MRI Probes. *Bioconjugate Chem.* **2007,** *18* (5), 1379-1382.

27. Yang, J.; Chen, H. T.; Vlahov, I. R.; Cheng, J. X.; Low, P. S., Characterization of the pH of folate receptor-containing endosomes and the rate of hydrolysis of internalized acid-labile folate-drug conjugates. *J Pharmacol Exp Ther* **2007,** *321* (2), 462-468.

28. Ilett, K.; Ong, R.; Batty, K.; Taylor, J. J. B. j. o. u., Effect of urine pH on the stability of doxorubicin and its recovery from bladder instillations. **1990,** *65* (5), 478-482.

29. Korsmeyer, R. W.; Gurny, R.; Doelker, E.; Buri, P.; Peppas, N. A., Mechanisms of Solute Release from Porous Hydrophilic Polymers. *Int J Pharm* **1983,** *15* (1), 25-35.

30. Dash, S.; Murthy, P. N.; Nath, L.; Chowdhury, P., Kinetic Modeling on Drug Release from Controlled Drug Delivery Systems. *Acta Pol Pharm* **2010,** *67* (3), 217-223.

31. Lee, P. I., Kinetics of drug release from hydrogel matrices. *Journal of Controlled Release* **1985,** *2*, 277-288.

32. Kim, H. C.; Hartner, S.; Hampp, N., Single- and two-photon absorption induced photocleavage of dimeric coumarin linkers: Therapeutic versus passive photocleavage in ophthalmologic applications. *J Photoch Photobio A* **2008,** *197* (2-3), 239-244.

33. Kim, H. C.; Kreiling, S.; Greiner, A.; Hampp, N., Two-photon-induced cycloreversion reaction of coumarin photodimers. *Chem Phys Lett* **2003,** *372* (5-6), 899-903.

34. Härtner, S.; Kim, H.-C.; Hampp, N., Photodimerized 7-hydroxycoumarin with improved solubility in PMMA: Single-photon and two-photon-induced photocleavage in solution and PMMA films. *Journal of Photochemistry and Photobiology A: Chemistry* **2007,** *187* (2-3), 242-246.

35. Buckup, T.; Dorn, J.; Hauer, J.; Hartner, S.; Hampp, N.; Motzkus, M., The photoinduced cleavage of coumarin dimers studied with femtosecond and nanosecond two-photon excitation. *Chem Phys Lett* **2007,** *439* (4-6), 308-312.

Chapter 6: Multi-responsive gels prepared without small molecule reactants or free-radical crosslinking by reversible light-triggered microgel interlinking

6.1 Abstract

Environmentally responsive hydrogels have been widely studied because of their attractive properties and potential for applications in areas ranging from biomedical implants to displays. In this chapter, multi-responsive hydrogels are constructed by using microgels (MG) from chapter 4 as building blocks with UV light (365 nm) irradiation without involving any free-radicals or small molecules. The hydrogel can be prepared by inter- and intra-particle dimerised coumarin formation (crosslinker). The dimerized coumarin can be cleaved to monomeric coumarin easily upon short wavelength of UV light (254 nm) illumination. I demonstrate facile preparation of triply responsive hydrogels that are reversibly responsive to light, pH and temperature using photo-triggered covalent interlinking of coumarin-based MGs. The gels have a phototunable modulus and swelling ratio. They also show light-assisted healing and re-shapeability. The gels can be formed as cyotocompatible actuators and grippers which are triply responsive and their use in an electrical circuit is also demonstrated. The fluorescence of the gels is reversibly light-tunable and undergoes a blue-shift in the photo-crosslinked state. This property is used to embed hidden information within the gels. The gels can also be constructed using either positive or negative photo-patterning using a shadow mask. These new gels as well as their construction method open the door to new smart biomaterial and anti-counterfeit applications.

6.2 Introduction

Hydrogels are crosslinked hydrophilic three dimensional polymer networks containing a large amount of water[1, 2]. Responsive hydrogels exhibit swelling or mechanical responses to pre-determined stimuli such as pH[3, 4], temperature[5, 6], light[7, 8], ionic[9] or redox[10] changes. They arise great interest for "smart" applications such as drug delivery[11, 12], robotics[13], bioelectronics[14], anti-counterfeit[15] and photonics[16]. For example, Gawade et al. put forwarded a modular semisynthetic method to govern the release of site-specifically modified proteins independently and sequentially from gels upon enzyme, reductant, and light stimulus[17]. Wang et al. reported light induced association or disassociation of host-guest complexes between α-CD and azobenzene using different wavelengths of light within gels. A remote control of the ionic mobility in the gel was realized by reversibly switching an electric circuit on and off by light irradiation[18]. Such hydrogels with reversible or tuneable functional groups provide enhanced potential for application as biomaterials[19] and maintenance-free self-healing materials[20] with an added recyclability[21]. However, most gels are prepared using either free-radical polymerization or small molecules, which often limits spatial and temporal control and may adversely affect cells[22].

Photo-curing is a good method to control gel formation spatially during gel construction[22-24]. However, it often involves small molecules such as photo-initiators which may diffuse away from the point of application or may be harmful to strongly proliferating cell types[25]. Coumarin is well known photo-sensitive chemical that can dimerize upon UV irradiation at wavelengths above 310 nm. The resulting coumarin dimers can be seperated into monomeric coumarin molecules upon UV irradiation at below 260 nm[26]. Some studies have reported that coumarin-based polymers exhibit photo-shapping[27], reversibility of sol-gel[28] and viscoelastic changes[29] solely by UV light irradiation.

In chapter 4, the triply-responsive MGs were introduced whose crosslinker density and pH- and thermally-triggered swelling ratio can be adjusted by two different UV wavelength. Herein, I study stimuli-responsive hydrogels constructed using this MG as a building block. These hydrogels are formed in the absence of a photoinitiator or other chemical reagents. In the beginning, The poly(MEO_2MA-co-MAA-co-CMA) MGs (denoted as MG-CMA) are prepared using 2-(2-methoxyethoxy)ethyl methacrylate (MEO_2MA), methacrylic acid (MAA) and 7-(2-methacryloyloxyethoxy)-4-methylcoumarin (CMA) via emulsion polymerization as shown in Scheme 6.1. The effects of photo-crosslinking and de-crosslinking on temperature- and pH-responsive behaviours of MG-CMA are then studied.

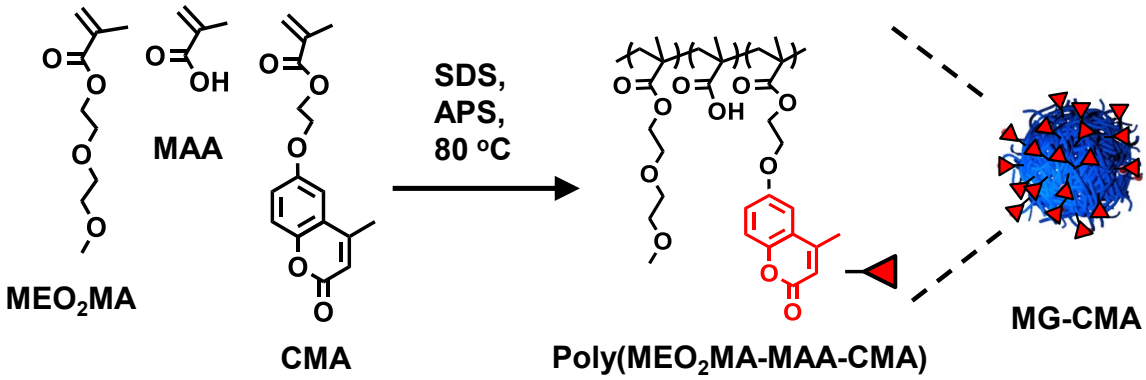

Scheme 6.1. Depiction of synthesis of CMA

The pH value of concentrated MG-CMA dispersion is then adjusted to 7.4 so that the MG polymer chains can interpenetrate and form a physical gel. The starting point is a shapeable physical gel of MG-CMA particles (Scheme 6.2A). It is then photo-crosslinked using 365 nm light due to photo-induced formation of cyclobutane rings (dimerisation) of CMA (Scheme 6.2B) and subsequently photocleaved to monomeric CMA using 254 nm light so the photo-de-crosslinked gel is formed (Scheme 6.2C).

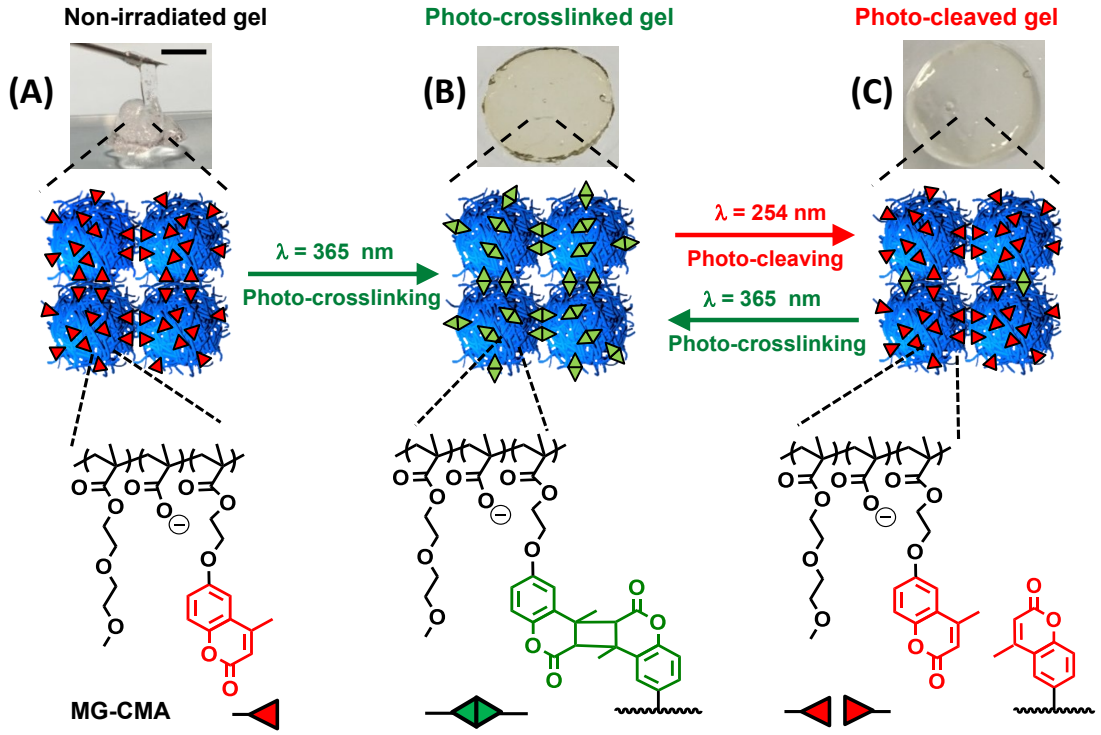

Scheme 6.2. Schematic illustration of the initial non-irradiated gel of **(A)** MG-CMA particles (no UV exposure), **(B)** photo-crosslinked gel (with 365 nm irradiation) and **(C)**photo-cleaved gel (with 254 nm irradiation), respectively. The non-irradiated gel is a physical gel and re-shapeable. The photo-crosslinked gel is an elastic gel. The photo-cleaved gel retains its original shape but is less stiff than the photo-crosslinked gel. The scale bar is 5.0 mm and applied in all images.

The gel shows pH-, temperature- and light-responsive behaviors as well as light-triggered self-healing and re-processing to different shapes. The modulus value is photo-tuneable via changing the wavelength of UV light. The gel is used to construct cytocompatible actuators for ON/OFF switching and gripping by combination the acrylamide (AAm) gel or MG/PEI gel, respectively. The gels can be photo-patterned to give various shapes or hidden messages for anti-counterfeit applications. Interestingly, these gels exhibit photo-reversible fluorescence blue-shift which is rarely reported for fluorescent gels. The gel can be photo-patterned. The data show that spatiotemporal construction of hydrogels using CMA-functionalised MGs is a potentially powerful method for constructing next-generation functional hydrogels.

6.3 Experimental detail

6.3.1 Materials

2-(2-methoxyethoxy)ethyl methacrylate (MEO_2MA, 95%), methacrylic acid (MAA, 98%), sodium dodecyl sulphate (SDS, 98%), ammonium persulfate (APS, 98%), potassium carbonate (K_2CO_3, ACS grade), $CHCl_3$ (≥ 99.5%), chloroform-d ($CDCl_3$, 99.8 atom % D), methanol (MeOH, ≥99.9%), methacryloyl chloride (97.0%), Rhodamine B, *N*-*N*′-Methylene bisacrylamide (BIS, ≥99.5%), acrylamide (AAm, ≥99.5%), 2,2′-Azobis(2-methylpropionamidine) dihydrochloride (V-50, 97%), ethylacrylate (EA, 99%) and divinylbenzene (DVB, 80%) were all purchased from Aldrich. 4-Methylumbelliferone (≥98%), 2-bromoethanol (95%), *N*,*N*-dimethylformamide (DMF, ACS grade), ethanol (100%), triethylamine (TEA, 99%), CH_2Cl_2 (≥99.8%), Nile blue A were purchased from Fisher Scientific. Methacryloxyethyl thiocarbamoyl Rhodamine B (Me-RDB), Branched polyethylenimine (PEI) with molecular weights of 10 kD were purchased from Polysciences. All materials were used as received. Ultrahigh purity water was used that had been doubly filtered and deionised.

6.3.2 Synthesis of MG-CMA

The synthesis route MG-CMA was similar MG-CMA1 in Chapter 5 but scale for 2 times. Briefly, SDS solution (0.22 g SDS in 39.2 g water) was add to three neck round flask equipped with magnetic stirrer and reflux condenser, heated to 80 °C and purged with N_2 for 60 min to de-oxygenate. Aqueous APS (0.8 g of solution with a concentration of 2.5 wt.%) was added to the reaction flask. A comonomer solution used to prepare microgels containing MEO_2MA (2.26 g, 12.0 mmol), CMA (0.418 g, 14.5 mmol) and MAA (0.365 g, 4.2 mmol) was feed into reaction flask at a uniform rate of 0.10 mL/min until the

required mass had been added. The reaction was continued for 1.0 h at 80 °C and the nitrogen atmosphere was maintained. The reaction mixture was then cooled to room temperature and the dispersion extensively dialysed MG against water for 7 days. The dialysed was washed with fresh $CHCl_3$ three times to remove un-reacted monomer and the residual $CHCl_3$ in the dispersion was removed by rotary evaporation at 25 °C. The dispersion was protected from light using aluminium foil.

6.3.3 Photo-crosslinking and photo-de-crosslinking for MG-CMA

Irradiation of all MGs dispersion was conducted using a CL 1000 Ultraviolet Crosslinker equipped with five lamps which provided a wavelength of 365 nm or 254 nm and an intensity of 14 mW/cm^2 and 10 mW/cm^2, respectively. The MG-CMA dispersions in quartz cuvettes were heated at 60 °C (pH 5.4) for 20 min and irradiated with UV light (365 nm) to photo-crosslink. The dispersion was then diluted in buffer solution (0.10 M) of the required pH to obtain dynamic light scattering (DLS) data. The dispersions were photo-de-crosslinked in the swollen state (typically pH 7.4) by irradiation with 254 nm UV light to obtain DLS data.

6.3.4 Photo-triggered gel preparation

To prepare the photo-triggered crosslinked gel, aqueous NaOH solution (4.0 M, 33 μL) was added to a concentrated MG dispersion (1.0 mL, 12.0 wt.%) and the dispersion mixed manually until homogeneous. The mixture became viscous when the pH was adjusted to 7.4 and this pH was used for gel preparation unless otherwise stated. The viscous mixture was transferred to an O-ring and sandwiched between two quartz glass slides and then fixed using clamps and cured with UV light (365 nm, 14 mW/cm^2) for 10 h. In the case of photo-de-crosslinking using short wavelength UV light (254 nm), the formed gel was

placed in an O-ring and sandwiched between two quartz glass slides and then irradiated by UV light (254 nm, 10 mW/cm^2) for 1 h.

6.3.5 Bilayer Hydrogel preparation

The first layer gel is the AAm-based non-responsive gel which is based on literature method[30] and the second layer gel is photo-crosslinked gel. AAm (62.9 mg, 2.08 mmol), BIS (1.8 mg, 11.7 μmol), Me-RDB (0.15 mg, 0.23 μmol), V-50 (1.06 mg) were dissolved 1.0 g water and mixed uniformly. Then, the mixture was transferred to O-ring (inner diameter = 15.0 mm and thickness = 1.5 mm), sandwiched between two quartz glass slides, fixed using clamps and cured with UV light at 365 nm for 10 min. After the first layer gel was formed, the gel was taken off from the O-ring and fixed to another O-ring (inner diameter = 15.0 mm and thickness = 2.5 mm). The concentrated MG dispersion (0.50 mL, 12.0 wt.%, pH 7.4) was added to the top of the first layer gel within the O-ring, sandwiched between two quartz glass slides and then fixed using clamps and cured at UV light at 365 nm for 10 h. The bilayer gel was taken from the O-ring and cut into rectangle shape (13.0 mm×6.0 mm× 2.5 mm).

6.3.6 Multi-responsive actuator circuit component for ON/OFF LED switching

An electrically conductive actuator was prepared as a bilayer gel. Firstly, the AAm gel was replaced with a cationic MG/PEI gel. The MG/PEI gel preparation is described in detail elsewhere[31]. Briefly, MG(EA-MAA-DVB) dispersion (0.50 mL, 18.0 wt.%) was transferred to a vial. (The MG(EA-MAA-DVB) dispersion was prepared according to the method reported[31]). PEI solution (10 kg/mol, 0.50 mL, 18.0 wt.%) was injected into the MG(EA-MAA-DVB) dispersion and mixed mechanically and vigorously by hand using a small spatula to form a white coloured pre-gel. A pre-cut circular sheet of Al foil

(thickness 10 μm) was placed in the O-ring. The MG(EA-MAA-DVB)/PEI pre-gel was added to the top of the Al foil within the O-ring (inner diameter = 13 mm and thickness = 1.5 mm) and heated at the 37 ºC for 20 h. The next step involved adding a photo-crosslinked MG-CMA layer and was the same as that used above for the bilayer gel. The Al foil and the photo-crosslinked MG-CMA gel can be attached to the MG(EA-MAA-DVB)/PEI gel due to the adhesive property of MG(EA-MAA-DVB)/PEI gel.

6.3.7 Reversibly transferring fluorescent images to the gels

To transfer images of the shadow mask a photo-crosslinked gel in an O-ring (inner diameter = 15 mm and thickness = 1.5 mm) was sealed with two slides and clamps. The shadow mask was placed on the top surface and irradiated at 254 nm for 1 h. To remove the encoding, the encoded gel was put in an O-ring, and sealed on both side using microscope slides fixed with clamps and then irradiated at 365 nm for 6 h.

6.3.8 Live/Dead and MTT assays

The Live/Dead and MTT assays experiments were conducted by Dr. Daman Adlam (School of Biological Sciences, University of Manchester). T/C28a2, immortalised human chondrocyte cells, were cultured in Dulbecco's modified Eagle's medium (DMEM) supplemented with 10% fetal bovine serum (FBS, Gibco) and antibiotic/antimycotic (Sigma-Aldrich, UK) at 37 °C in a humidified 5% CO_2 atmosphere. Cells were seeded at a density of 5×10^4 onto 13 mm glass coverslips in 24 well plates. Exposure to 30 mg of gel was achieved via 0.4 μm cell-culture inserts (BD Biosciences). The viability of the cells was determined at 24, 48 and 72 hour time-points versus gel-free controls by live/dead assay (Life Technologies, UK) and MTT assay (Sigma-Aldrich) as per manufacturers instructions. Images and absorbance were obtained with an Olympus

BX51 fluorescence microscope and a FLUOstar OMEGA plate reader respectively.

6.3.9 Physical Measurements

^{1}H NMR spectra were measured using a B400 Bruker Avance III 400 MHz spectrometer. UV-visible spectra were measured using a PerkinElmer Lambda 25 UV/VIS spectrometer. FTIR spectra were measured using Nicolet 5700 ATR-FTIR spectrometer. Titration measurements were conducted in the presence of aqueous NaCl (0.050 M) using a Mettler Toledo titration instrument. The photoluminescence (PL) spectra were obtained using Edinburgh Instruments FLS980 spectrometer and the excitation wavelength was 302 nm. TEM images were obtained using a FEI Tecnai 12 BioTwin instrument and were stained using uranyl acetate solution (0.50 wt.%). Number-average diameters from TEM images were obtained using Image-J software. Samples for SEM were freeze-dried and coated with Au/Pd. All SEM data were obtained using a FEI Quanta 650 FEG-SEM at 10 kV. DLS data and electrophoretic mobility data were obtained using a Malvern Zetasizer NanoZS instrument fitted with a 20 mW HeNe laser and the angle of detection was set at 173°. Dynamic rheology measurements were conducted with a TA Instruments AR G2 rheometer. A 20 mm diameter plate geometry was used and the gap was set to 2500 μm.

The volume swelling ratio values for the gel (Q) were determined gravimetrically. The photo-crosslinked gel and photo-de-crosslinked gel were placed into 0.10 M buffer solution and weighed once daily for 3 days after being carefully wiped using tissue paper. The Q values were calculated using equation (6.1).

$$Q = \rho_p \left(\frac{Q_m}{\rho_s} + \frac{1}{\rho_p} \right) - \frac{\rho_p}{\rho_s} \qquad (6.1)$$

Where Q_m is the ratio of swollen gel mass to the dry mass. The parameters ρ_p and ρ_s are the densities of water and the polymer (1.2 g/mL), respectively.

6.4 Results and Discussion

6.4.1 Characterization of MG-CMA

The TEM images in Figure 6.1A show that the MG-CMA was a spherical particle (d_{TEM} = 37 nm). The intensity DLS distribution data in poor solvency conditions, pH 5.4 and 60 °C, is shown in Figure 6.1B. The z-average diameters (d_z = 41 nm) are larger than the respective d_{TEM} values because the MGs dispersion contain residual water and strong dependence of d_z values on scattering form the largest particles. The CMA content in the MGs was determined using UV-visible spectra (Figure 6.1C) and the absorption maximum at 320 nm from CMA according to Beer-Lambert law. The CMA content was calculated as 7.4 mol%. Potentiometric titration data (Figure 6.1D) were used to determine the MAA contents and this was 28.9 mol%. The apparent pK_a value for the MG-CMA was 6.2 (Figure 6.1E).

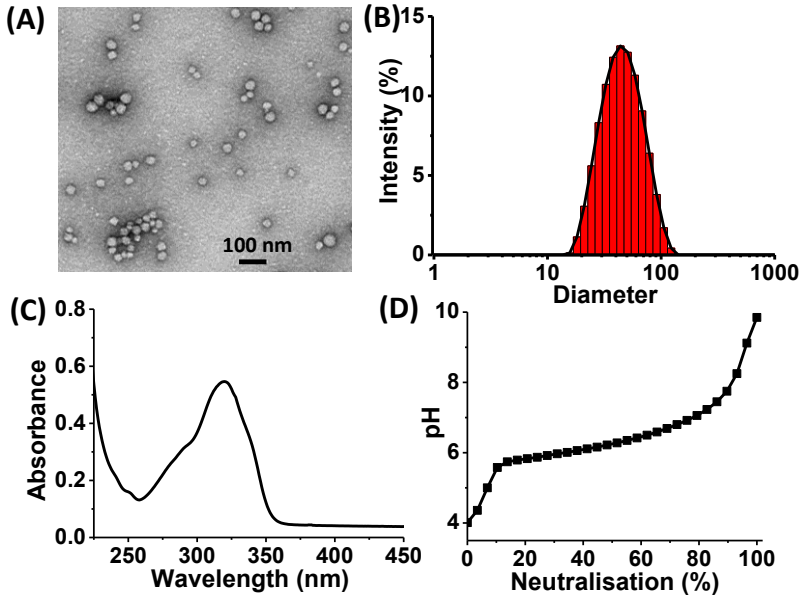

(E)

MEO_2MA/ mol%	MAA/ mol%	CMA/ mol%	pK_a	d_z (pH 6.0, 60°C)/nm	d_z (pH 7.4, 25°C)/nm	d_z (TEM)/nm
63.7	28.9	7.4	6.2	41	107	37

Figure 6.1. (A) TEM images of MG-CMA, **(B)** DLS distribution data of as-made MG-CMA at pH 5.4, 60 °C. **(C)** UV-visible spectra of MG-CMA **(D)** Titration data for MG-CMA. (E) Composition and properties of the MG.

The variation of d_z with pH was measured at 25 °C for the as-made, photo-crosslinked and photo-de-crosslinked MG-CMA dispersions (Figure 6.2A). For both of them, the d_z values increased as the pH approached the respective apparent pK_a values due to increasing electrostatic repulsion between -COO^- groups (Figure 6.2B). However, the swelling ability for the photo-crosslinked MG-CMA (365 nm) was smallest and that for the as-made, photo-de-crosslinked MG-CMA was much stronger.

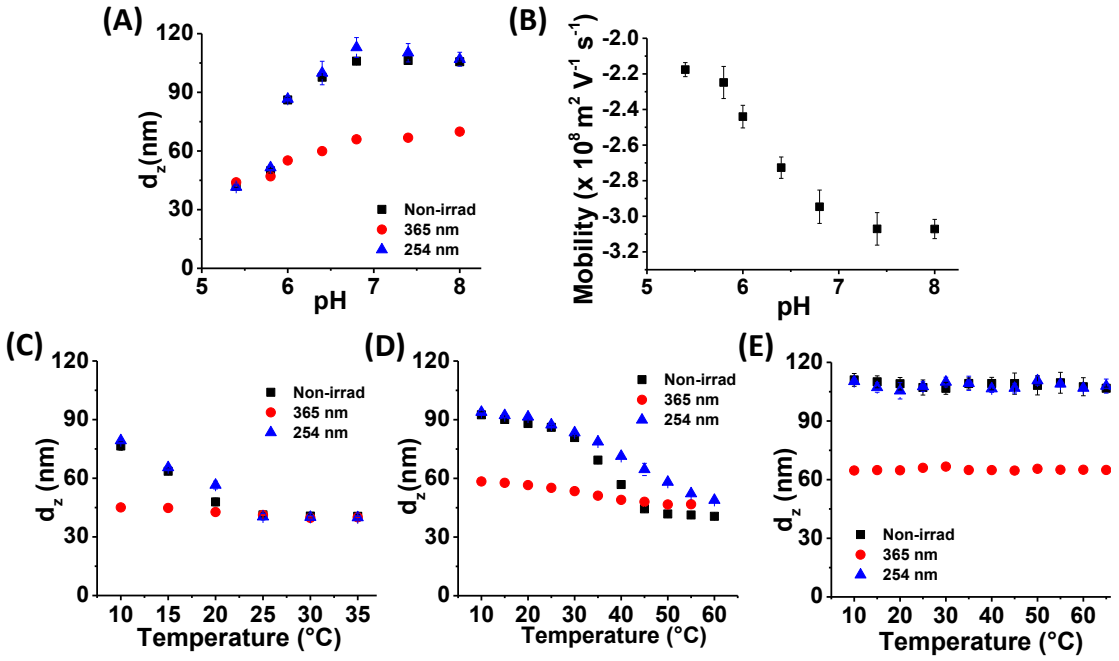

Figure 6.2. (A) d_z vs pH for as made (Non-irrad), photo-crosslinked (365 nm) and photo-de-crosslinked (254 nm) MG-CMA at 25°C. **(B)** Zeta potential vs pH for as made MG-CMA (Non-irrad) at 25°C. Variation of d_z with temperature at pH 5.4 **(C)**, pH 6.0 **(D)** and pH 7.4 **(E)** for as made (Non-irrad), photo-crosslinked (365 nm) and photo-de-crosslinked (254 nm) MG-CMA.

Variable temperature DLS data were measured for MG-CMA at pH 5.4, 6.0 and 7.4 (Figure 6.2C - E). At pH 5.4, with increasing the temperature, the d_z decreases from 45 nm to 40 nm for the photo-crosslinked MG-CMA, 77 nm to 41 nm for as made and 79 nm to 40 nm for photo-de-crosslinked one (Figure 6.2C). The d_z change for the photo-crosslinked MG-CMA was much smaller than the as-made and photo-de-crosslinked one. At pH 6.0, the d_z decreases from 55 nm to 47 nm for the photo-crosslinked MG-CMA, 86 nm to 41 nm for the as-made and 88 nm to 49 nm for photo-de-crosslinked one,

respectively (Figure 6.2D). At pH 7.4, the d_z remained stable at ~ 65 nm for photo-crosslinked MG-CMA, at ~ 110 nm for as-made and photo-de-crosslinked one (Figure 6.2E).

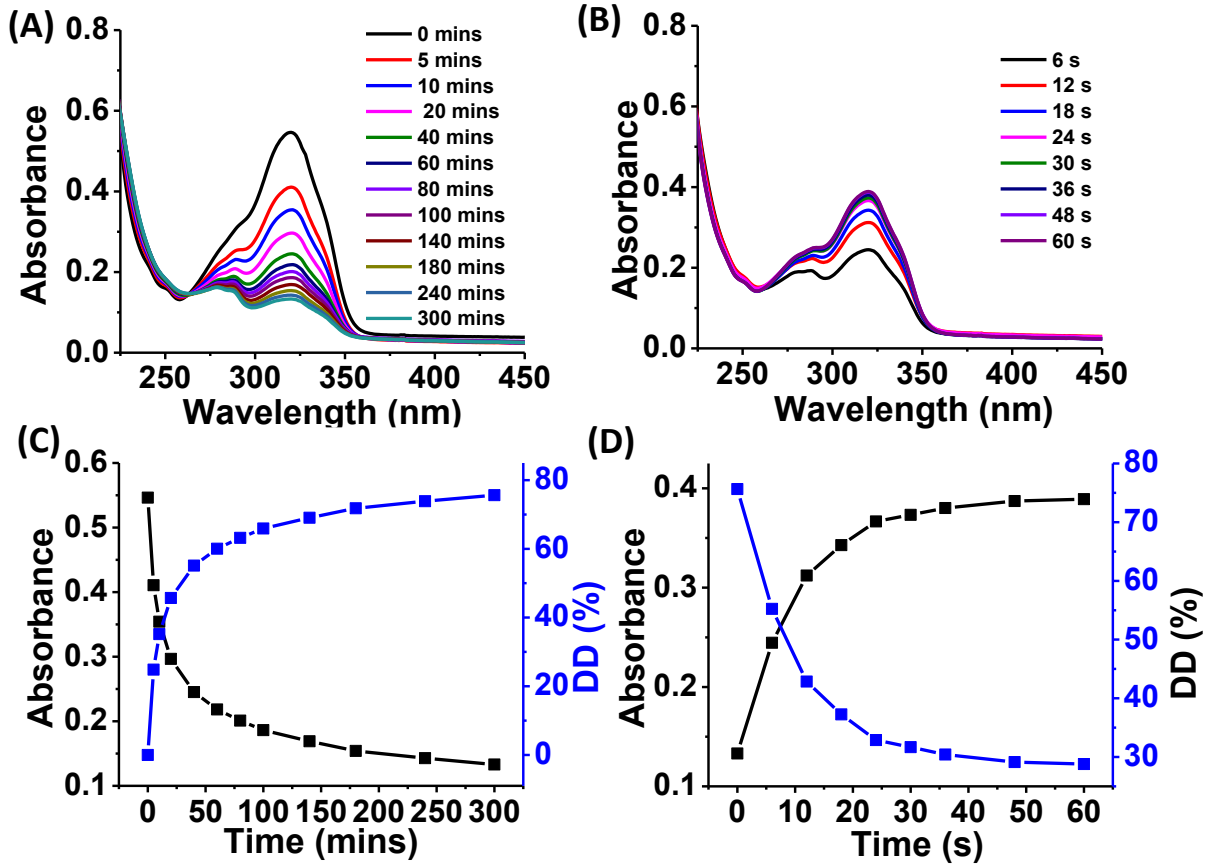

Figure 6.3. UV-visible spectra of MG-CMA measured during photo-crosslinking at 365 nm irradiation **(A)** and photo-de-crosslinking at 254 nm irradiation **(B)**. The absorbance at 320 nm with UV-vis and the calculated dimerization degree (DD) change during photo-crosslinking at 365 nm irradiation **(C)** and photo-de-crosslinking at 254 nm irradiation **(D).**

The d_z varation of MG-CMA at swollen state is due to dimerisation of CMA at 365nm UV light irradiation. This leads to high crosslinker density and restricts the swelling. Figure 6.3A and C shows the absorption of CMA at 320 nm decreases and the dimerization degree (DD) increases to ~80 % upon irradiation at 365 nm. The DD is calculated according to equation 5.1 in Chapter 5. However, 254 nm light can cleave the dimerised CMA so the absorption at 320 nm increases again and the DD decreases to 29 % (Figure 6.3D). This contributes to the increase of swelling ability.

6.4.2 UV-triggered Morphology changes of the gels

The pH of concentrated non-irradiated MG-CMA dispersion (12.0 wt.%) was adjusted to 7.4 to form a physical gel and the neighboring MGs then covalently interlinked using photo-crosslinking of peripheral CMA groups to form a gel of covalently interlinked MGs. The crosslinked gel can transform to de-crosslinked gel with low crosslinker density upon 254 nm light illumination. SEM images for the freeze-dried gels are shown in Figure 6.4.

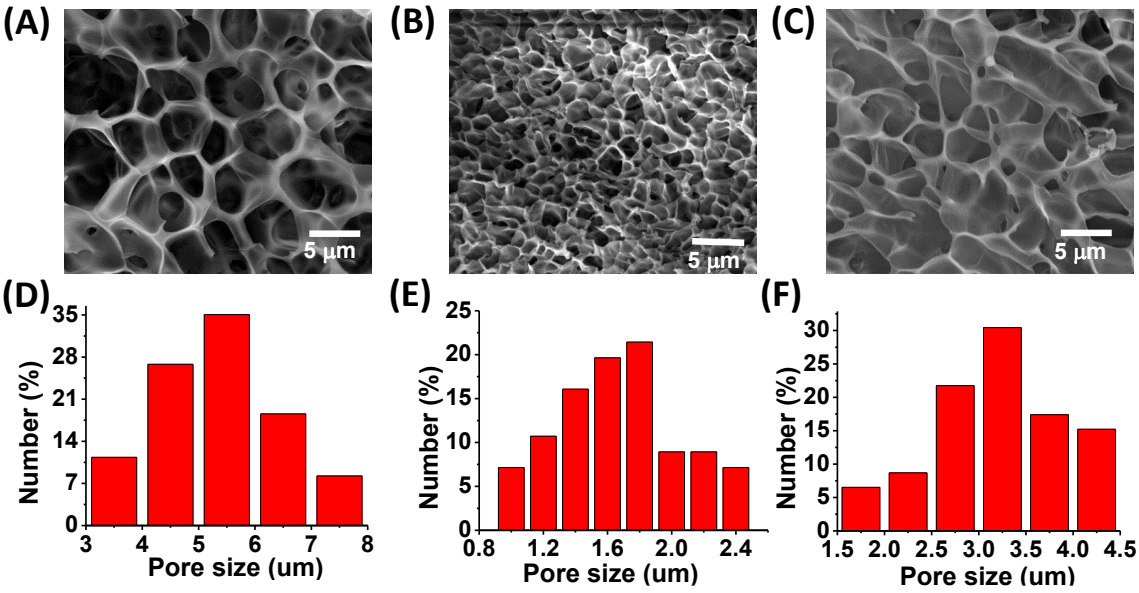

Figure 6.4. SEM images of **(A)** Non-irradiated, **(B)** photo-crosslinked (365 nm) and **(C)** photo-cleaved (254 nm) gels. Pore size distributions for **(D)** physical gel (Non-irrad), **(E)** photo-crosslinked gel (365 nm) and **(F)** photo-cleaved gel (254 nm).

The pore size is photo-tuneable. The non-irradiated gels (Figure 6.4A) and photo-crosslinked gels (Figure 6.4B) had the largest (5.6 µm) and smallest (1.7 µm) average pore sizes, respectively. The pore size for the photo-cleaved gel (3.14 µm) was between those values (Figure 6.4C). Pore size distributions for three gels are shown in Figure 6.4D - F.

6.4.3 UV-triggered FTIR spectra changes of gels

In Figure 6.5, the FTIR spectra for the non-irradiated gel shows a photo-labile band at

1620 cm^{-1} due to C=C stretching[32]. Photo-crosslinking at 365 nm caused coumarin photo-dimerisation and the absorbance of the C=C stretching band decreased due to formation of the cyclobutane ring via [2πs+ 2πs] cycloaddition[33]. Subsequent photo-cleavage of the dimers (by 254 nm irradiation) reformed the C=C bonds and the absorbance at 1620 cm^{-1} increased.

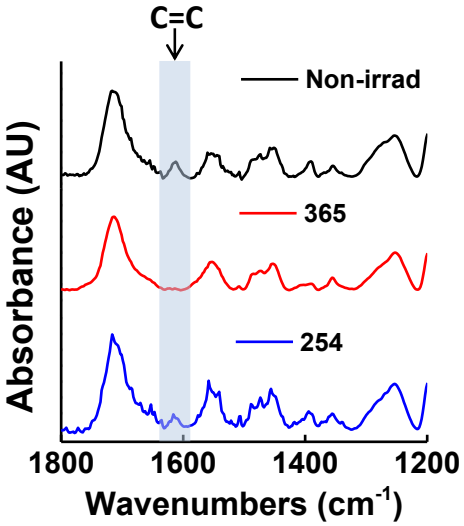

Figure 6.5. FTIR spectra for the non-irradiated, photo-crosslinked (365 nm) and photo-cleaved (254 nm) gels.

During the photo-crosslinking process, the C=C stretching of CMA is decreasing from 0 h to 4 h with increase time of light irradiation (365 nm) (see Figure 6.6A). Subsequently, the C=C stretching occurs reversely upon irradiation at 254 nm for 1 h and does not further increase after longer time irradiation (Figure 6.6B).

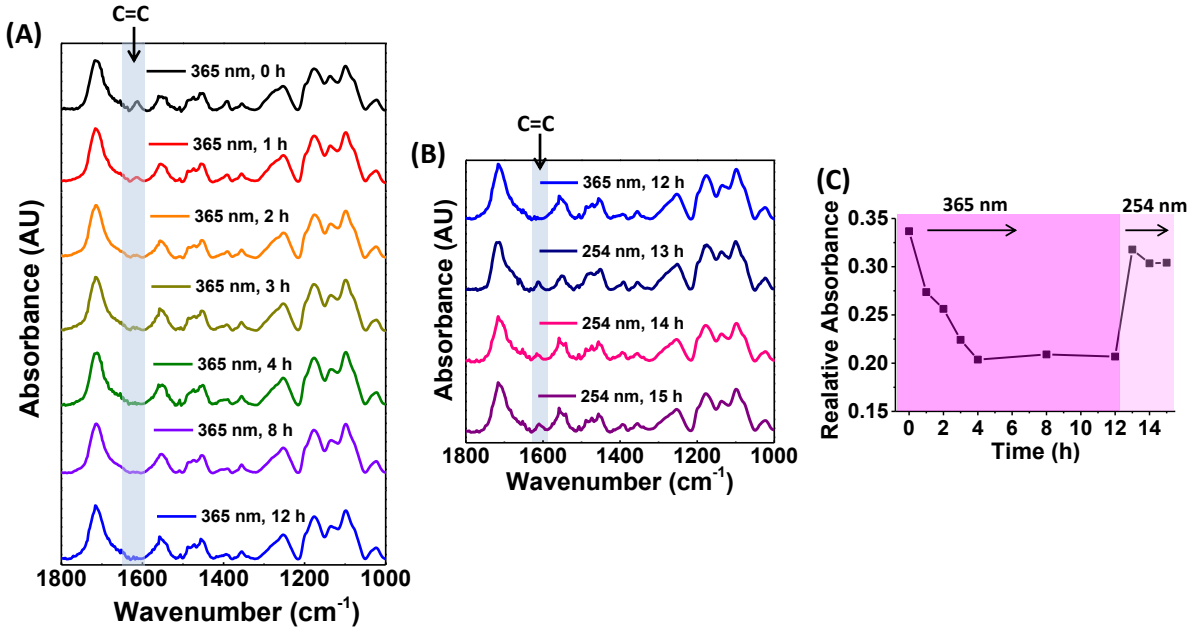

Figure 6.33 (A) FTIR spectra measured for concentrated MG-CMA (pH 7.4) during photo-crosslinking (365 nm irradiation) for different irradiation times and **(B)** subsequently photo-cleaved (254 nm irradiation). **(C)** Relative absorbance for the C=C stretch vs. time. The latter is the peak area ratio between 1620 cm^{-1} and 1710 cm^{-1}. Note that the point for "0" in (A) and (C) corresponds to the initial non-irradiated gel.

In order to study the change of peak at 1620 cm^{-1} with treatment of UV light, the peak area ratio between 1620 cm^{-1} and 1710 cm^{-1} was calculated. As shown in Figure 6.6C, the ratio decreases from 0.34 to 0.21 with first 4 h and remained stable at 0.20 for further 8 h with 365 nm irradiation. With further treatment with 254 nm light, the ratio increases to 0.32 and is stable at 0.30. Hence, photo-cleavage is ~ four times faster than photo-crosslinking. This is because the latter is a bi-molecular process[33].

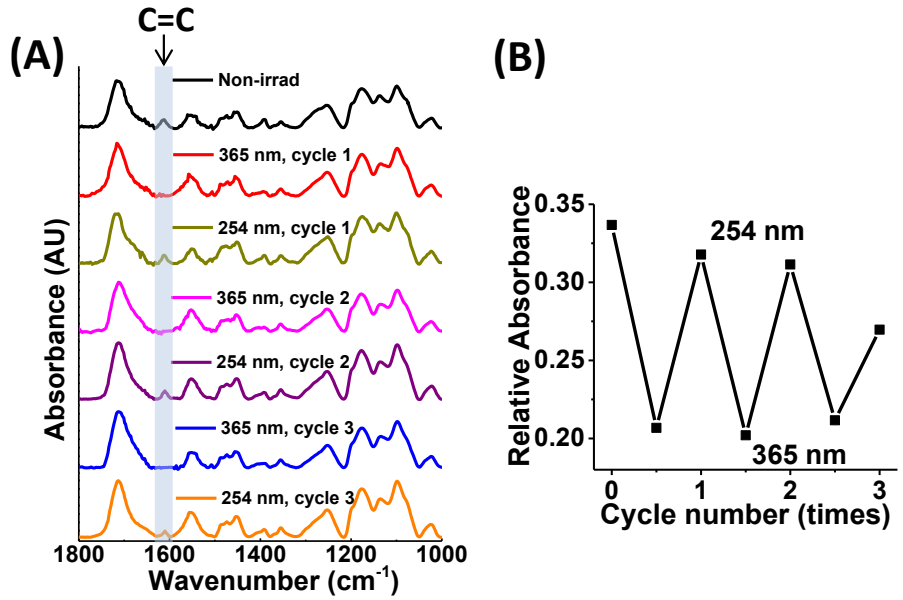

Figure 6.7. (A) FTIR spectra for the gels after photo-crosslinking (365 nm) and photo-cleaving (254 nm) cycles. **(B)** Variation of relative absorbance from FTIR spectra with cycle number. The latter is the peak area ratio between 1620 cm^{-1} and 1710 cm^{-1}. Note that the point for "0" in (A) and (B) corresponds to the initial non-irradiated gel.

The reversibility of photo-dimerisation and photo-cleavage of coumarin in the gels was probed by FTIR spectra. It can be seen in Figure 6.7A that the peak at 1620 cm^{-1} from the C=C stretching band decreased and grew when the gel was repeatedly irradiated at 365 nm and 254 nm, respectively. However, the reversibility of peak area ratio between 1620 cm^{-1} and 1710 cm^{-1} decreased with cycling (Figure 6.7B). This may be due to stable photo reaction side-products such as anti-head-to-tail coumarin dimers[34,35] being formed that are difficult to photocleave.

6.4.4 UV-triggered mechanical property change of gel

The physical gel (12.0 wt.%, Non-irrad), photo-crosslinked gel (365 nm) and photo-cleaved gel (254 nm) were investigated using dynamic rheology.

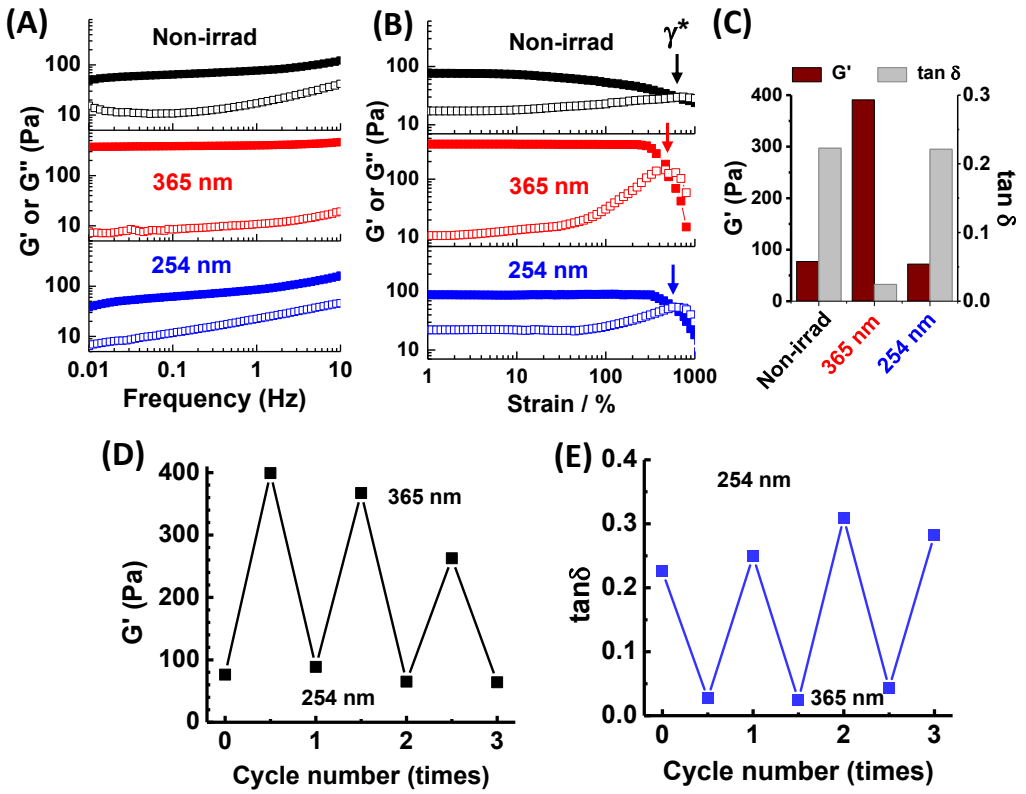

Figure 6.8. (A) Frequency-sweep and **(B)** strain-sweep rheology data for the gels. G′ and G″ are the storage modulus and loss modulus, respectively. The arrows in (B) show the yield strain (γ*). **(C)** G′ and tan δ (= G″/G′) for the non-irradiated, photo-crosslinked and photo-cleaved gels. **(D)** G′ and **(E)** tan δ variation with photo-crosslinking / photo-cleaving cycles. Note that the point for "0" in (D) and (E) corresponds to the initial non-irradiated gel.

Frequency-sweep (Figure 6.8A) and strain-sweep (Figure 6.8B) rheology data for the gels show mechanical property photo-tuning. The photo-crosslinked gel (365 nm) showed an almost frequency independent storage modulus (*G′*). The non-irradiated and photo-cleaved gels had frequency-dependent *G′* as expected for viscous gels. The curves for strain-sweep rheology data (Figure 6.8B) started with linear viscoelastic behaviour at a low strain before the gel can no longer withstand the strain and began to break. Subsequently, the G′ started to decrease because of the breaking of elastic networks. The G″ values increased until reaching its maximum when G′ and G″ crossed. After that, the gel networks were increasingly destroyed and both G′ and G″ decreased. Figure 6.8B also showed major changes upon photo-crosslinking with a strong maximum of the loss

modulus (G''). The yield strain (γ*) is a measure of ductility and was determined from the cross-over point of G' and the loss modulus (G'')[36]. The γ* values for the non-irradiated, photo-crosslinked and photo-cleaved gels were 740%, 400% and 660%, respectively, and they were all ductile. The storage modulus (G') for the photo-crosslinked gel (390 Pa) was five times higher than that for the parent non-irradiated gel (77 Pa) and decreased to 72 Pa upon photo-cleaving at 1 Hz and 1% strain (Figure 6.8C). Values of $tan\,\sigma$ ($= G''/G'$) less than 1.0 are signatures of elastic behavior[37] and are lowest for the photo-crosslinked gel. This is due to the higher number-density of elastically effective chains afforded by the coumarin dimers at 365 nm treatments compared to the gels not with UV light and also the 254 nm treatment. The reversibility of modulus photo-tuning was probed (Figure 6.8D - E). The modulus could be repeatedly increased and then decreased. Also, tanδ can be repeatedly decreased and then increased. These changes occurred using alternate cycles of irradiation at 365 nm and 254 nm.

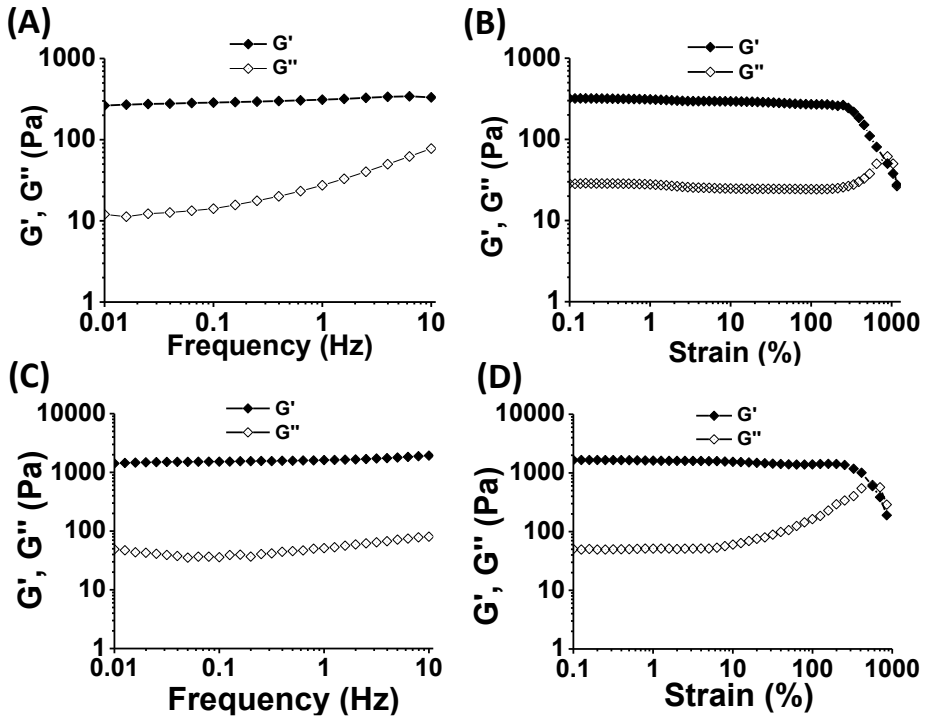

Figure 6.9. Frequency-sweep **(A)** and strain-sweep **(B)** rheology data for photo-crosslinked-gel (365 nm) after 2 h UV light treatment using 225 mW/cm^2 irradiation. Frequency-sweep **(C)** and strain-sweep **(D)** rheology data for a gel prepared from high concentration MG-CMA (22.0 wt.%).

From Figure 6.6, the photo-crosslinking process needs to at least 4 hours to be completed. In order to decrease the irradiation time, the higher intensity irradiation (225 mW/cm^2) was used to shorten the photo-crosslinking time to 2 h. The polymer content of gel was kept at 12.0 wt.%. The obtained gel showed an almost frequency independent storage modulus (G'), indicating that the elastic state is achieved (Figure 6.9A). The G′ can reach to 311 Pa (Figure 6.9B) which means that the photo-crosslinked gel can be formed more quickly by increase the light intensity. The modulus also can be adjusted by the concentration of MG-CMA. The high concentrated MG-CMA (22.0 wt.%) was treated with UV light and formed the more stiff hydrogel and G′ can increase to 1619 Pa (γ^* value is 566 %) ((Figure 6.9C - D).

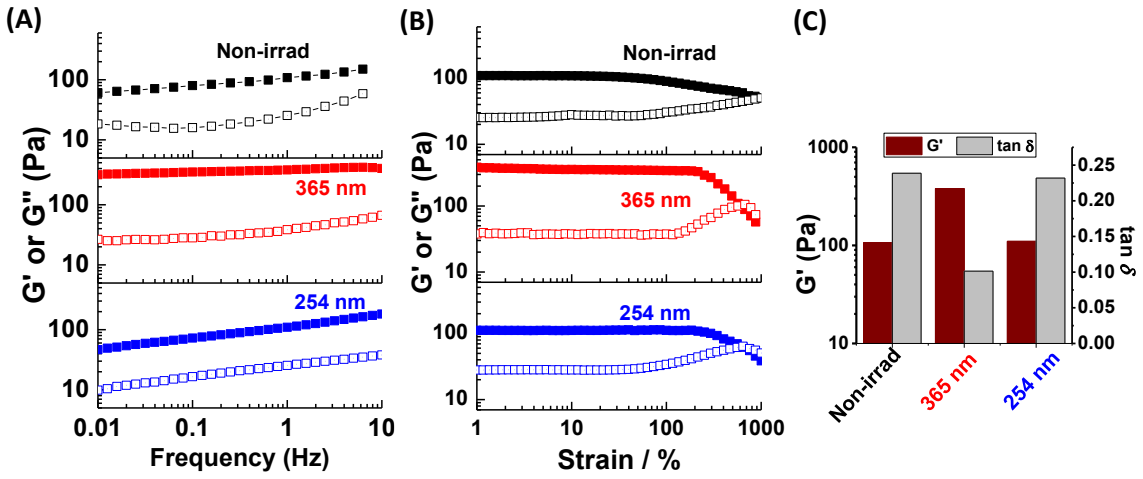

Figure 6.10. Frequency-sweep **(A)** and strain-sweep **(B)** rheology data for physical gel, photo-crosslinked-gel and photo-cleaved gel in DMF solvent. **(C)** Variation of the storage modulus (G′) and tan δ (= G″/G′) for the gels.

I studied the effect of several parameters on the gels mechanical properties. To demonstrate versatility non-aqueous gels (donated as Non-aqu gel) were prepared by exchanging water to DMF. The MG-CMA (13.0 wt.%) can swell in DMF and the physical non-aqueous gels formed. The crosslinked and photo-cleaved non-aqueous gels were obtained using UV light treatment (365 nm and 254 nm, respectively). The photo-crosslinked non-aqueous gel has almost frequency independent storage modulus (G′) while the non-irradiated and photo-cleaved non-aqueous gels had frequency-dependent G′ values (Figure 6.10 A). The values of G′ for the physical (110 Pa) photo-cleaved non-aqueous (112 Pa) were around a factors of 4 less than the photo-crosslinked one (386 Pa). The γ* values for these gels are 1002%, 871% and 673% respectively (Figure 6.10 B - C).

6.4.5 UV-triggered self-healing and reshaping of gel

The photo-reversible covalent bonding enabled light-triggered self-healing and re-shaping. Two halves of a photo-cleaved gel from a disk that had been severed were stained with two dyes (Rhodamine B and Nile Blue A).

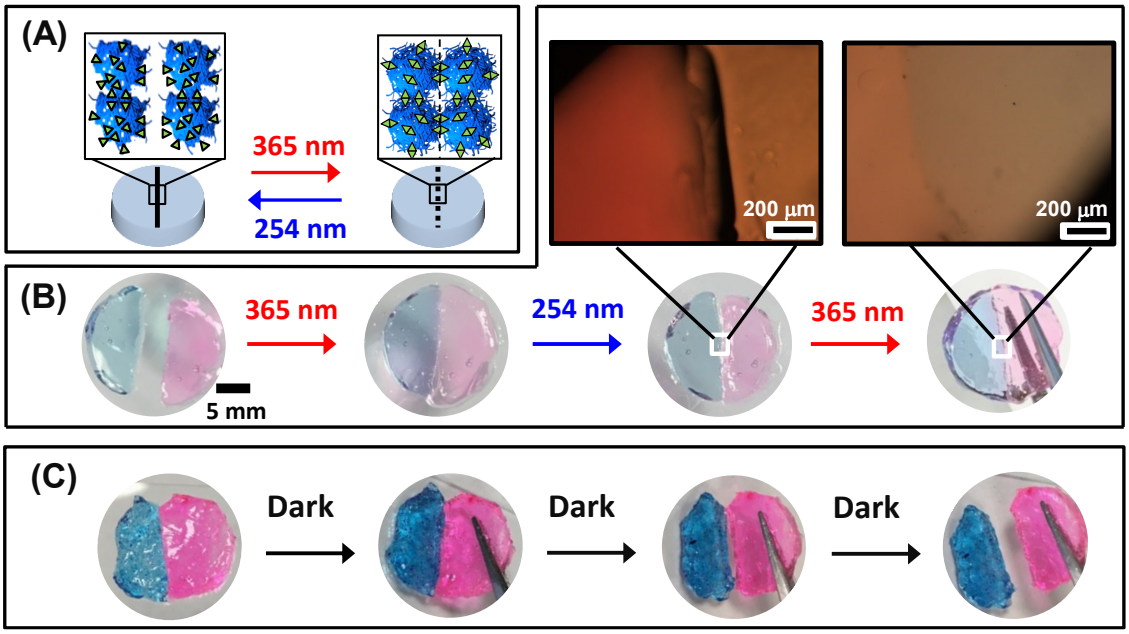

Figure 6.11. (A) Depiction of light-triggered self-healing. **(B)** Reversible self-healing using photo-crosslinking (365 nm) and photo-de-crosslinking (254 nm). The two halves of a photo-cleaved gel were reversibly joined and separated with the aid of 365 nm or 254 nm light. A control experiment **(C)** where two halves of a photo-cleaved gel were kept in the dark and pushed together resulted in them separating without self-healing. The scale bar is applied in all images.

Figure 6.11A depicts the mechanism of light triggered self-healing. As shown in Figure 6.11B**,** the two halves of the gel could be joined together by photo-crosslinking (365 nm). The joined gel could then be easily separated upon photo-cleaving (254 nm) and re-joined with 365 nm irradiation. The re-joined hydrogel cannot separate even it was suspended. Optical microscopy showed that the crack vanished due to photo-crosslinking. In contrast, self-healing did not occur when the gel was kept in the dark (Figure 6.11C).

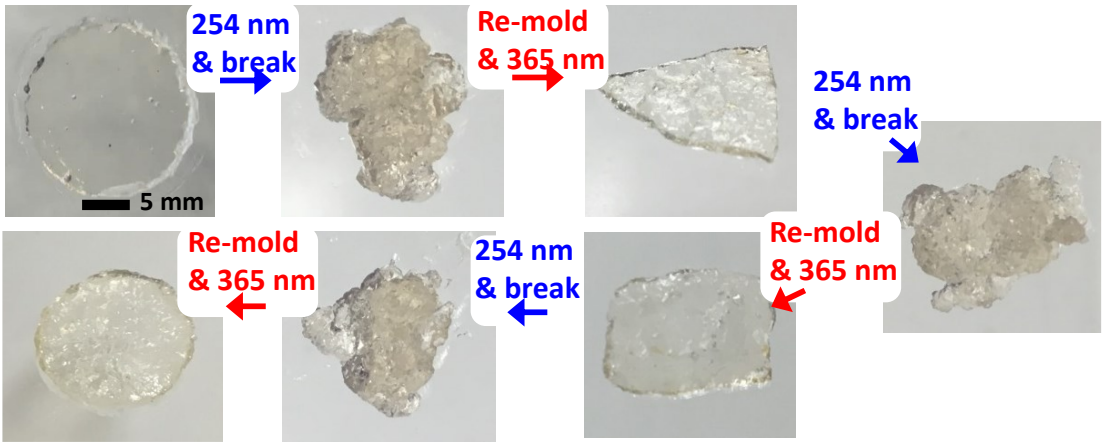

Figure 6.12. Light-assisted re-shaping of photo-crosslinked gels into a triangular, rectangular and circular shapes using photo-de-crosslinking followed by mechanical breaking and photo-crosslinking. The scale bar is applied in all images.

Because of the reversible nature of cycloaddition (UV, 365 nm) and photo-cleavage (UV, 254 nm) of coumarin, this hydrogel had another benefit, which allowed the de-crosslinked hydrogel to be recycled different shape hydrogel. Figure 6.12 shows the light-assisted reshaping of gel. A circle crosslinked hydrogel disc was decrosslinked by UV light (254 nm) irradiation and shear into small fragments and reprocessed into a triangular shape via UV light (365 nm) illumination for 6 hours. This triangular hydrogel can be transferred to a square one by photo-cleaving with UV light (254 nm), shearing, re-crosslinked with UV light (365 nm). After being reshaping according to the same procedure, a disc specimen was achieved. The light-assisted re-shaping was performed several times, which is a potential advantage for gel re-processing.

6.4.6 The effects of pH, temperature, UV light on the swelling of the gels

The triple sensitivity (light, pH and thermal) of gels was investigated using the volume swelling ratio (Q). Figure 6.13A shows the Q for the photo-crosslinked gel at three different temperatures and pH values. The smallest Q is 1.4 at pH 5.4 buffer solution and 37 °C, which is due to temperature-triggered hydrophobic interaction between MEO_2MA

segments as well as pH-triggered hydrogen bond formation between protonated –COOH groups within MAA[38, 39]. *Q* increase with decreasing temperature cause the hydrogel bond formation between poly(MEO_2MA) and water. There is a similar trend for *Q* at pH 6.0 (Figure 6.13A). The difference of *Q* values is not as distinct as the one at pH 5.4. At pH 7.4 the gels swelled strongly ($Q = 48$) because of electrostatic repulsion between $-COO^-$ groups and the *Q* values did not change significantly because the electrostatic repulsion is strong enough to inhibit temperature-triggered hydrophobic-hydrophobic interactions. Figure 6.13B shows the *Q* values for the photo-cleaved gel. The Q values at pH 6.0 and 7.4 at all temperatures are much higher than the photo-crosslinked gel. This is because of a low degree of cross-linking within polymer network contributed to stronger swelling. The temperature-triggered *Q* values changes at pH 5.4 are similar for the photo-cleaved and photo-crosslinked gel. Hydrogel bond form between -COOH and -COOH group as well as poly(MEO_2MA) and -COOH group at low pH (smaller than pK_a). The polymer network mainly occupied by poly(MEO_2MA) and poly(MAA), hence the effect of hydrogen bond exceeds the effect of crosslinker density changes on *Q* values.

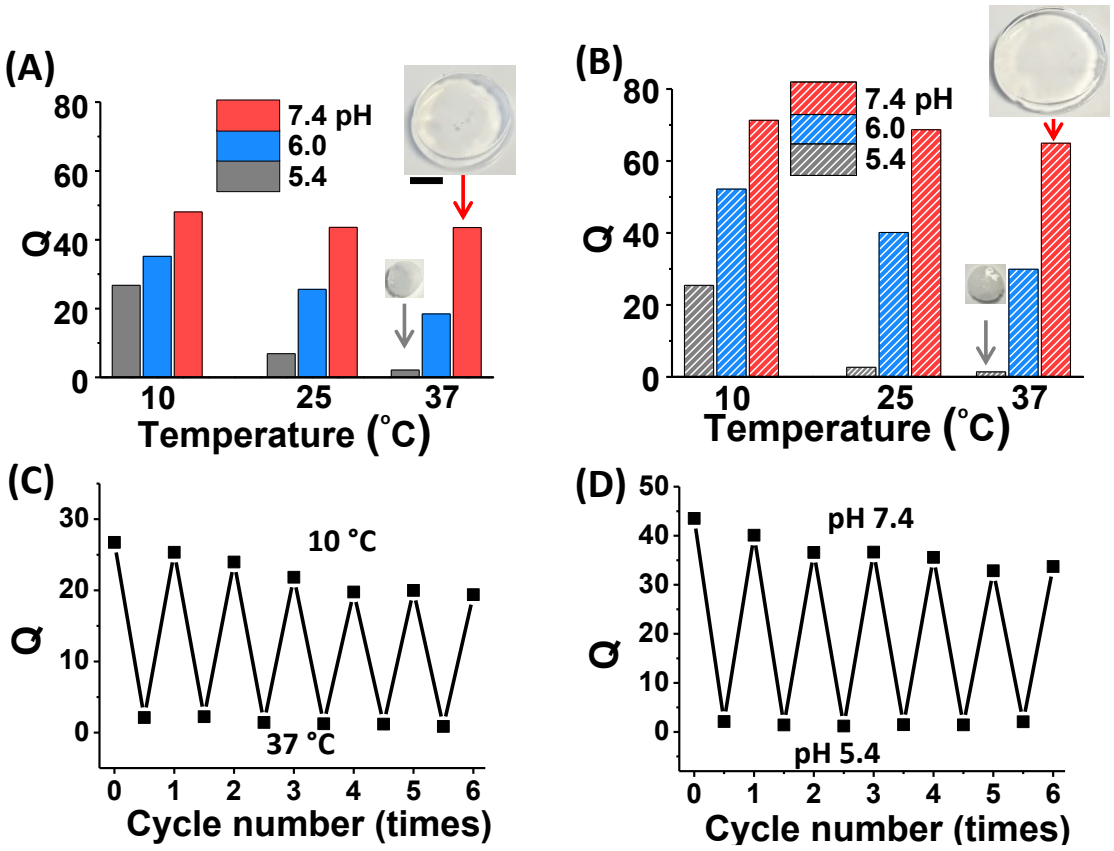

Figure 6.13. Volume swelling ratio (Q) for (**A**) photo-crosslinked (**B**) and photo-cleaved gel. The values of Q can be changed by pH, temperature and light irradiation. The scale bar is 5.0 mm and applies to all images. Variation of Q with **(C)** temperature cycling at pH 5.4 and **(D)** pH cycling at 37 °C for the photo-crosslinked gels.

The reversibility of Q to temperature and pH switching response for the photo-crosslinked gel was also studied (Figure 6.13C - D). The temperature dependence of Q at pH 5.4 can be reversed for 6 cycles but gradually decreases at low temperature (10°C). This may be due accumulated hydrogen bonding between poly(MEO_2MA) and -COOH groups at low pH and high temperature (37°C) for each cycle (Figure 6.13C). This leads to a decrease swelling of the hydrogel at low temperature. The pH dependence of Q at 37°C can also be reversed for 6 cycles and exhibits a small decrease (Figure 6.13D). This may be due to an increase of the ionic concentration in pH cycling.

6.4.7 Multi-responsive actuator

Bilayered hydrogels or hydrogel actuators have attracted great research interests because of the anisotropic deformation (expansion or contraction), causing bending[40, 41], walking[42], folding[43, 44]. Herein, the multi-responsive gel actuator was constructed by adsorbing the multi-responsive MG gel layer onto a non-responsive polyacrylamide (PAAm) gel and subsequent photo-crosslinking (see Experimental detail and Figure 6.14A). The PAAm layer contained a cationic dye (Me-RDB) to enhance visibility. The dye also provided a positive charge to the surface which assisted adhesion of the negatively charged MGs (Figure 6.2B). Figure 6.14B depicts swelling changes of the MG gel layer as well as the bending angle.

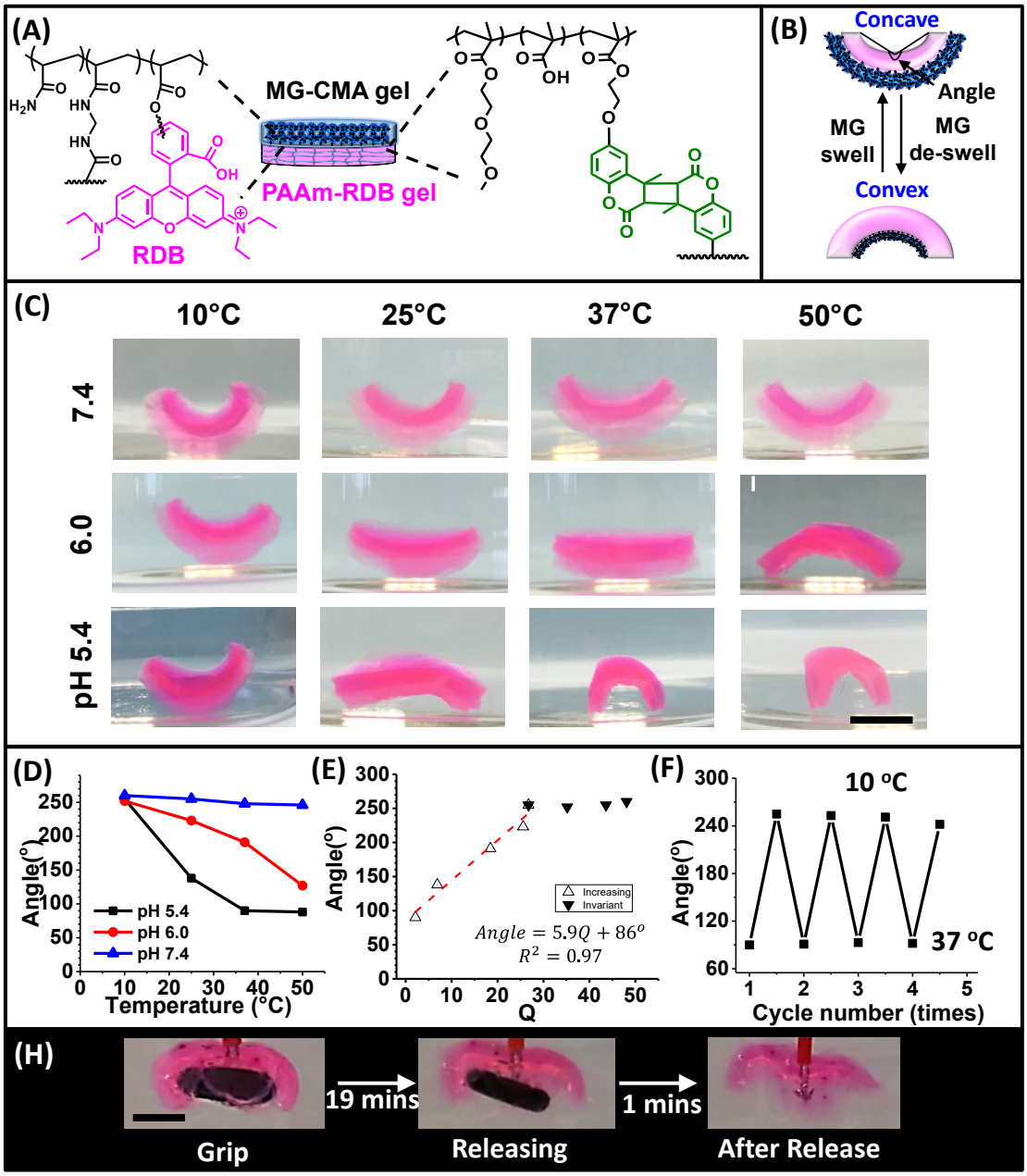

Figure 6.14. (A) Bilayer hydrogel actuator design. (**B**) Depiction of changes of the MG gel layer causing actuation as well as the bending angle. **(C)** The temperature-responsive bending and shrinking behaviours of the bilayer gel at pH 5.4, 6.0 and 7.4 as well as temperatures between 10 °C and 50 °C. The scale bar is 10.0 mm and applied to all images. **(D)** Effects of temperature and pH on the actuator bending angle. **(E)** Variation of bending angle with volume swelling ratio (Q) of the gels. **(F)** Reversibility of actuation behavior at pH 5.4 due to temperature switching. **(H)** The actuator could be used as a gripper by increasing the pH from 4.5 to 7.4 at 25 °C. The scale bar is 10.0 mm and applied to all images.

At pH 7.4 the actuator was concave and the bending angle stabilised at around 250°

(Figure 6.14D) at all temperatures (top row of Figure 6.14C) due to a high Q for the MG gel layer (Figure 6.13A). At pH 6.0 (middle row of Figure 6.14C) the actuator changed from concave at 10 °C to convex at 50 °C with bending angle changing from 200° to 127°(Figure 6.14D) because the Q value was temperature dependent at this pH (Figure 6.13A). At pH 5.4 the temperature-triggered changes were very large with convex bilayer resulted at 37 ºC and 50 ºC (bottom row of Figure 6.14C). This is because the pH-dependence of Q was strongest at pH 5.4 (Figure 6.13A). The bending angle had a change of 167° at pH 5.4 (Figure 6.14D). The data show that actuation was tuneable by pH and temperature in physiological conditions. The actuator bending angle was proportional to Q (for $Q < 30$) as shown in Figure 6.14E which is potentially useful for application. The bilayer also showed very good reversibility to temperature-triggered actuation (Figure 6.14F). A gripper was constructed that released a load (an O-ring, 85 mg) via a pH-triggered increase (from 4.5 to 7.4) as shown in Figure 6.14H. The bilayer gel did not exhibit any detectable cytotoxicity to chondroycte cells (Figure 6.15). Hence, the data raise the interesting prospect of using such actuators as biomedical micro-grippers[45] in the future.

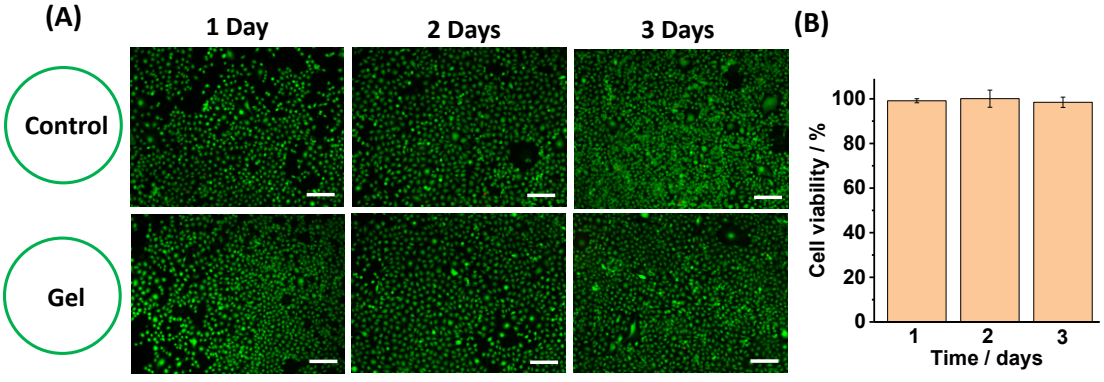

Figure 6.15. (A) Live/Dead cell assay and **(B)** cell viability calculated from the MTT assay for the bilayer gel used to construct the actuator. The chondrocyte cells were used. The control is the cells in the absence of the gel. The scale bar is 200 μm.

Subsequently, the swelling actuator (pH 7.4) was irradiated by 254 nm UV light. As

shown in Figure 6.16A, the height of second layer gel increase from 0 min to 20 min irradiation due to the photo-cleavage the dimers within polymer network of the crosslinked gel. This caused the gel to swell further at pH 7.4. After that, the height started to decrease until to second layer hydrogel totally disassociated. This is due to 254 nm UV light further cleaves the dimerised coumrine and the ignorable covalent bonds were not strong enough to keep the MG layer hydrogel intact. At the same time, the bending angle decrease gradually from 245° to 182° (Figure 6.16B). The bending angle for resulting one layer gel cannot change and remains stable at 180° at pH 6.0 at variation temperatures (Figure 6.16C). It is conclude that the pre-swelling of the crosslinked gel decreased the MG particle concentration and the strength of the residual crosslinking. This property was taken advantage of during bilayer construction so that photo-cleavage could be used to permanently remove the MG layer at pH 7.4. Hence, actuation could be terminated using 254 nm irradiation.

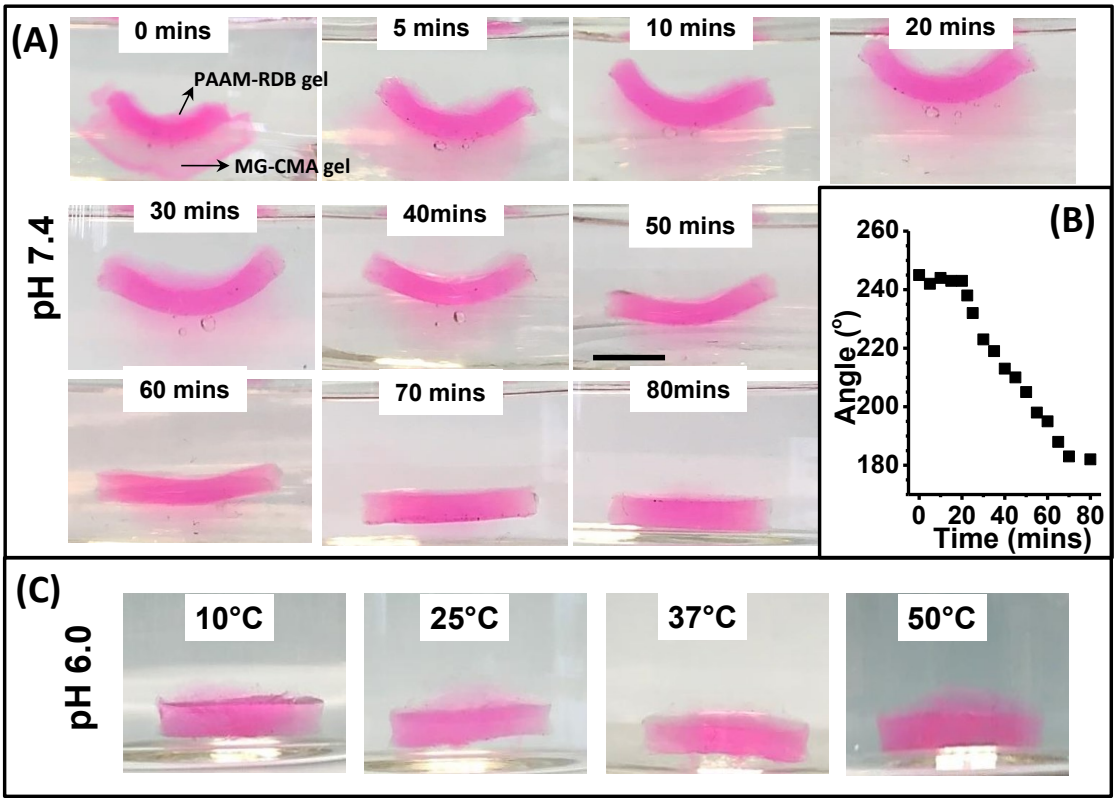

Figure 6.16. (A) Images and **(B)** Change of bending angle of the actuator during photo-cleaving (254 nm irradiation). **(C)** Temperature variation no longer has any effect on the photo-cleaved system. The scale bar is 10.0 mm and applied to all images.

The multi-responsive actuator can be used to control current flow. A conductive bilayer actuator was constructed using the photo-triggered crosslinked gel at the surface of MG(EA-MAA-DVB)/PEI hydrogel. The other side of MG(EA-MAA-DVB)/PEI hydrogel was absorbed to a thin layer of aluminate foil due to gel's adhesive property. The MG(EA-MAA-DVB)/PEI hydrogel is adhesive because the ionic crosslinker. The device design and properties are shown in Figures 5.17A.

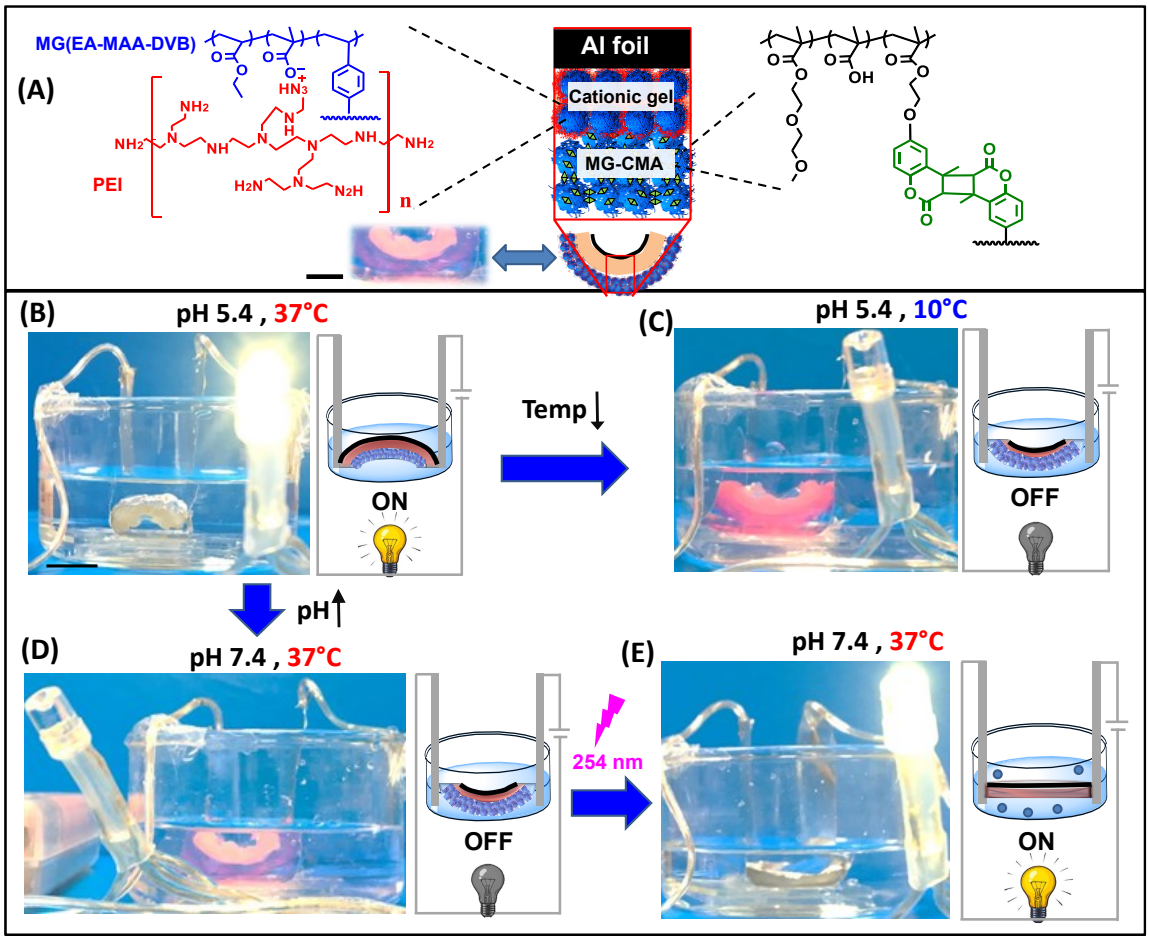

Figure 6.17. (A) Schematic of a circuit containing the actuator consisting of Al foil, a cationic adhesive gel layer and the multi-responsive MG layer. The Al foil touches both electrodes (ON state) in (B) to complete the circuit when the MG layer is de-swollen. The current can be interrupted (OFF state) by (C) decreasing the temperature or (D) increasing the pH. The current can be re-connected to give a permanent ON state by photo-cleaving (E) to remove the MG layer. The scale bar in (A) is 5.0 mm. The scale bar in (B) is 10 mm and applies to (B) - (E). Rhodamine B was absorbed into the MG layers in (A), (C) and (D) to improve the visual contrast.

The conductive actuator completed the circuit when convex (ON state) by allowing the top Al foil to touch two electrodes when the MG layer was in the de-swollen state and the actuator was convex (Figures 5.17B). When the MG gel was in the swollen state, the actuator became concave and the current flow was interrupted (OFF state) because the connection between the electrodes and aluminate foil was removed. This could be achieved by increasing the pH to 7.4 or decreasing the temperature to 10 °C (Figures

5.17C - D). Furthermore, the MG layer of this device could also be removed by photo-cleaving (ON state) (Figures 5.17E).

6.4.8 Studying the photochromic behaviour of the gels

The MG-CMA dispersions are fluorescent due to the coumarin groups[46] (Figure 6.18A). For the dilute dispersions (0.01 wt.%), there a emission peak at 380 nm for monomeric coumarin (Figure 6.18B**)**. The PL spectra (Figure 6.18B) show that the intensity decreases strongly upon photo-crosslinking due to a loss of conjugation as a result of photo-dimerisation of CMA[47]. This suggestion is supported by UV-visible spectra (Figure 6.3A) which show a decrease of the CMA absorption band. Figure 6.18B shows that most of the intensity lost due to photo-crosslinking is mostly recovered upon photo-cleaving. It is important to note that the wavelength of maximum intensity (λ_{max}) for the dispersions is not affected by irradiation (Figure 6.18C). The pictures of diluted dispersion at three stages are shown in Figure 6.18A. The colours of the MG-CMA dispersion without UV treatment and 254 nm irradiation are dark blue. The colour becomes much light blue with UV light irradiation at 365 nm. This is due to a decrease in CMA fluorophore concentration upon 365 nm light irradiation.

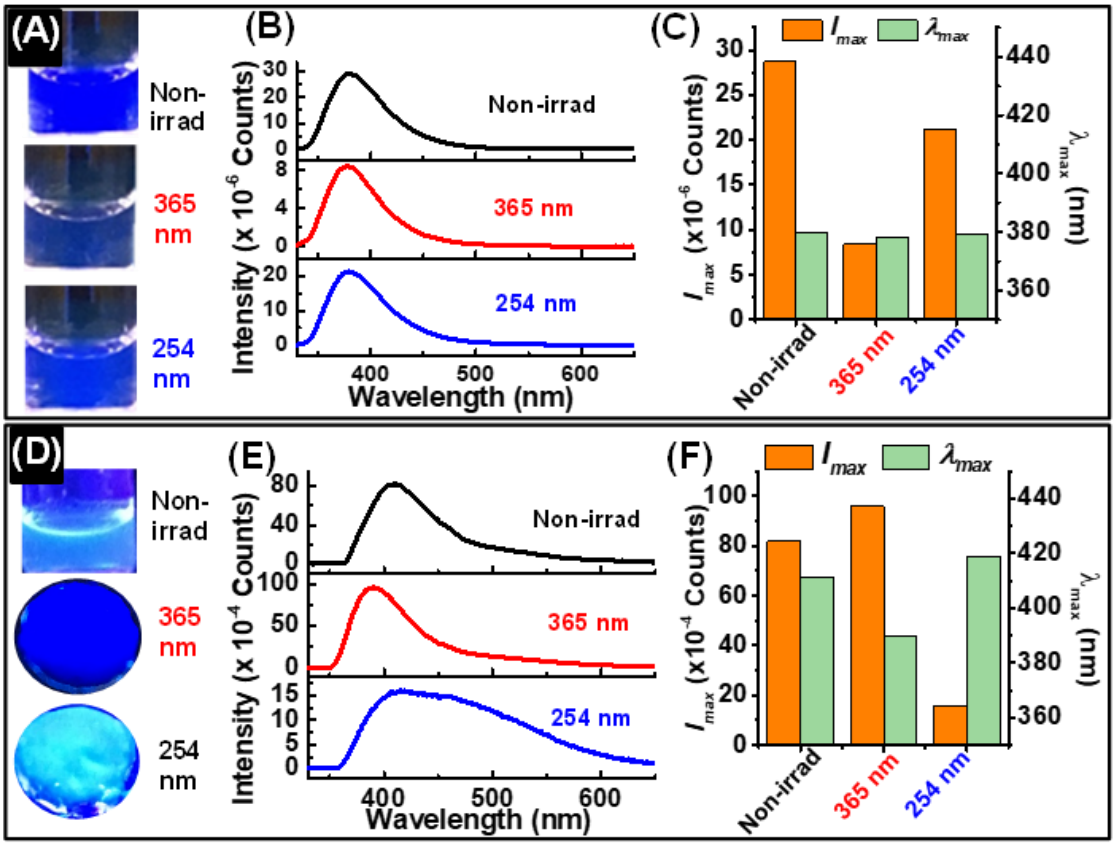

Figure 6.18. (A) Photographs of MG-CMA dispersions (0.010 wt.%) under UV light (302 nm) after various treatments. **(B)** Photoluminescence (PL) spectra for MG-CMA dispersion as made (non-irradiated), after photo-crosslinking (365 nm) and photo-cleaving (254 nm). (**C**) Maximum PL intensity (I_{max}) and wavelength at I_{max} (λ_{max}) for the dispersions. **(D)** Photographs of the gels (12 wt.%). The non-irradiated physical gel is in a tube. **(E)** PL spectra for the gels. **(F)** I_{max} and λ_{max} for the gels. Tube and gel diameters: 10 mm.

However, the MG-CMA gels showed very different fluorescent behaviours compared to the dilute dispersions. The concentrated (12.0 wt.%) non-irradiated physical gel and also the photo-cleaved gel were light blue (Figure 6.18D); whereas, the photo-crosslinked gel (365 nm) was deep blue. The PL spectra (Figure 6.18E) show a blue-shift upon photo-crosslinking which is followed by a red-shift when subsequently photo-cleaved (254 nm). The λ_{max} shifts may be due to π-π* overlap of coumarin groups[48]. Furthermore, the maximum PL intensity (I_{max}) increases and decreases, respectively, for the photo-crosslinked and photo-cleaved gels compared to the non-irradiated gel (Figure 6.18F). The I_{max} changes are indicative of an inner-filter effect[49]. Such effects have been

previously used for analyte detection[50, 51], whereas, here this effect is used to reversibly encode hidden information in gels.

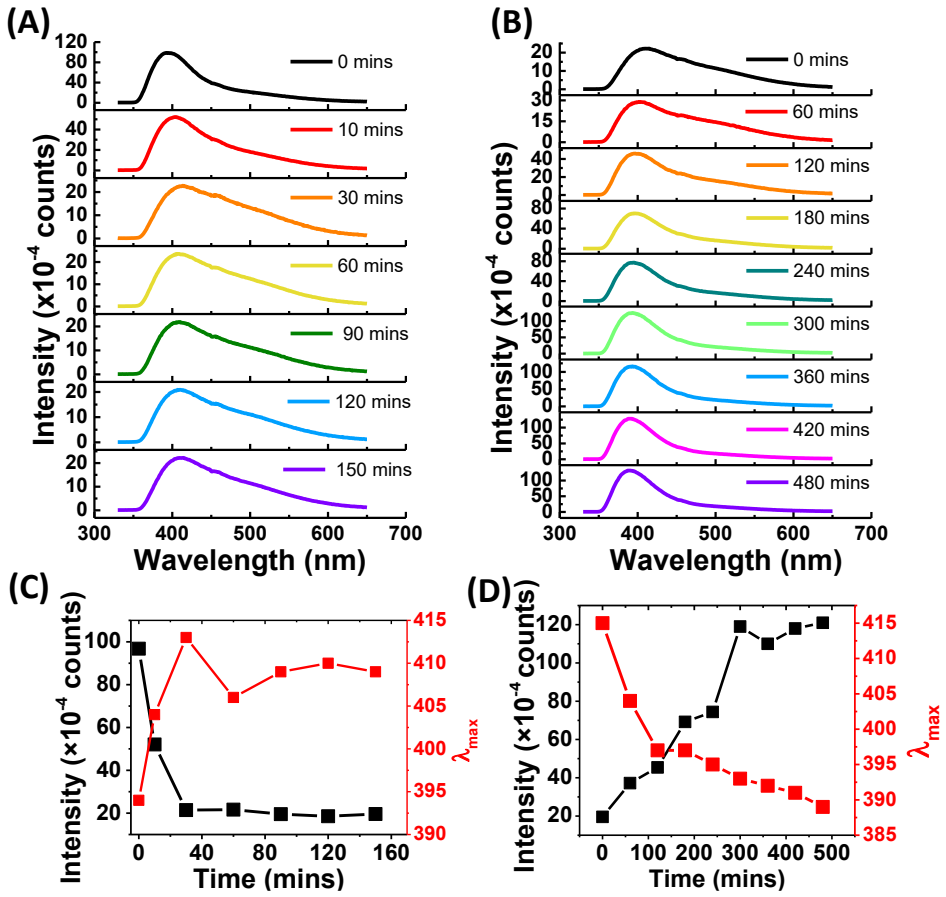

Figure 6.19. Changes of PL spectra for the gel during UV light at **(A)** 254 nm and **(B)** 365 nm irradiation. The PL intensity changes at 394 nm and the wavelength at maximum intensity from (A) and (B) are shown in **(C)** and **(D)**, respectively.

The trend in the PL spectra change of gel upon irradiation was studied as a function of irradiation time (see Figure 6.19). The PL intensity decreased from ~10^{-6} counts to 2 ×10^{-5} counts and red-shifted from 394 nm to 413 nm and the high-wavelength shoulder appeared after 30 min when the photo-crosslinked gel was irradiated with 254 nm light and then stabilised (Figure 6.19A and C). Subsequently, the photo-de-crosslinked gel was photo-crosslinked by 365 nm irradiation and the intensity increased to above 10^{-6} counts over a period of 300 min. The red-shift was mostly lost after 120 min of irradiation and the maximum intensity increased (Figure 6.19B and D).

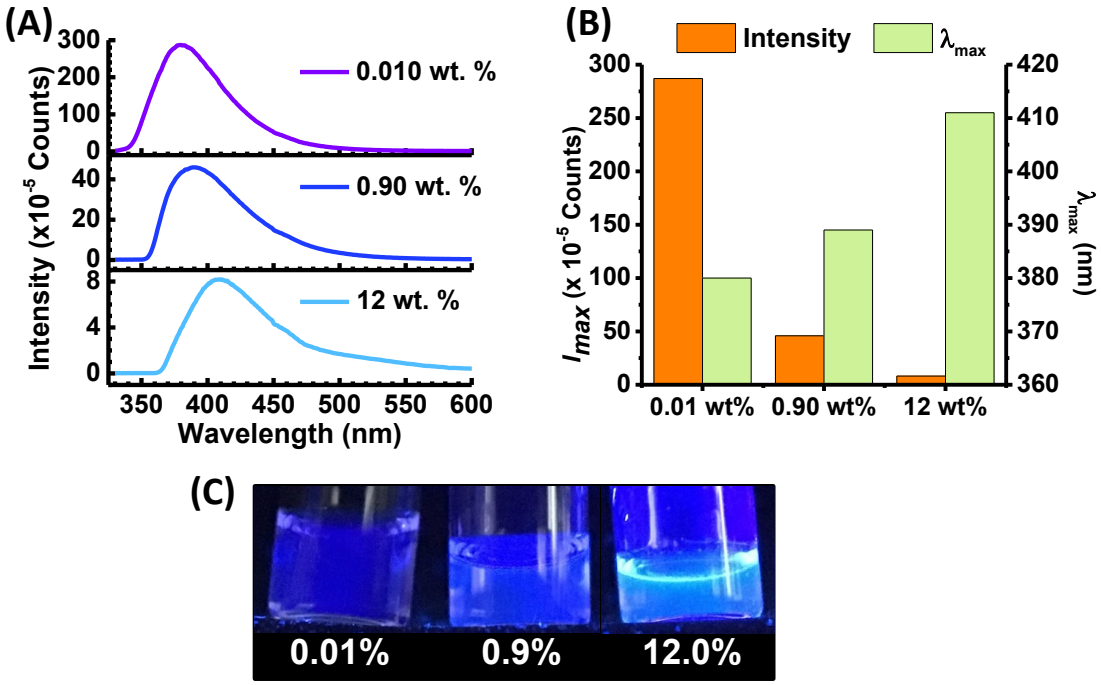

Figure 6.20. (A) PL spectra for MG-CMA dispersion obtained using different concentrations (shown). **(B)** Maximum intensity and wavelength of maximum intensity for the dispersions. **(C)** Digital photographs of the dispersions obtained using UV-light (302 nm).

The coumarin groups are closely located in the gels. Indeed, increasing the concentration of MG-CMA (without irradiation) caused a red-shift of λ_{max} and also decreased I_{max} (Figure 6.20). These results confirm that the red-shift is due to coumarin overlap and that I_{max} decreases when the coumarin concentration increases. For the gels in Figure 6.18D, photo-crosslinking (365 nm irradiation) decreases the concentration of coumarin, resulting in less π-π* overlap and a blue shift. Because the chromophore concentration decreases and less light is absorbed due to the inner filter effect, increased light penetration occurs and the emitted PL intensity increases from the remaining groups.

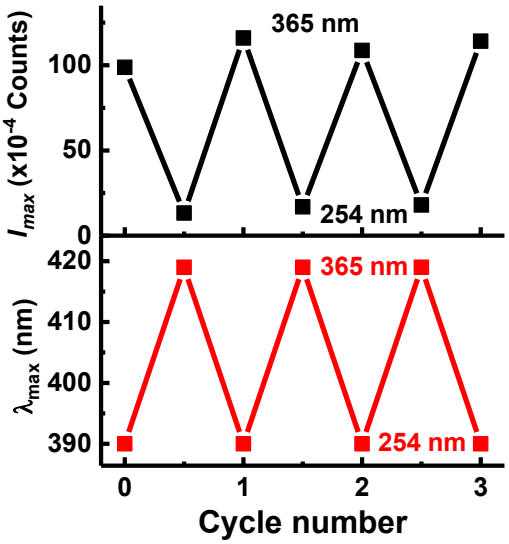

Figure 6.21. PL intensity and wavelength at maximum intensity (λ_{max}) for the gels after repeated photo-cleaving/photo-crosslinking cycles. Note that the point for "0" corresponds to the initial non-irradiated gel.

The light-triggered changes for I_{max} and λ_{max} show very good reversibility (Figure 6.21). Hence, the emission wavelength and intensity of these gels are photo-reversible. In contrast to other approaches that require complementary dyes to achieve such effects[52], the present system used only built in fluorescence of the photo-responsive CMA crosslinker.

Because a colour change occurred that was only visible in UV light and was reversible using the irradiation wavelength, I sought to demonstrate that hidden images could be transferred from a shadow mask to the gel and subsequently photo-erased.

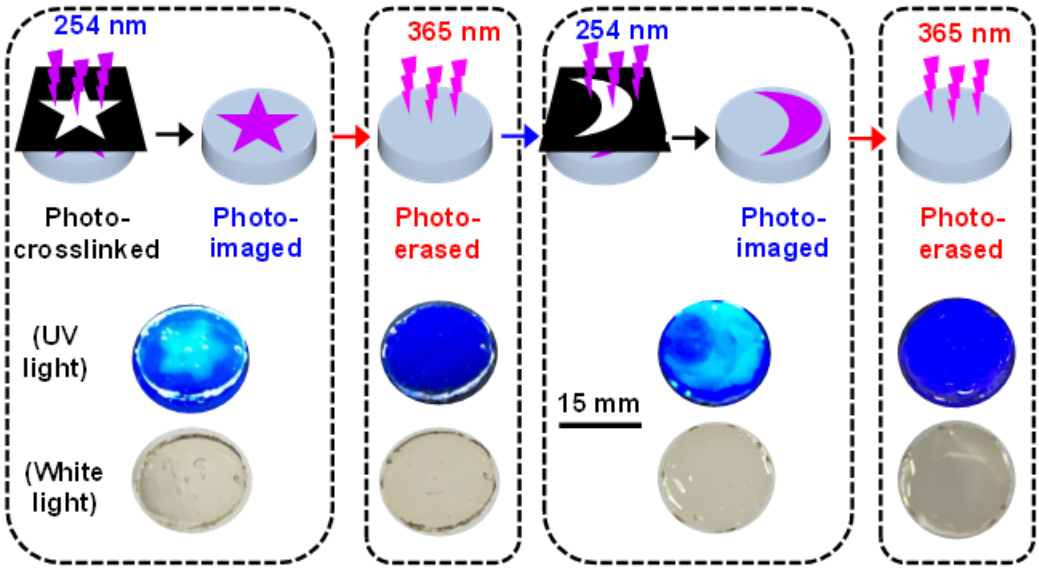

Figure 6.22. Depiction of reversible photo-imaging of a mask pattern using a photo-crosslinked gel (top row). The gels were viewed using UV light (302 nm, 2nd row) and white light (3rd row). The scale bar applies to all images.

As shown in Figure 6.22, photo-patterning at specific regions of the blue fluorescent photo-crosslinked hydrogel was realised by using a photo mask to direct the UV irradiation (254 nm) for 60 min. The fluorescent colour of UV-exposed regions changed from dark blue to light blue, whereas the protected regions maintained the dark blue fluorescent colour. The fluorescent pattern was displayed on the gel under UV light irradiation because of the considerable contrast of distinct fluorescent colours between the irradiated and protected regions. The colour of the treated region of gel can be photo-erased by photo-crosslinking (365 nm). The "star" and "moon" shape can be patterned and removed reversibly by switching the wavelength of UV light. However, the irradiated and protected region of gel was transparent under daylight because of the high transmittance of the blue fluorescent hydrogels over the range of visible light (bottom row). Such a gel could be an ideal material for an anti-counterfeit system.

6.4.9 The photolithography of gels

Different shape gels can be formed by using concentrated non-irradiated gels. In a *positive* photopatterning mode the non-irradiated MG-CMA physical gel was placed in an O-ring on a glass slide and another slide was placed on the top. A flower shape shadow mask was placed on the top of slide (Figure 6.23A). The gel was then photo-crosslinked (365 nm) in the exposed flower-shaped region. The gel was swollen in water and the non-photo-crosslinked gel in the shadow mask protected region re-dispersed in water to provide a flower shaped photo-crosslinked gel. *Negative* photopatterning was also demonstrated (Figure 6.23B). A photo-crosslinked gel was swollen in water. Next, a "heart" shape shadow mask was placed on top of the gel, and the gel photo-cleaved (254 nm) to photo-de-crosslink the exposed regions. These photo-cleaved sections detached. The gel protected from irradiation by the shadow mask remained intact so that the heart-shaped gel was formed.

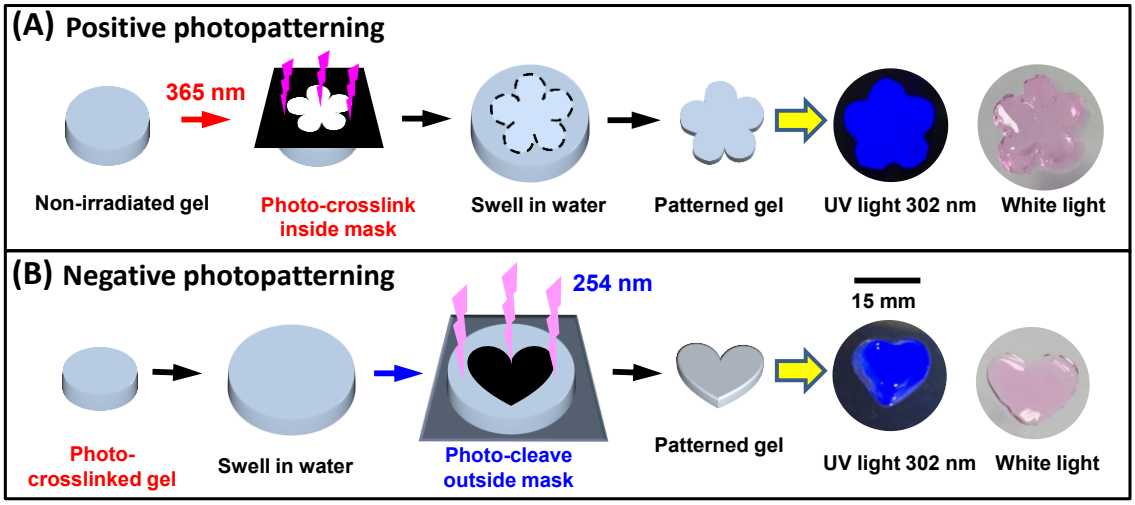

Figure 6.23. (A) Schematic (top row) and example preparation (bottom row) of flower shaped gel using *positive* photo-crosslinking and a shadow mask. **(B)** Schematic and example of preparation of heart shape gel-CMA by *negative* photo-patterning. The scale bars are 15.0 mm and apply to all images. Gel images were obtained under 302 nm or white light. The pink colour of the gels when viewed under white-light is due to an added Rhodamine B. The pH was 7.4.

6.5 Conclusions

In this chapter, a new method was introduced for fabrication of hydrogels with the help of UV light using only multi-responsive MG-CMA as the building blocks. MG-CMA contained coumarin groups. The pH and thermal triggered size change of MG-CMA was photo-tuneable. MGs enabled light to direct gel assembly and tune the mechanical and swelling properties without the use of small molecules or free-radical polymerization. The gels were triply-responsive with photo-tuneable modulus values. They were used to demonstrate multi-responsive cytocompatible actuators, grippers and ON/OFF circuit components via combining the non-responsive AAm gel and cationic gel, respectively. A reversible light-triggered blue-shift provided an anti-counterfeit property. The gels could be photo-patterned and exhibited light-triggered self-healing and re-processing. This chapter showcases the increased versatility to be obtained by including photo-crosslinkable groups within responsive MG-CMA building blocks. The results indicated that this approach should be quite general and is likely to apply to other aqueous and non-aqueous MG-CMA and nanogel gels. In terms of potential application, the actuators may lead to development of biocompatible micro-grippers for biomedical applications.

6.6 References

1. E. M. Ahmed, *J. Adv. Res*. 2015, **6**, 105-121.
2. A. M. Jonker, A. Borrmann, E. R. van Eck, F. L. van Delft, D. W. Löwik and J. C. van Hest, *Adv. Mater.* 2015, **27**, 1235-1240.
3. J. Gačanin, J. Hedrich, S. Sieste, G. Glaßer, I. Lieberwirth, C. Schilling, S. Fischer, H. Barth, B. Knöll and C. V. Synatschke, *Adv. Mater.* 2019, **31**, 1805044.
4. J. D. Tang, C. Mura and K. J. Lampe, *J. Am. Chem. Soc.* 2019, **141**, 4886-4899.
5. X. Wang, H. Huang, H. Liu, F. Rehfeldt, X. Wang and K. Zhang, *Macromol. Chem. Phys.* 2019, **220**, 1800562.
6. Y. Ke, C. Zhou, Y. Zhou, S. Wang, S. H. Chan and Y. Long, *Adv. Funct. Mater.* 2018, **28**, 1800113.
7. Z. Z. Ming, X. Ruan, C. Y. Bao, Q. N. Lin, Y. Yang and L. Y. Zhu, *Adv. Funct. Mater.* 2017, **27**.
8. Y. Takashima, S. Hatanaka, M. Otsubo, M. Nakahata, T. Kakuta, A. Hashidzume, H. Yamaguchi and A. Harada, *Nat. Commun.* 2012, **3**, 1270.
9. J. J. Shang and P. Theato, *Soft Matter* 2018, **14**, 8401-8407.
10. Z. Y. Li, G. Davidson-Rozenfeld, M. Vazquez-Gonzalez, M. Fadeev, J. J. Zhang, H. Tian and I. Willner, *J. Am. Chem. Soc.* 2018, **140**, 17691-17701.
11. R. Langer and D. A. Tirrell, *Nature* 2004, **428**, 487-492.
12. M. P. Lutolf and J. A. Hubbell, *Nat. Biotechnol.* 2005, **23**, 47-55.
13. T. Matsuda, R. Kawakami, R. Namba, T. Nakajima and J. P. Gong, *Science* 2019, **363**, 504.
14. H. Yuk, B. Lu and X. Zhao, *Chem. Soc. Rev.* 2019, **48**, 1642-1667.
15. S. Han, H. J. Bae, J. Kim, S. Shin, S.-E. Choi, S. H. Lee, S. Kwon and W. Park, *Adv. Mater*, 2012, **24**, 5924-5929.

16. S. H. Jung, J. Jeon, H. Kim, J. Jaworski and J. H. Jung, *J. Am. Chem. Soc.* 2014, **136**, 6446-6452.

17. P. M. Gawade, J. A. Shadish, B. A. Badeau and C. A. DeForest, *Adv. Mater.* 2019, 1902462.

18. H. Wang, C. N. Zhu, H. Zeng, X. Ji, T. Xie, X. Yan, Z. L. Wu and F. Huang, *Adv. Mater.* 2019, **31**, 1807328.

19. J. Lou, F. Liu, C. D. Lindsay, O. Chaudhuri, S. C. Heilshorn and Y. Xia, *Adv. Mater.* 2018, **30**, 1705215.

20. M. Nakahata, Y. Takashima, H. Yamaguchi and A. Harada, *Nat. Commun.*, 2011, **2**, 511.

21. B. Rybtchinski, *ACS Nano* 2011, **5**, 6791-6818.

22. Z. Liu, Q. Lin, Y. Sun, T. Liu, C. Bao, F. Li and L. Zhu, *Adv. Mater*. 2014, **26**, 3912-3917.

23. B. D. Fairbanks, M. P. Schwartz, A. E. Halevi, C. R. Nuttelman, C. N. Bowman and K. S. Anseth, *Adv. Mater*. 2009, **21**, 5005-5010.

24. H. Shin, B. D. Olsen and A. Khademhosseini, *Biomaterials* 2012, **33**, 3143-3152.

25. C. G. Williams, A. N. Malik, T. K. Kim, P. N. Manson and J. H. Elisseeff, *Biomaterials* 2005, **26**, 1211-1218.

26. S. R. Trenor, A. R. Shultz, B. J. Love and T. E. Long, *Chem. Rev.* 2004, **104**, 3059-3078.

27. Y. M. Zhang and L. Ionov, *Langmuir* 2015, **31**, 4552-4557.

28. C. P. Kabb, C. S. O'Bryan, C. C. Deng, T. E. Angelini and B. S. Sumerlin, *ACS Appl. Mater. Interfaces* 2018, **10**, 16793-16801.

29. R. Tamate, T. Ueki, Y. Kitazawa, M. Kuzunuki, M. Watanabe, A. M. Akimoto and R. Yoshida, *Chem. Mater.* 2016, **28**, 6401-6408.

30. M. N. Zhu, D. D. Lu, S. L. Wu, Q. Lian, W. K. Wang, A. H. Milani, Z. X. Cui, N. T. Nguyen, M. Chen, L. A. Lyon, D. J. Adlam, A. J. Freemont, J. A. Hoyland and B. R. Saunders, *ACS Macro Lett.* 2017, **6**, 1245-1250.

31. S. L. Wu, M. N. Zhu, D. D. Lu, A. H. Milani, Q. Lian, L. A. Fielding, B. R. Saunders, M. J. Derry, S. P. Armes, D. Adlam and J. A. Hoyland, *Chem. Sci.* 2019, **10**, 8832-8839.

32. A. Concellón, T. Liang, A. P. H. J. Schenning, J. L. Serrano, P. Romero and M. Marcos, *J. Mater. Chem. C* 2018, **6**, 1000-1007.

33. S. R. Trenor, A. R. Shultz, B. J. Love and T. E. Long, *Chem. Rev.* 2004, **104**, 3059-3078.

34. Y. Chen and J. L. Geh, *Polymer* 1996, **37**, 4481-4486.

35. N. Yonezawa, T. Yoshida and M. Hasegawa, *J. Chem. Soc., Perkin Trans. 1* 1983, 1083-1086.

36. Y. Yuan, S. Basu, M. H. Lin, S. Shukla and D. Sarkar, *ACS Appl. Mater. Interfaces* 2019, **11**, 31709-31728.

37. R. Tamate, T. Ueki, Y. Kitazawa, M. Kuzunuki, M. Watanabe, A. M. Akimoto and R. Yoshida, *Chem. Mater.* 2016, **28**, 6401-6408.

38. M. Boularas, E. Deniau-Lejeune, V. Alard, J.-F. Tranchant, L. Billon and M. Save, *Polym. Chem.* 2016, **7**, 350-363.

39. L. Teng, Y. Chen, M. Jin, Y. Jia, Y. Wang and L. Ren, *Biomacromolecules* 2018, **19**, 1939-1949.

40. C. Yao, Z. Liu, C. Yang, W. Wang, X. J. Ju, R. Xie and L. Y. Chu, *Adv. Funct. Mater.* 2015, **25**, 2980-2991.

41. Y. Tan, D. Wang, H. X. Xu, Y. Yang, X. L. Wang, F. Tian, P. P. Xu, W. L. An, X. Zhao and S. M. Xu, *ACS Appl. Mater. Interfaces* 2018, **10**, 40125-40131.

42. C. Yang, W. Wang, C. Yao, R. Xie, X. J. Ju, Z. Liu and L. Y. Chu, *Sci. Rep.* 2015, **5**.

43. J. C. Breger, C. Yoon, R. Xiao, H. R. Kwag, M. O. Wang, J. P. Fisher, T. D. Nguyen and D. H. Gracias, *ACS Appl. Mater. Interfaces* 2015, **7**, 3398-3405.

44. E. Wang, M. S. Desai and S. W. Lee, *Nano Lett.* 2013, **13**, 2826-2830.

45. K. Kobayashi, C. Yoon, S. H. Oh, J. V. Pagaduan and D. H. Gracias, *ACS Appl. Mater. Interfaces*, 2019, **11**, 151-159.

46. J. S. de Melo and P. F. Fernandes, *J. Mol. Struct.* 2001, **565**, 69-78.

47. X. Zhang, Y. P. Wang, G. Li, Z. T. Liu, Z. W. Liu and J. Q. Jiang, *Macromol. Rapid Commun.* 2017, **38**.

48. R. R. Cui, Y. C. Lv, Y. S. Zhao, N. Zhao and N. Li, *Mater. Chem. Front.* 2018, **2**, 910-916.

49. D. Cortecchia, H. A. Dewi, J. Yin, A. Bruno, S. Chen, T. Baikie, P. P. Boix, M. Grätzel, S. Mhaisalkar, C. Soci and N. Mathews, *Inorg. Chem.* 2016, **55**, 1044-1052.

50. L. Shang and S. Dong, *Anal. Chem.* 2009, **81**, 1465-1470.

51. A. S. Tanwar, S. Hussain, A. H. Malik, M. A. Afroz and P. K. Iyer, *ACS Sens.* 2016, **1**, 1070-1077.

52. D. Wang, T. Zhang, B. Wu, C. Ye, Z. Wei, Z. Cao and G. Wang, *Macromolecules* 2019, **52**, 7130-7136.

Chapter 7: Conclusions and future work

7.1 Summary of conclusions

The main aim of this research was design and develop most of the multi-responsive (pH, temperature, and light) microgels (MGs) and doubly crosslinked microgels (DX MGs) for potential use in biomedical applications, such as drug delivery and degenerated intervertebral disc (DIVD) repair. The light sensitivity of MGs and DX MGs were specially focused upon as light can control the mechanical property of gels directly and remotely. Besides, other properties like swelling properties and cytotoxicity were also studied to comprehensively understand MG and DX MGs.

At the beginning of the project, the UV-C light induced MG-*x*-nPh degradation and enhancement of mechanical property of DX MG-*x*-nPh were studied (Chapter 4). The DX MG-*x*-nPh was constructed from the concentrated vinyl functionalised MG-*x*-nPh in the presence of an initiator. The degradation speed and degree of mechanical property enhancement induced by UV light (254nm) is related to the content of copolymerised photo-cleavage crosslinker (nPh). The degradation rate was shown to be strongly dependent on the crosslinker amount copolymerised in MGs. It is possible to load the drug to MGs and design the MGs with different crosslinker amount according to the release rate of drug via UV irradiation. A higher crosslinker content increased the stiffness of gels due to the formation of multiple ionic crosslinks between $-COO^-$ groups and photogenerated $–NH_3^+$ groups. Both MG-*x*-nPh and DX MG-*x*-nPh were pH- and temperature- responsive. High pH and low temperature can trigger MG and DX MG swelling, while low pH and high temperature deswell MG-*x*-nPh and DX MG-*x*-nPh. The

live/dead assay for the gels demonstrates the gels were not toxic, which indicates the gel had potential application in biomaterials such us IVD repair.

Next, I replaced the photo-cleavage crosslinker (nPh) in Chapter 4 with the reversible photo-dimerisation/cleavage monomer (CMA). Four different size poly(MEO_2MA-MAA-CMA) MGs (MG-CMA) which are photo-, pH-, temperature- responsive were synthesised. The crosslinker density can be increased or decreased reversibly by switching the wavelength of light (365 nm and 254 nm). Hence, the UV light can adjust the pH- and temperature- induced swelling of the MGs. Unexpectedly, the time of dimerisation degree to equilibrium is faster for the smaller diameters of the as-made MGs. These MGs can be used to enhance the anticancer drug release, which indicates that it has potential application in real time drug delivery and release. As the different sized MGs exhibits different drug release rates due to the size of the porous water filled pores in the matrix[1-2], it would be useful to control the release rate by adjusting the size of MGs. This could also combinate two or more drugs with requirement of combination therapies such as those used to treat cancer[3] and HIV[4].

Concentrated swollen MGs are constructed to form CMA-based gels. This method for fabrication of hydrogels uses only multi-responsive MGs as the building blocks via photo-crosslinking peripheral CMA groups without the use of small molecules or free-radical polymerization. The gels were triply-responsive with photo-tuneable modulus values, light-assisted healing and re-processing capacity. The light-controllable reparability and re-processability can realize intelligent resolution of recyclability and sustainable development of hydrogel or polymer. They can be constructed as multi-responsive cytocompatible actuators, grippers and ON/OFF circuit components. The gel with those properties could be exploited in chemical and mechanical systems, including on-demand

drug delivery platforms[5] and microfluidic valves[6] which control the drug release and fluidic flow respectively remotely by light. The gels also can be photo-patterned and photo-imaged. Such hydrogels provide an idea plan to protect information with improved security. Hence, the hydrogels in this study could be exploited novel methods to design multi-function and multi-application materials.

7.2 Future work

The results from Chapter 4 to Chapter 6 indicate that new gels were prepared successfully. The mechanical property and the swelling behaviour of those gels can be adjusted remotely by UV light (254 nm and 365 nm). However, the UV light ($\lambda < 360$ nm) hardly penetrates to tissue (< 0.5 mm)[7], which limited the application of this gels and MGs into DIVD. UV irradiation may also cause negative effect such as erythema, shin ageing, strong pigmentation and skin cancer[7]. To surmount those, two-photon absorption (TPA) via stimulataneously absorbing two low energy near infrared (NIR) photons is proposed. NIR light can penetrate deeper (5 - 10 mm)[8] because skin consists of a range of chromophores which have scattering and absorption coefficients which are highly wavelength dependent[9-11]. To control the local stress distributions of gels in the DIVD via a non-invasive way, NIR light is worthwhile to use. The photo-degradation of *o*-nitrobenzyl moiety via TPA has been fully studied[12-14]. The use of TPA process instead of UV light is reported for the cyclo-reversion reaction of comarin as well [15-17].

More investigations of the NIR irradiation of TPA for the photo responsive DX MG-*x*-nPh are required in future studies. For the DX MG-*x*-nPh prepared from the vinyl functionalised MG-*x*-nPh via free radical polymerisation in Chapter 4, more study about the injectability of physical gel and the NIR light tuneable modules of chemical gel within DIVD should be carried on. This hydrogels also were proposed as gel implants which

report sterilisation. Hence, the sterilisation ability of UV-A light (254 nm) to this gel will be studied in the future.

The photo-enhancement of the anticancer drug (DOX) release from MG-CMA and photo-tuneable modulus values of CMA-based gels were achieved in Chapter 5 and Chapter 6, respectively. Loading the growth factor or protein into MG-CMA and mixing the encapsulated MG-CMA with concentrated swollen MG-CMA and then NIR light triggered formation the CMA-based gels within the DIVD are also worthwhile to study. They can both provide NIR light-controlled tuning of the mechanical properties and releasing the growth factor that can promote the repairing of DIVD.

Our group has established ratiometric fluorescent nanosensor based on dye labelled pH-responsive nanoprobes and core-shell-shell nanoparticles which can report the strain distribution of gels based on Förster resonance energy transfer (FRET)[18-20]. Next, the new theranostic methodology could be forwarded via combining the NIR responsive injectable gels and nanosensor to provide an injectable load supporting NIR gels medical device that has mechanical property tuning capabilities, repairing the DIVD and strain-reporting.

7.3 References

1. Gurny, R.; Doelker, E.; Peppas, N. J. B., Modelling of sustained release of water-soluble drugs from porous, hydrophobic polymers. **1982,** *3* (1), 27-32.

2. Varma, M. V.; Kaushal, A. M.; Garg, A.; Garg, S. J. A. J. o. d. d., Factors affecting mechanism and kinetics of drug release from matrix-based oral controlled drug delivery systems. **2004,** *2* (1), 43-57.

3. Mokhtari, R. B.; Homayouni, T. S.; Baluch, N.; Morgatskaya, E.; Kumar, S.; Das, B.; Yeger, H. J. O., Combination therapy in combating cancer. **2017,** *8* (23), 38022.

4. Arts, E. J.; Hazuda, D. J. J. C. S. H. p. i. m., HIV-1 antiretroviral drug therapy. **2012,** *2* (4), a007161.

5. Zhang, J.-T.; Keller, T. F.; Bhat, R.; Garipcan, B.; Jandt, K. D. J. A. b., A novel two-level microstructured poly (N-isopropylacrylamide) hydrogel for controlled release. **2010,** *6* (10), 3890-3898.

6. Lee, E.; Kim, D.; Kim, H.; Yoon, J. J. S. r., Photothermally driven fast responding photo-actuators fabricated with comb-type hydrogels and magnetite nanoparticles. **2015,** *5*, 15124.

7. Ash, C.; Dubec, M.; Donne, K.; Bashford, T., Effect of wavelength and beam width on penetration in light-tissue interaction using computational methods. *Laser Med Sci* **2017,** *32* (8), 1909-1918.

8. Teraphongphom, N.; Kong, C. S.; Warram, J. M.; Rosenthal, E. L., Specimen Mapping in Head and Neck Cancer Using Fluorescence Imaging. *Larynscope Investig* **2017,** *2* (6), 447-452.

9. Young, A. R., Chromophores in human skin. *Phys Med Biol* **1997,** *42* (5), 789-802.

10. Anderson, R. R.; Parrish, J. A., The Optics of Human-Skin. *J Invest Dermatol* **1981,** *77* (1), 13-19.

11. Brenner, M.; Hearing, V. J., The protective role of melanin against UV damage in human skin. *Photochem Photobiol* **2008,** *84* (3), 539-549.

12. Zhao, H.; Hou, B.; Tang, Y. F.; Hu, W. B.; Yin, C.; Ji, Y.; Lu, X. M.; Fan, Q. L.; Huang, W., O-Nitrobenzyl-alt-(phenylethynyl)benzene copolymer-based nanoaggregates with highly efficient two-photon-triggered degradable properties via a FRET process. *Polym Chem-Uk* **2016,** *7* (18), 3117-3125.

13. Aujard, I.; Benbrahim, C.; Gouget, M.; Ruel, O.; Baudin, J. B.; Neveu, P.; Jullien, L., o-Nitrobenzyl photolabile protecting groups with red-shifted absorption: Syntheses and uncaging cross-sections for one- and two-photon excitation. *Chem-Eur J* **2006,** *12* (26), 6865-6879.

14. Wang, X.; Werner, S.; Weiss, T.; Liefeith, K.; Hoffmann, C., ortho-Nitrobenzyl alcohol based two-photon excitation controlled drug release system. *Rsc Adv* **2012,** *2* (1), 156-160.

15. Kim, H. C.; Kreiling, S.; Greiner, A.; Hampp, N., Two-photon-induced cycloreversion reaction of coumarin photodimers. *Chem Phys Lett* **2003,** *372* (5-6), 899-903.

16. Härtner, S.; Kim, H.-C.; Hampp, N., Photodimerized 7-hydroxycoumarin with improved solubility in PMMA: Single-photon and two-photon-induced photocleavage in solution and PMMA films. *Journal of Photochemistry and Photobiology A: Chemistry* **2007,** *187* (2-3), 242-246.

17. Buckup, T.; Dorn, J.; Hauer, J.; Hartner, S.; Hampp, N.; Motzkus, M., The photoinduced cleavage of coumarin dimers studied with femtosecond and nanosecond two-photon excitation. *Chem Phys Lett* **2007,** *439* (4-6), 308-312.

18. Zhu, M. N.; Lu, D. D.; Wu, S. L.; Lian, Q.; Wang, W. K.; Milani, A. H.; Cui, Z. X.; Nguyen, N. T.; Chen, M.; Lyon, L. A.; Adlam, D. J.; Freemont, A. J.; Hoyland, J. A.; Saunders, B. R., Responsive Nanogel Probe for Ratiometric Fluorescent Sensing of pH and Strain in Hydrogels. *Acs Macro Lett* **2017,** *6* (11), 1245-1250.

19. Zhu, M. N.; Lu, D. D.; Wu, S. L.; Lian, Q.; Wang, W. K.; Lyon, L. A.; Wang, W. G.; Bartolo, P.; Saunders, B. R., Using green emitting pH-responsive nanogels to report environmental changes within hydrogels: a nanoprobe for versatile sensing. *Nanoscale* **2019,** *11* (24), 11484-11495.

20. Shanks, H. R.; Milani, A. H.; Lu, D. D.; Saunders, B. R.; Carney, L.; Adlam, D. J.; Hoyland, J. A.; Blount, C.; Dickinson, M., Core-Shell-Shell Nanoparticles for NIR Fluorescence Imaging and NRET Swelling Reporting of Injectable or Implantable Gels. *Biomacromolecules* **2019,** *20* (7), 2694-2702.